VICTORIA UNIVERSITY OF WELLINGTON

Microemulsion Electrolytes for Electrochemical Energy Storage Devices

by

Fraser R Hughson

A thesis submitted in partial fulfillment for the
degree of Doctor of Philosophy

in the
Faculty of Science
School of Chemical and Physical Sciences

August 2021

Declaration of Authorship

I, Fraser Hughson, declare that this thesis titled, ‘Microemulsion Electrolytes for Electrochemical Energy Storage Devices’ and the work presented in it are my own. I confirm that:

- This work was done wholly or mainly while in candidature for a research degree at this University.
- Where any part of this thesis has previously been submitted for a degree or any other qualification at this University or any other institution, this has been clearly stated.
- Where I have consulted the published work of others, this is always clearly attributed.
- Where I have quoted from the work of others, the source is always given. With the exception of such quotations, this thesis is entirely my own work.
- I have acknowledged all main sources of help.
- Where the thesis is based on work done by myself jointly with others, I have made clear exactly what was done by others and what I have contributed myself.

Signed: ____

Date: ____

VICTORIA UNIVERSITY OF WELLINGTON

Abstract

Faculty of Science
School of Chemical and Physical Sciences

Doctor of Philosophy

by Fraser R Hughson

The demand for electrical energy storage technology is growing at a rapid pace. The current market leader is the lithium ion battery which has found use in many applications from stationary, grid level storage to transportation and smaller applications like mobile phones.

Supercapacitors are an up-and-coming alternative energy storage technology that compliments lithium ion batteries in many ways. Where lithium ion batteries have a high energy density, delivering energy for a long time, supercapacitors have a high power density which means they are capable of being charged and discharged within seconds.

Both of these technologies rely on organic electrolytes that are toxic and flammable. Replacing these organic electrolytes with alternatives would go a long way to improving their sustainability and lessening the environmental impact. Using a water based electrolyte is an attractive option however water is limited by its electrochemical window. Above a voltage of 1.23 V it is thermodynamically favourable for water to be split into hydrogen and oxygen gasses. This voltage restriction limits the energy density of water based batteries and supercapacitors making them economically non-viable.

The research in this thesis was investigating the use of microemulsions as an alternative class of electrolytes in ion batteries and supercapacitors. Microemulsions are a thermodynamically stable mixture of two immiscible phases. Despite being mostly made up of water, microemulsions can have a greatly extended electrochemical window, as much as 5 V. This means that they could have all of the benefits of aqueous and organic electrolytes in one solvent.

Microemsulions have never been applied to supercapacitors or ion batteries before. They were found to retain their enhanced electrochemical stability and still allow for the devices to perform. In almost all aspects the devices presented within out-perform any other water based electrolyte in the literature and in many cases show comparable performance to organic electrolytes.

Acknowledgements

Firstly, I must express my deepest respect and gratitude to my research advisor and supervisor Prof. Thomas Nann. His continued support and his trust in me to get in the lab, have ideas, make mistakes, and find my own way forward will have a lasting impact. I could never have imagined all of the amazing opportunities he gave me throughout my PhD which have challenged me in many exciting ways. I am also forever indebted to Prof. James Johnston who took over the role of VUW supervisor when Thomas departed for Australia. Despite my research being a bit outside of his usual scope he accepted me with open arms, his assurance in the first week that this was not an "in name only commitment" were the most reassuring words I could have heard. He stepped up and fought for me when he could have been passive, and made my life much easier as a result. Such a commitment to integrity is not something I will forget quickly.

Thanks must also go to Ashwath Sundaresan of Wellington UniVentrures. Before this PhD I never thought that commercialisation would become such a large part of my professional identity. Ash has encouraged that development over the past few years and is the only reason I got an Emerging Innovator award from Kiwinet which has been an amazing experience.

Also the MacDiarmid Institute must be mentioned for the continued funding and opportunities they have provided to me over the years. In particular, Covid lockdown would have been a much more stressful experience were it not for the scholarship extension they provided. The symposiums and boot camps have been some of the best experiences of my PhD.

I would also like to thank David Flynn, for teaching me how to use the electron microscopes and his commitment to helping me figure out how to do anything I wanted with them. Also to Mathew Cairns for teaching me how to do XRD (once the machine was finally working again), without his expertise (and knowledge of calcium carbonate) it would have taken me a lot longer to get my results.

One of the things I will look back on the most fondly is the Nann group. While it was in disarray for a little bit there, from joining the group in early 2016 for my honours project to now, they have remained committed to research excellence, pushing each other with insightful and constructive feedback and mostly just being all around good people. Erin, Kathryn, Siobahn, Garima, Renee, Geoffry, Vaibhav, Zeineb, Helen and Nicolo all made the lab a great place to be. Also to Jim's group for being so accepting of me during a time when I could have ended up quite isolated. Special mention must go to Rohan for doing a lot of the ground work on the microemulsion project and for being the only one

who I think comes as close as I do to understanding just how weird and wonderful they can be. There is a long way to go but I'm excited to see what they will throw at us next.

Of course, I can't not mention Dr. Shalini Divya. When I first started making batteries she was there showing me how to do it all. That alone would have been enough, but she has stayed behind me (literally and figuratively) every step of the way. From reading emails to make sure they strike the right tone before I send them, to hearing out my frustrations, to helping me interpret results and sharing in my excitement when things went well, I could not have asked for a better lab mate and friend during this time.

Also to my family who have encouraged me at every step, thank you for not asking how much longer its going to take or what I'm going to do afterwards too often, your love and support has been very meaningful for me.

Finally, I must thank the person without whom I probably would have never gotten a PhD scholarship in the first place, my incredible, intelligent, gorgeous, loving, partner Cara. Her help and support during this 3-ish years cannot be understated. I am grateful for you and the life we have together every single day and I cannot wait for what the future has in store for us.

Contents

List of Figures

Abbreviations

XRD	X-ray Diffraction
XPS	X-ray Photoelectron Spectroscopy
SEM	Scanning Electron Microscope
TEM	Transmission Electron Microscope
CV	Cyclic Voltammetrey
GCDC	Galvanostatic Charge Discharge
ME	Microemulsion
SEI	Solid Electrolyte Interphase
EEI	Electrode Electrolyte Interphase
SDS	Sodium Dodecyl Sulfate

Conferences

1. **F. Hughson**, R. Borah and T. Nann “Suppressing water splitting for high voltage aqueous ion batteries” The International Coalition for Energy Storage and Innovation (**ICESI**) Conference 2020, Sydney.
2. **F. Hughson**, R. Borah, J. Johnston and T. Nann “Supressing water splitting for high voltage aqueous ion batteries” **TechConnect** Washington D.C., USA, 2020. Abstract accepted, conference cancelled (due to COVID-19)
3. **F. Hughson**, R. Borah and T. Nann “A 2.7 V aqueous supercapacitor” Australasian Colloid and Interface Symposium (**ACIS**) 2021, virtual conference.

Symposia

1. **F. Hughson**, and T. Nann “Electrospun Sillica Nanofibres” Victroria University of Wellington - Massey University Symposium, 2018, New Zealand
2. **F. Hughson**,“History of Lithium Ion Batteries” Novel Prize Public Lecture at Victoria University of Wellington 2019, New Zealand
3. **F. Hughson**, R. Borah and T. Nann “A 2.7 V aqueous supercapacitor”, MacDiarmid Institue Annual Symposium, 2021, Rotorua, New Zealand

Publications

1. R. Borah, **F. Hughson**, J. Johnston, T. Nann “On Battery Materials and Methods” [12]
2. N. Canever, **F. Hughson**, T. Nann “Solid electrolyte interphases (SEI) in non-aqueous aluminium-ion batteries” [13]
3. **F. Hughson**, R. Borah, T. Nann “A 2.7 V aqueous supercapacitor using a microemulsion electrolyte” [14]
4. **F. Hughson**, R. Borah, T. Nann “High voltage aqueous ion batteries using microemulsion electrolytes”. To be submitted.

Chapter 1

Introduction

1.1 The climate crisis

Anthropogenic climate change is perhaps the biggest challenge ever faced by humanity. With greenhouse gas emissions around the globe still increasing, it is becoming evident that technological advances have to come along with social changes to stop climate change. Of principle concern is the use of fossil fuels such as coal and oil for transportation and grid power generation. There has been a large increase in the adoption of renewable energy sources. In 2019 renewable energy overtook fossil fuels as the dominant source of energy in the UK [15]. In November of 2020, Tasmania in Australia declared that it was fully powered by renewable energy [16]. However, these advancements alone are not enough to secure a complete departure from fossil fuel use.

1.2 Renewable energy and energy storage

As the world moves away from fossil fuels, the largest remaining question is one of energy security: What happens when the sun doesn't shine and the wind doesn't blow? Coal and oil do not suffer from this intermittency and so replacing them wholesale is a difficult task. This is because in many places around the world the peak energy consumption is during the evening/at night, whilst the peak of solar energy production is during the day. Figure 1.1 shows solar and wind power output alongside grid demand [17].

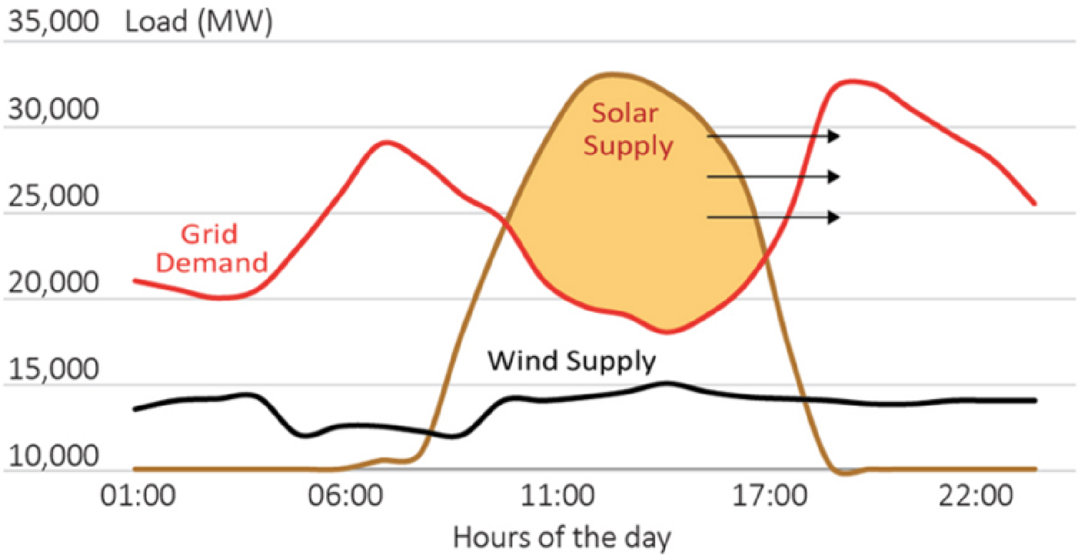

FIGURE 1.1: The output of solar and wind power do not match with the peak demands of the grid, this makes adoption of renewables difficult because the power comes at the wrong time. Reproduced with permission from auclimate.wordpress.com/2018/04/17/battery-storage-the-answer-to-renewable-energy-intermittency/

In order to 'shift' the energy generated at off-peak times, as indicated by the arrows in Figure 1.1, energy must be stored during times of over-production and then released when it is needed most. There are many methods for storing energy, most of which are summarised in Figure 1.2.

Figure 1.2 shows that there are not only many different types of energy storage, there are also many different applications where each is most suitable. How and why these different forms of storage are needed is illustrated by the energy grid (see Figure 1.3).

Pumped hydro is an example of an energy storage technology available on a large scale. However, it takes a long time for these systems to be charged and discharged. Pumped hydro is therefore an attractive option for grid level storage as it can supply large amounts of energy for a long amount of time. However, such large systems are not very dynamic, their energy output can not easily respond to fluctuations in demand [18]. Energy production can be increased for known peak time periods, but matching the instantaneous demand on a minute by minute basis can be difficult. Pumped Hydro, or some other large scale energy storage method such as compressed air storage, could provide 'base-load' power, the amount of energy the grid needs regardless of the time of day.

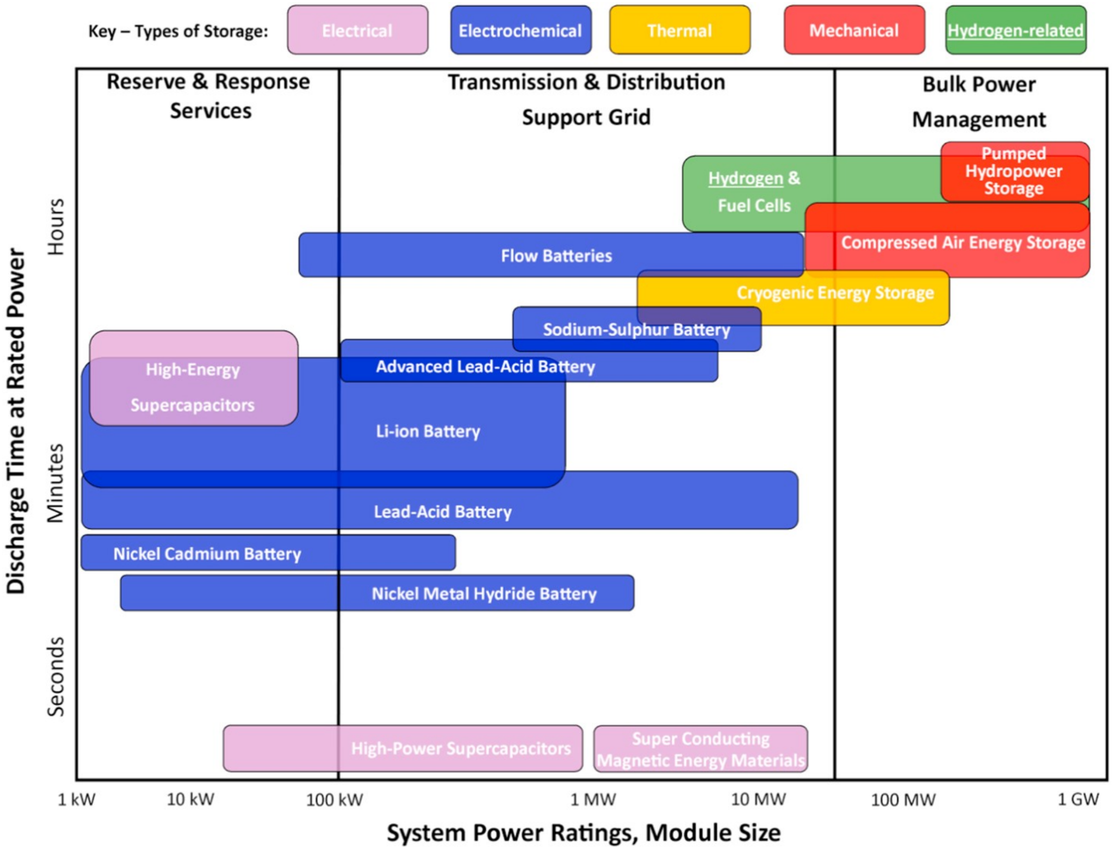

FIGURE 1.2: There are many different kinds of energy storage available. This plot compares them based on method, power rating and discharge time.[1]

More responsive systems are needed to deal with surges in demand. However these systems still need to store a lot of energy to keep up with demand over hour long time scales. This is where batteries could be utilised effectively. Being charged when demand is low (and the spot price for energy is low) and being discharged when demand is high (and the spot price for energy is high). There are many types of battery as shown in Fig 1.2 but the types most often referenced for this application are lithium ion batteries and redox flow batteries [19, 20]. Both can be scaled to appropriately large sizes, are able to handle frequent charge and discharge, and can be held at various states of charge for extended periods of time. This last point in particular is where lead acid batteries perform poorly in grid scale applications [21, 22].

The final element of the grid is frequency regulation. Power grids around the world operate on an alternating current with a frequency of either 50 or 60 Hz. Any device connected to the grid is designed to receive this frequency only (within a small margin of error). Any prolonged period where the grid is not supplying the rated frequency can cause serious damage to the grid as a whole and any device connected to it. To maintain

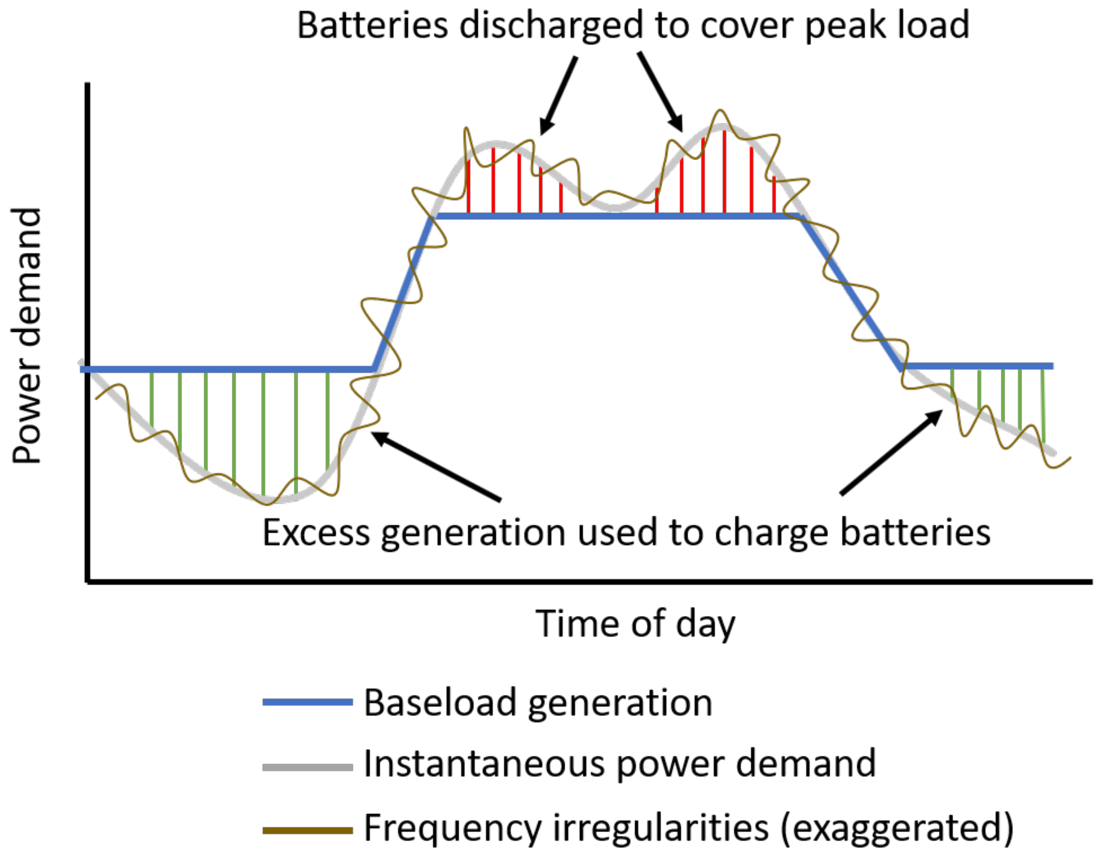

Figure 1.3: The instantaneous power demand fluctuates throughout the day (grey line) The base load (blue line) can ramp over many hours to meet a forecast rise but cannot be scaled quickly enough to meet demand exactly. With energy storage systems, excess energy generation can be used to charge the system (green lines) and then it can be discharged to meet peak demands (red lines). Using renewables also introduces the possibility of frequency irregularities (gold line) a fast responding (on the order of seconds) energy storage device is required to correct these or else irreparable damage can be done to anything powered directly by the grid.

frequency, the energy into the grid must match the energy out of the grid [23] If they are not matched then the frequency will slowly start to rise or fall. Modern grid level generators are equipped with sensors to detect these frequency shifts and can generally adjust power output minutely over the course of a few seconds to maintain this balance.

However as the grid moves towards renewable energy, frequency regulation could become a bigger problem [24]. The power output of solar or wind energy cannot be controlled as easily as steam powered generators. If the wind speed was to pick up or drop off suddenly, or a cloud were to pass over a solar farm, the grid could become destabilised due to a quick change in energy input into the grid. The solution is to have a fast acting energy storage device that can, on a second by second basis, take in excess energy generated by the grid or push extra energy into the grid rapidly to make up any shortfall.

Most batteries are not well designed for frequency regulation as their power rating, in Watts (or Js^{-1}) is generally too low to suppourt rapid uptake and release of energy in an efficient manner. [12]. In the case of lithium ion batteries, charging or discharging them too fast can also cause irreparable damage to the cells and drastically shorten their lifespan [12].

Electrical double layer capacitors or supercapacitors (also often referred to as ultracapacitors) are ideal for this high power application. They can be charged and discharged rapidly (100-1000 times faster than a lithium ion battery) and can be cycled over 1 million times with very small capacity losses [25].The downside with supercapacitors is they cannot store a lot of energy at one time (10-100 times less than a lithium ion battery by per unit volume or mass)[26]. This makes them unsuitable for peak energy management (minute to hour long usage) but ideal for frequency regulation (seconds of usage at a time).

Another area where supercapacitors and batteries can work in tandem is in electric vehicles [27]. When accelerating, a vehicle uses a burst of energy over a short time span. When maintaining a constant speed, the instantaneous energy demand is lower, but the power system needs to be able to meet that demand for a long period of time. Due to their high power capabilities, supercapacitors can be used to accelerate the car then the high energy capabilities of the battery can take over when the instantaneous energy demand is lower. The battery lifetime is extended due to not having to be discharged too quickly during acceleration and the vehicle range is kept high due to the battery compensating for the supercapacitors lack of overall energy.

1.3 Energy storage metrics

Before continuing, it is pertinent to give a brief introduction to the metrics used to compare energy storage devices and how they are calculated.

- *Capacity:* This is how much charge (often reported in milliamp-hours, mAh) can be stored in the device. To allow for comparison between systems, this is often normalised by either the mass, which gives specific capacity in milliamp-hours per gram ($mAhg^{-1}$), or by volume, which gives volumetric capacity in milliamp-hour per centimetre cubed ($mAhcm^{-3}$).[1]In literature, capacity is generally calculated by multiplying the current used to charge or discharge the device by the time the current was applied for. More correctly, capacity should be calcuated as by integrating the current over the discharge time. A high capacity means that the battery can provide energy for a longer period of time so ideally this number is as large as possible.

- *Voltage:* This is the potential difference (V) between the two electrodes. For batteries, this is the potential of the redox reaction that occurs within the cell, and for supercapacitors it is the maximum voltage applied across the plates. Again this should be as large as possible.

- *Energy:* This is how much energy is stored in the device, measured in Watt-hours (Wh). Again this is often normalised by mass to give Whg^{-1} or by volume to give $Whcm^{-3}$. The energy density (Whg^{-1}) is the number quoted most often when trying to establish the capabilities of an energy storage system. For batteries, this is most commonly calculated by multiplying the capacity and voltage together. For supercapacitors, it is calculated by by taking half the capacitance (see Section 1.4) multiplied by the maximum voltage squared. ($0.5CV^2$). The higher the energy density, the more successful the device.

- *Power:* This is a measure of how rapidly energy can be extracted from the system. It is usually measured in Watts or kilowatts per gram (Wg^{-1} or kWg^{-1}). This can be calculated in a variety of different ways for the different devices. For supercapacitors, the maximum power is related to the internal resistance of the cell (See Section 2.8.1). For batteries, this is often established by increasing the current used to charge and discharge the cell and seeing how the capacity of the cell behaves. If the cell maintains its capacity, even at high currents, then it is deemed to have good power density [28, 29]. Again, the power density should be as high as possible.

---

[1] This can be complicated by how exactly the masses and volumes used in these calculations are used. Commercial cells use the mass and volume of the final fully packaged cell. However this is unrealistic for many lab scale operations. Instead, the mass of the electrode material used in the cell should be used. One electrode is usually in vast excess so that only the mass of the relevant electrode is used. Some groups report the mass calculated based only on the active material in the electrode (removing conductive agent and the binder that are often included alongside the active material) This has an effect

1.4 Supercapacitors - Overview and working principle

All capacitors consist of two electrodes, anode and cathode, separated by a dielectric material. Dielectric materials are insulating materials that can be polarised by an applied electric field, many materials fit this description including glass, plastics and metal oxides. When a voltage is applied across the two plates, charge accumulates on the electrodes driven by the difference in potential. Since the dielectric is non-conducting, electrons cannot flow across the electrode-dielectric boundary and so the charge is 'stored' on the surface of the electrodes at a potential equal to that of the applied voltage. No actual electron transfer (redox reaction) takes place.

The 'capacitance' of a capacitor is measured in Farads (F) which is defined as the ratio of charge stored on the plates and the voltage applied across them,

$$C = Q/V \tag{1.1}$$

Where Q is measured in Coulombs and V is measured in Volts. Any capacitor with a 'very high' capacitance is deemed to be supercapacitor [30]. There has been much discussion the literature as to where exactly the line between a non-supercapacitor and a supercapacitor is in terms of a capacitance value [25].

Most supercapacitors are electrical double layer capacitors or EDLCs. They rely on a liquid electrolyte with a salt dissolved in it. A purely capacitive double layer is generally accepted to have 4 reigons, the Inner Helmholtz plane (IHP), the Outer Helmholtz Plane (OHP), the diffuse layer and the bulk, indicated in Figure 1.4.

The IHP is made of adsorbed ions that either have no solvation shell or only a partial one, the thickness of this plane is taken as the centre of the adsorbed ions. The OHP is made up of fully solvated ions and so they exist slgihtly further away from the electrode surface. The thickness of the OHP is taken as the centre of these solvated ions. The thickness of these layers is dependant on the size of the ions in the solution, but in common aqueous electrolytes such as KCl they are on the order of a few Angstroms [25]. Often the IHP and OHP are referred to collectively as the Stern layer.

---

of artificially inflating numbers, especially in the case of sulfur batteries, where the sulfur loading in the electrode could be as low as 50% of the electrode mass). In this thesis, all mass calculations will be done using the mass of the limiting electrode, inclusive of the binder and conductive agent.

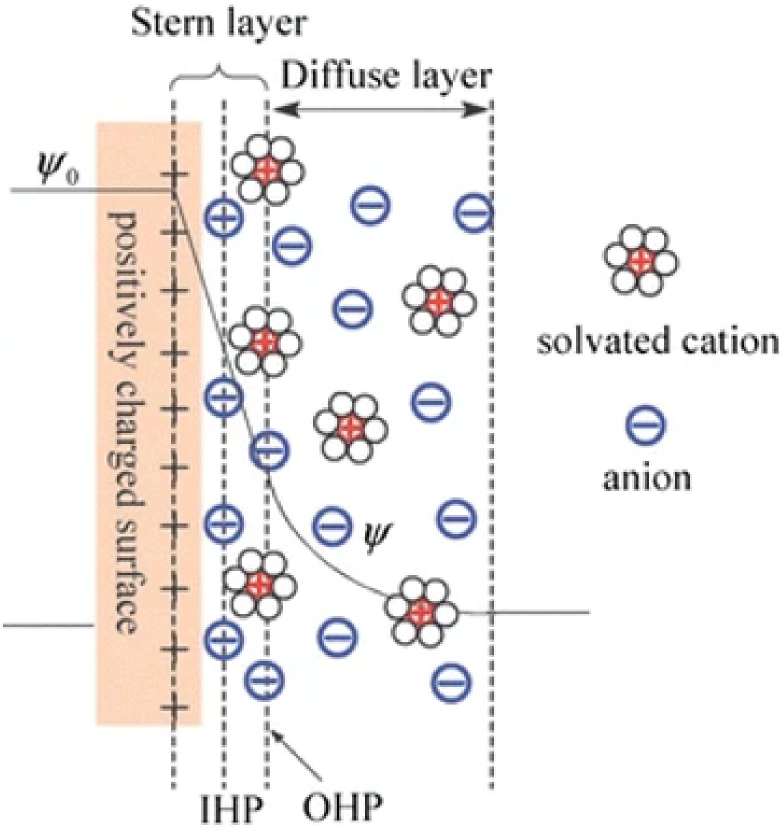

Figure 1.4: An illustration of the electrical double layer that forms at planar electrodes in solution. Reproduced with minor alterations with permission from Du *et al.*, [2]

As the distance from the electrode increases beyond the OHP, the concentration of ions (and thus the potential) will still be slightly higher than the bulk concentration. Eventually, the effects of the electrode are no longer felt by the solution and the ion concentration becomes identical to the bulk. This distance from the OHP until the ion concentrations reaches its bulk value is called the diffuse layer. This model of course works best for a planar electrode.

For electrode materials, activated carbon is the most common for both the anode and cathode. Activated carbon is a form of carbon that has been 'activated' through action of a strong acid or base. This activation corrodes the sample and creates many pores of various sizes in the material giving it a large surface area. This large surface area is what gives rise to the high capacitance. As shown in Figure 1.5, increasing the surface area allows more charge to be stored on the electrode. Therefore a high capacitance value is obtained. How well the double layer formed in these materials relates to the theory described above depends on the size of the pores relative to the size of the IHP, OHP and diffuse layer.

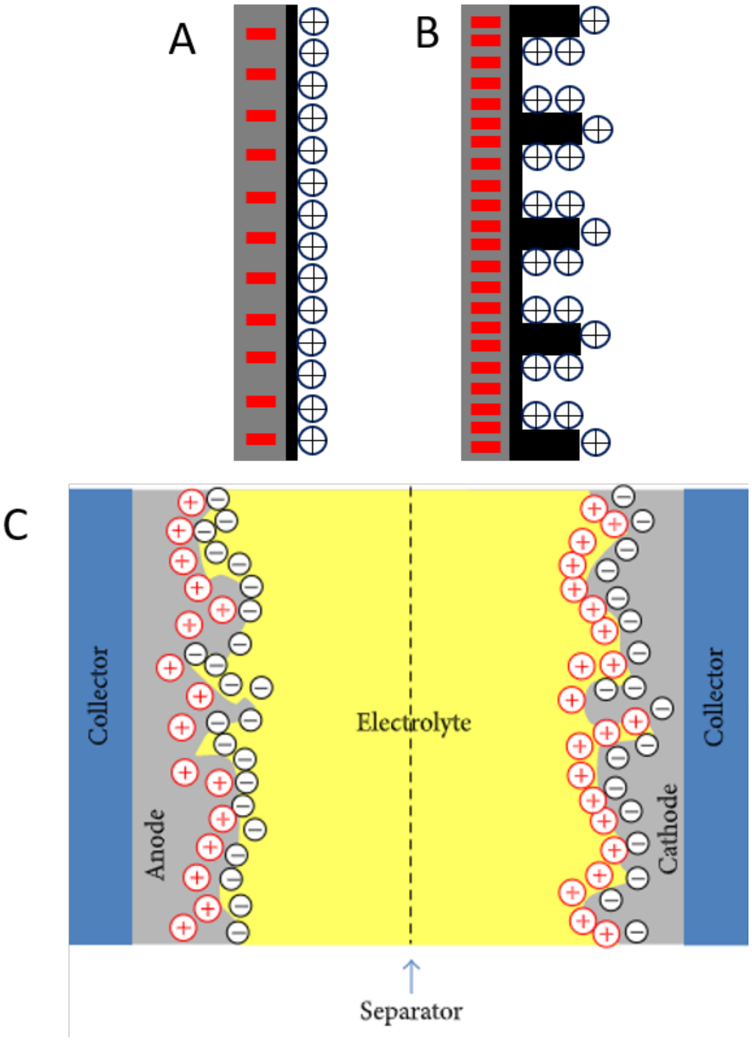

Figure 1.5: A) An electrode with a low surface area. B) An electrode with a larger surface area which is able to store more charge on the surface as a result. C) A sketch of a full supercapacitor with both current collectors both electrodes and the electrolyte and separator. C reproduced from Saleem *et al.*, [3] with minor alterations under Creative Commons Attribution Licence

Graphene has been extensively investigated over the past few years due to its high conductivity and high surface area [31–34]. However, activated carbon still remains the electrode material of choice for most academic and commercial supercapacitors due to its low cost and natural abundance. Most activated carbons on the market are derived from coconut husks as they have been shown to have ideal pore sizes [35, 36]. Alternatively, activated carbon can be derived from metal carbide precursors; though this is generally a much more expensive synthetic route [37, 38]

The electrolyte in traditional supercapacitors is most commonly acetonitrile as a solvent with a quarternary ammonium salt e.g. tetrabutylammonium tetrafluoroborate

($N(C_4H_9)_4BF_4$) or tetraethlyammonium tetrafluoroborate ($N(C_2H_5)_4BF_4$) [39]. Propylene carbonate is an alternative to acetonitrile as a solvent, however it used much less often due to the lower power densities obtained when using it [40, 41].

The energy stored in a supercapacitor is given by Equation 1.2

$$E = 0.5CV^2 \tag{1.2}$$

Where E is the energy stored in Joules, C is the capacitance in Farads and V is the max voltage of the supercapacitor (in Volts). As the capacitor is discharged, the voltage drops linearly with time (assuming the current drawn is constant). This leads to Voltage-Charge curves such as Figure 1.6.

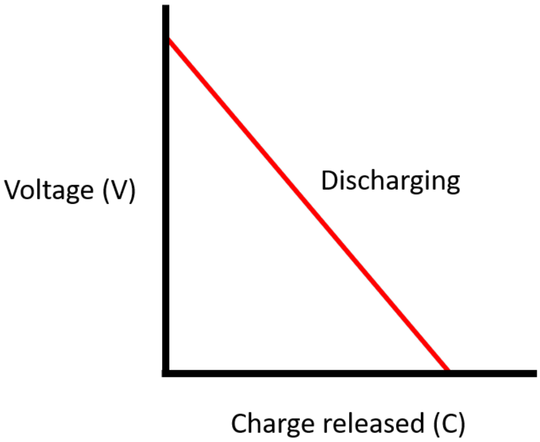

Figure 1.6: The discharge profile of an ideal supercapacitor. The voltage decreases linearly less charge is stored on the surface of the capacitor.

By substituting Equation 1.1 into Equation 1.2 the following expression for the energy can be obtained.

$$E = 0.5QV \tag{1.3}$$

Therefore, the area under this discharge curve is equal to the energy stored in the device. From Equation 1.1 it can also be seen that the gradient of this curve is equal to the inverse capacitance (1/C) of the device. A device with a higher capacitance will lose its charge more slowly and consequently such a curve will have a lower gradient.

1.5 Ion batteries - Overview and working principle

Ion batteries also consist of a cathode and anode with an electrolyte between the two electrodes. Unlike supercapacitors, the anode and cathode materials used in ion batteries are not the same as each other. The other major difference between supercapacitors and ion batteries is that redox reactions occur inside the cell in an ion battery. This is best represented by the following two equations that occur in a typical lithium ion battery,

$$\text{Cathode: } CoO_2 + Li^+ + e^- \underset{\text{charging}}{\overset{\text{discharging}}{\rightleftharpoons}} LiCoO_2$$

$$\text{Anode: } LiC_6 \underset{\text{charging}}{\overset{\text{discharging}}{\rightleftharpoons}} C_6 + Li^+ + e^-$$

Due to this electron transfer process, the amount of charge stored is not limited by the surface area of the electrode as it is with supercapacitors. The intercalating ions can diffuse through the solid structure of the electrode material to occupy sites in the lattice. This means that the amount of charge stored in a battery is a lot higher than in a supercapacitor. However, because the process is no longer purely surface based and relies on solid state diffusion of the ions through the electrode, the rate at which these reactions happen is a lot slower than the surface adsorption of ions in a supercapacitor. Consequently, batteries generally have lower power outputs than supercapacitors.

The voltage of a battery is determined by the equilibrium potential of the redox reaction, such as the one shown in Figure 1.7, which has a nominal potential of 3.8 V [12]. The voltage-charge curves for a battery therefore look very different compared to a supercapacitor. In an ideal case, the voltage at which the redox reaction occurs is independent of the amount of charge stored in the battery. This means that the voltage of the cell remains constant during discharge until the reaction has gone to completion at which point the difference in potential between the electrodes drops to zero.

Like a supercapacitor, the energy stored in an ion battery is calculated by finding the area under the voltage-charge curve. In the ideal case, as depicted in Figure 1.8 the energy is given by the voltage multiplied by the total charge stored in the cell. Ion batteries can maintain their voltages for longer than supercapacitors. Coupled with the naturally higher capacities, ion batteries are capable of storing much more energy than a

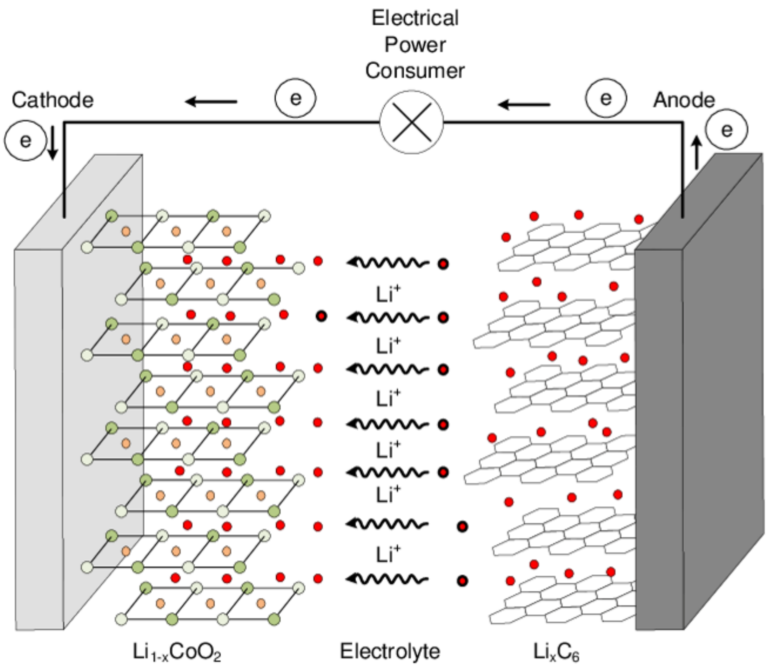

FIGURE 1.7: A schematic of a "typical" lithium ion battery based on a graphite anode and a cobalt oxide cathode. The discharge reaction is being shown. The lithium ions move from the anode to the cathode through the electrolyte and the electrons move from the anode to the cathode through the external circuit. Reproduced with permission from Novinsky *et al.* [4].

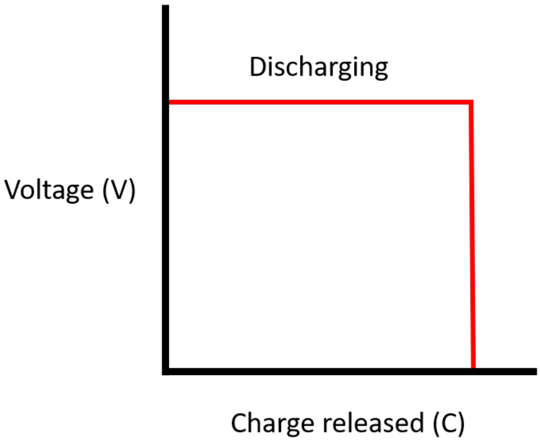

FIGURE 1.8: The discharge profile of an ideal battery. The voltage is fixed at the voltage of the redox reaction inside the cell until the charge in the cell is depleted.

supercapacitor, but, as previously mentioned, they cannot deliver their energy payload as quickly.

The electrode materials used in ion batteries are much more diverse than supercapacitors. Cathodes can range from transition metal chalcogenides such as CoO_2 or MoS_2 to phosphates such as $Fe(PO_4)$ or organic compounds [12]. Anodes are ideally the parent metal but other examples are known such as graphite or TiO_2 for lithium ion batteries [42].

Common ion battery electrolytes are based on organic carbonates, such as propylene carbonate (PC) or diethyl carbonate(DEC), often a mix is employed e.g. 1:1 PC:DEC, as this gives a better performance than one solvent alone. The salt used is often a hexafluorophosphate or perchlorate salt of the ion [43].

1.6 Electrolytes

In its most simple form, an electrolyte consists of a salt dissociated in a solvent. The role of the electrolyte is to complete the circuit by allowing the transport of ions between the two electrodes. Any electrolyte used in a battery or supercapacitor system must meet several key criteria (in rough order of importance):

1.6.1 Electrochemical window

The electrochemical window is defined as the potential range over which a particular solvent does not undergo decomposition. For example, at 1.23 V vs the standard hydrogen electrode, water is oxidised into oxygen gas. At 0.00 V vs the standard hydrogen electrode, protons are reduced to hydrogen gas. This means that, thermodynamically at least, water has an electrochemical window of 1.23 V. Practically this can be extended if the electrodes used are particularly unfavourable for one or both of those reactions (see section 1.7). For example the lead acid battery is able to operate at 2 V, despite using an aqueous electrolyte, because the hydrogen evolution reaction is quite unfavourable on the lead surface [44].

Ideally the electrochemical window of the electrolyte is as large as possible. A larger electrochemical window corresponds to a higher maximum voltage for both batteries and supercapacitors. A supercapacitor or battery that uses a solvent with an electrochemical window of only 0.5 V could only be charged to a maximum voltage of 0.5 V. If a solvent with a 5 V window was used instead, then the supercapacitor could theoretically be charged to 5V. According equation 1.2 this would result is a 100 fold increase in the energy stored in the supercapacitor. In general, water is viewed as being quite unstable electrochemically and has one of the smallest windows of readily available solvents. Aprotic organic molecules such as acetonitrile or cyclohexane generally have much larger electrochemical windows [45].

1.6.2 Ionic conductivity

In order for an electrolyte to be used in a cell, it must be able to conduct ions. Excluding ionic liquids, where the liquid is made from charged species, this is usually attained by dissolving a salt in the chosen solvent. Water has an advantage here as it is able to dissolve a wide variety of 'simple' salts such as sodium chloride, in high concentrations due to its polarity. Organic solvents such as acetonitrile cannot dissolve these inorganic salts in high enough concentrations to be usefully conductive and so must use quaternary ammonium based salts such as those mentioned in section 1.4. Non-polar organic solvents such as cyclohexane cannot dissolve any salts and are therefore not used as electrolytes.

1.6.3 Thermal stability/volatility

Batteries and supercapacitors ideally have a large operation range in terms of temperature. It not only diversifies their potential applications, but also limits the possibility of failure should unexpected conditions arise. For example, acetonitrile based supercapacitors are usually rated to perform between -40 and +70 degrees Celsius which is considered to be an acceptable temperature range for general use [46]. Again, water has an advantage here, with the addition of additives, the freezing point of water can be lowered and a higher maximum temperature can be achieved. The use of volatile solvents with low boiling points and flash points such as tetrahydrofuran is highly unfavourable as gas evolution in the cell can not only reduce cell performance but can also be dangerous [47].

1.6.4 Cost

Low cost is essential for establishing long term viability of commercial devices. Ionic liquids are very expensive and so are not generally favoured. Acetonitrile and other organic solvents are not quite as expensive as ionic liquids, e.g. a typical price of acetonitrile is 2 USD/kg at scale. However, most of the cost of the standard electrolyte for supercapacitors comes from salt that is used. Readily available salts like chlorides or sulfates do not easily dissolve in acetonitirle and so more expensive salts based on quarternary ammonium cations must be used.

For Ion batteries the organic carbonates used for the electrolytes, like acetonitrile, are not expensive on their own, but the salts used in conjunction with them such as $LiPF_6$ are much more expensive than cheaper alternatives such as LiCl. Using non-aqueous systems such as these also increases production cost further as the solvents are required to be anhydrous as any water in the electrolyte can undergo electrolysis inside the cell.

The requirement for dryness can also add cost to other areas of production. For example the electrodes must be thoroughly dried, usually by placing them in an oven at high temperature for a long period time, before they can be used in cells.

Water is much cheaper than any organic solvent and the potential use of simple inorganic salts like NaCl as a source of conductivity represents a further massive cost reduction [48]. The processing costs of such electrolytes would be much lower as they would not need to be dried extensively before use. Using water would also eliminate the need to dry the electrode before use which cuts costs further and could enable faster production.

1.6.5 Safety and environmental impact

Safety and environmental impact are much more pertinent to batteries, but are also factors to consider for supercapacitors. Lithium ion batteries regularly make headlines due to malfunctions, which can lead to catastrophic failure [49]. This is not only a result of the chemistry of the cell but also the flammable organic electrolytes used. Choosing a non-flammable electrolyte would reduce the safety concerns significantly. Furthermore, many organic solvents are toxic and environmentally harmful which can make dealing with cells at the end of life more difficult [50]. Using an aqueous electrolyte would solve this problem.

1.6.6 Compatibility

The electrolyte must be compatible with commonly used (and inexpensive) battery materials. For example, steel is an ideal current collector for batteries or supercapacitors due to its low cost. However, chloride containing electrolytes corrode steel at relatively low potentials and as such the two are not compatible [51]. Even if the electrolyte components are cheap, if they are only compatible with expensive metals such as molybdenum or tantalum then the electrolyte may end up not being scaleable [52]. Highly acidic or basic aqueous electrolytes are often not compatible with many materials. The compatibility of materials with organic solvents is more case-by-case. In the case of magnesium ion batteries for example, many organic solvents are known to decompose on the magnesium metal surface, forming an impenetrable solid electrolyte interphase (SEI) which stops cell function [51].

1.6.7 Summary

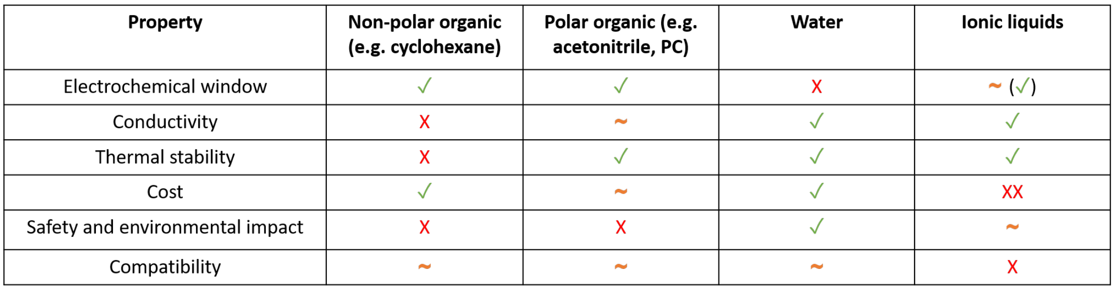

Property	Non-polar organic (e.g. cyclohexane)	Polar organic (e.g. acetonitrile, PC)	Water	Ionic liquids
Electrochemical window	✓	✓	X	~ (✓)
Conductivity	X	~	✓	✓
Thermal stability	X	✓	✓	✓
Cost	✓	~	✓	XX
Safety and environmental impact	X	X	✓	~
Compatibility	~	~	~	X

Figure 1.9: A summary of electrolyte requirements listed in the previous section. All common classes of solvents are evaluated based on their performance in a certain category. Ticks indicated the solvent performs well in that criterion, crosses imply poor performance and tilde represent middling performance. Ionic liquids have a large variation in properties, some do have large electrochemical windows while others do not [5]. Compatibility is also on a more specific solvent-material basis as previously mentioned. Ionic liquids are generally very corrosive and so are only compatible with a few materials [6].

From Figure 1.9 it can be seen that while water appears to be the best solvent, the one major drawback is its electrochemical window. This lower electrochemical window leads to lower voltages and thus, greatly reduced energy densities. The drop in energy density is most pronounced for ion batteries, where commercial cells which employ polar organic solvents, routinely reach 4 V.

The reduced energy density alone makes water not viable as a solvent for modern energy storage applications (with the exception of the lead acid battery). Modern commercial ion batteries and supercapacitors use polar organic solvents such as acetonitrile or a mixture organic carbonates in order to achieve the energy density required for modern applications.

If this one drawback could be overcome, the impact would be far reaching.

1.7 Water splitting

As mentioned previously in section 1.6.1 the thermodynamic potential at which water is split into hydrogen and oxygen is 1.23 V

$$\mathrm{H_2O\,(l) \longrightarrow H_2(g) + 0.5\,O_2(g)} \qquad E^{\mathrm{o}} = -1.23V \tag{1.4}$$

However the potential at which this reaction actually occurs also depends on various over-potentials present in the system.

$$\mathrm{H_2O\,(l) \longrightarrow H_2(g) + 0.5\,O_2(g)} \qquad E^{o} = -1.23V + \eta \tag{1.5}$$

Over-potentials can come in many forms. For simplicity, over-potentials can be separated into anode and cathode and “other” contributions which includes terms like the over-potential (η) that arises form the solution resistance. Therefore increasing the over-potentials for the water splitting reactions on the electrodes is a viable way to increase the operating voltage of aqueous electrolytes. This is the strategy employed in lead acid batteries to attain their 2 V operating voltage.

However, simply having a large anode or cathode over-potential on its own is not enough. As soon as the over-potential for one of the reactions is surpassed then that reaction will start to occur and electrolyte decomposition will begin. This will be discussed further in section 1.8

1.8 Extending the Electrochemical Window of Water

Given the clear advantages of water as an electrochemical solvent, it is not surprising that many attempts have been made to extend the electrochemical window of water and open up higher energy densities as a result. This section will detail some of the methods employed in the literature thus far for both ion batteries and supercapacitors.

1.8.1 Artificial Solid-Electrolyte interphases

The notion of a solid electrolyte interphase (SEI) has been around since the conception of the lithium ion battery. During the first few cycles of a lithium ion battery, the anode undergoes a reaction with the electrolyte and a passivation layer forms on the anode surface. This layer is comprised of a complex mixture of species that are dependent on the exact nature of the electrolyte [53, 54]. The SEI is still ionically conductive and so Li^+ ions are still able to pass through to the graphite. However, further side reactions with the electrolyte are prevented. Therefore the formation of the SEI is advantageous for lithium ion batteries and is one of the reasons that traditional cells are able to achieve such high voltages [55].

Many groups have tried to develop 'Artificial SEI's' which they can coat on to electrode materials to suppress water splitting. The underlying concept is that if one can prevent water from reaching the electrode, then water splitting will be observed. Using this methodology Yang *et al.*[56] were able to achieve a 4 V aqueous battery using a highly fluorinated ether, coated on the lithium surface prior to cell assembly. During the first charge, the ether was selectively reduced on the surface, which created a hydrophobic SEI that repelled water from the interface but allowed Li ions to still pass through. The electrolyte used was a water in salt electrolyte, which is discussed in more detail in Section 1.8.5. Using this methodology a 4 V battery was constructed that was compatible with both graphite and lithium metal anodes.

Artificial SEIs can also be prepared prior to assembling the cell. Subramanya *et al.* [57] formed a carbon-TiO_2 composite by thermally decomposing glucose on the surface of TiO_2 particles enabling an aqueous battery that could be charged to 2 V. Zhi *et al.* [58] used a Langmuir trough based technique to coat their anodes with reduced graphene oxide films. Lithium ion batteries made with these coated cathodes were able to achieve 1.9 V in 1 M Li_2SO_4.

Beyond lithium batteries, a zinc battery was constructed by Han *et al.* [59] with an artificial SEI deposited on a V_2O_5 cathode. This artificial SEI was made *in situ* by polymerising various heterocyclic monomers onto the cathode surface. Zinc batteries are lower in voltage than lithium ion batteries and therefore water splitting is not generally a major concern, the main advantage was that the thermal stability of the system was drastically improved by the SEI.

As evidenced, in batteries, SEIs can perform a useful function. As long as they are ionically conductive, the passivation they provide can extend the voltage window of the electrolyte and extend the lifetime of the cell. For supercapacitors however, SEIs are detrimental. As discussed in Section 1.4 the higher the surface area of the electrode, the higher the capacitance of the cell. The formation of an SEI would lead to a decrease in the active surface area as the micropores are filled with solid deposits. Over time SEIs do still form in supercapacitors [60]. These decomposition reactions are driven by reactive functional groups, such as carboxylic acids, that remain on the surface of the activated carbon electrodes after the activation process. These trigger decomposition of the electrolyte and electrode which results in the formation of an SEI and a decrease in the performance.

One rare example of an artificial SEI in a supercapacitor was presented by Hong *et al.* [61] where they used atomic layer deposition to coat activated carbon particles with 2 nm of Al_2O_3. This thin layer protected the reactive functional groups on the surface and extended the electrochemical window in a non-aqueous electrolyte to 3 V without adversely affecting the porous structure.

1.8.2 Electrode functionalisation

The main method used to extend the electrochemical window of non-aqueous supercapacitors from an electrode engineering perspective, is rigorous purification of the activated carbon or use of materials such as carbon nanotubes that do not contain these functional group impurities in the first place [62]. Izadi-Najafabadi *et al.* [63] were able to obtain a 4V supercapacitor using a non-aqueous (acetonitrile) electrolyte using carbon nanotube electrodes which were free of functional group impurities. Generally, acetonitrile based electrolytes only achieve 2.7 V on activated carbon due to the impurities mentioned previously.

Purification of the activated carbon is not widely used on aqueous supercapacitors however. The reason for this is that these functional group impurities impurities are actually advantageous in an aqueous system. These functional groups improve the wetabillity of the electrode (this is important for all the available surface area being used) and can increase the capacitance (and subsequently the energy density as per Eq 1.2) as a result of the pseudocapactive contributions [64–66].

1.8.3 Mass balance

As shown in Figure 1.6 and 1.8 the way in which the voltage of the device changes as it discharges is different between ion batteries and supercapacitors. In ion batteries the voltage (difference in potential between the electrodes) stays more or less constant as the cell is charged and discharged, which means both the anode and cathode remain at approximately constant potential during discharge.

For supercapacitors , the voltage of the cell decreases linearly with charge, and therefore the potentials of both the anode and the cathode must also be constantly changing. In an ideal case, this change in potential will be linear according to equation 1.3. This is shown in Figure 1.10

Starting from the equilibrium potential (blue dot) at 0 charge, the cell is charged and the potential (ϕ) of both the anode and cathode change linearly with an absolute gradient of 1/C for that particular electrode. In the example in Figure 1.10 both electrodes have equal capacitance values and so they change potential at the same rate. However, because of the position of the equilibrium potential relative to the electrochemical window, the cathode (in blue) reaches the upper potential limit of the electrolyte before the anode (in yellow) reaches the lower limit. Because the electrode is now at a potential sufficient to reduce the electrolyte, the cathodic decomposition reaction will begin taking place. Therefore the maximum difference in potential attainable by this supercapacitor is less than the full voltage window of the solvent.

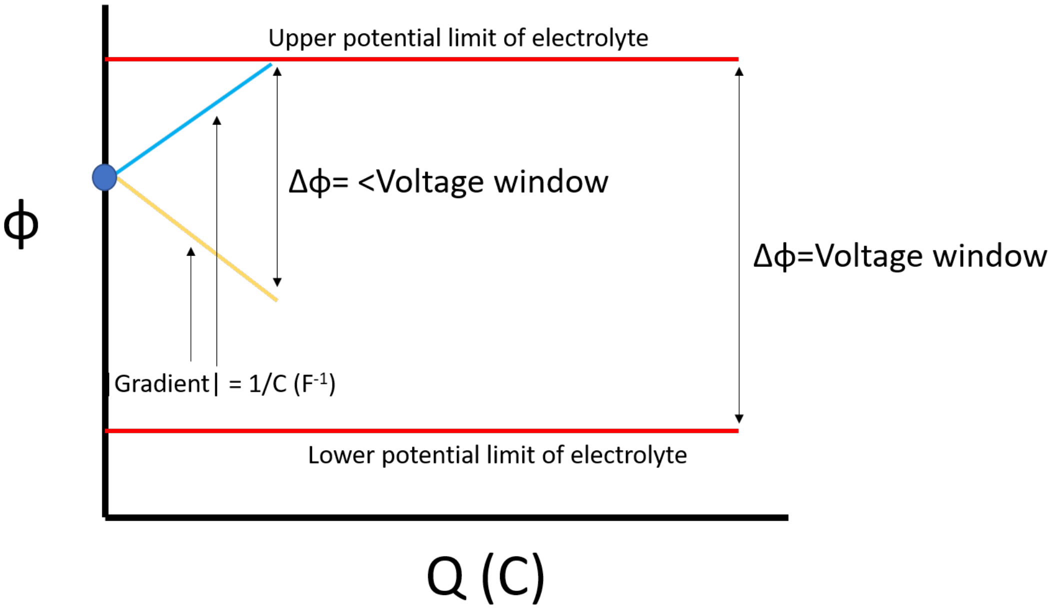

Figure 1.10: The variation in potential (ϕ) of both the cathode (blue) and anode (yellow) as a function of charge stored on the electrodes. The upper and lower potential limits of the electrolyte are indicated as well as the voltage window, which is the difference in potential between the two limits.

With this model in mind, the effect of both changing the mass loading of each electrode and the equilibrium potential can be investigated. First by altering the mass balance, the capacitance of the electrode is changed.[2] This changes the gradient of the line. In Figure 1.11 the mass of the cathode has been increased relative to the anode meaning the gradient (1/C) has decreased.

As a result, the maximum difference in potential achieved is increased compared to the non-mass balanced case (Figure 1.10). Vaquero *et al.* [67] were able to demonstrate that for aqueous supercapacitors based on a K_2SO_4 electrolyte, changing the mass ratio of m^+: m^- from 1:1 to 2.46:1 improved the stability of the device at high voltages; though degradation was still observed. Redondo *et al.* [26] were able to achieve a voltage of 3.2 V in acetonitrile by mass balancing their activated carbon electrodes and finding the optimal amount of graphene doping. This approach was aimed at improving energy density and so both specific capacitance and voltage were considered in crafting their optimal device.

---

[2] Note, the specific capacitance (Fg^{-1}) or volumetirc capacitance Fcm^{-3} are unchanged as they are inherent to the material, however, since there is a different amount of material the total capacitance in Farads will change.

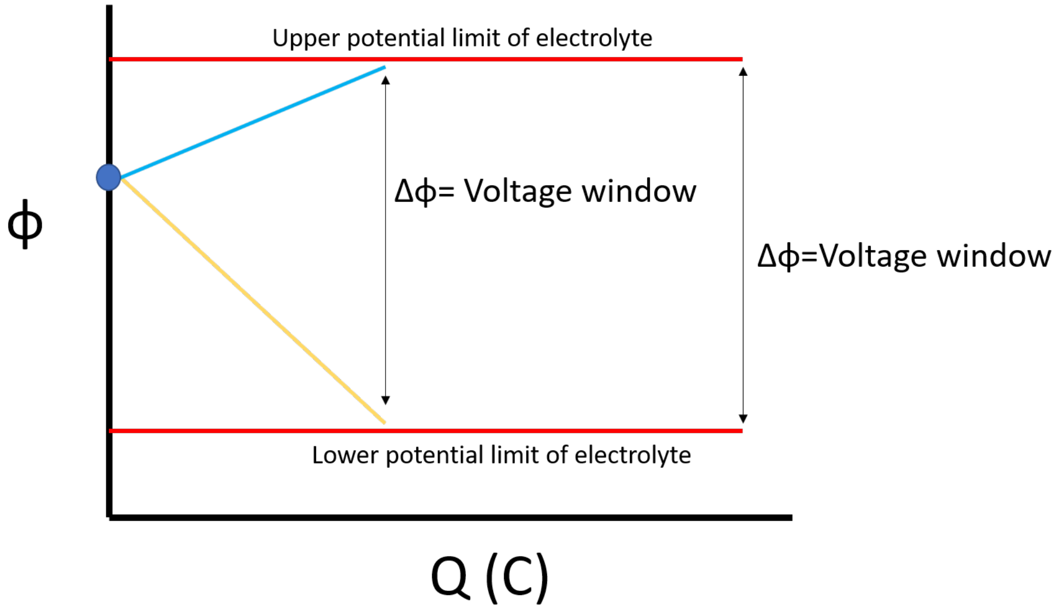

FIGURE 1.11: The variation of potential of both the cathode (blue) and anode (yellow) as a function of charge stored on the electrodes. In this example, the positive electrode (cathode) has a greater mass loading than the negative electrode (anode). This means the capacitance value of this electrode is higher and so the gradient of this line (1/C) is lower. If adjusted correctly, the potential window can be widened as a result of both electrodes hitting the electrolyte potential limits at a similar amount of charge.

This approach is also used widely in asymmetric capacitors (and ion batteries), where the two electrodes have different specific capacitances (or specific capacities) to begin with, however, in these cases, it is mainly for the purpose of not having any wasted material on a given electrode rather than to improve the operating voltage.

1.8.4 Adjusting pH

Although the difference in potential between the two water splitting reactions is always 1.23 V, the potential at which the individual reactions occur is pH dependent. For each pH point increase the standard potential of both oxygen and hydrogen evolution decreases by 59.2 mV, this is shown in the Pourbaix diagram in Figure 1.12.

From Equation 1.5, this thermodynamic limit may not be the actual onset potential for water splitting observed due to the presence of over-potentials. If the over-potential of these water splitting reactions is pH dependant, then it makes sense to adjust the pH to maximise the potential window. If these reactions are not pH dependant then the pH

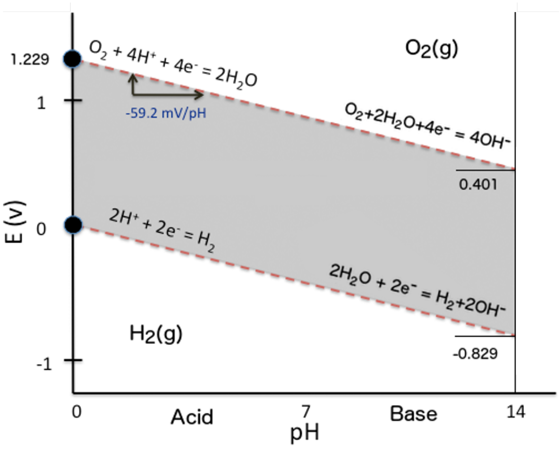

Figure 1.12: A Pourbaix diagram of water showing the pH dependence of the two water splitting reactions, hydrogen evolution and oxygen evolution. The difference in potentials is always 1.23V, however the potential of each reaction changes with pH. ©Wikimedia Commons 2017, used under Creative Commons licence

will determine the combination of electrode materials that can be used as the stability window will be the same over all pH values.

Aside from a few other special cases such as this, the widest electrochemical windows are almost always observed in neutral solutions. Consider the four reactions in Figure 1.12: The reactions responsible for the evolution of hydrogen both increase the pH of the solution, either by consuming H^+ at low pH or producing OH^- at high pH. While these reactions, will not have a large effect on the pH in the entire electrolyte, they will heavily impact the local pH. In the case of hydrogen evolution, it will make the local environment more basic, which will shift the potential of this reaction to more negative potentials, which makes it more thermodynamically unfavourable. Likewise for the oxygen evolution reactions, both result in a large, local, pH decrease when they occur. This decrease shifts these reactions to higher potentials. This negative feedback loop is most pronounced when the concentration of both H^+ and OH^- is low in solution i.e.at pH 7, as the local pH swing will be the largest under these conditions.

This is backed up by many experiments on both supercapacitors and ion batteries, all concluding that the voltage window of an electrolyte is the widest when the pH is neutral, with values of 1.6 V and even 1.8 V being commonly quoted numbers [68–75].

1.8.5 Water-in-salt electrolytes

In recent years, the most noticeable advance in aqueous energy storage technologies is the development of the 'water in salt' electrolyte. Water-in-salt electrolytes were first demonstrated by Suo *et al.* and can have electrochemical windows as wide as 3 V [7]. Lithium bis(trifluoromethane)sulfonimide (LiTFSI) was used as the salt in the original publication and was prepared in concentrations as high as 22 molkg^{-1}. At this high concentration, there are not enough water molecules to fully solvate the ions, hence the term 'water-in-salt'. Because there are no free water molecules, the potential of the water splitting reactions deviate from the standard reduction potentials significantly. Figure 1.13 C shows that for a 21 m (molal, molkg^{-1}) LiTFSI electrolyte the electrochemical window is 3 V.

Since this initial publication, water in salt electrolytes have attracted a large amount of attention in the literature for both ion batteries and supercapacitors. In 2017, Suo *et al.* also showed an aqueous sodium ion battery capable of being charged to 1.6 V in an electrolyte based on sodium trifluoromethane sulfonate (NaOTf) which had an electrochemical window of 2.5 V at 9.26 m concentration [76]. This highlights an issue in the development of high voltage aqueous electrolytes for ion batteries that is mostly absent for supercapacitors. The maximum potential of an ion battery is determined by the chosen electrode materials. Even if the electrochemical window of the solvent is 4 V, if the chosen materials have a potential difference of only 0.5 V then the final cell will have a maximum voltage of 0.5 V. The challenge becomes finding electrode materials that fit at the extremes of the solvent window so as to maximise the cell voltage. If even one of the half reaction potentials of the electrode material lie outside of the electrochemical window of the solvent then solvent splitting will be favoured and the cell will not function.

Most of the wide library of electrode materials for ion batteries has been developed with the constraints of the window of the standard organic electrolytes in mind. When a new solvent system is developed that has a potential window in a different position to that of the standard electrolytes, in order to maximise the window of the new electrolyte, new electrode materials must be developed along side it.

Jiang *et al.* were able to improve the voltage of their water-in-salt sodium ion battery to 1.74 V by altering the electrode materials and also were able to extend the window

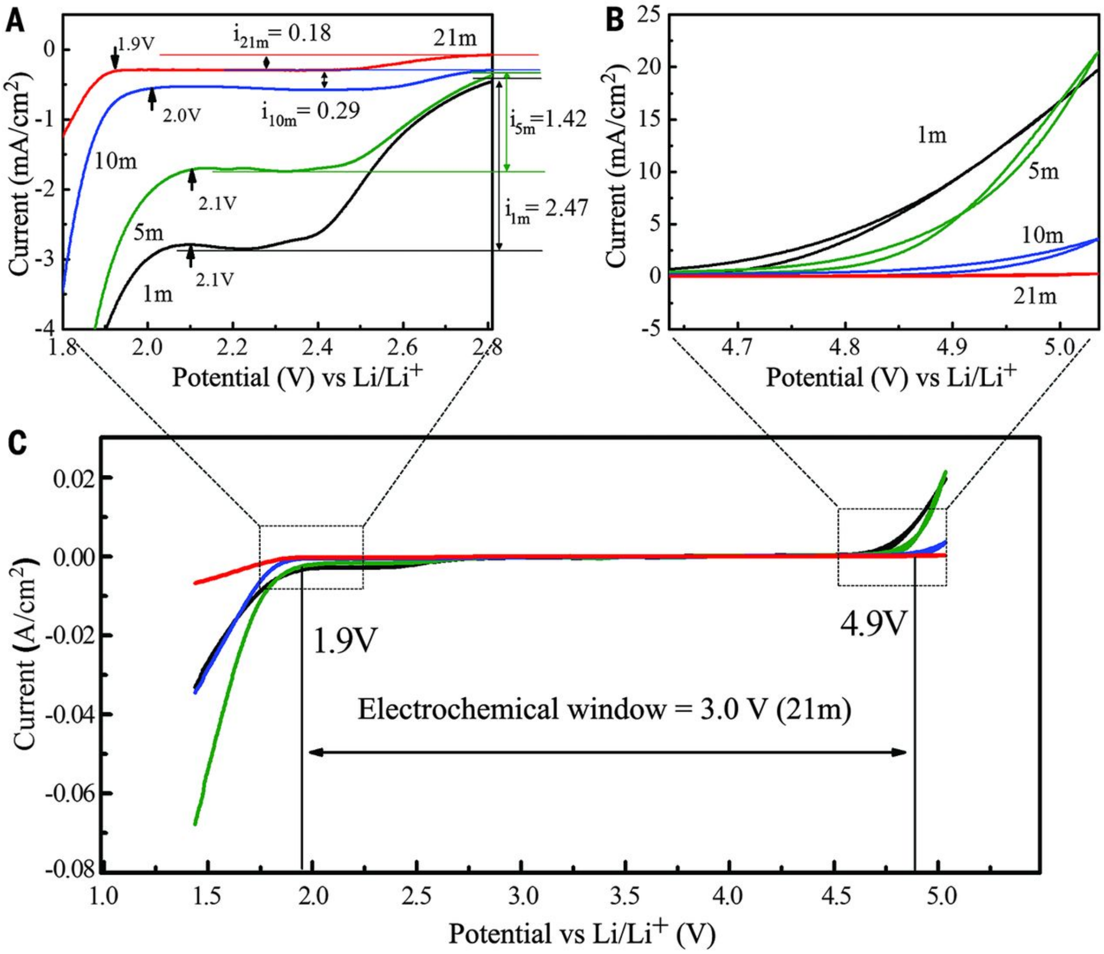

FIGURE 1.13: The electrochemical window of LiTFSI based water in salt electrolytes at various concentrations. A) The reductive stability of the electrolytes is shown, there is a reduction of the current density in this regon as the concentration in increased. The 21 m (molal, molkg^{-1}) sample in red, shows the greatest stability over the potential range. B) The oxidiative stability of the electrolytes is shown. Again there increase in concentration results in a lowered current density. C) The overall window of the eelctrolytes is shown vs Li/Li$^+$. For the 21m sample it is shown to be 3 V. Reproduced with permission from The American Association for the Advancement of Science Copyright © 2015 from Suo *et al.* [7]

of 9 m NaOTf by including 22 m tetraethylammonium trifluoromethane sulfonate as an inert cation [77]. The achieved capacity was more than double that reported by Suo *et al.* for thier system.

A potassium ion battery has also been made with a water-in-salt methodology by Leonard *et al.* [78]. The advantage of this system was that is was able to achieve an extended electrochemical window of 3.2 V with potassium acetate at a concentration of 30 m. Most other water-in-salt based batteries rely on heavily fluorinated sulfones which are much more expenisve and hazardous than acetate ions are. This electrolyte was co-opted by Han *et al.* who used a mixture of sodium acetate (8 m) and potassium acetate (32 m) to create an electrolyte for a sodium ion battery. This cell was only able to achieve 1.2 V. It was again constrained by availability of viable electrode materials in the appropriate potential range.

Supercapacitors are not limited as much as ion batteries by electrode materials. Despite this, the application of water in salt electrolytes to supercapacitors has been met with limited success. Bu *et al.* used a 17 m solution of sodium perchlorate ($NaClO_4$) to produce a capacitor capable of reaching 2.3 V. This is still below the standard 2.7 V mark achieved by acetonitrile based electrolytes. The rate capability of this system was very high, showing a capacitance retention of 88.5% when the charging/discharging current was increased from 1 Ag^{-1} to 20 Ag^{-1}.

Water-in-salt electrolytes represent a large advance in the viability of water based electrolytes due to their extended electrochemical window. However, much work is still needed to assess their long term stability. The most popular salts (TFSI based) are prohibitively expensive which thereby negates one of the main advantage of water over other alternative solvents.

1.8.6 Miscellaneous

The approaches listed in the preceding sections are currently the most common methods of extending the electrochemical window of water. Further attempts have been made to tackle this problem from unique angles.

Cai *et al.* recently used heavy water (D_2O) as a solvent to obtain a 2.3 V supercapacitor [79]. They used computational studies to show that the activation barrier to water splitting is greatly increased in D_2O compared to H_2O which in turn led to the higher operating voltage of their 1 m Na_2SO_4 supercapacitor. Although there is a cost advantage to not having to use large amounts of salt, using heavy water undoubtedly impacts the scalability of these devices due to cost.

1.8.7 Summary

Water is clearly a desirable base for an electrolyte in both ion batteries and supercapacitors. While many accept water's failings and make devices that are 1 V or lower, there is a large amount of research going in to determining how to extend the electrochemical window of water. Doing so would enable a large increase in energy density compared with existing aqueous systems while also being far cheaper and environmentally friendly than current organic solvents.

1.9 Microemulsions

Microemulsions (MEs) are thermodynamically stable mixtures of two or more immiscible liquids. Generally these are water and an 'oil' which is any liquid immiscible with water. A surfactant and co-surfactant are also usually included in the composition. Because of their amphiphillic nature, the surfactants reduce the surface tension between the polar and non-polar phases to such an extent that it is thermodynamically favourable to mix the two. This is determined by the following equation

$$\Delta G = \gamma \Delta A - T \Delta S \tag{1.6}$$

For spontaneous formation of the microemulsion the ΔG must be negative. The ΔS term is the entropy of mixing, which will always be positive. ΔA, the change in surface area, is always very large given that the dispersed droplets will have a much larger interfacial surface area than when the two phases are separated. The surface tension γ will always be a positive value, therefore, it must be reduced significantly to overcome the effects of the large ΔA term. Doing so allows the TΔS term to dominate and make ΔG negative overall.

One example of a stable ME composition is 84 wt% distilled water, 4 wt% sodium dodecyl sulfate (SDS), 9 wt% n-butanol and 3 wt% cyclohexane. In this example, SDS is acting as the surfactant and *n*-butanol is a co-surfactant. Upon mixing the components in the required ratios, a cloudy solution is observed. Over time however, the solution becomes clear, indicating the formation of a microemulsion.

While MEs are macroscopically homogeneous, they are microscopically heterogeneous. The microstructure of MEs is also very complex and can differ a lot depending on the exact composition. Broadly speaking there are three categories of microemulsion: oil in water (o/w), water in oil (w/o), and bicontinuous. Examples of the microstructure of these types is shown in Figure 1.14

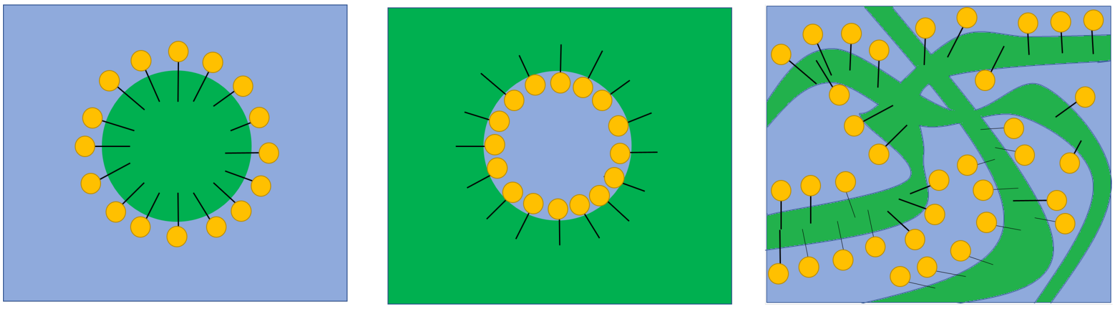

Figure 1.14: Three broad types of microemulsion that can be made. From left to right, oil in water, water in oil, and bicontinuous. Yellow represents the polar head group of the surfactant and the black line is the non-polar tail.

In water in oil systems, the surfactant and co-surfactant (if required) form micelles around water with oil as the bulk phase. This is reversed for oil in water systems. Bicontinuous systems are more complex, no discrete micelles exist, instead, the phases are somewhat evenly interspersed with one another.

Which type of microemulsion is present depends on the components used, their ratios and the temperature. For a given set of components a phase diagram can be constructed which represents the different possible outcomes. In order to simplify systems with more than three components, the ratio of one set of compounds e.g. the surfactant and co-surfactant, is kept constant. This simplifies the diagram to a ternary phase diagram. An example of such a phase diagram is shown in Figure 1.15

Microemulsions are widely used in many fields such as food products, pharmaceuticals, cleaning products, pesticides, cosmetics, catalysis and polymer synthesis. They are also used in the materials chemistry literature as a way of synthesising nanoparticles [80].

1.9.1 Microemulsions as electrolytes

Despite having the propensity to act as an incredibly versatile solvent, microemulsions have not been used widely in electrochemistry. One of the first, researchers to investigate the use of microemulsions as an electrolyte in electrochemical systems was J. F. Rusling in 1987, on an electrocatalytic reduction in what was referred to as “a surfactant stabilised emulsion” [81]. The goal of the research was to investigate the reduction of

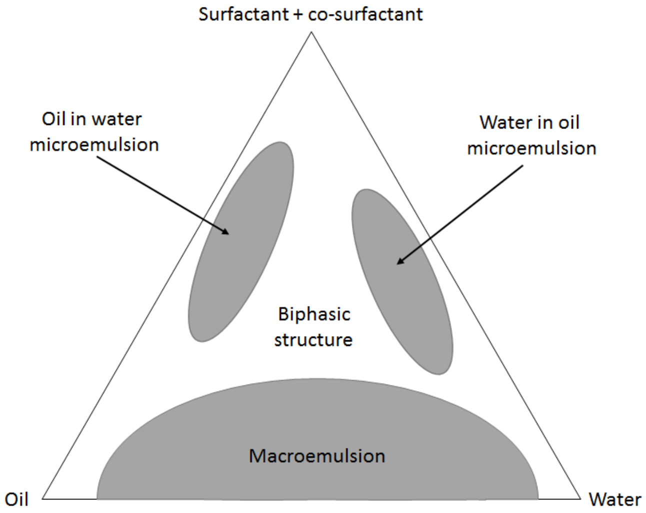

Figure 1.15: An example of a ternary phase diagram for a oil/water/surfactant-cosurfactant mix. In order to simplify the diagram to three phases, the surfactant and co-surfactant ratio is kept constant. Various compositions result in different outcomes in terms of microemulsion structure.

ethylene dibromide, which is an envrionmentally hazardous lead scavenger used in gasoline. The reduction of ethylene dibromide is electrocatalysed by Vitamin B12. However, Vitamin B12 is water soluble whereas the analyte of interest is dispersed in the gasoline. Therefore, an emulsion system was used so that the catalyst and analyte could be mixed effectively.

A follow up article in 1990 demonstrated the use of bicontinuous MEs as an electrolyte [82]. The system used in the 1987 article was a w/o emulsion. The conductivity of the resulting solution was low [81]. By changing to a bicontinuous ME the conductivity increased and allowed for effective study of a variety of analytes such as ferrocyanide and $[Ru(NH_3)_6]^{3+}$ as well as more non polar species such as perylene and ferrocene. It was found that the diffusion coefficients of the species were similar to those observed in neat solutions and the charge transfer kinetics were broadly unaffected.

Most of the research from Rusling to date has focused on electrocatalysis or electrosynthesis [83] [84] [81] [85] [86] [87] [88]. Various models of what the electrode/electrolyte interface looks like have been posited. In one instance, the rate of competing reactions was controlled by a film of adsorbed surfactant molecules [88]. In another it was observed that electron transfer could be as fast as in a homogeneous solution [84].

Another major researcher in this field is M. Kunitake who first investigated the electrochemistry of microemulsions in 2002 [89] where they proved that both the aqueous phase and oil phase could be active electrochemically by probing both ferrocene and ferricyanide in the same solution. The biggest contribution made by this group has been a more in-depth probing of the electrode/electrolyte interface.

In 2016 this group investigated a solution of both ferricyanide and ferrocene in a bi-continuous microemulsion on different electrodes. By changing from hydrophilic indium tin oxide (ITO) to amphiphilic gold and glassy carbon through to hydrophobic highly oriented pyrolytic graphite (HOPG) differing redox activity was observed (Figure 1.16). Both species were observed electrochemically by cyclic voltammetry on the amphiphilic surfaces. However, only the water soluble ferricyanide was observed in the cyclic voltammogram on the hydrophilic ITO and only the oil soluble ferrocene was observed on the hydrophobic HOPG as seen in Figure 1.16.

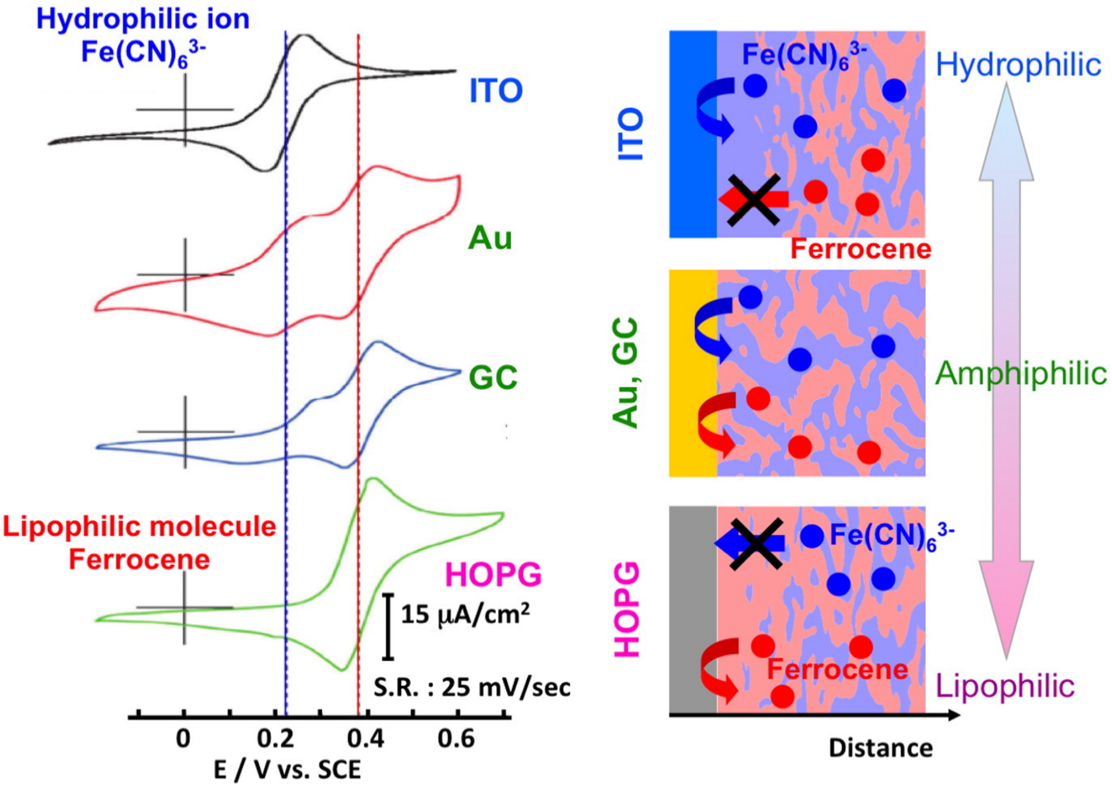

Figure 1.16: Cyclic voltammograms measured in solutions with both ferrocyanide and ferrocene. The ferrocene redox potential is shifted in the microemulsion so both species can be observed separately. On the hydrophillic ITO surface only the peak from ferricyanide is seen in the cyclic voltammogram (black). On the amphiphillic surfaces both species are observed electrochemically shown by two distinct peaks appearing the the cyclic voltammogram. One the lipohillic highly oriented pyrolytic graphite (HOPG) on the peak for the ferrocene is observed in the cyclic voltammogram (green). Reproduced with permission from Elsevier [8]

The most recent investigation on microemulsion electrolytes comes from Peng *et al.*

[90]. They went a step further than Kunitake *et al.* and used neutron scattering to investigate the structure of the interface between the electrode and electrolyte. These studies were not carried out on their working electrode however. Instead, they used a silicon wafer with an oxide surface layer that was modified with a poly(ethylene oxide) containing silane. This gave a similar hydrophobicity to glassy carbon (measured by contact angle). From this study they developed the model shown in Figure 1.17. The surfactant (Tween 20) arranges its hydrophobic tail on the hydrophobic surface in a monolayer. The polar head group then facilitates a water rich layer (D_2O was used in the study to increase neutron diffraction) which then leads to the bulk ME.

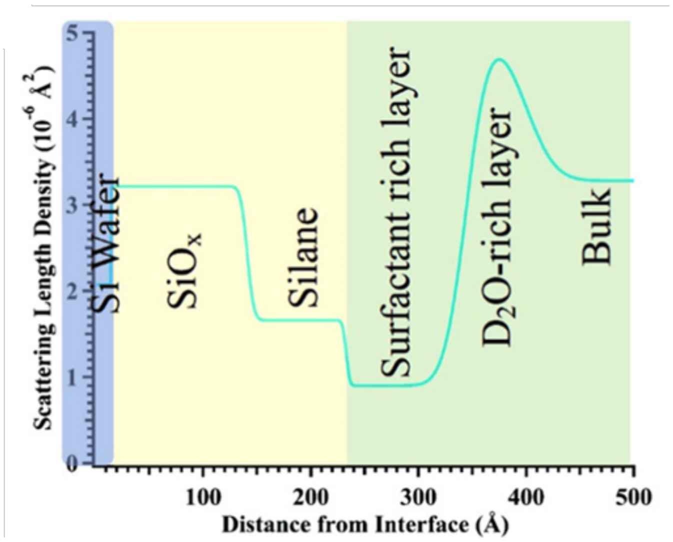

FIGURE 1.17: Neutron scattering study done by Peng *et al.* showing the distinct layers at the electrode/electrolyte interface. Adapted with permission from Peng *et al.* ACS Appl. Mater. Interfaces 2020, 12, 36, 40213–40219. Copyright 2020 American Chemical Society

The interaction of surfactants on electrodes has been well established [91] and has even been used in a Zn/Na battery as a way of extending the electrochemical window of the aqueous solvent [92]. This alone was only able to extend the electrochemical window of water to 2.5 V.

1.10 A new discovery

Before this research began, our research lab was already investigating microemulsions for their ability to dissolve a wide range of organic compounds while remaining conductive. In order to use a redox acitve organic molecules (such as quinones or ferrocene) as the active material in a redox flow battery, one must either use some polar organic solvent with some expensive supporting electrolyte such as tetrabutylammonium hexafluorophosphate (TBAP) or derivatise the molecule so that it is soluble in water where much cheaper supporting electrolytes such as KCl can be used. Both of these options are expensive and time consuming and reduce the performance of the resulting battery.

Microemulsions get around these issues by having the solubility of the oil phase such that un-derivatised organic molecules can be used, but retaining the conductivity of the aqueous phase so cheap suppourting electrolytes can be used. While running cyclic voltammetrey experiments on blank microemulsions an unexpected electrochemical property of the microemulsions was discovered that opened up the possibilities beyond the original intended application.

Microemulsions also have a greatly extended electrochemical window compared to that of water even though water can be the major component by mass. This was sometimes as wide as 5 V (See Figure 1.18). Previously microemulsions had mainly been studied as a medium that overcame solubility issues of analytes, allowing both water soluble and water insoluble species to be analysed at the same time. However, this discovery of the extended electrochemical window creates opportunities for the use of MEs and opens up a wider range of applications based on MEs. In particular, MEs have never been used as electrolytes in energy storage devices before.

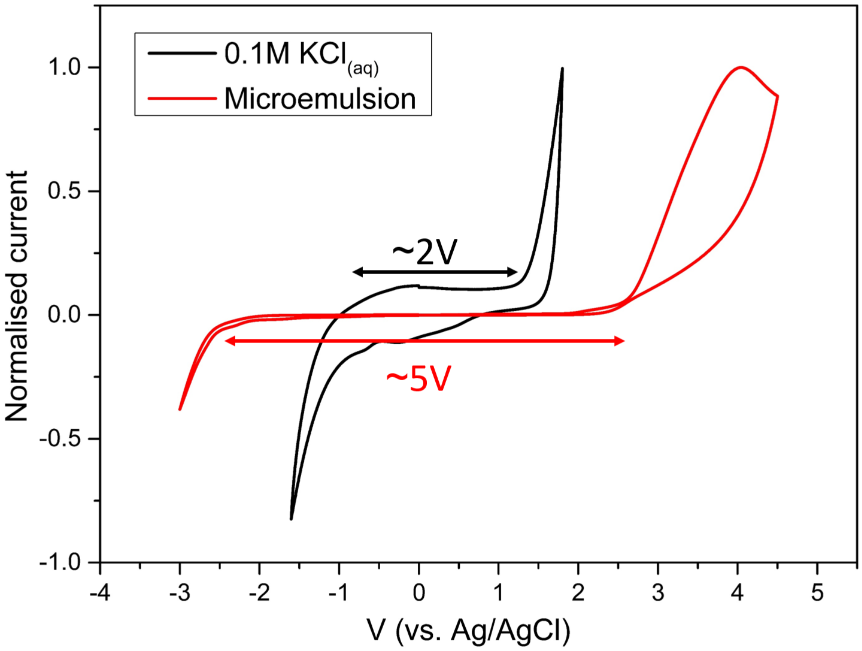

Figure 1.18: Electrochemical window of a microemulsion electrolyte compared to a 0.1 M aqueous KCl electrolyte. The electrochemical window of the microemulsion is much larger than that of the aqueous electrolyte.Both scans were recorded on a glassy carbon electrode surface at a scan rate of 100 mV/s. The microemulsion used was based on sodium dodecyl sulfate and is described in Section 2.5

A provisional patent application was filed based on our findings [93] (see Appendix B), with the main focus being on this extended electrochemical window effect and its application into electrical energy storage devices.

As previously mentioned, the ability to use an electrolyte that has all the best features of water and non-polar organic solvents combined, is potentially of great interest to both academia and industry.

1.11 Research aims

The overall goal of this PhD project is to investigate the use of microemulsions as electrolytes in electrical energy storage devices. More specifically the research aims are:

- Discover a cell format that is compatible with the microemulsion electrolytes. This includes not only the form factor of the cells but also the current collectors.

- Design and use a microemulsion as an electrolyte in a supercapacitor and evaluate its performance compared to the state of the art of other electrolytes. This includes:
    - Selection/design of an appropriate microemulsion for use in supercapacitors
    - Selection of appropriate electrode materials that will be compatible with the microemulsion and give a high voltage and capacitance
    - Electrochemical testing such as cyclic voltammetry and galvanostatic charge/discharge to evaluate the capacitance and power of the system
    - Ageing tests to establish the stability of the system over long periods of time
    - Comparing the results of the above tests to standard acetonitrile based electrolytes.
- Design and use a microemulsion as an electrolyte in a lithium ion and sodium ion battery, potassium, calcium, magnesium, and zinc ion batteries. This includes:
    - Selection/design of an appropriate microemulsion for use in ion batteries as it will most likely differ form that used in supercapacitors.
    - Selection of appropriate electrode materials that will be compatible with the microemulsion and also be electrochemically active for redox reactions.
    - Electrochemical testing to establish the capacities and working voltages of the assembled cells
    - Establishing the mechanism of any working batteries discovered by physical characterisations such as X-ray diffraction and scanning electron microscopy.

Chapter 2

Experimental methods

2.1 Galvanostatic Charge and Discharge

Galvanostatic charge/discharge (GCDC) experiments are used to evaluate the amount of charge stored in a device and also observe electrochemical reactions. The experiment is run by using a galvanostat to set a current that is kept constant at all times. The cell adjusts its potential in order to maintain the specified current. For a charge curve, the potential keeps increasing until the upper cut-off voltage (which is set by the user) is reached. At this point the current reverses direction and the cell begins to discharge. Again the potential of the cell adjusts itself in order to deliver the set amount of current. The potential continues to drop until it reaches a lower cut-off. This is one cycle.

2.1.1 GCDC - Ion Batteries

An example of the plots generated from these experiments is shown in Figure 2.1. In these curves, any plateaus (such as the one at around 1 V in the discharge curves of Figure 2.1) are indicative of a faradaic reaction occurring. The cell is able to maintain this potential as the redox reaction "powers" the current by providing electrons. An ideal case of this is shown in Figure 1.8.

Whilst the ideal case is a completely flat discharge curve, it is very common to have a sloping discharge curve. This is because the potential of the redox reaction occurring is not constant. As mentioned in Section 1.5 the redox reaction of the electrode is almost

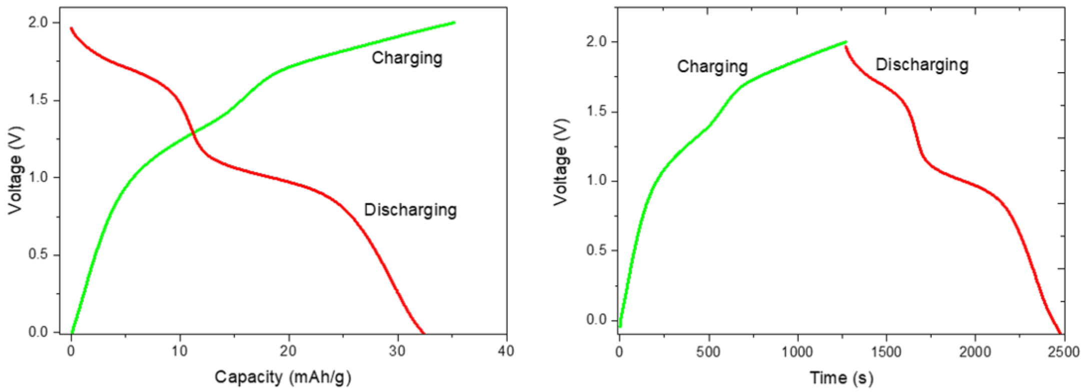

FIGURE 2.1: An example of a sodium ion battery that was charged and discharged at a rate of 50 mA g^{-1} Left: A galvanostatic charge/discharge curve that shows the charge and discharge capacities of the battery. Right:A chronopotentiogram that plots the voltage of the cell against time. Both experiments show voltage plateaus, where redox reactions occur.

always accompanied by intercalation of the active ion. This intercalation can distort the lattice of the solid electrode material and slightly adjust the redox potential of the reaction occurring [94]. However, flatter curves are more desirable for many commercial applications as the voltage output is more stable.

The energy density can be calculated by measuring the area under the discharge curve. Only the discharge curve is used in calculations as it represents the amount of usable or extractible energy in the cell. The nominal voltage of the cell can also be calculated from these curves. This should be taken as the midpoint of the plateaus on the discharge curve [12]. Many groups define the nominal voltage as where the charge and discharge curves intersect, which is reasonable in an ideal system, however this has a tendency to overestimate the voltage, especially in cases where the internal resistance of the cell is high. In cases where multiple redox events occur, such as in Figure 2.1, individual voltages should be reported for each plateau.

2.1.2 GCDC - Supercapacitors

For supercapacitors, GCDC experiments are also performed. However, there are no redox reactions occurring so the voltage profile is (in an ideal case) a straight diagonal line (see Figure 1.6). The energy density of the supercapacitor is given by the area under the voltage-capacity curve.

The capacitance of the supercapacitor can also be calculated from these curves. From Equation 1.1 it is known that the charge stored by the capacitor is equal to the capacitance of the device multiplied by the voltage at which the charge is stored. The amount of charge stored is calculated by multiplying the applied current by the time taken for the device to discharge.

$$\frac{I \times t}{\Delta V} = C \tag{2.1}$$

The ΔV term is the difference between the upper and lower voltage cutoffs. In all cells there is some amount of internal resistance. This can come from a variety of places such as the wire contacts to the cells, the current collectors, and the solution resistance. Some of the voltage of the cell is lost. This means that the ΔV term in this should be the difference between the final and initial potentials after taking into account the voltage losses across the internal resistance. This is commonly referred to at the IR drop. An example of an IR drop is shown in Figure 2.2. In this case, the cell was charged and discharged between 0 and 2.6 V. However there is an IR drop of approximately 80 mV. This means that when using Equation 2.1, a value of 2.52 V should be used for the ΔV term and not 2.6 V. Not doing so would underestimate the capacitance and energy density [1].

2.1.3 Coulombic Efficiency

By taking the ratio of the discharge capacity to the charge capacity the coulombic efficiency is obtained for both batteries and supercapacitors. This figure of merit shows how efficient the device is. A coulombic efficiency of 100% would indicate that all of the charge is stored reversibly. For both supercapacitors and ion batteries this number should be as close to 100% as possible. However, this is unachievable due to inevitable factors such as internal resistance. Commercial devices will have a coulombic efficiency of at least 99.9%. For lab scale supercapacitors a figure close to this is attainable. For ion batteries however, lab scale cells often achieve slightly lower coulombic efficiencies, around 90-95%, as the faradaic reactions that drive them are not perfectly reversible.

---

[1] IR drop is also present in ion batteries. However, it is not as important in lab scale cells. Any voltages used in calculations should be the voltages of the plateaus in the GCDC curve and not maximum voltage as it is in supercapacitors.

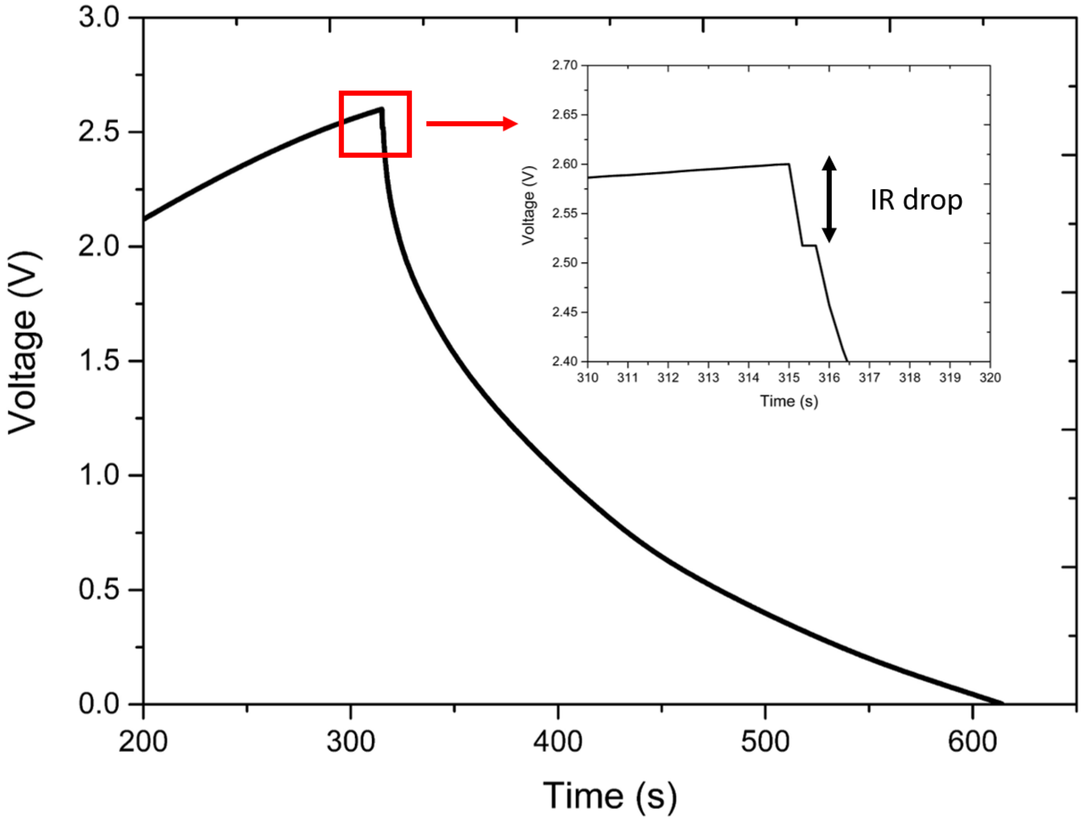

Figure 2.2: An example of a supercapacitor GCDC experiment. Inset is a zoomed in portion at the beginning of the discharge curve. A sharp drop in potential is seen which corresponds to the voltage loss across the internal resistance of the cell. In theory this should be a vertical line, however, the software in this case was only recording the potential of the cell once every second. The software interpolates the potential over this time which leads to the curve appearing sloped, followed by a horizontal line

2.2 Cyclic Voltammetry

Cyclic voltammetry (CV) is a technique that measures how current changes with potential in an electrochemical cell. This can be used to indirectly observe redox events within a battery or lack of redox peaks in a supercapacitor. An example of a cyclic voltammogram is shown in Figure 2.3. As the voltage is swept from the lower vertex to the upper vertex (the postive or anodic scan), electrochemical reactions will occur at certain voltages. These reactions produce a current leading to peaks as is seen at 1.5 V in Figure 2.3. The potential is then swept back from the higher vertex to the lower vertex (the negative or cathodic scan).

CVs can be recorded in either a three electrode or two electrode set up. In a three electrode set up, there is a working electrode, a counter electrode (also sometimes referred to as an auxiliary electrode) and a reference electrode. The electrochemical reactions

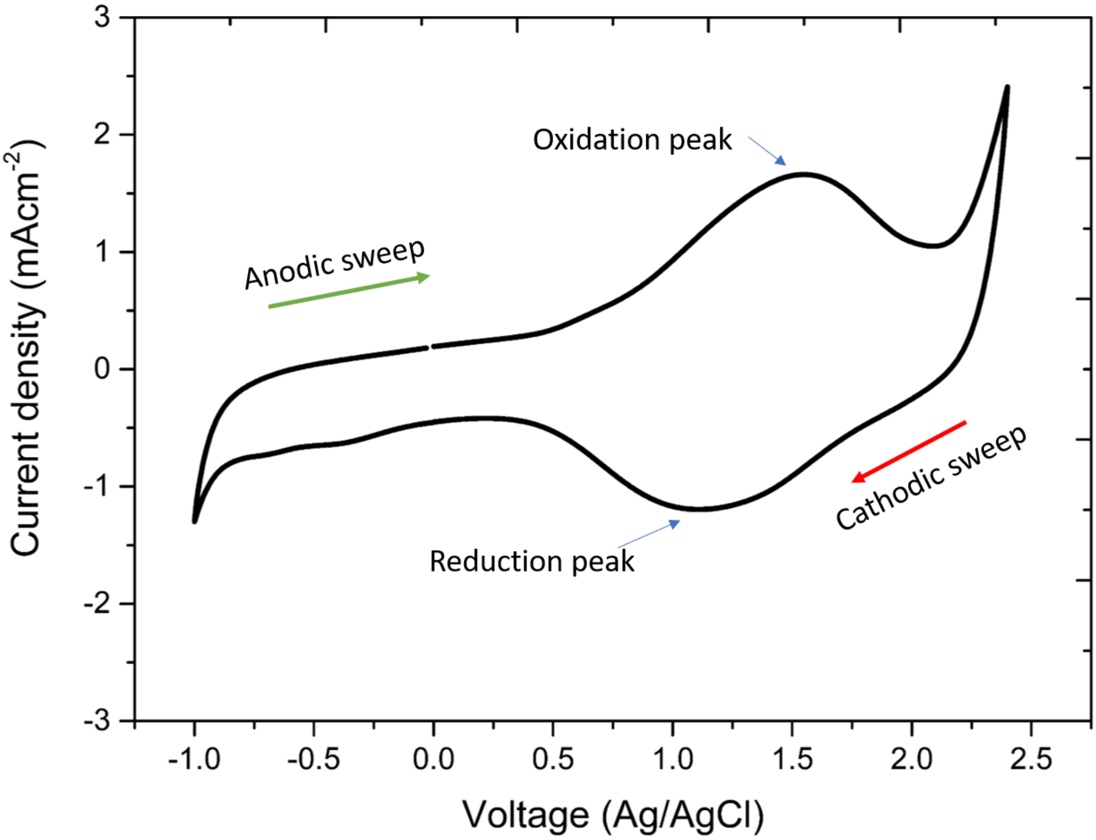

FIGURE 2.3: An example of a cyclic voltammogram of a Prussian blue electrode in a ME electrolyte. The scan rate was 100 mV s^{-1} and the reference electrode was Ag/AgCl in saturated KCl.

that happen are analysed at the working electrode. The current is measured between the working and counter electrodes. The potential of the working electrode is measured or set relative to the reference electrode. In Figure 2.3, the reference electrode used was a silver/silver chloride reference electrode in saturated KCl. The potential of this electrode is kept constant as no current flows through it. Any redox reaction that occurs is referenced relative to the reference electrode e.g. the oxidation peak in Figure 2.3 occurs at +1.5 V vs. Ag/AgCl.

In a two electrode cell, the reference and counter electrode are the same. When testing a battery or supercapacitor, the anode is used as the counter and reference electrode simultaneously and the cathode is used as the working electrode. This means that the 0 V point is where the difference in potential of the anode and cathode is 0. A positive voltage implies that the cathode is at a positive potential relative to the anode (hence why the electrodes are connected in this way). Any negative voltages essentially swap which electrode is acting as the anode and cathode and so going below 0 V in a two electrode set up, especially for batteries, has little merit unless there is a reaction at potentials close to 0.

In a three electrode set up, it is common to use platinum as the counter electrode as it has a high exchange current density and is catalytic for many reactions therefore it is able to keep up with any reactions that happen at the working electrode. The potential of the counter electrode is not checked, it floats constantly to satisfy the reactions that happen at the working electrode. If an oxidation happens at the working electrode then a reduction must happen at the counter electrode. Which reduction reaction specifically occurs is not important and the counter electrode changes its potential to drive a reaction.

In a two electrode setup, it is still true that if an oxidation occurs at the working electrode a reduction reaction must occur at the counter electrode. In a battery, both of these reactions are important. A single oxidation peak means that there must be an oxidation occurring at the cathode (the working electrode) and a reduction reaction at the anode (counter electrode). It is impossible to decouple these reactions in a two electrode cell but the peaks are still significant. A peak implies that a reaction is able to happen at *both* electrodes. The midpoint of the oxidation and reduction peak gives the formal potential of a given electrochemical reaction. These can be translated into where plateaus would be expected in GCDC experiments.

The rate at which the potential is swept, known as the scan rate and given the symbol ν, is also important in CV experiments. Faster scan rates lead to higher currents for both faradaic and coulombic reactions. However, faster scan rates (e.g. 1 V s^{-1} can tend to smear faradaic peaks making them broader and less well defined. If two reactions have a similar potential then they may appear as one broad peak at higher scan rates. Also if a reaction is particularly slow, such as one that relies on solid state diffusion then the reaction may not be seen at a higher scan rate. Going to slower scan rates (e.g. 1 mV s^{-1}) can resolve these processes but does result in lower currents. Changing the scane rate is also important to establish the reversibility of a redox process. If the potential of a peak in a CV is invariant with scan rate then this process is more reversible. If the peak ‘drifts’ with increasing scan rate then this is a less reversible reaction.

CVs are also important for determining the electrochemical window of the cell i.e. the maximum voltage it can be charged to. In Figure 2.3 the upper limit for this cell appears to be at +2.3V and the lower limit appears to be -0.8V, this gives an overall electrochemical window of 3.1V. This does not mean that the cell will be able to be charged to 3.1 V however. If the equilibrium point (point where the cell is at 0 V) of the full cell is at 0.5 V vs Ag/AgCl for example, the cell would only be able to achieve a voltage of 1.8 V as at this point it would hit the upper stability limit of the electrolyte.

2.3 Electrochemical impedance spectroscopy (EIS)

While CV and GCDC are direct current (DC) techniques, EIS uses alternating current (AC) at different frequencies to uncover information about the processes inside a cell. As the frequency of the AC signal changes the impedance of the connected device is measured. The data can be presented in a Bode plot, which plots the log of the absolute impedance versus the log of the frequency used. For electrochemical devices, it is more common to use a Nyquist plot which plots the imaginary and real components of the impedance versus each other. An example of a Nyquist plot is shown in Figure 2.4

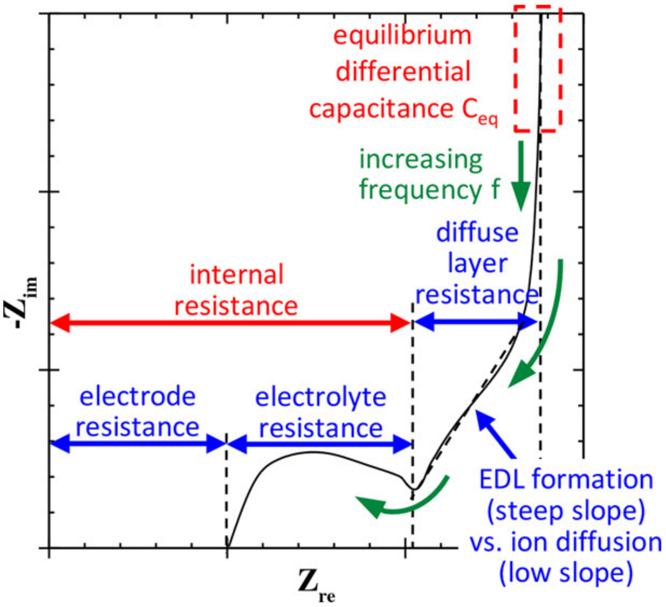

FIGURE 2.4: An example of a Nyquist plot showing the various metrics that can be extracted from a scan of an electrical double layer capacitor. Reprinted with permission from Physical Interpretations of Nyquist Plots for EDLC Electrodes and Devices by Mei *et al.*, [9]. Copyright 2017 American Chemical Society.

In order to extract information out of a Nyquist plot, an equivalent circuit must be constructed. An example of such a circuit is the Randles circuit shown in Figure 2.5. The Randles circuit is the most simple model that can be applied to an EIS experiment.

Data obtained from an EIS spectrum can be fitted to the model circuit to extract values for the various components. The most common method of fitting is a non-linear least-squares regression analysis which is common to most EIS software.

Care must be taken when assembling a model circuit. Adding more components can lead to a better fit of the data, however each component should be a physical representation of a process inside the cell. If a poor equivalent circuit is selected then there is a risk of reaching incorrect conclusions about the system even if the model fits the experimental data well.

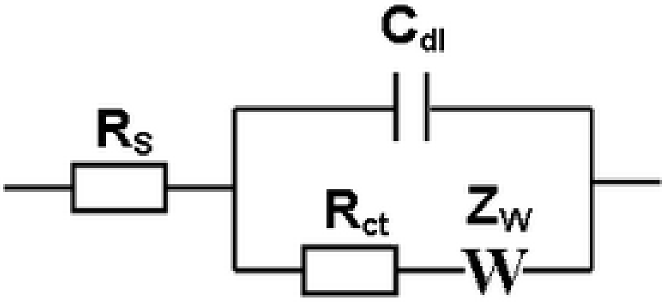

FIGURE 2.5: The Randles circuit which is used to fit EIS data. R_s is the solution resistance, R_{CT} is the charge transfer resistance, C_{DL} is the double layer capacitance and Z_W is the Warburg impedance, which may or may not be included in the model

Figure 2.4 was the result of a first principles modelling approach by Mei *et al.* [9] where they were able to fit a Nyquist plot of an electrical double layer capacitor. By removing the need to fit an equivalent circuit for this type of device, some unequivocal physical interpretations could be made. This allowed for parameters like the internal resistance of the cell to be determined for such a device. However, extending this to more complex systems where electron transfer is occurring for example, has not been done.

2.4 Electrode preparation

A battery electrode is made by pasting a slurry of the active material, a binder and a conductive agent on a current collector. Usually the current collector is a metal foil but for this work the material used was carbon foil (0.127 mm thickness, purchased from Ceramaterials).

The active material performs the desired function, whether adsorbing the charges on the surface for a supercapacitor e.g. activated carbon or performing redox reactions for a battery e.g. cobalt oxide or graphite. The binder is used to bind the material to the current collector. Polytetrafluoroethylene (PTFE) or polyvinyl difluroide (PVDF) are the most common materials used for this purpose. The binder has the side effect of decreasing the conductivity of the mixture. A conductive agent is added to counteract the loss of conductivity introduced by the binder. Common examples of conductive agents used are: Super-P, acetylene black, or Ketjen Black.

To form the slurry, all the components are mixed together with the active material (85 wt% of the dry mass), 9 wt% binder (PVDF, MTI Corporation) and 6 wt% Super-P conductive carbon (99+% metals basis, Alfa Aesar). Once these powders are mixed, they are stirred magnetically. N-methyl pyrollidone (NMP) (Sigma, 99.9%) is added as a solvent. NMP is used as an industry standard as its use is known to result in smooth and homogeneous slurries. NMP was added until the desired consistency was achieved. Ideally, the slurry should be thick and smooth but still able to be spread on the current collector. Usually slurries were left under stirring for 24 hours to ensure they were well mixed.

The slurries are 'doctor-bladed' onto the current collector at the desired thickness. For most materials, the mass loading was 11 mg cm^{-2}. After the current collectors were coated, they were placed in a vacuum oven (DZF-6020) and dried at 120 °C for 12 hours to remove the solvent and form the film. If the film was too thick, it had a tendency to flake off.

2.5 Electrolyte preparation

Microemulsions can be prepared from a ternary phase diagram as seen in Figure 1.15. If a phase diagram exists for a given system, it can be used to find a composition of interest. This is shown in Figure 2.6. After a point is chosen, three lines are drawn from the chosen point to each of the edges. These lines are drawn parallel to the side opposite the 100% point for that particular component. For example, a solution in the bottom right corner (marked C) would be 100% component C.

Figure 2.6 shows an example of this calculation. With the point in green selected, to figure out how much of component C is in the composiiton, a line is drawn parallel to the side marked 'mol% A' until it intersects the side marked 'mol % C'. This results in the red line shown. Where the drawn line intersects the edge gives the mol% of C in the desired composition, in this case, approximately 28%. This is repeated for the other components until all three are known.

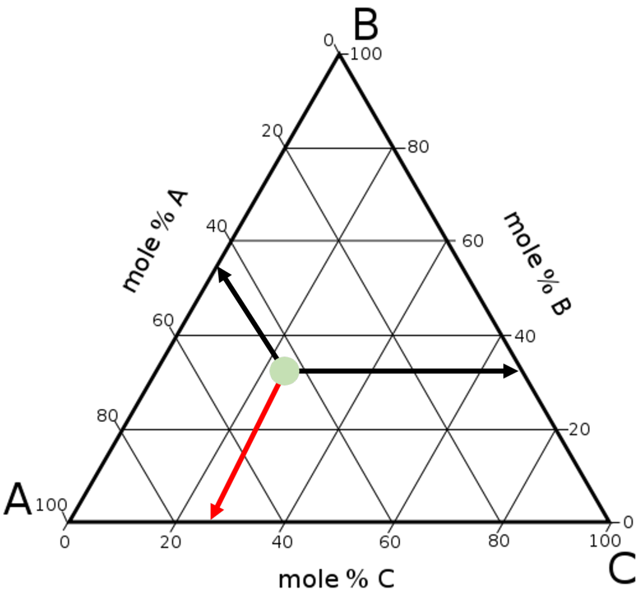

FIGURE 2.6: An example of a ternary phase diagram being used to find the composition of a point of interest (in green).

This method works well if there is a well established phase diagram for a particular system. If a phase diagram is not already known for a system, but a similar one is known, it can be used as a starting point. For example, an SDS-butanol-toluene-water ME system was well known within the lab group. Since toluene and cyclohexane are similar in their hydrophobicity, a 1:1 swap was attempted where toluene was replaced with an equal mass of cyclohexane. This ME stabilised immediately indicating the phase diagram is suitably similar for the two systems. If no similar systems can be found, or additions are being made to a known system (i.e. salts) then it is best to use a titration method. In this method, an initial composition is chosen, then more of one component is added until a stable mixture is achieved. A stable ME is noticed by the solution becoming clear.

Many small scale samples (approx. 10 ml) can be prepared in parallel. Different amounts of the extra component can then be added to separate samples to speed this process up. The stabilisation process is often not fast and so to avoid false negatives, it is often pertinent to leave samples overnight. If possible, samples should be placed in an ultrasonic bath as this can speed up the stabilisation process.

The two main microemulsion ‘bases’ used in this research were;

- 84 wt% distilled water, 4 wt% sodium dodecyl sulfate (SDS) (99.9% TCI), 9 wt% n-butanol (>99.5% Aldrich) and 3 wt% cyclohexane (99.9%, Fisher scientific)
- 72 wt% distilled water, 1.33 wt% cyclohexane (99.9%, Fisher scientific) and 26.7 wt% Triton X-100 (Sigma).

The SDS based emulsion was taken directly from literature[95] whereas a phase diagram was constructed for the Triton system (Figure 2.7) with the one above being chosen.

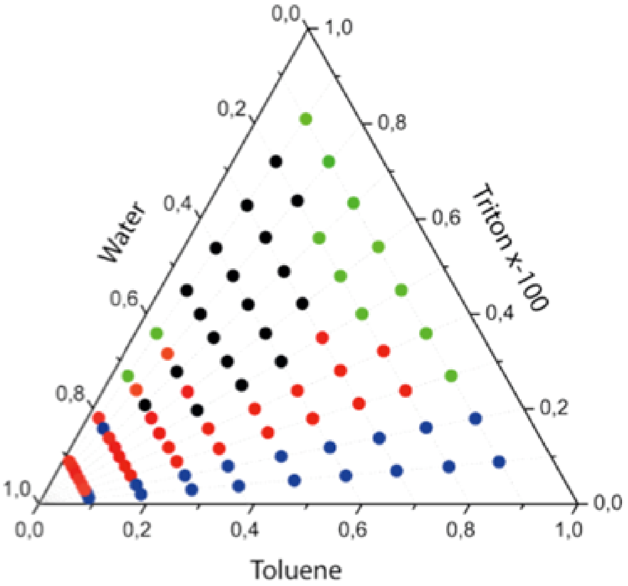

FIGURE 2.7: A ternary phase diagram that was constructed based on trials of various ratios of Triton X-100, water and toluene, as stated previously since toluene and cyclohexane have similar hydrophobicites it is possible to swap out one for the other in a phase diagram without altering the results drastically. Red dots indicate the formation of a turbid single phase, blue dots represent compositions that phase separated, black dots represent compositions that formed gels and green dots are compositions that formed a clear single phase.

A Triton X-100 based composition with higher oil content was also tested (65.45 wt% water, 24.18 wt% Triton X-100 and 10.3 wt% cyclohexane). According to tests detailed in Chapter 5 the behaviour of the two compositions was identical and so the lower oil content ME was favoured to reduce the environmental impact of the research.

Once a stable composition was discovered, samples were usually prepared on a 100 g scale. Additions of the required salts for the ion batteries were made at this point, LiCl (TCI), NaCl (Fisher scientific), KCl (Fisher scientific), $CaCl_2$ (Sigma Aldrich),

$MgCl_2$ (Sigma aldrich), were all weighed out separately and added to the stablised ME as required to bring it to the desired molality. The salts were added after the ME had already stabilised as the MEs generally re-stabilised much more quickly after addition of salt if they had already formed.

By definition, MEs are thermodynamically stable and so theoretically should never separate. Samples of the SDS base that are over two years old and samples of the Triton emulsion that are over one year old were still stable, with no visible signs of cloudiness or separation.

Many other ME compositions are known within the group and could be used in the continuation of this research, refer to Appendix A for details.

2.6 Cell assembly

For details on the choice of materials for the cells and the reasons behind the chosen form factor refer to Chapter 3. To assemble both the supercapacitors and ion batteries, the first electrode was placed inside the cell and glass microfiber (Grade GF/D, Whatman) placed on top to act as a separator. Approximately 70 μL of the electrolyte were used to wet the separator. The final electrode was placed on top with the active material facing into the cell. The current collectors were pressed together to ensure good contact between the components. The cell caps were screwed on to hand tightness. All cell assembly for the ME containing cells was done on a bench top under ambient conditions.

2.7 Electrochemical Analysis

Cyclic voltammetry (CV) experiments on full cells were run using a potentiostat (eDAQ EA 160, ecorder-401). CV experiments on full supercapacitor and ion battery cells were carried out using the anode as the reference and counter electrodes and the cathode as the working electrode. No degassing was performed prior to electrolytes being loaded into the cells.

Degassing can be achieved in multiple ways, with freeze-pump-thaw, sonication and bubbling nitrogen or argon gas through the solution being the most popular methods.

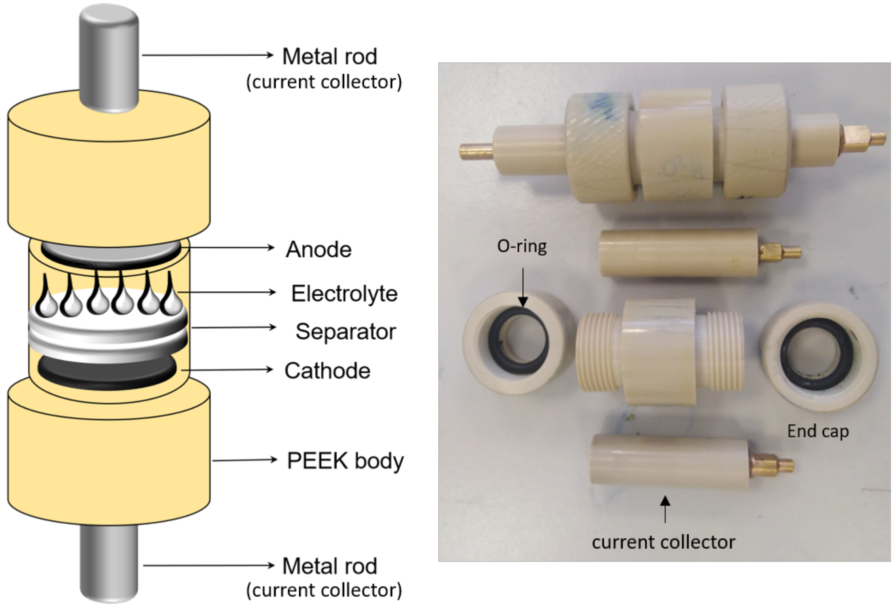

Figure 2.8: Left: A schematic of the cell Swagelok cell form factor with all parts labelled. Right - Top a fully assembled cell, Bottom a cell that has been disassembled with parts labelled.

Most liquids will have varying degrees of dissolved oxygen in them. This dissolved oxygen can interfere with with electrochemcial measurements due to the high reactivity of oxygen. For most electrochemical measurements, aqueous or non-aqueous, it is common to perform some sort of degassing step to remove any unwanted impurities leading to side reactions.

This is a problem for microemulsions however, especially the ones used in this study. Both Triton X-100 and SDS are detergents. SDS in particular is used in many cleaning products (often under the name sodium lauryl sulfate). Both of these have a tendency to form bubbles in solution when gas is blown through them. As such this is an ineffective method for degassing and can lead to large loss of sample which may alter the composition of the ME. Sonication and freeze-pump-thaw are more viable, however the problem with MEs is that they are multiple component systems. The different components of the ME will have different volatilities and so will evaporate at different rates. The ME could also break at lower temperatures as the thermodynamics change to disfavour the formation of the ME as per Equation 1.6. Determining the rate at which this evaporation occurs and if any change in compositing occurs over a period of time is difficult. Both other methods were also avoided as it was deemed that keeping the system sealed to retain the composition was more important than any oxygen artefacts in the electrochemical measurements.

One other alternative involves degassing the individual components separately. However, measuring the components out and mixing them together afterwards will cause a certain amount of agitation which could reoxygenate them. Assembly inside a glovebox is also not an option considering the major component of the ME is water. In future, more detailed analysis on the degassing and its effect on the cells will be undertaken as it likely does have some effect on the long term cell performance.

Galvanostatic charge discharge experiments were performed using a battery analyser system (NEWARE BTS CT-4008-5V10mA-164, MTI Corp.). EIS experiments were done on a Palmsens 3 potentiostat using the PSTrace software.

2.8 Battery analyser protocols

After a cell has been assembled for GCDC experiments it must be connected to the battery analyser. This is shown in Figure 2.9. The anode is connected to the negative wire (black in image) and the cathode is connected to the positive wire (red in image). Then a testing protocol is entered into the analyser, which can perform a variety of experiments with varying levels of complexity. In the most simple cases, a current rate, upper and lower voltage cutoff and number of cycles is set. The following sections will detail how each of these parameters is chosen.

2.8.1 Current rate

To compare batteries and supercapacitors to those in the literature, it is important to use similar testing regimes. For example, slower charging rates generally produce higher capacities which lead to more ‘publishable’ results. However, slow charging and discharging is not really reflective of a real world scenario. For example, supercapacitors are attractive because they are capable of being charged and discharged quickly. Therefore reporting performance at low charging rates will misrepresent the technology.

2.8.1.1 Ion batteries

For established battery technologies the ‘C’ terminology is used. A cell being discharged at 1 C will be discharged in one hour. At 2 C, the cell would be discharged in 30

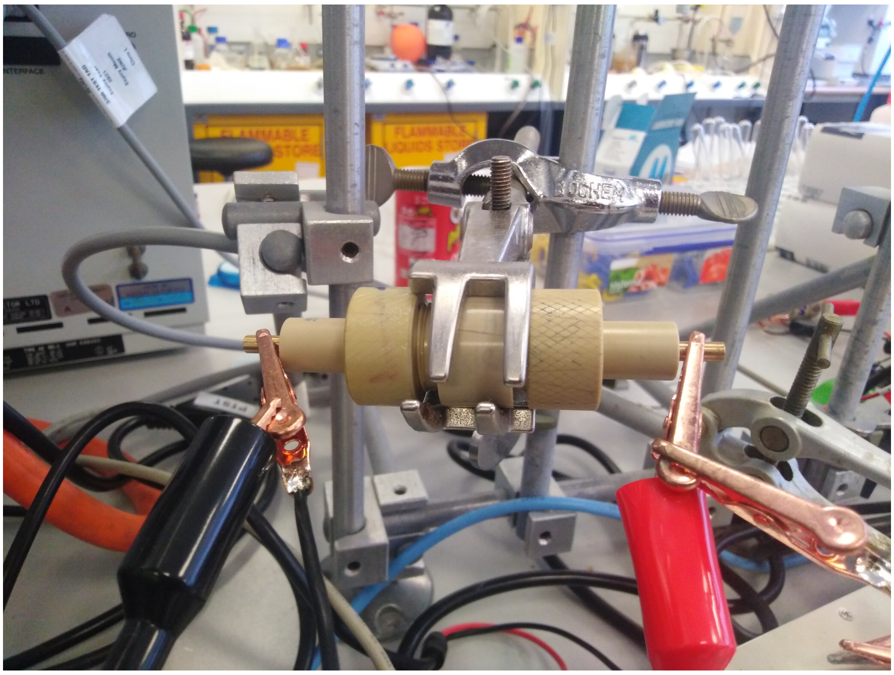

FIGURE 2.9: A cell connected to the battery analyser with the black clip connected to the anode and the red clip connected to the cathode.

minutes, at C/2 it would take 2 hours to charge or discharge the cell. This only works if the capacity of the cell is known and well characterised such as modern lithium ion batteries or lead acid batteries. For new chemistries, the two most common current rates for new systems are 50 and 100 mA g^{-1}. These strike a balance between being realistic but also showing relatively high capacities. Charging much slower than this causes the current demand to be very low at all times e.g. a cell with 1 mg of active material being charged at 1 mA g^{-1} would require 1 microamp of current. This is not an undetectable amount of current by any means, but it can introduce artefacts into the curves such as those shown in Figure 2.10.

The current rate can also be increased to investigate the power density of the battery. A battery that retains its capacity at high current rates is deemed to have good rate capability even at a figure such as 10 C [96]. This is particularly relevant for applications where fast charging is desireable such as electric vehicles.

2.8.1.2 Supercapacitors

For supercapacitors, it is suggested that a current rate of at least 500 mA g^{-1} be used [25] as this is sufficient to not artificially over-inflate the capacitance values calculated but low

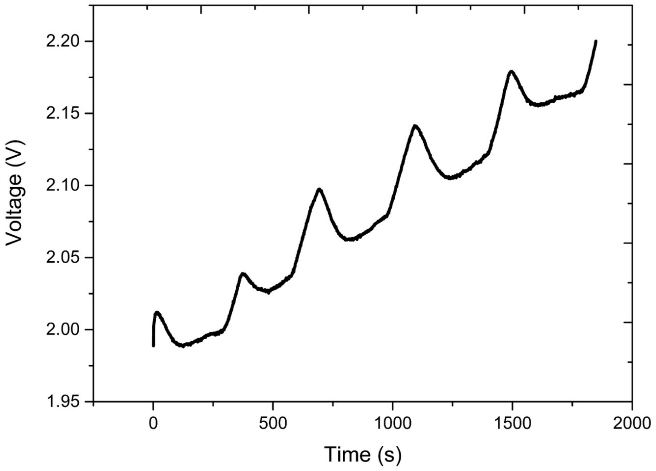

FIGURE 2.10: An example of a sodium ion battery that was charged at a rate of 1 mA g^{-1}. The cell was charging: however, due to the low current rate small and regular fluctuations in the voltage are observed.

enough that any supercapacitor should be able to behave in an expected manner. The upper limit of the current rates that can be used for supercapacitors varies depending on the chemistry and materials. 2 A g^{-1} is commonly seen, though highly optimised devices such as those involving graphene can reach 10 A g^{-1} or higher [97].

Supercapacitors also have a more well defined way to calculate the maximum power density. The internal resistance of the cell, also known as the equivalent series resistance (or ESR) is calculated by the following formula.

$$R = \frac{V_{IR-drop}}{i} \tag{2.2}$$

Where the IR drop is determined as shown in Figure 2.2. This can then be used to calculate the maximum power that can be extracted from the supercapacitor.

$$P_{max} = \frac{V^2}{4R} \tag{2.3}$$

V is the voltage of the cell after taking into account the IR drop. R is the ESR as calculated in Equation 2.2. While this represents a theoretical maximum it is still pertinent to cycle supercapacitors at high current rates in order to establish their true rate capability, which may be a lot less than the number calculated.

2.8.2 Voltage cut offs

As explained in Section 2.1, an upper and lower voltage cutoff must be established for cycling tests. This can be done by taking a CV to establish the upper and lower limits of the stability of the cell which then can be set as the cut-off. For lab cells, the lower limit is generally taken as 0 V (or -0.01 V due to the programming of the battery analyser) unless there are other unwanted side reactions at low potential. Cut-offs can also be adjusted sequentially to determine the upper stability limit of the cell.

2.8.3 Cycle life

The cycle life of both supercapacitors and ion batteries is established in literature by cycling between the upper and lower cut-offs continuously. Commercial cells require much more rigorous tests to determine life times such as accelerated ageing or float tests. A general benchmark for when a cell is considered to have reached end of life is when the capacity or capacitance reaches 80% of the original value. This metric is not appropriate for lab scale cells as it may still be of interest to see how the capacity or voltage profile of a cell changes until the cell shorts or reaches very low capacities.

2.9 X-ray diffraction

X-ray diffraction (XRD) studies are commonplace in battery research as it is important to understand how the electrode materials change structurally as this gives insights into the mechanism which in turn can help optimisation of the materials. XRD studies are not usually done on supercapacitor electrodes as no structural change occurs during operation.

The pinnacle of this technique for battery research is *operando, in situ* XRD which takes scans as the battery is being charged or discharged (in operation) and shows how the materials are changing. This technique is still highly specialised and not widely available.

As a substitute, *ex situ* XRD studies can reveal changes but getting samples at various states of charge is difficult. *Ex situ* XRD is also difficult for non-aqueous systems as these are often air and moisture sensitive so disassembling the cell to investigate its electrodes can cause degradation of the sample. Thankfully, aqueous systems do not suffer from this issue and samples will be more stable in the air once the cell has been taken apart.

XRD studies in this research were done on electrodes that were pristine (i.e. not having been in a battery yet), in a charged, and discharged state. Both charged and discharged samples were collected from cells that had run for 100 cycles. Discharged cells were discharged to 0 V before disconnecting the cell and taking it apart. Charged cells were charged to 2.4 V before disconnection and disassembly. Both charged and discharged electrodes were washed with water to remove any electrolyte as some of the salt may have crystalised out which would show up on the XRD scans. This also removed any of the glass microfiber separator that may have been left behind on the electrodes. This was important to remove as it would show up as a broad amorphous peak in the XRD which may obscure important reflections. Once cleaned and dried, samples were stuck onto a glass slide, active material facing upwards, using double sided tape.

XRD measurements were done on prepared electrodes using done using PANalytical X'Pert operated at 40 kV and 40 mA using Cu Kα radiation, from 10-80° 2θ over a period of 10 hours.

2.10 Scanning electron microscopy

Scanning electron microscopy (SEM) can be used to study the surface of electrodes. This is another *ex situ* technique that might not be well suited to non-aqueous systems. While XRD experiments reveal much more information about large scale structural changes in the electrode itself, SEM images can show changes in the surface of the electrode which may be important for establishing the formation of an SEI layer.

As all electrodes were conductive, they did not need to be coated before being imaged. Samples were imaged on a JEOL 6500F FE-SEM. Samples were mounted on aluminium stubs using carbon tape.

Chapter 3

Current Collector Development

3.1 Introduction

Realising the potential of using microemulsions in electrochemical applications, the attention turned focus of this project is in fully assembled supercapacitors and ion batteries. Before this could be achieved, changes to the traditional lab cell design were needed. In particular the current collectors, which the anode and cathode sit on and also provide the points of connection from the cell to the potentiostat and or battery analyser (see Figure 2.8), needed to be redesigned from the ground up. This chapter will detail the model that has been hypothesised by our lab as to why MEs show extended electrochemical windows and how that informed the development of appropriate current collectors for use in full cells.

3.2 Model for the extended electrochemical window

Following the first observation of the extended electrochemical window by our group, a hypothesis needed to be developed to explain this phenomenon. Several hypothesis already existed in literature such as the one presented by Kunitake *et al.* as shown in Figure 1.16. Based on various pieces of evidence, this model was modified to better fit those observations.

Firstly, the water splitting reactions happen at the electrode surface and the potetnial they are observed at is also in part determined by said surface. Given the results shown in Figure 1.18 which use the same electrode surface just a different electrolyte, the microemulsion must be altering the surface of the electrode such that the potentials of these reactions are shifted. While the exact products of these reactions occurring at the potential limits are unknown, gas evolution at the working electrode is observed at these potentials.

If it is to be assumed that these reactions at the edge of the window are water splitting, then these shift in potential can be investigated using the Nernst equation, Equation 3.1. Where R is the gas constant, T is the temperature, z is the number of electrons transferred in the reaction, F is Faraday's constant and Q is the reaction quotient.

$$E = E^0 - \frac{RT}{zF} lnQ \tag{3.1}$$

Such a large shift in the observed potential window (3 V) would imply a very large value for the reaction quotient. This in turn implies the activity of water at the electrode surface is reduced dramatically to be close to zero. If the reactions observed at the stability limits are not the result of water splitting, then the argument remains the same, the activity of water at the electrode surface must be so low that other components of the electrolyte are breaking down before the water is.

In practical terms, this implies that little to no water is reaching the electrode surface. This in turn implies that one or more components of the ME must be forming some form of blocking layer that is preventing water from reaching the electrode. When an electrode is placed into solution something in the solvent must be sitting on the surface of the electrode. In an aqueous solution only water can fill this role. However, in the ME, there are several options as to what could sit on the surface and depending on the nature of the electrode one of the components may be preferred over the other. Glassy carbon is a hydrophobic surface and so it would be reasonable to assume that the hydrophobic components of the ME (both the hydrophobic part of the surfactant and the oil) would preferentially adhere to that surface in solution.

How these surfactant molecules would arrange themselves on the surface is unclear. A reasonable first approximation would be that the surfactant molecules arrange themselves in a monolayer on the surface. A schematic representation of the proposed electrode electrolyte interphase (EEI) is shown in Figure 3.1.

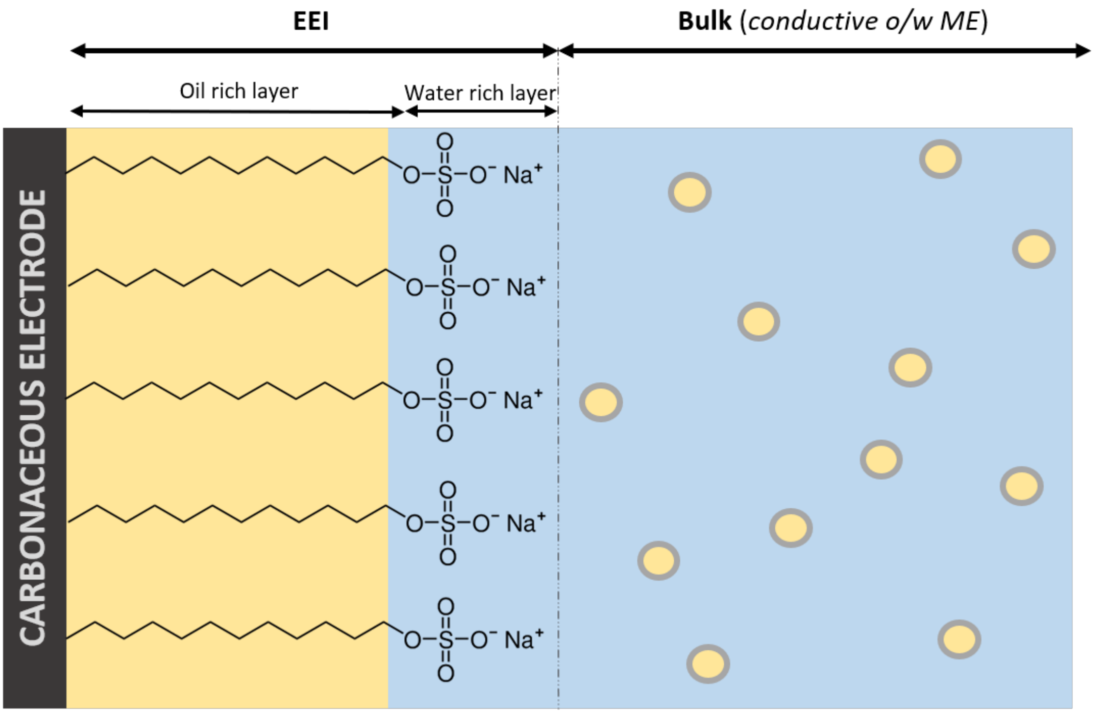

Figure 3.1: The EEI model we propose. The hydrophobic surfactant tail adheres to the hydrophobic electrode. The oil dominates in this layer, then there is a water rich layer around the polar head group before reaching the bulk solution. Here the bulk is shown as being an o/w ME but in theory any type of ME could be present.

The oil phase is still present in this monolayer whereas water is confined to a water rich layer near the polar head group. Then the bulk solution which contains oil droplets exists further out. It is assumed that the co-surfactant is interspersed throughout the EEI, either existing with the polar head-group in the water rich layer or existing fully in the oil rich layer or some combination thereof.

This model would explain why the extended electrochemical window is observed. Much like the artificial SEIs discussed in Section 1.8.1, by preventing water from reaching the electrode the water cannot be oxidised or reduced and so water splitting is not observed.

Figure 3.1 is simply one moment in time, how dynamic this EEI is, is uncertain. Often, monolayers are made such that there is a covalent bond between the surface and the molecule e.g. dodecanethiol on a gold surface. This system lacks that covalent bond, relying solely on hydrophobic interactions (e.g. dispersion forces) to maintain contact. Thus it is likely that this EEI is much more dynamic that classic monolayers in literature. This may be advantageous as it my result in a self-healing property but could also be a downside as it may not be as resistant to changes in chemical or electrical environment.

Of course, it is possible that the surfactant molecules are not arranged in a monolayer and the true structure is almsot certianly much more complex. Fundamental investigations into the EEI are still ongoing, using techniques such as EIS and atomic force microscopy as well as modelling, it is hoped a better understanding can be obtained. The focus of this work was to improve the IP around of this discovery in terms of constructing devices to show application. The iteration of the EEI hypothesis presented here was sufficient to inform the experiments conducted however it is acknowledged that this is likely an incomplete model. One piece of evidence in literature does exist that supports this hypothesis was done byt Peng et al. [90] with their neutron diffraction studies (Figure 1.17).

This extended electrochemical window, is the key argument for using microemulsions in energy storage devices. The biggest insight that this EEI model gives into how the ME works is that it all hinges on a suitably hydrophobic electrode surface such that the EEI can form. This is not an issue in standard three electrode electrochemical cells as there are plenty of electrode materials available to use, glassy carbon being the most common. However, when it comes to making a proper full device in a lab scale form factor such as a Swagelok-type cell or a coin cell, the challenge becomes apparent. The current collectors used in both of these cell types are exclusively metallic. Since metallic surfaces are generally more hydrophilic than hydrophobic, the EEI will not be able to form and the electrochemical window will not be extended.

Therefore, this was the first major hurdle to overcome during this research. How to build a device in an acceptable form factor with the constraint of not having any exposed metal inside the cell.

3.3 Swagelok-type cells and Coin cells

On a lab scale the two most common form factors for testing full cells are Swagelok-type cells or coin cells (sometimes known as button cells). Both of these form factors are suitable for ion batteries and supercapacitors and so neither can be discounted on this alone.

Coin cells are made by layering one electrode and the separator then adding the electrolyte and topping with the other electrode. This is then pressed and crimped together into a sealed cell. They are useful because they are compact, well sealed (so that they can be taken out of a glove-box for testing for example), and quick to produce. However they have limitations in that the casings which act as the current collectors, are only commercially available in a small number of materials, primarily steel. This makes this format inappropriate for the ME chemistry as the EEI would not be able to form.

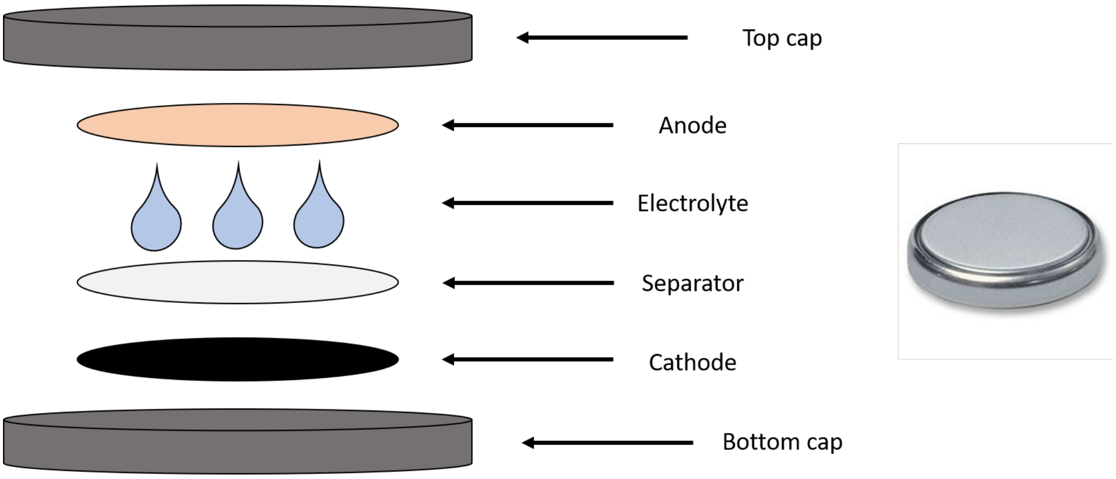

Figure 3.2: A schematic of a coin cell showing all of the components, and a fully assembled and crimped cell.

Therefore a Swagelok-type cell was the most appropriate form factor to develop. Swagelok-type cells comprise a tubular casing as seen in Figure 2.8 and 3.3. As with coin cells, electrodes, separators and electrolyte are layered inside. Then, this stack is compressed by two plungers which act as current collectors. These current collectors can be clipped to an electrochemical workstation to perform tests as seen in Figure 2.9. These are a lot bulkier than coin cells, however they can be made out of a wide variety of materials some of which are well suited to the ME chemistry.

While the casing is easily constructed out of some inert plastic such as polyether ether ketone (PEEK), the current collectors that sandwich the cell together present an issue. Traditionally these are made out of a metal such as steel as it is easy to shape and cheap. As already established, the ME chemistry does not work on these metallic current collectors. This is shown in the chronopotentiogram in Figure 3.4. This cell has no active electrode material and an ME electrolyte containing SDS, cyclohexane, n-butanol, water and 1 mol kg^{-1} (m) NaCl. This cell is barely able to reach 1 V and shows evidence of irreversible side reaction due to the roughness and irregularity of the charging curve. Because the cell is not able to reach even 1.23 V (the minimum potential for water splitting) the reaction that is occurring is probably corrosion of the steel due

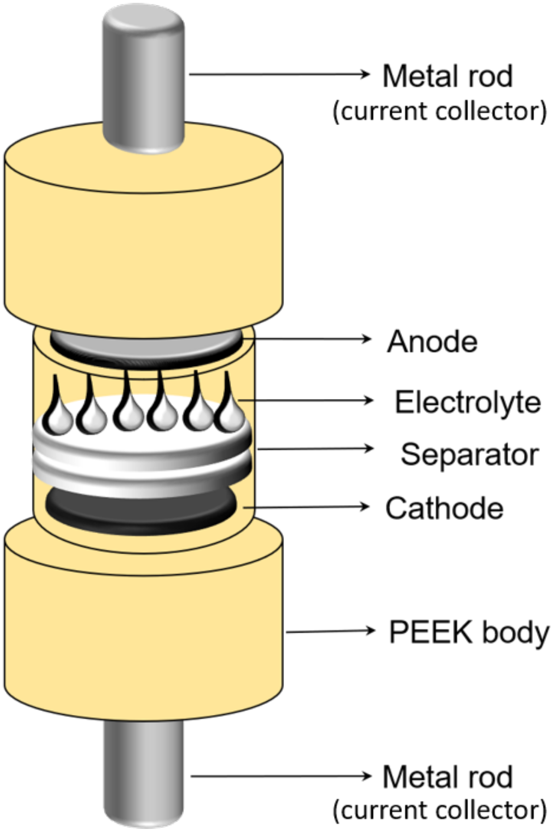

FIGURE 3.3: A schematic of a Swagelok-type cell showing all of the components and how they fit together.

to the chloride ions in the electrolyte. Evidence of corrosion was seen on the current collectors in the form of reddish discolouration after the experiment was over and the cell deconstructed.

This combined with the results in Figure 3.5, confirmed the hypothesis that metallic current collectors are not compatible with ME electrolytes and so alternate current collectors needed to be developed that could allow MEs to achieve their full potential.

The following tests in this chapter are all done using cells assembled with no active material present, i.e. the anode and cathode shown in Figure 3.3 are not used. Instead the current collectors act as the anode and cathode. This is because the primary objective in this phase of the research was to find a current collector capable of suppourting the EEI and the extended electrochemical window that comes with it. Therefore only the maximum voltage that is achieved by the cells is of interest in these tests.

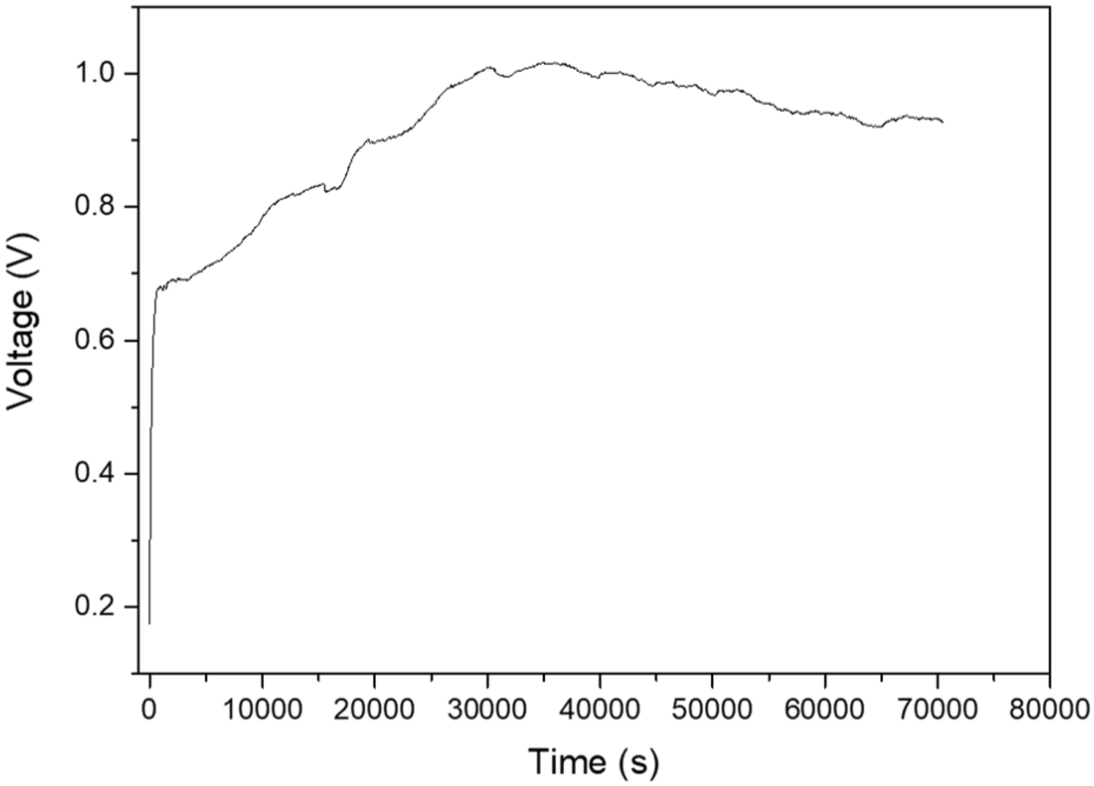

FIGURE 3.4: A cell constructed using a steel current collector. The steel begins to corrode at around 0.7 V, which is below the 1.23 V potential for water splitting. this shows the incompatibility of metal current collectors with the ME system

3.4 Coating Metallic current collectors

The first attempt to work around this issue was to coat the current collectors directly with a conductive yet hydrophobic (i.e. carbonaceous) material. Two methods were attempted for this. Firstly, carbon coating using a carbon coater usually reserved for coating scanning electron microscopy (SEM) samples. Thicknesses of 5 nm and 15 nm were applied. These thicknesses were chosen so as to limit any capacity contributions from the coating but to still achieve the hydrophobic coating. In an ideal case, current collectors are electrochemically inert and act purely as conductors. If the current collector undergoes any redox reaction then it will contribute to the capacity of the device which means incorrect conclusions may be drawn about the active material. It should also not contribute meaningfully to coulombic reactions so the surface area should generally be minimised to combat this.

This method was unsuccessful, producing similar results to those observed in Figure 3.4. The coating could be increased; however it was noticed that the coating was not very robust and easily removed from the metal rod. This is because no chemical bonds at all were being formed, carbon was simply being sprayed onto the surface. Any "weak spots" in the coating would allow water to come into contact with the metal which allows for the corrosion/water splitting to occur. While this method would have been a simple solution, it was ultimately abandoned.

The next method employed was to make a coating that could be "painted" on the rods. This could provide a robust coating that would prevent the electrolyte from coming in to contact with the metal. The "paint" was made by mixing Super-P carbon (92 wt%) (a conductive additive used in electrode slurries), and PVDF (8 wt%) with NMP as a solvent, as described in Chapter 2.10). This slurry was coated on the surface of the rod that would be exposed inside the cell and then placing it in a vacuum oven at 120 degrees Celsius for 12 hours.

This approach was tried on both steel and molybdenum rods. The steel rods showed similar results to those in Figure 3.4. This indicates that the coating was somewhat permeable to water and allowed the solvent to eventually reach the metal underneath. On molybdenum, the corrosion effect of the chloride ions should not have been as pronounced as on steel. The results of these tests (with no active material) are shown in Figure 3.5.

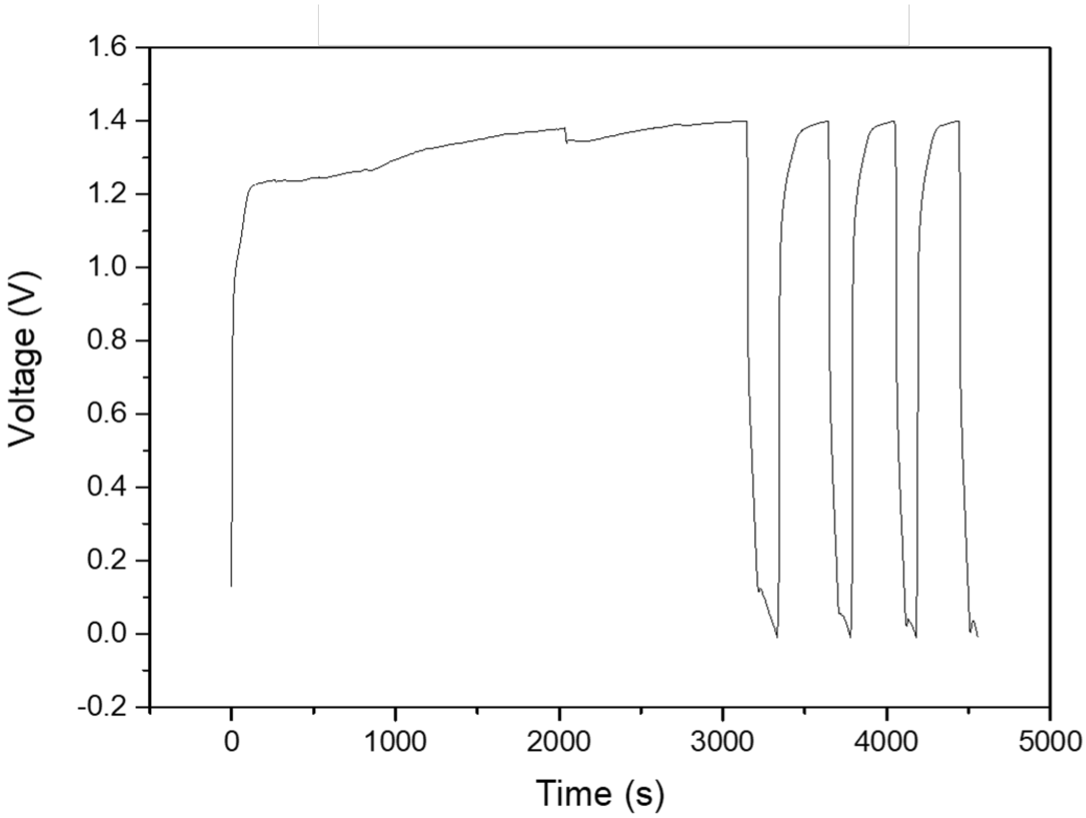

FIGURE 3.5: A cell constructed using Mo current collectors covered with a Super-P binder slurry that had been dried. This device, with no active material between the rods, is able to be charged to 1.4 V. Unlike steel it does not show the corrosion effects below 1 V however it is still only able to barely exceed the 1.23 V thermodynamic limit of water splitting

These cells were able to reach a voltage of 1.4 V which is above the 1.23 V limit. They could be charged and discharged between these limits. However, evidence of solvent splitting was observed at higher voltages. The coulombic efficiency of these cycles was 20% on average which means there were a lot of irreversible faradaic reactions occurring. Not all of the 80% loss can be ascribed to water splitting since there will be some losses due to the internal resistance (IR) of the cell.

As with the tests on steel, there was still evidence of this rod being in contact with the electrolyte. While this was not surprising, it meant that another approach had to be attempted to find an appropriate current collector.

3.5 Graphite Rods

The next attempt was to use rods made of graphite. These are much more delicate than the metal current collectors and much harder to make, which is why they were initially avoided in favour of the coating approaches. Examples of the rods are shown in Figure 3.6.

FIGURE 3.6: The graphite current collectors (top) compared to a Mo current collector (bottom). The graphite rods were manufactured to fit into the Swagelok-type cells that were available. 11 mm diameter and 5 cm long

Tests with these graphite cells were promising. Cells assembled with no active material were able to be charged to 2.6 V which is a large improvement over any previous results. However, the charge capacity of the graphite on its own, as shown in Figure 3.7, was not negligible. The corresponding discharge capacity was very low, with an IR drop of 2.4 V. This alone means that the current collectors had a very high resistance which makes them unsuitable to act as current collectors. The reason for the high charge capacity is probably due to the porous nature of the current collectors which means the surface area of the electrodes is high which leads to high capacitance. The large resistance of the current collectors is most likely due to the amporphous nature of these rods. Crystalline graphite rods would have a much more uniform conductivity throughout the whole structure. Tests with a multi-meter gave resistance values of approximately 17 Ω which is high compared to metal rods. This number may not be representative of the electrode when it is used in combination with an electrolyte.

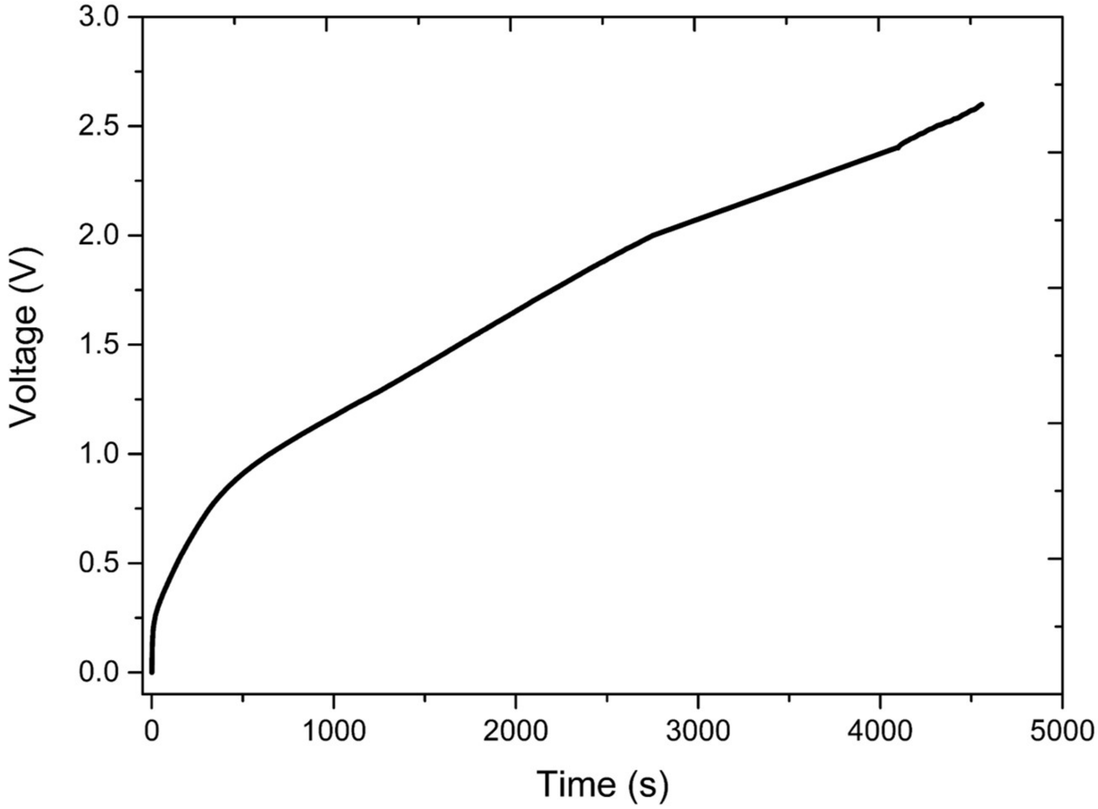

Figure 3.7: A charging curve for a supercapacitor using graphite rods as current collectors. The cell could be charged to 2.6 V, which showed that these electrodes were sufficiently hydrophobic to extend the electrochemcial window.

However, after only a few cycles, the cell stopped working. The nature of the failure (as shown in Figure 3.8) indicated a loss of electrical contact rather than a short circuit. Post-mortem analysis of the cell revealed the cell to be completely dry on the interior with white power covering the current collectors and separators. The powder was assumed to be a mixture of SDS and NaCl left behind as the solvent evaporated. It was determined that the porosity of the graphite rods was such that the electrolyte was being transported through the rods by capillary forces before evaporating out the other side of the rods. To counter this, the cells were pre-soaked with the electrolyte by fully immersing them in electrolyte overnight. The cells were wrapped in parafilm as much as possible to prevent evaporation. While this did extend the time the cells were active slightly, the cells eventually ceased function in a similar manner as before. As a result, these graphite rods were also abandoned as current collectors.

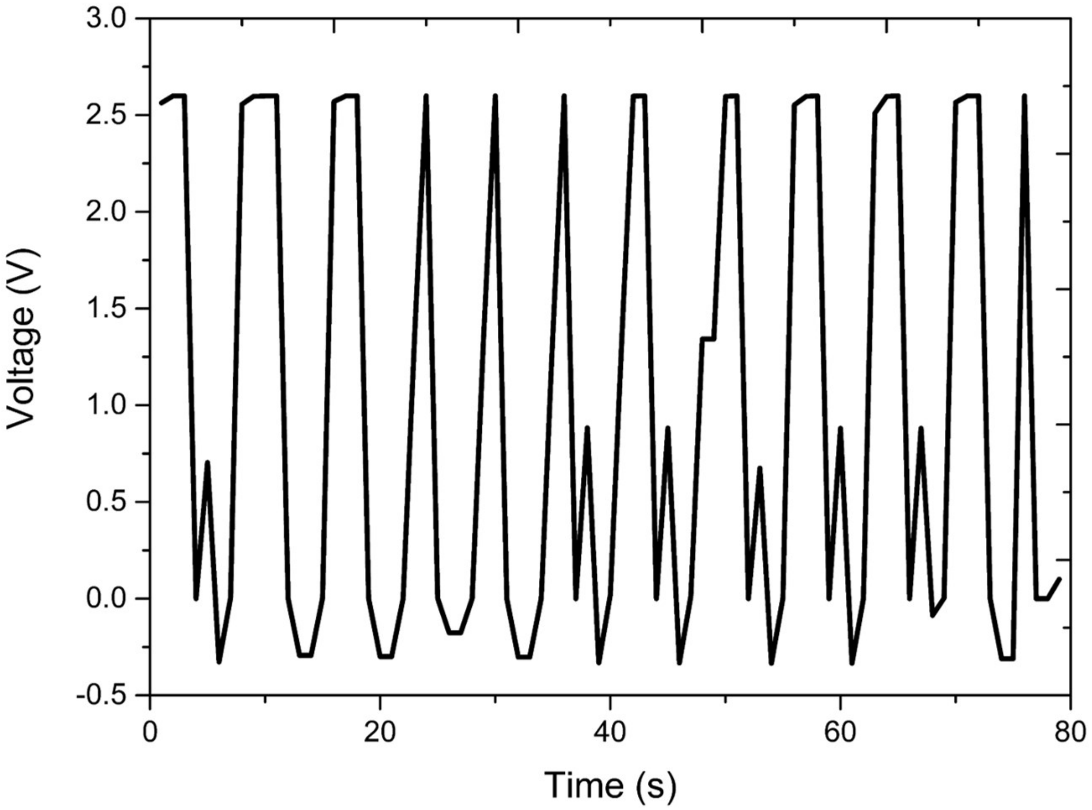

FIGURE 3.8: GCDC curves of a cell using graphite current collectors once it shorted. The very short cycles (1-2 seconds) and the irregular fluctuations in the voltage indicate a loss of contact between the two electrodes.

3.6 Glassy carbon current collectors

An alternative hydrophobic and conductive material other than graphite is glassy carbon. This is the material that was used in the initial tests of the extended electrochemical window so it was known that the EEI would form on the surface of this material. It had been avoided up until this point because of the prohibitive cost of a glassy carbon rod with dimensions similar to those shown in Figure 3.6.

A design was developed in conjunction with the VUW workshop that would allow for a much smaller piece of glassy carbon to be used. As only the face exposed inside the cell matters, it would be much more economical to use a much shorter stub of glassy carbon and build the rest of the current collector around it. The initial design is shown schematically in Figure 3.9

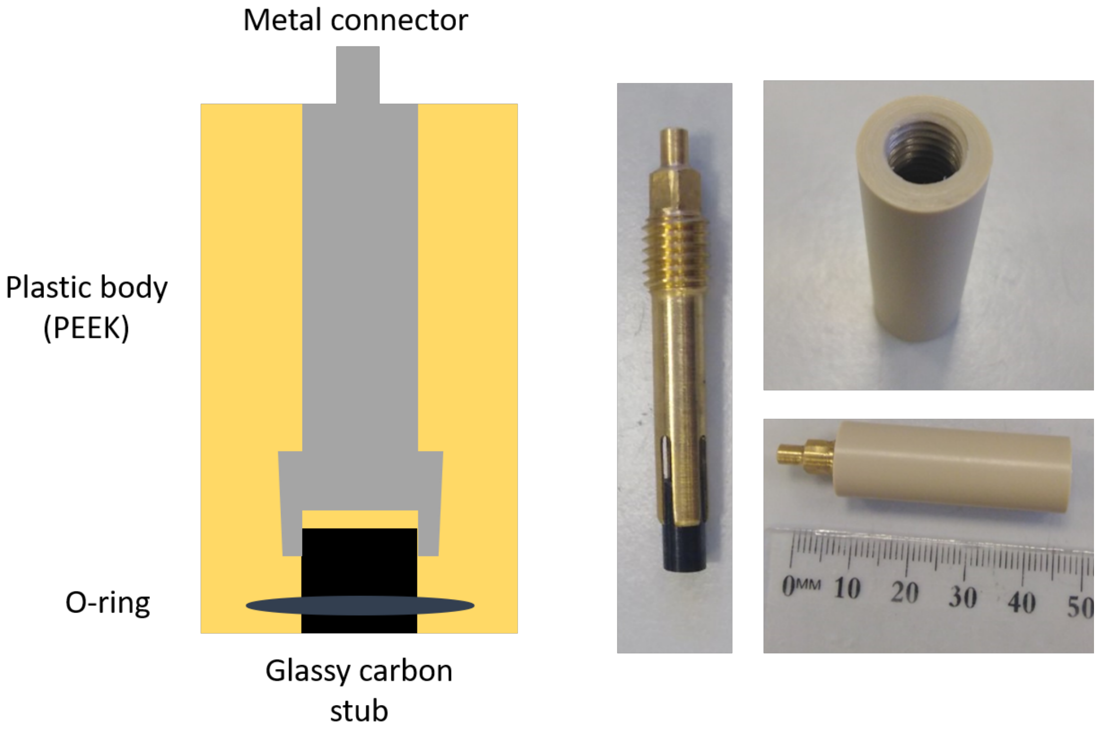

FIGURE 3.9: A schematic of the first design of the glassy carbon current collector. The metal chosen was brass. This version was able to be disassembled.

The glassy carbon stub is held in a pincer-like fashion by a brass rod. This is to keep a good electrical contact between the glassy carbon and the metal. There is an O-ring around the base of the stub to seal the interior from contact with the electrolyte. If any electrolyte were to leak through and make contact with the brass then the extended window effect would not be observed.

Initial tests with these current collectors were promising. Three electrode CV tests on 0.1 M aqueous potassium ferricyanide (99.9% Sigma) which used these current collectors as working electrodes showed a peak separation of approximately 70 mV. This shows that the surface of the glassy carbon was relatively active and well polished (Figure 3.10).

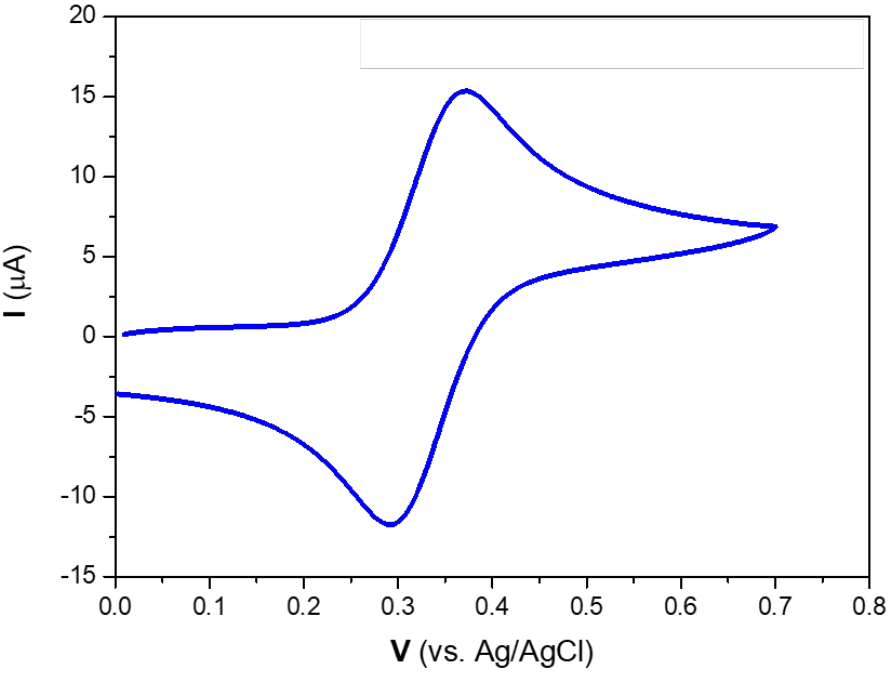

FIGURE 3.10: A 3 electrode cyclic voltammogram of 0.1 M ferricycanide in aqueous solution to test the activity of the electrode. The reference used was Ag/AgCl in saturated KCl.

GCDC tests of cells with no active material were successful and voltages of 3.4 V were obtained with an SDS based ME. There is evidence of some side reactions happening above 3 V, which could be the upper limit of the ME stability window or the oxidation of the glassy carbon surface. Regardless, a 3 V stability window of the MEs in these cells is a vast improvement over any previous attempt. When the tests were repeated with an aqueous electrolyte, the cells could reach approximately 1.9 V. This too, represents an extended window compared to the metallic current collector tested earlier. This is not unexpected as glassy carbon is not very active for the water splitting reactions. However, the aqueous window has not been widened to the extent shown by the ME in Figure 3.11, which indicates the formation of the EEI.

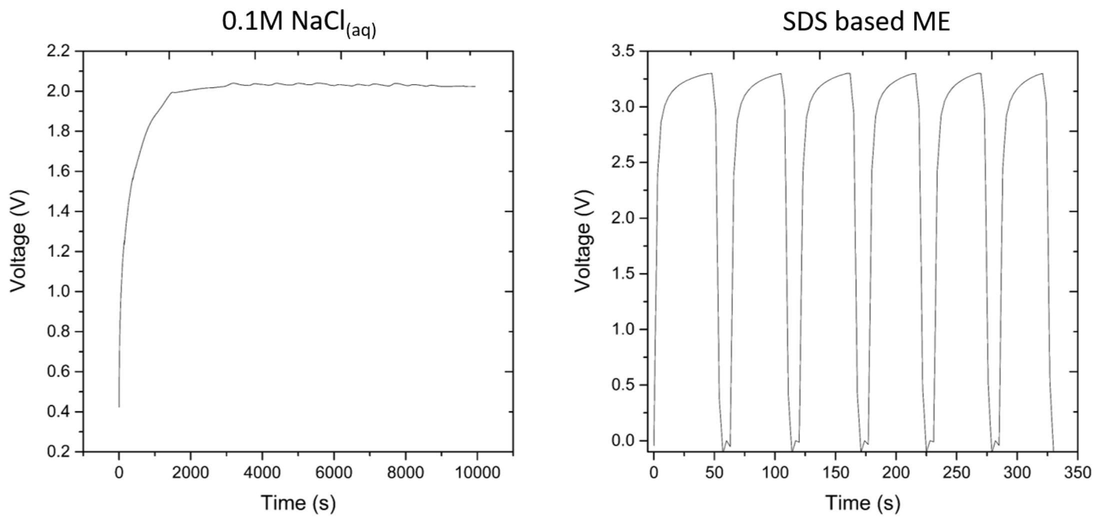

FIGURE 3.11: Full Swagelok type cell constructed with two glassy carbon current collectors. For aqueous electrolytes only voltages of 1.9 V were achieved before water splitting was observed. A max cell voltage of 3.4 V was achieved with SDS based MEs.

However, some cells failed in a manner reminiscent of Figure 3.5 where some "infinite charging" behaviour was observed at relatively low potentials. Upon disassembly of the current collector to investigate, corrosion, was observed on the brass connector (Figure 3.12).

FIGURE 3.12: Corrosion on one of the brass connectors from a failed cell. This is assumed to be from a bad seal around the O-ring allowing electrolyte to leak into the chamber and react with the brass.

From this, is was evident that the seal around the glassy carbon stub made by the O-ring on this particular rod was not complete which allowed electrolyte to leak inside the body of the electrode and react with the metal surface. This was only observed on one out of six current collectors made but does highlight the importance of the having no metallic surfaces in electrochemical contact with the electrolyte.

3.7 Conclusion

In conclusion, in order for microemulsions to be used as high voltage aqueous solvents, a hydrophobic surface is necessary. Therefore the development of a suitable current collector is vital when it comes to constructing full cells. Over the course of this work, many different options were tried. Finally, glassy carbon current collectors were constructed that worked as desired but also kept costs relatively low.

These electrodes, while fit for purpose, are not suitable for scale up as the cost is exceedingly high, each stub costing around 100 NZD. If microemulsions are to be commercialised the development/discovery of a suitable current collector is going to be one of the main hurdles that needs to be overcome. Investigations are currently underway with suitably passivated, yet still conductive metal surfaces or free standing carbon felts/fibers potential candidates.

Chapter 4

Supercapacitors

4.1 Introduction

After the development of a current collector that was compatible with ME electrolytes, attention turned to applications that exploited their extended electrochemical window to the fullest. As detailed in Chapter 1, both aqueous supercapacitors and ion batteries have had limited commercial success due to their inherently low voltage. With their extended electrochemical windows, MEs are able to overcome this low voltage limitation.

This chapter will detail the development of a supercapacitor using ME electrolytes and the use of electrochemical methods to characterise their performance compared to standard non-aqueous electrolytes.

4.2 Cell assembly

First, an appropriate electrode material must be selected. Of those available the most widely used is activated carbon. This is advantageous for the microemulsions as this surface is mostly hydrophobic, which means the EEI can be formed. Slurries of an off-the-shelf activated carbon (Commodities NZ) derived from coconut husks (the industry standard) were made according to the procedure outlined in Chapter 2.10.

Active material slurries are usually pasted onto a metal foil, which acts as a platform for the material and allows for post mortem analysis of the cell as these discs can be easily removed (see Figure 3.3). These foils also act as a secondary current collector. As was outlined in Chapter 3 this is not viable for the ME electrolytes. This problem is more straightforward to solve compared to the issues detailed in Chapter 3. It is possible to purchase carbon foils which are usually highly oriented pyrolytic graphite (HOPG). These do not have a large surface area that can contribute meaningfully to the capacitance but are conductive and easy to work with. Such a foil was used as the backing for all coatings.

Cells were assembled and tested with techniques outlined in Chapter 2.10. For each cell, the mass loading of each electrode was kept equal. However, different mass loadings should be examined in future work (see Section 1.8.3). All cells were assembled on a bench top under ambient conditions with no degassing of the solutions prior to assembly.

4.3 Electrochemical tests

4.3.1 Cyclic voltammetry

Cyclic voltammetry was performed first to evaluate the potential window of the assembled supercapacitors. Results from CV experiments are displayed in Figure 4.1

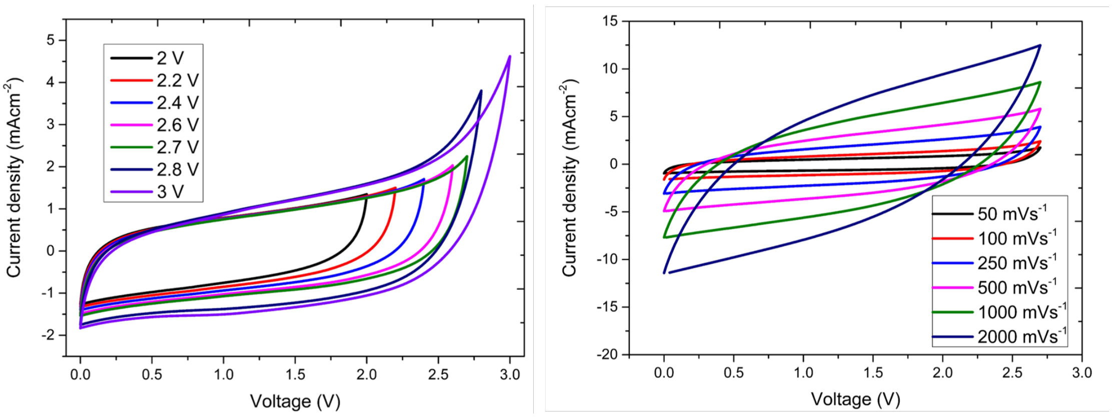

Figure 4.1: Cyclic voltammetry of supercapacitors using a two electrode set-up. A) Sequential increasing of the upper voltage cutoff in 0.2 V increments from 2 V-3 V at 100 mVs^{-1} including 2.7 V. B) Cyclic voltammograms at various scan speeds using 2.7 V as the cutoff. All show deviation from the ideal square wave shape due to the internal resistance of the cell.

An ideal supercapacitor would show a square wave shape in the CV rather than the lenticular shapes seen in Figure 4.1. This deviation from the ideal is due to the internal resistance of the cell. While there is some resistance expected from the solution, there is also most likely a non-negligible contribution from the current collectors. In a Swagelok-type cell these would usually be solid metal rods with very low resistivity. Glassy carbon however, has a much higher resistivity than steel and so the resistance from the current collectors was quite large comparatively.

The EEI was another source of resistance. The contribution of the EEI was much harder to quantify. The flow of charge in the oil-rich layer will be impeded significantly, which will also increase the internal resistance of the cell as well as extend the electrochemical window.

By sequentially raising the upper voltage limit in these scans, it is possible to determine the maximum voltage of the cell. The large increase in current density when the upper cut off is changed to 2.8 V in Figure 4.1 A was evidence of electrolyte/electrode break down. From these measurements it was shown that the maximum voltage was somewhere between 2.7 and 2.8 V. Commercial supercapacitors that use activated carbon electrodes almost always have a voltage of 2.7 V even though the window of the acetonitrile electrolyte is much wider than that. Above this voltage, it is the activated carbon that breaks down rather than the electrolyte. In particular, it is the oxygen containing functional groups such as carboxylic acids and ketones, left over by the activation process that break down [98]. Extensive purification of the carbon, or deriving the carbon from another source, e.g. metal carbides instead of coconut husks, can lead to a higher maximum voltage such as 2.8 V or 3 V, being achieved as these impurities are eliminated.

This experiment shows that the microemulsion stability is similar to acetonitrile when applied to supercapacitors using activated carbon. This overcomes one of the biggest hurdles for the application of aqueous electrolytes in energy storage devices.

The capacitance of the device can be evaluated from CVs using the following method.

$$C_s = \frac{Q}{mV} \tag{4.1}$$

Where C_s is the specific capacitance, Q is the charge stored on the plates in Coulombs, V is the potential difference between the two plates in Volts and m is the mass of the electrode material in grams.

Given that:

$$Q = I \times t \tag{4.2}$$

By substituting Equation 4.2 into Equation 4.1 it can be shown that:

$$C_s = \frac{(I \times t)}{mV} \tag{4.3}$$

If the numerator and denominator of Equation 4.3 are divided by t, the following expression is obtained.

$$C_s = \frac{I}{m(\frac{V}{t})} \tag{4.4}$$

The V/t term in Equation 4.4 is the scan rate of the CV experiment which is represented by ν. Hence the following expression is obtained:

$$C_s = \frac{I}{m\nu} \tag{4.5}$$

In a cyclic voltammogram, the current is a function of the voltage which can be written in integral form as

$$\int_{V_1}^{V_2} I(V)\,dV = Q \tag{4.6}$$

By substituting Equation 4.5 into Equation 4.6 the following is obtained

$$\int_{V_1}^{V_2} (C_s \times m \times \nu)\,dV = Q \tag{4.7}$$

It is also true that Equation 4.6 is an expression for the area under the CV curve. Therefore it can be shown that:

$$\int_{V_1}^{V_2} (C_s \times m \times \nu)\,dV = Area \tag{4.8}$$

Since C_S, m and ν are all constant, the integral can be evaluated as

$$(V_2 - V_1) \times C_s \times m \times \nu = Area \tag{4.9}$$

for the positive scan (which nominally goes from the low V_1 to the higher V_2), or

$$(V_1 - V_2) \times C_s \times m \times \nu = Area \tag{4.10}$$

for the negative scan where the potential is swept from V_2 to V_1.

The area of interest is the area inside the CV curve. To calculate this Equation 4.10 can be subtracted from 4.9

$$Area = (V_2 - V_1) \times C_s \times m \times \nu - (V_1 - V_2) \times C_s \times m \times \nu \tag{4.11}$$

$$Area = 2[(V_2 - V_1) \times C_s \times m \times \nu] \tag{4.12}$$

$$\frac{Area}{2[(V_2 - V_1) \times m \times \nu]} = C_s \tag{4.13}$$

Using this method, the capacitance of the cell shown in Figure 4.1 was calculated to be 42 Fg^{-1} at 100 mVs^{-1} and 20 Fg^{-1} at 2000 mVs^{-1} when cycled between 0 V and 2.7 V.

For an ideal capacitor, the capacitance is expected to be independent of the scan rate, however capacitance of a real device is expected to decrease with scan rate. Firstly, as the scan rate increases, the diffusion processes that govern supercapacitors have much less time to occur, the ions have less time to fit into the pores efficiently. This would result in a decrease in the observed capacitance. Also at higher scan rates, the IR drop within the cell is more pronounced, as observed by the “twisting” of the CVs as faster scans are performed (see Figure 4.1). This internal resistance also reduces the observed capacitance as the ΔV in Equation 4.10 (V_1-V_2), which represents the potential difference across the plates, will not remain consistent in regards to the initial and final voltages as some of that voltage will be lost due to the internal cell resistance.

This method for determining capacitance assumes that all the current over the scan leads to charge that is stored coulombically, not faradaically. Looking at the CVs in Figure 4.1 this assumption appears to be valid to a first approximation as there were no clearly well defined peaks, which indicate redox reactions. However, there was the possibility that there were some pseudocapacitive reactions with surface impurities in the activated carbon that did not have a well defined potential. This would have lead to difficult to notice broad peaks.

4.3.1.1 Pseudocapacitance

As outlined in Sections 1.5 and 1.4, the major difference between batteries and supercapacitors is that batteries store charge through faradaic processes and capacitors store charge through surface based coulombic processes. Pseudocapacitance is where the line between the two becomes blurred. For a pseudocapacitive process there is an electron transfer event, however, these faradaic processes occur only at the surface or very close to it. As a result, pseudocapacitive processes are still very fast. The line between what is a pseudocapacitive process and what is battery-like behaviour is not very clear and is the subject of some debate [25].

Transition metal oxides such as ruthenium(IV) oxide or manganese (IV) oxide, are the most investigated materials that have this property [99–101]. The reaction that takes place most commonly is proton insertion near the surface. Organic materials with redox active groups such as ketones or quinones are also popular for pseudocapacitors [102–104]. As previously mentioned, commercial activated carbon has some level of oxygen containing functional groups on the surface which can contribute to the capacity of the device through pseudocapacitance.

Pseudocapacitance can be seen in the form of a peak in a CV. Usually these are broad and show very little peak separation which is not influenced by the scan rate. This is because these reactions are very fast and reversible since they happen at the surface. Unlike other faradaic reactions, the current from pseudocapacitance scales linearly with the scan rate of the CV [25].

4.3.1.2 faradaic vs. coulombic reactions

One way in which coulombic interactions can be distinguished from Faradic reactions in a more rigorous manner than inspecting the shape of the CV curve is by analysis of how the current changes with the scan rate. The total current at any point is given by:

$$I_{total} = I_{faradaic} + I_{coulombic} \tag{4.14}$$

By taking Equation 4.2 and writing it in differential form:

$$I_{coulombic} = \frac{dQ}{dt} \tag{4.15}$$

and substituting it into Equation 4.14

$$I_{total} = I_{faradaic} + \frac{dQ}{dt} \tag{4.16}$$

If the scan rate is defined as:

$$\nu = \frac{dV}{dt} \tag{4.17}$$

It can be substituted into Equation 4.16

$$I_{total} = I_{faradaic} + \frac{dQ}{dV} \times \nu \tag{4.18}$$

dQ/dV is defined as the capacitance as per Equation 1.1 (in differential form) which leads to the relation

$$I_{total} = I_{faradaic} + C\nu \tag{4.19}$$

In an ideal supercapacitor C is constant with the scan rate. While this has already been shown to be incorrect for this system (see Figure 4.1) what is shown in Equation 4.19

is that the current from a purely coulombic process should vary linearly with the scan rate.

The faradaic current is given by the Randles-Ševčík equation

$$I_{faradaic} = 0.4463nFAC(\frac{nF\nu D}{RT})^{\frac{1}{2}} \tag{4.20}$$

It can be seen that for faradaic reactions the current varies proportionally with the square root of the scan rate.

Therefore, for any current, there are two contributions, faradaic and coulombic, which can be separated by recording CVs at different scan rates and plotting the results. The two factors of this equation can be combined and written as

$$I_{total} = a\nu^{b} \tag{4.21}$$

Where the a value incorporates all the other terms from Equations 4.19 and 4.20 and the b value can vary from 0.5 (for a fully faradaic process) to 1 (for a fully coulombic process). This method is exemplified by Wang *et al.,* [105] who used it to determine the relative contributions of these two currents for an anatase TiO_2 film in a lithium ion battery.

By plotting the log of the current vs. the log of the scan rate, a straight line graph is obtained, of which the gradient is the b value from Equation 4.21. By repeating this analysis at many potentials, a series of b values can be obtained for the whole scan.

However, this method is not appropriate for the devices investigated in this study. Firstly, there is a large internal resistance in the cells. This means that at low potentials (E.g. below 0.5V in Figure 4.1) the current actually decreases with scan rate. This means that any b value obtained from this analysis would be negative for these voltages.

Also, this method does not take into account pseudo-capacitance. Pseudo-capacitance reactions are faradaic in nature, but do not follow the Randle-Sevcik equation because they happen only at the surface of the electrode, as a result, pseudo-capacitance processes also scale linearly with the scan rate [25]. This method is unable to distinguish between

Scan	b value
1V positive scan	0.36
1.5V positive scan	0.44
2V positive scan	0.48
1V negative scan	0.57
1.5V negative scan	0.64
2V negative scan	0.81

Table 4.1: b values calculated by taking the absolute current at the voltage shown at various scan rates. The log of the currents was plotted against the log of the scan rate to produce a straight line, the gradient of which is the b value as per Equation 4.21

pseudo-capacitance and capacitance. Pseudo-capacitance is most commonly observed in metal oxide electrodes, it is only seen on activated carbon when there is a high degree of functionalisation (in particular oxygen containing functional groups) as these groups can undergo redox reactions. Given the ability of the capacitors to be charged to 2.7 V it can be assumed that the degree of surface functionalisation is sufficiently low to keep said surface hydrophobic enough for the EEI to form which would limit the capacity arising from pseudocapacitance. However, further investigations would be required to confirm this hypothesis.

Doing this analysis for 1 V, 1.5 V and 2 V on both the positive and negative scans yielded b values summarised in Table 4.1. Note that for negative scans the absolute current was used.

From these values it is clear that this analysis is not appropriate for the devices investigated. A *b* value of less that 0.5 should not be possible yet all of the positive scan data shows this. For the negative scan data the values are all still very low which would indicate that mostly faradaic processes occurred. This does not seem reasonable given the shape of the CVs. It is possible that there was such heterogenaeity in the redox sites that the peak that should appear when there is one defined redox potential such as that seen in Figure 3.10 would be smoothed out and look a lot like capacitive contributions. However, this is unlikely.

While there is almost certainly some pseudocapacitance present in the deivce due to surface impurities, it was unlikely to be the dominant charge storage mechanism given the results from the CV results. Galvanostatic experiments might be able to distinguish any redox reactions that do occur. These will be discussed in a later section.

4.3.2 Electrochemical impedance spectroscopy

In order to quantify the resistance of these cells electrochemical impedance spectroscopy (EIS) was performed. This is a versatile technique that can be used to uncover some processes that occur inside the cell. The results of these studies are summarised by the Nyquist plot in Figure 4.2. Three cells were tested in total. One with a 0.1 M aqueous NaCl electrolyte (blue triangles) one with the SDS based ME electrolyte that had been freshly prepared (red circles) and one with the SDS based ME electrolyte that had been cycled 10000 times (black squares) between 0 and 2.7 V at a rate of 500 mA g^{-1}.

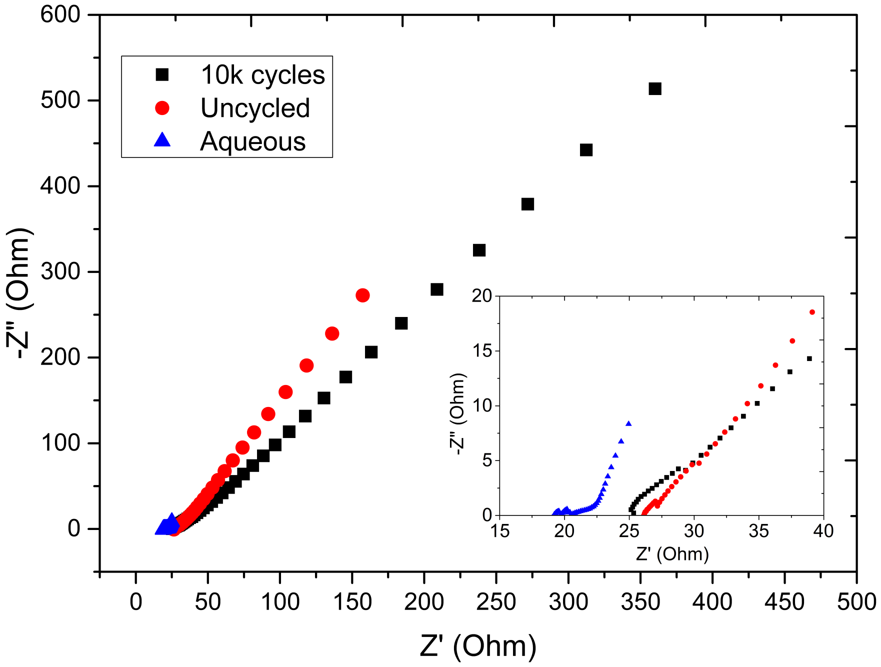

Figure 4.2: An EIS spectrum of 3 different supercapacitors, one with an 0.1 M NaCl aqueous electrolyte (blue), One with the ME electrolyte (red) and one with an ME electrolyte after it had been cycled 10,000 times (black). The applied voltage was 0 V with an amplitude of 5 mV over a frequency range of 0.1 to 10,000 Hz. Inset: a magnified portion of the graph showing the X-intercepts.

Firstly, the X intercepts in Figure 4.2 are a rough estimate of the internal resistance of the cell (see Figure 2.4). For the aqueous cell the resistance is much lower than the ME cells but is still high at 20 Ω. The internal resistance of the cell did not increase greatly upon cycling. This is important as an increase in internal resistance is a sign of ageing in a supercapacitor. When the resistance increases the efficiency and power density of the supercapacitor decreases, so having a cell that maintains its resistance over cycling is a sign that the ME/EEI is stable over this time and operating within its stability limit. In this case it remains roughly constant at 25 Ω. The comparatively large internal resistance explains the shape of the CVs observed in the previous section.

The other noticeable feature of these graphs is in the low frequency region (far right of the graph) In this region the capacitance dominates. The slope of this part of the graph is proportional to the capacitance. By comparing the two ME cells (before and after cycling) it was found that the capacitance did decrease over cycling which was not unexpected. Comparing both of these to the aqueous NaCl electrolyte, it was seen that the aqueous electrolyte had a higher capacitance. This too was not unexpected given the proposed EEI model.

Aqueous electrolytes are well known to have higher capacitance values for a given electrode [106]. This arises from the definition of capacitance (Equation 1.1) Q=CV. The more charge that can be stored on the surface of an electrode at a given potential, the higher the capacitance value. Charge dependant capacity is a function of surface area (as outlined in Figure 1.5) but is also a function of the size of the adsorbed ions. In aqueous electrolytes the salts used are made up of comparatively small ions, NaCl, KCl, H_2SO_4, $HClO_4$. Therefore it is possible to fit a lot of them on to the surface of the electrode which leads to a higher capacitance. In acetonitrile electrolytes however, the salts used, e.g. tetrabutylammonium tetrafluoroborate, are much larger and so less ions can be packed onto the surface.

How this translates in the case of ME electrolytes is uncertain. The EEI model explains the extended electrochecmical window, however it does not allow for charged species to be easily adsorbed onto, or interact with, the surface of the electrode.

As discussed in Section 4.3.1 Mei *et al.,* [9], developed a model for a supercapacitor that allowed for unambiguous interpretation of the Nyquist plot. This model was developed for a traditional supercapacitor. Therefore it would be inappropriate to draw any concrete conclusions or numbers from the EIS scans presented in Figure 4.2.

In order to interpret the EIS fully, an appropriate equivalent circuit would have to be devised and fit the data. However, in a complex system such as the ME with the EEI model, this is difficult to do accurately. In a similar manner, simulations could be performed that could deepen the understanding of this system. This was beyond the goals of the current project but is work that will be carried out in future studies.

4.3.3 Galvanostatic cycling

With an electrochemical window established, cycling tests were performed at various charge rates and over a long period of time to test the stability of cells.

First, charge-discharge experiments were performed on solutions of both aqueous 0.1 M NaCl and 4.9 wt% SDS to evaluate the effect that adding the active material had on the electrochemical window of water and surfactant solutions.

The aqueous cell achieved similar results to those observed in Figure 3.11. It was never able to achieve a voltage of 2 V and the irregularities in the charging curve indicated that some solvent splitting or other side reaction was taking place.

The inset on the right hand side of Figure 4.3 is a zoomed in portion of the same curve showing irregular charging behaviour indicative of solvent splitting reactions occurring inside the cell. The cell was able to achieve a voltage of 2.4 V eventually and complete a discharge cycle, however, due to the irregularities observed in the charging curve the experiment was not continued. The IR drop was substantial at around 500 mV, which was an order of magnitude greater than that observed for the SDS microemulsion cells, which was around 50 mV.

The results of GCDC cycling of a supercapacitor with a ME electrolyte are shown in Figure 4.4.

The main advantage of supercapacitors is that they can be operated at high rates without much loss of capacity. Therefore, it is important to evaluate this rate capability, how the capacitors perform at high charging and discharging currents. The capacitance was calculated by using the following formula.

$$C = \frac{I \times t}{\Delta V \times m} \tag{4.22}$$

Where I is the discharging current used, t is the discharge time of a particular discharge step, V is the difference in voltage between the beginning and end of the cycle (Here it is

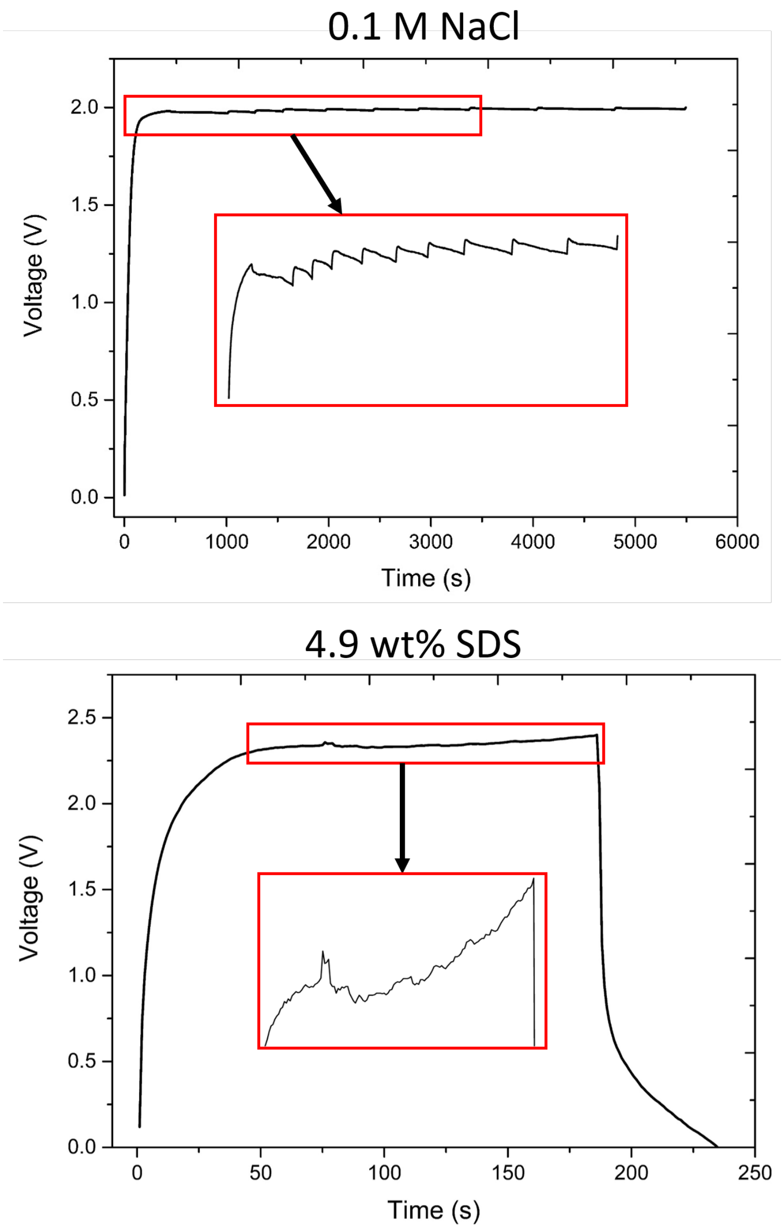

FIGURE 4.3: Galvanostatic charge-discharge curves for 0.1 M NaCl and 4.9 wt% SDS solutions. The aqueous solution shows a window similar to that seen in Figure 3.11 with irregular behaviour around 1.9 V (indicated) which is evidence of solvent splitting. The SDS solution is able to achieve a voltage of 2.4 V however, there was evidence of solvent splitting around 2.3 V. For both cells the charging current used was 500 mA g^{-1}.

taken as the voltage after the IR drop has been taken into account and 0 V) and m is the mass of the electrode material. This assumes that the discharge curve is linear, which is accurate to a first approximation, especially for higher discharge rates. If there is any non-linearity (due to pseudocapacitive effects) then this method could over-estimate or underestimate the capacitance depending on the exact shape of the curve.

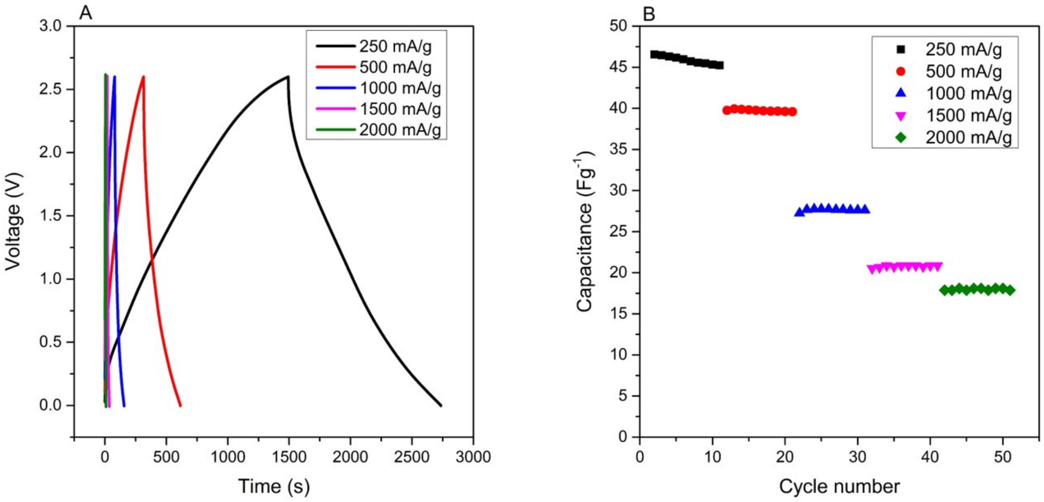

Figure 4.4: A: Charge discharge curves for a supercapacitor assembled with an ME electrolyte. B: Calculated capacities at various rates over 10 cycles for the same supercapacitor.

In order to evaluate how appropriate this assumption was for calculating the capacitance, the values obtained from the CV experiments in Section 4.3.1 could be compared to the ones obtained here. Given that the capacitance changes with scan rate and discharging current, it is hard to compare the results in a one to one manner. However the results were in a similar range to what was observed from the CV results (20-40 Fg^{-1}) which shows the methods are somewhat consistent.

As expected, the capacitance of the cell decreased as the current rate was increased. Ideally the percentage change in the capacitance should be small; however, here it is quite large. This is likely due to the EEI influencing the rate at which the electrical double layer can be formed. Through further optimisation of this interphase and the electrode material this could be improved. For instance, changing the oil phase for a solvent with a higher dielectric constant may allow for a stronger electric field to be developed more quickly. A shorter chain surfactant could be utilised to create a thinner EEI, this however may cause it to be less robust and not increase the electrochemical window as much. Salt concentration could also be a factor in the rate capability as a higher conductivity would result in the ions being able to move faster through the solution.

Determining the exact capacitance values can be difficult due to the difficulty in assigning whether charge is stored in a coulombic or faradaic way. The calculated energy densities are more unambiguous, as this number takes into account both the capacitive and pseudocapacitve contributions. The calculated figure of 41 Whkg^{-1} at 500 mA g^{-1} for the device shown in Figure 4.4 is difficult to compare to commercial cells since they report energy density based on the mass of the cell as a whole where as these calculations are based on the mass of just the electrode material. However, they are comparable to some results available in the literature that also use activated carbon.

Finally, long term cycling data is desirable to see the stability of the system. In literature it is most common to see continuous charge-discharge tests.

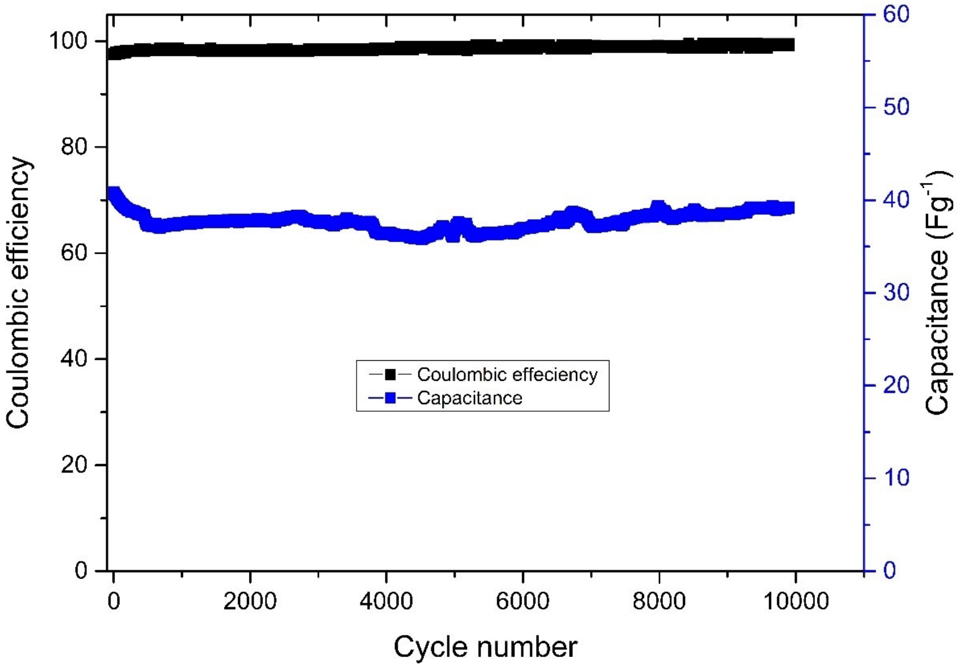

FIGURE 4.5: Long term cycling data for a supercapacitor with a microemulsion electrolyte. 10,000 cycles were completed at a charge and discharge rate of 500 mA g^{-1}. This cell was able to maintain a capacitance value of around 40 Fg^{-1} over this time period with a coulombic efficiency of close to 100%

Figure 4.5 shows the performance of one cell over 10,000 cycles of continuous charge and discharge at 500 mA g^{-1} between 0 V and 2.7 V. Over this period, the cell was able to maintain a capacitance of just under 40 Fg^{-1}. The coulombic efficiency was also close to 100% which shows that not many faradaic, irreversible, side reactions were occurring. The loss in efficiency was probably due to the high internal resistance of the cell.

A capacitance of 40 Fg^{-1} is quite low compared to a lot of supercapacitors in the literature. Activated carbon capacitors regularly reach close to 100 Fg^{-1} but can be much higher [107–110]. As discussed previously, there must be a match between the activated carbon and the electrolyte. In particular, the pore sizes of the material must adequately match the charge carrying species in the electrolyte. With a new electrolyte (and a new electrode-electrolyte interphase) to contend with it is likely that modifications would need to be made to the standard carbon materials available which have been optimised for standard electrolytes. Showing that a moderately high capacity can be maintained over the course of 10,000 cycles is a good stepping off point for ME electrolytes in supercapacitors.[1]

The low capacitance values could just be inherent to the carbon used. While a coconut derived carbon was used, as is the industry standard, there is still large variance between different coconut derived carbons. In order to test the capacitance of the carbon under more standard conditions, some cells with a quarternay ammonium based salt in acetonitrile as the electrolyte were assembled. Acetonitrile cells were prepared in a nitrogen filled glovebox. Prior to going into the glovebox the electrodes used in the acetonitrile tests were heated 120° for a further 12 hours under vacuum to ensure they were fully dried. The electrolyte used was 1 M tetrabutylammonium tetrafluoroborate (TBAB) (99.5% Aldrich) in acetonitrile (anhydrous, Aldrich). The use of a glovebox for these cells is important as it is known that water hinders the performance of acetonitrile based cells significantly due to the tendency of water to turn into oxygen and hydrogen gasses at the voltages of these supercapacitors.

The results of these studies are shown in Figure 4.6. The capacitance of these cells at current rates of 250 and 500 mA g^{-1} was similar to what was observed in the ME electrolytes in Figure 4.4. However, it is apparent that the rate capability of the acetonitrile electrolytes was much better. At very high current rates of 2000 mA g^{-1} the capacitance was still approximately 75% of what it was at 250 mA g^{-1}. For the ME electrolyte however, the capacitance dropped to under 40% of what it was at a slower rate. This drop could occur for many reasons, but the root was likely in the EEI. The rate at which charges can be transported across the layer (if they are at all) will be lower than in an electrolyte without it due to the unfavourable interactions between the charges and the non-polar phase.

---

[1] It is also often hard to compare specific capacitance values to the literature as the mass values are often misrepresented. The mass values reported in this research are based on the mass of both the anode and cathode combined as this is what it takes to make the whole device work. Research that calculates these numbers based purely on one electrode, despite other calculations being based on the device as a whole, over-represents the specific capacitance of the device.

Attempts to find a stable ME composition that used TBAB as an additive in the SDS ME base were unsuccessful. TBAB is soluble in water but when added to the SDS base, the sample gradually destabilised even at low concentrations (0.01 m). In future studies, finding an ME composition that is stable towards TBAB would allow further elucidation of the mechanism behind the ME based supercapactiors.

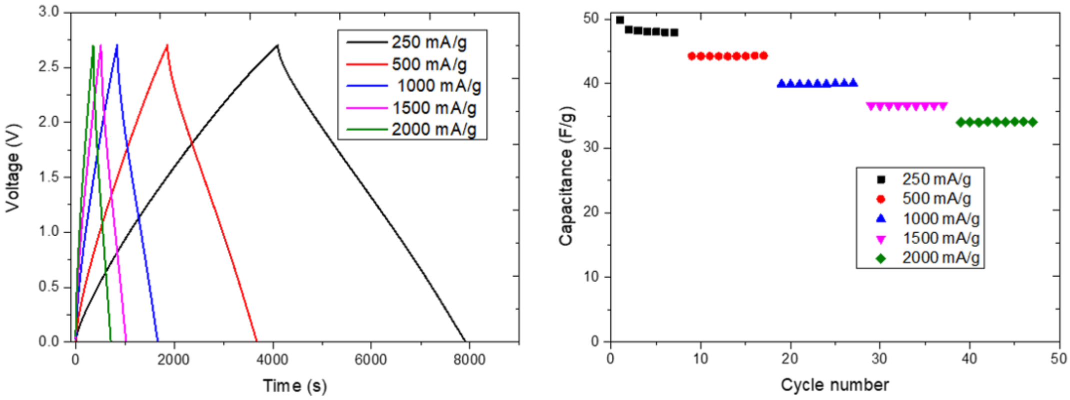

FIGURE 4.6: Long term cycling data for a supercapacitor with an acetonitrile electrolyte. It shows stable rate performance over the currents tested.

While continuous charge-discharge tests are the ones most often performed to establish cycle life for supercapacitors in the literature, voltage hold or ‘float’ tests are much more relevant for industrial applications. This is because a commercial supercapacitor spends most of its life floating at the maximum voltage, either being disconnected from the circuit meaning no charge is lost or ”trickle charged” to account for any losses over time. Most commonly supercapacitors are only used when necessary, e.g. when a power outage occurs. Therefore a supercapacitor has to be able to survive being held at a high voltage for a long period of time.

This is exemplified by Weingarth *et al.* [111], who compared voltage hold tests to continuous cycling tests for supercapacitors. The electrolyte used was an ionic liquid on a carbon black electrode so the voltage achieved was much higher than traditional market supercapacitors.

Figure 4.7 shows that during a cycling test, even if the upper voltage cut off is above the stability limit of the electrolyte, only spend a short amount of time there. This means that even though these tests may run for a long amount of time, they may not show the whole story. In the bottom left of Figure 4.7 The results of cycling tests with a 3.5 V and 3.75 V upper cut-off are shown, the difference over the 12000 cycles (and 1000 hours

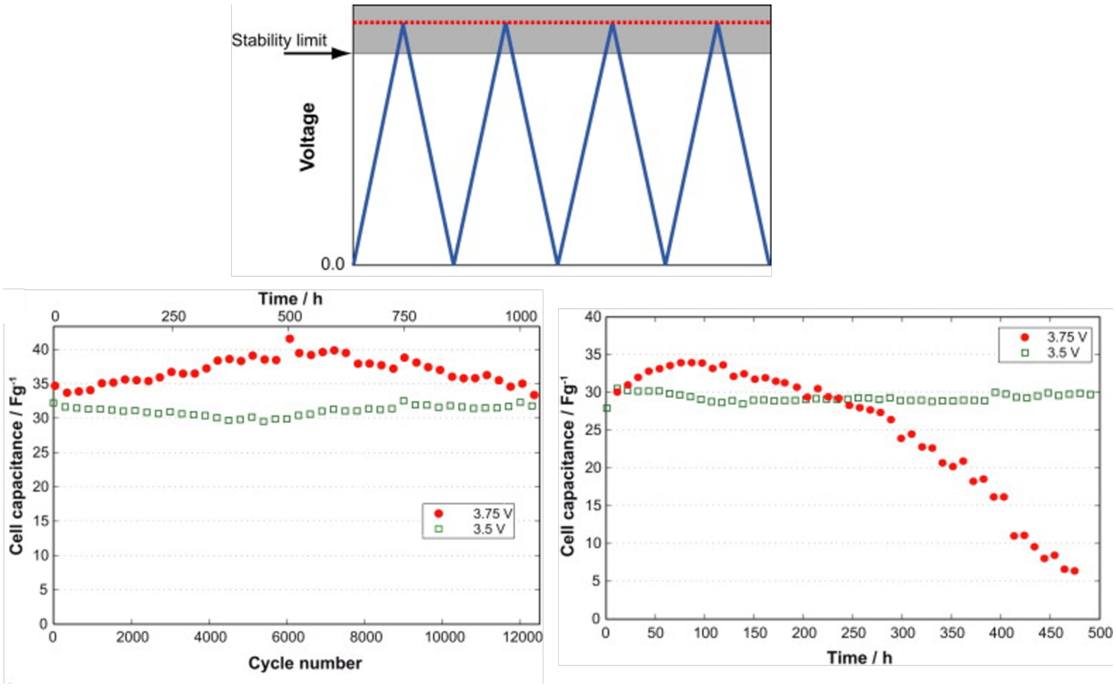

FIGURE 4.7: Top: Cycling of an idealised supercapacitor where the maximum voltage exceeds the stability limit of the electrolyte but only for a short time. Bottom left shows the results of cycling two real capacitors with different upper cut off voltages. Bottom right shows results for the same cells but for a voltage hold tests instead. By looking at the voltage hold tests it is clear that 3.75 V is above the stability limit of this electrolyte despite the difference not being noticeable over in the cycling tests. Reprinted with minor alterations from Cycle Versus Voltage Hold – Which Is the Better Stability Test for Electrochemical Double Layer Capacitors, Vol 225, D.Weingarth A.Foelske-Schmitz R.Kötz, pg 84-88, Copyright (2013), with permission from Elsevier.

the test was running) was minimal, it might even be concluded that 3.75 V is better as it gives higher capacitance values on average. However, the results of the voltage hold tests (bottom left in Figure 4.7) reveal a different story. These tests are conducted by raising the cell voltage to the maximum then holding it there *via* trickle charging (a constant voltage measurement) for 10 hours, three cycles are then performed to evaluate the capacitance of the cell at which point the cell is recharged to the maximum voltage and held for another 10 hours. These tests show that after 100 hours the cell held at 3.75 V begins to degrade rapidly whereas the 3.5 V cell retains its capacitance. The conclusion from this test is that 3.75 V was above the upper cut-off for the electrolyte in this system. This shows the value of carrying out voltage hold tests.

Voltage hold tests are quite harsh and it is difficult for unoptimised lab based cells to withstand them. Therefore when these tests were performed, they were carried out alongside cells that used standard electrolytes. It is known that acetonitrile-TBAB electrolytes stand up well to this test in optimised commercial cells. By using this standard electrolyte in the lab cells available, the performance of the SDS based ME can be compared to it in a relative manner.

Tests were carried out in triplicate. The method used was the same as that of Weingarth *et al.* [111] except that the upper cutoff used for both cells was 2.7 V. Results are shown in Figure 4.8.

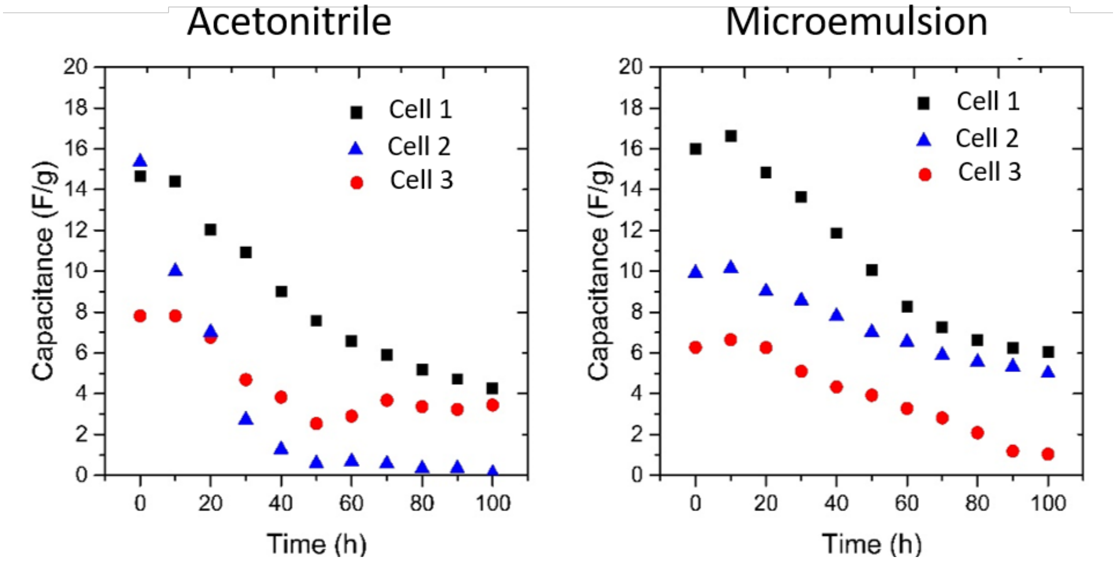

FIGURE 4.8: Voltage hold tests for acetonitrile electrolytes and the ME based electrolytes. Each colour represents a different cell. Performance between the electrolytes was similar.

It is apparent that neither electrolyte withstands this test particularly well. Also there is some variance between cells observed. This is somewhat expected given that these cells were assembled by hand. However it could be determined that both electrolytes performed similarly in this test.

There could be multiple reasons for the poor performance of both electrolytes. Firstly the carbon mix used was not optimised, as previously stated. The reason for the low voltage window of supercapacitors is generally the decomposition of impurities in the activated carbon. A cleaner more processed carbon would reduce this. Also the electrochemical workstation was located outside of the glovebox. This meant that cells had to be sealed as best they could with parafilm when they left the glovebox. It is known that water has a detrimental effect on acetonitrile electrolytes so this could have had an impact on the performance of those cells.

As mentioned in Section 1.6, degassing of solvents is an important step in electrochemistry experiments as it removes reactive oxygen. Degassing of MEs is difficult as the solution tends to foam extensively. However, if a solution could be devised for this it might improve the long term cycling performance of the ME cells.

4.4 Conclusion

In conclusion, MEs show promise as electrolytes for supercapacitors. The performance of cells with ME electrolytes was comparable to cells based on acetonitrile electrolytes in both long term cycling and voltage hold tests. The ME electrolytes were able to achieve a voltage of 2.7 V and an energy density of 40 Whkg^{-1}.

The ME electrolytes did not show as good rate capability as acetonitrile due to the postulated EEI impeding charge movement in the vicinity of the electrode. By adjusting the ME composition or changing the surfactant mix, a solution could be developed. However, there will be a fine line between achieving an extended electrochemical window effect of the EEI but making charges mobile through the EEI. In particular, choosing an oil phase that imparts electrochemical stability but allows for the solubilisation of salts like TBAB could be a solution.

Exactly how the double layer is forming in these electrolytes is another area that needs to be investigated further. It is unlikely that charges like Na^+ ions are migrating into the oil rich layer of the EEI to any reasonable extent. It is possible that the double layer is forming in the water rich layer of the EEI some distance from the electrode itself though exactly how this would be possible is unresolved. Some form of modelling will have to be undertaken in order to fully understand the complex interaction of the components at the EEI in order to truly optimise the system and fully exploit ME electrolytes.

The activated carbon used is another area that requires further investigation. As mentioned throughout this chapter, oxygen contamination and the formation of oxygen containing functional groups are a common issues with the activation process. These can be beneficial as they can provide extra charge storage in the form of pseudocapacitive charge transfer reactions. However in the case of ME electrolytes they could also provide hydrophilic sites where the EEI could not form and allow access of water to the electrode where it could be split. Exactly how much of a problem this was in the current set up was hard to evaluate. Another form factor such as a pouch cell would be an improvement because it can be fully vacuum sealed which allows easy identification of gas evolution. The Swagelok-type cells were sealed, but not as effectively as pouch cells. This meant the Swagelok-type cells could release gas over time, so no pressure build up was noticeable.

By refining the carbon mixture used, as well as adjusting the ME make up and composition, the performance of the ME cells could be pushed to surpass the current acetonitrile electrolytes used in industry.

Chapter 5

Lithium Ion Batteries

5.1 Introduction

Another research goal of this thesis was to apply microemulsion electrolytes to ion batteries. Lithium ion batteries have the most well established catalogue of electrode materials from which to pull and so they were investigated in depth. Also, lithium ion batteries have been shown to work with both non-aqueous and aqueous electrolytes, which makes them ideal to test a new electrolyte that combines aspects of both.

In this chapter, the choice of electrode materials, alterations to the electrolyte used in Chapter 4, and the performance of the assembled batteries are discussed in detail.

5.2 Lithium ion battery electrodes

Before constructing the cell the electrode materials had to be chosen. The primary limitation for aqueous lithium ion batteries is the anode material. Many materials have been used in literature, however, an off-the-shelf material was desired as the focus of this research was on the electrolyte. The three main materials used as anodes in commercial lithium ion batteries are lithium metal, graphite, and lithium titanate.

Lithium metal is incompatible with microemulsions, not only because the metallic surface would not allow formation of the EEI, but also because of the possibility of the lithium metal violently reacting with the water. Graphite is attractive because of its hydrophobic yet conductive nature. However, the issue in this system is the potential of the lithium intercalation reaction. The potential of lithium insertion into graphite to form the corresponding graphite intercalation complex, sits just 0.2 V above the reduction potential of lithium [12]. This low reduction potential is a huge advantage in traditional lithium ion batteries, as it reduces the safety concerns that are associated with lithium metal while maintaining a high energy density. In the ME systems, the lower potential limit of the electrochemical window sits well above where graphite intercalation is expected to occur. This makes graphite an unsuitable candidate for ME based lithium ion batteries.

This brings back a point mentioned in Section 1.8: The voltage of a battery is determined by the difference in potential energy of electrons in the cathode and anode material. Therefore, not only must the electrochemical window of electrolytes be made wider, materials that fit inside this window must also be found.

Therefore lithium titanate would have been chosen as the anode material, as it has a substantially higher reduction potential than graphite (approximately +1.5 V vs. Li/Li^+) which should place it inside the window of the ME. Due to the supply issues, lithium titanate could not be used in this study. Anatase phase titanium dioxide was used as a replacement. Anatase has been shown to be useful as an electrode material [112–114].

On the cathode side, there are a wide variety of materials available, but again, international availability of industry standards like lithium cobalt oxide, $LiCoO_2$ or iron phosphate, $FePO_4$ slowed progress. Vanadium pentoxide, V_2O_5 was selected from the range of materials available on hand as a material that has shown to be useful across a range of ion batteries and has a well established lithium chemistry [115–118].

5.3 Electrolyte alterations

The next issue tackled was that of the electrolyte. Until this point, the ME used for all tests was an SDS-cyclohexane-butanol base ME. However, this ME has sodium ions in the solution which may interfere with the lithium ion chemistry at the electrodes. Any anionic surfactants such as sodium sterate are going to have the a similar issue unless they use lithium as a counter ion. These lithium based surfactants are either not commercially available or prohibitively expensive.

Therefore, alternative microemulsions based on alternative surfactants were developed. The two options aside from anionic surfactants, are non-ionic surfactants or cationic surfactants. MEs prepared with Cetrimonium chloride (CTAC) as a cationic surfactant, showed very little tolerance to any added lithium salts and so were avoided. One of the most widely available classes of non-ionic surfactants is the Triton series with the most common being Triton X-100.

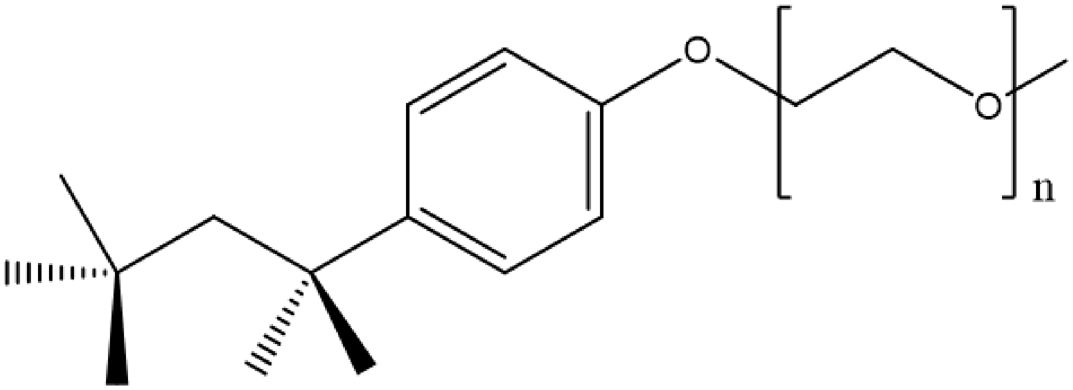

FIGURE 5.1: Triton X-100, n =9.5 on average.

Microemulsions prepared using Triton X-100 showed good stability in the presence of added salts, in most cases being able to reach 1 m concentrations. These MEs also did not require a cosurfactant as with the SDS based MEs. However they did require a much larger proportion of surfactant compared to the SDS MEs. The final composition used was 72 wt% distilled water, 1.33 wt% cyclohexane and 26.7 wt% Triton X-100 as this mixture showed good stability in the presence of added salt with 1m concentrations of LiCl being easily achieved.

In order for the ME EEI effect to be in play, the electrode had to be sufficiently hydrophobic. Electrodes were prepared as described in Chapter 2.10 with 9 wt% conductive carbon, 6 wt% PVDF as a binder. Both of these components are hydrophobic and so there is the possibility the the EEI could form on these surfaces, even though it may be less robust than on a carbonaceous surface.

Wetting tests of MEs in our lab showed interesting results. When water was placed on the surface of the electrodes it did not wet the surface fully. The MEs, however, appear to wet any surface regardless of its hydrophobicity.

The reason liquids wet, (or do not wet) a surface is due to the surface tension between the substrate and the liquid. A low surface tension means that it is favourable for the liquid to wet the surface whereas a high surface tension leads to beading of the liquid on the surface. MEs contain surfactants which are in the solution to reduce the surface tension between the aqueous phase and the oil phase. Therefore it is unsurprising that MEs wet any surface. The action of the surfactants reduces the surface tension regardless of the phase that preferentially adsorbs on to the surface and the hydrophobicity of that surface. As a result, wetting tests were not sufficient to establish whether the surface was sufficiently hydrophobic for the EEI to form. Instead electrochemical tests were performed to establish whether or not the EEI was forming on these electrodes.

For initial tests, the composition of the electrode slurries was kept the same as those in Chapter 2.10. If these were unsuccessful, then the composition would be altered to increase the hydrophobic content and encourage the formation of the EEI.

A further complication came from using Triton X-100 as the surfactant in the ME. SDS, the primary surfactant used in the MEs Chapter 4, has a small polar head group and a long non-polar tail. This leads to an EEI as shown in Figure 3.1. Triton X-100 however, has a small non-polar head group and a large polar tail (see Figure 5.1). This will lead to a much thinner EEI compared to the SDS based MEs. The water splitting suppression effect may be lessened compared to the SDS based emulsions as it may be easier for the water to traverse the oil layer and come into contact with the electrode.

In order to establish the extent of the EEI on the electrodes, cells with 1 M aqueous LiCl were constructed using the Anatase and V_2O_5 as described above. The results are shown in Figure 5.2. The water splitting onset at 1.9 V was similar to what was observed in Figure 4.3 which indicates that these electrodes did not have any more affinity for water splitting than the glassy carbon current collectors. If full cell tests showed a similar pattern to what was seen in Figure 5.2, the conclusion would have to be that the EEI did not form and something in the electrode composition would have to be altered.

5.4 Initial full cell tests

The first cells assembled with the electrodes and the Triton X-100 based ME showed very poor performance as shown in Figure 5.3. The discharge capacity was very low at 1.4 mA g^{-1} after 20 cycles and remained approximately constant over this time. The sharp drop in potential followed by a linear decrease upon discharge suggested that there

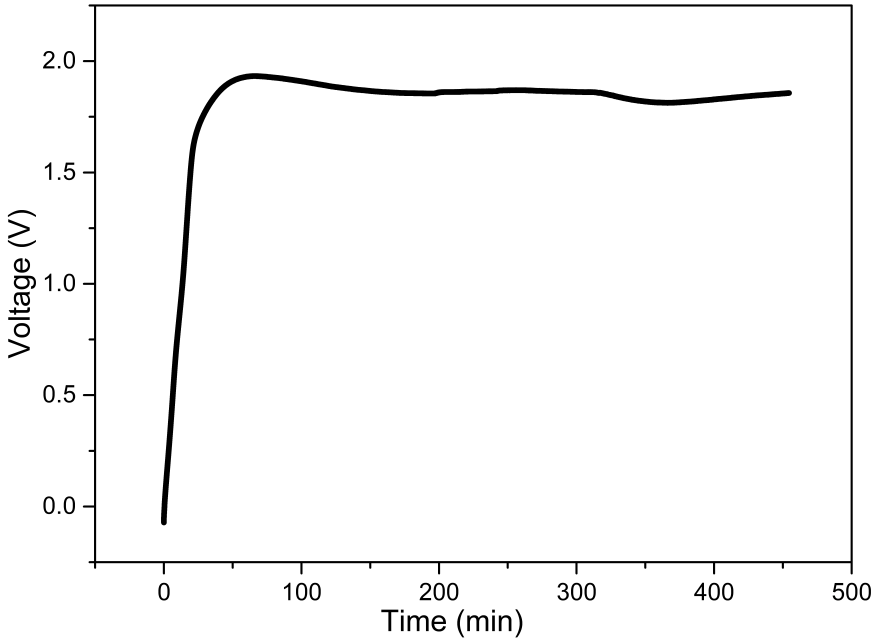

FIGURE 5.2: A test of 1 M aqueous LiCl using a TiO_2 anode and V_2O_5 cathode. A similar water splitting onset is observed in Figure 4.3.

is some redox activity, as a purely coulombic process would only have the linear decrease as seen throughout Chapter 4.

This result was observed over many cycles even after changing current rates, mass loading on electrodes and adjusting of the voltage cut offs and was consistent when cells were remade.

The solution to this problem involved a close examination of the EEI theory that had been well supported throughout the research so far. As mentioned in Chapter 4, for a decent capacitance to be observed, some charged species needed to adsorb onto the electrodes. It is still not clear exactly what is happening at the immediate electrode/electrolyte interface and how the hypothesised EEI model plays into it for supercapacitors, e.g. what the species is being adsorbed (if any). For an ion battery however, the conditions are much more rigorous. For the battery to function there must be intercalation of the active species into the electrode material. Otherwise, as the redox reaction proceeds, there is a charge imbalance at each end of the cell as electrons are pumped from one electrode to the other. Therefore the active species (in this case lithium ions) must traverse the EEI and reach the electrode for the cell to function.

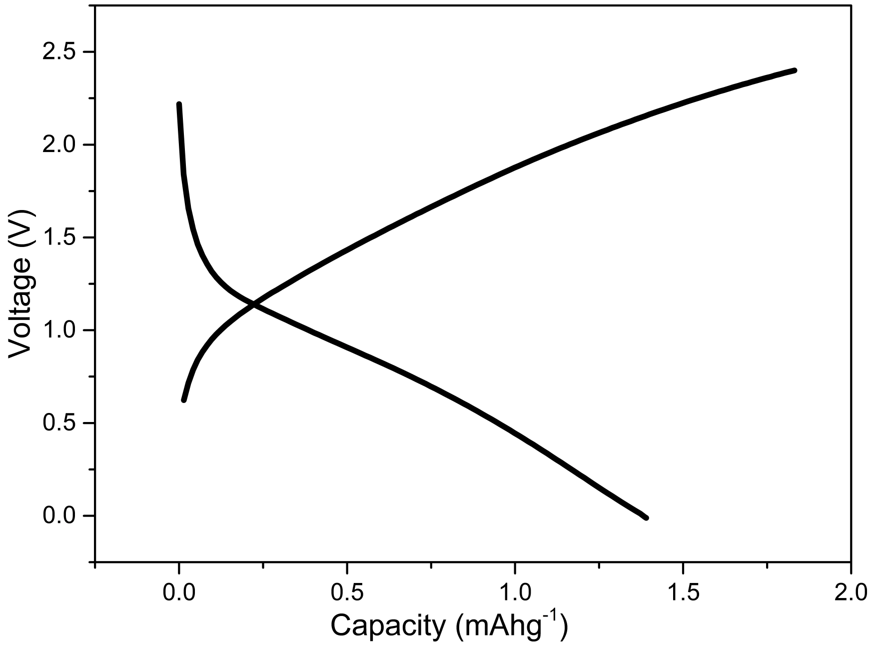

FIGURE 5.3: GCDC curve of one of the first Li ion batteries assembled using TiO_2 as an anode and V_2O_5 as a cathode. The current used was 50 mA g^{-1}

.

When lithium chloride is dissolved in the electrolyte, the lithium ions will exist as a tetraaqua complex $[Li(H_2O)_4]^+$. This species is has a relatively high charge density and its hydrogen bonding capability will mean that it is highly favourable for it to remain in the aqueous phase. It will also be highly unfavourable for it to move through the oil-rich EEI to reach the electrode. If the lithium ions are never reaching the electrode then no intercalation can occur so the battery cannot be charged or discharged.

A solution was devised using the methodology of a phase transfer catalyst. If the metal ions could be complexed with a ligand that would displace water and make a complex ion that was hydrophobic enough to penetrate the EEI, the ions would be able to reach the electrode and intercalate into it.

A ligand like tetrahydrofuran (THF) could result in an appropriately hydrophobic complex, however, water will be in vast excess in the ME. Even if the binding of THF and water were comparable in strength, the equilibrium will always favour the ligation of water, with a very low proportion of ions being completely complexed by THF due to this large excess of water. Therefore, the ligand has to bind strongly enough to fully displace water from the complex.

However, in order to intercalate into the solid electrode, the ligands must also de-complex from the ion. If the ligand was bound too tightly, then this desolvation process would be unfavourable and hinder the intercalation process. This rules out strong complexing agents like crown ethers or cryptands.

In order to effectively displace water while not binding too strongly to the ion, a ligand capable of forming a chelate could be used. When a ligand chelates a metal ion, it displaces multiple monodentate ligands at once which leads to a large increase in entropy, making the reaction more favourable. Using this chelate effect, the strong interactions of the water with the metal ions could be overcome without having to use a ligand that displaces water on bond strength alone.

The first family of ligands investigated that fit this criteria, being chelating ligands that will bind strongly to alkali metal ions, were glymes also known as glycol ethers. In particular, dimethoxyethane (DME) and bis(2-methoxyethly) ether (also known as diglyme) were used (see Figure 5.4).

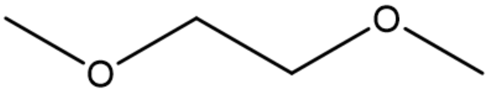

dimethoxyethane

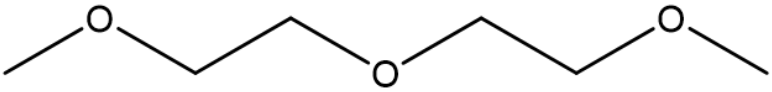

bis(2-methoxyethyl) ether

FIGURE 5.4: Structure of two glymes that were trialled as phase transfer catalysts to allow the metal ions to pass through the non-polar EEI

First, DME was added to the ME described in Section 5.3 to a concentration of both 5 and 10 wt%. At both of these percentages the emulsion destabilised immediately. Upon increasing the surfactant ratio or decreasing the oil content still no stable composition could be found. Thus DME was abandoned as a phase transfer catalyst.

The same was attempted with diglyme. Diglyme was added to give a final composition of 5 wt% and 10 wt%. Both MEs were stable. The final composition used was the 10 wt% version, as this would maximise the chance of a significant amount of the lithium being complexed. This meant that in solution there was a 1:1.2 molar ratio of diglyme to lithium ions. Diglyme complexes lithium in a tridentate mode to form a $[\mathrm{Li(diglyme)_2}]^+$ complex [119]. This means that a good proportion of lithium ions in the solution will exist as this bis complex. Ideally this ratio of liglyme to lithium would be raised even further to ensure all the lithium ion solution could form the bis complex. At higher diglyme concentrations the ME began to destablise. Therefore inital tests were done with a 10 wt% diglyme Triton X-100 ME with 1m LiCl. The electrodes used were TiO_2 as the anode and V_2O_5 as the cathode.

5.5 Cell tests - Diglyme

With the diglyme electrolyte, the assembled cells behaved very differently. The charge-discharge results of cycle 1, 50 and 100 are shown in Figure 5.5. What is noticeable is that the initial discharge capacity for cycle 1 has increased by a factor of 10 over what was seen without diglyme in Figure 5.3. Secondly, there was some evidence of redox activity in the first cycle. The inflection point around 1.25 V indicated that there was a redox process occurring and it was not purely a capacitive process. There is some evidence of the reverse process as well with some bowing in the discharge curve beginning at around 1 V.

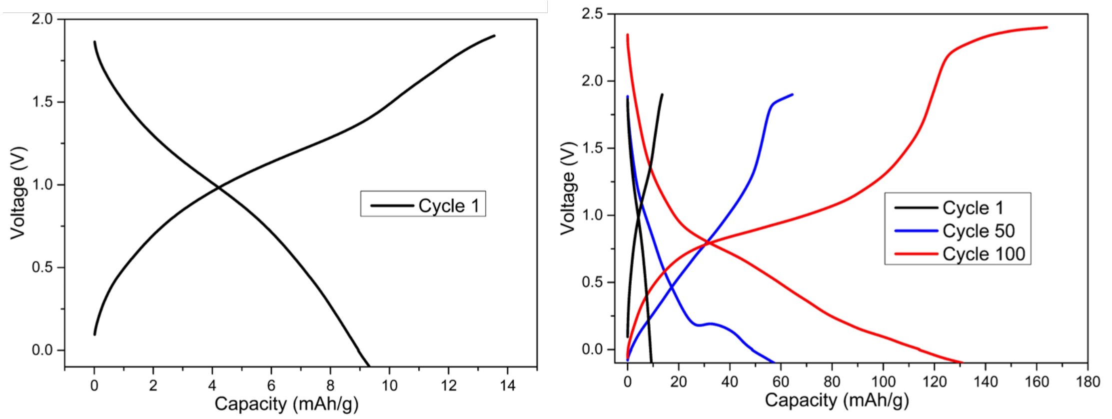

FIGURE 5.5: Left Cycle 1 and Right: Cycles 1, 50 and 100 of a lithium ion battery assembled with the diglyme-triton electrolyte. Charging and discharging rates were 50mA g^{-1} and the voltage cutoff was started at 2 V but was raised to 2.4V

Cycle 50 however, showed very unusual activity. Firstly, the discharge capacity had dramatically increased over the first 50 cycles. Usually it is anticipated that discharge capacity decreases after the first cycle. Potentially, as the cell was ”conditioned” in the first few cycles, a capacity increase might be expected, but having a sustained increase over the first 100 cycles was definitely unusual.

The other point of note about cycle 50 is the region around 0.25 V in the discharge curve, where the voltage increased slightly. As described in Chapter 2.10 during a discharge, the voltage of the cell is adjusted until the discharging current is met. In a discharge, the potential difference between the two electrodes is lowered as this drives current in the desired direction. To have the voltage increase in such a manner during a discharge was most likely related to a phase change within one of the materials. As it underwent this phase change, it might be easier for lithium ions to move in or out of the structure which meant that current might start flowing faster for a given voltage. To meet the required current, the voltage had to increase to slow down the current rather than decrease to speed it up, which is usually the case.

This increase in capacity might also be attributed to improved wetting of the electrode. It is common for the first few cycles of an ion battery to show irregular capacities [120–122]. This is often referred to as a conditioning step where the cells are cycled a few times to make sure the electrolyte has fully permeated the electrode. SEIs are also formed during these first few cycles which stabilise the chemistry of the cell. Once the electrode is fully wet and any SEIs formed, the entire electrode is electrochemically accessible which means the capacity should be stable at its full value. Usually this takes less than 5 cycles.

This wetting can also be achieved by letting cells rest once fully assembled. This is obviously less viable industrially, but is appropriate on a lab scale. In order to see if letting the cells rest had an effect, 2 cells were assembled, one was put to cycling immediately whereas one was left for 48 hours before being cycled. Both cells returned similar results and so the conclusion was that these cells required *electrochemical* conditioning rather than just letting the electrode fully wet.

The most likely explanation for this outcome was the state of the electrode materials. A commercial lithium ion battery is assembled in the discharged state with lithium cobalt oxide as a cathode and graphite as an anode. During the first charge the lithium ions are de-intercalated from the cobalt oxide and intercalated into the graphite.

In this cell, using a V_2O_5 cathode and TiO_2 anode, the anode was in the discharged state but the cathode was in the charged state. This mismatch meant the capacity would naturally be lower for the cells as assembled. During the initial charge, lithium ions from the solution should be intercalated into the TiO_2, however this process also required the titanium centres to be reduced with electrons. Normally these electrons would come from the cathode but since it was already in the fully charged state it had no more electrons to donate. As a result, intercalation into the anode was initially limited and could only be driven by irreversible Faradic reactions at the cathode.

Once a small amount of intercalation had occurred at the anode, this could drive intercalation into the cathode upon discharge but only to a similar extent as what was driven into anode during the initial charge. If more and more intercalation driven by irreversible side reactions happened each cycle and the reversible capacity established in previous cycles carried over, then the capacity would increase over time. This would have resulted in a slightly lower coulombic efficiency over these cycles which was observed.

How the charge and discharge capacities as well as the coulombic efficiencies of these cycles developed is presented in Figure 5.6. The capacity increases in a roughly exponential manner over these cycles. The coulombic efficiency also generally increased from around 80 % to 90% over this time frame. Ideally the coulombic efficiency would be as close to 100% as possible. The reason for the low value is probably a combination of internal resistance of the cell and some irreversible faradaic reactions occurring. These were unlikely to be solvent decomposition as the efficiency is roughly constant. If the efficiency was more irregular and much lower, then that would be a sign solvent decomposition was occurring.

By cycle 100 this process was no longer occurring to the same extent, but the capacity had more than doubled again to reach 130 mAhg^{-1}. This is among the highest capacities ever recorded for an aqueous ion battery using intercalation electrodes.

At cycle 80 the upper voltage cut off was raised to investigate the voltage stability of the system. As the voltage cut off is raised, it is expected that the discharge capacity increases. As it takes more charge being stored to reach a higher voltage, when the

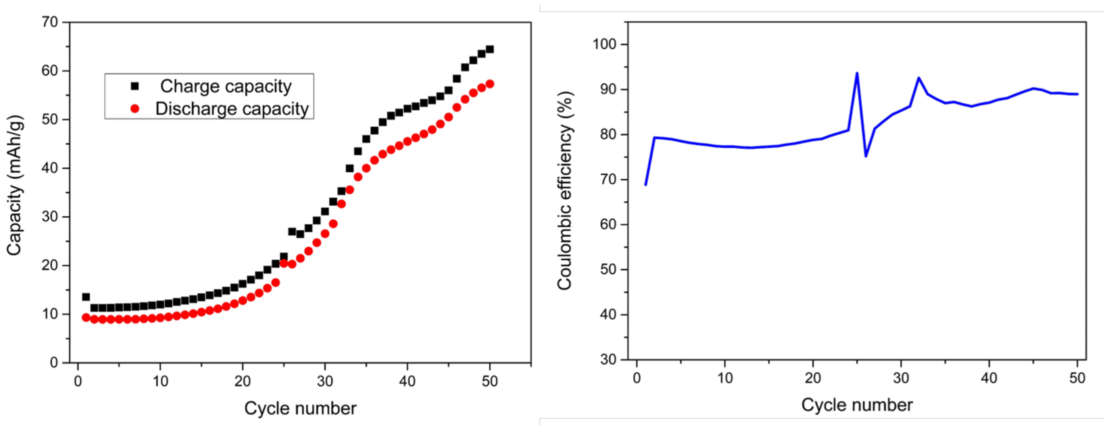

FIGURE 5.6: Left: The charge and discharge capacities of the first 50 cycles for the lithium ion battery presented in Figure 5.5 Right: the coulombic efficiency of those cycles

cell is discharged, there is more charge stored so the discharge capacity is higher. This battery was able to be charged to 2.4 V without evidence of solvent splitting though the coulombic efficiency of these cycles did drop to 80% on average, indicating that some more irreversible side reactions may have been occurring.

GCDC experiments were also carried out to see the rate capability of this battery. By increasing the rate to 500 mA g^{-1} it was expected that the capacity would decrease. A faster current rate means that the rate of the reactions is forced to increase. If reactions are slow such as with solid state diffusion, then they will not be able to keep up with the faster current rate which decreases the capacity. If the reactions occurring are reversible in nature, the capacity should be regained upon slowing the current rate down to where it originally was. This is shown in Figure 5.7

Upon increasing the current rate, the discharge capacity did indeed decrease from between 125 and 150 mAhg^{-1} to 50 mAhg^{-1}. Upon decreasing the current rate back to 50 mA g^{-1} the capacity returned to the value that it was before. The coulombic efficiency of the cycles at the fast current rate was also much higher (close to 100%) compared to the approximately 80% efficiency of the slower current rate cycles. This indicated that maybe the loss of efficiency was due to unwanted side reactions. At higher current rates, these have less time to occur than at slower current rates and so are seen less. It is hard to determine what these side reactions were exactly but from the shape of the curves they were probably not gas evolution or electrolyte breakdown as those features would be very distinctive (wavy lines in GCDC graphs).

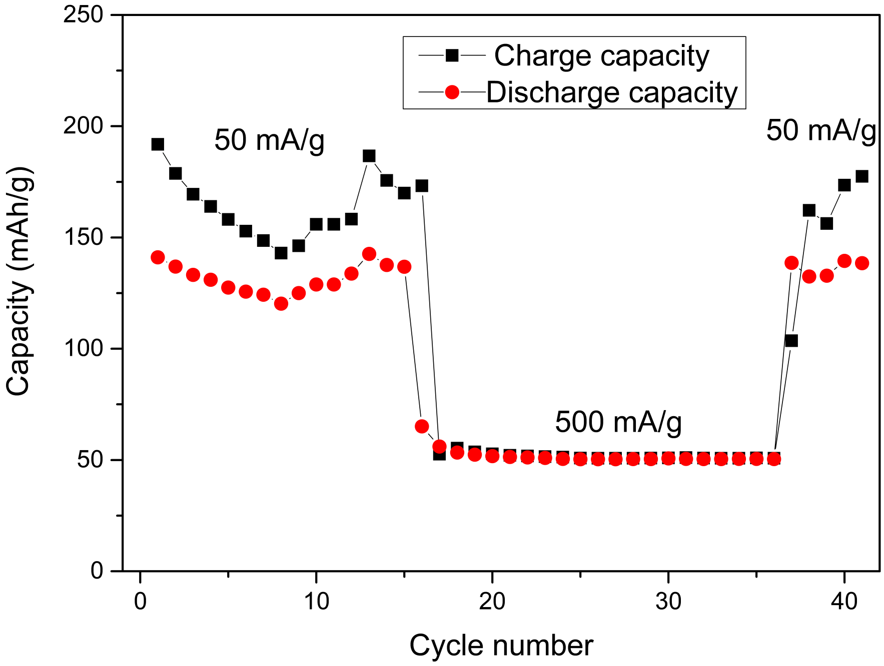

FIGURE 5.7: The results of changing the current rates in the lithium ion battery from 50 mA g^{-1} to 500 mA g^{-1} and back again. It was observed that the capacity was regained after re-lowering the current rate which was a sign of reversibility

Looking at the GCDC curves for cycles at the two current rates it was clear that the redox reactions were still occurring at both current rates. In Figure 5.8, it was seen that the curves take the same basic shape when the cell is charged at 50 mA g^{-1} and 500 mA g^{-1}.

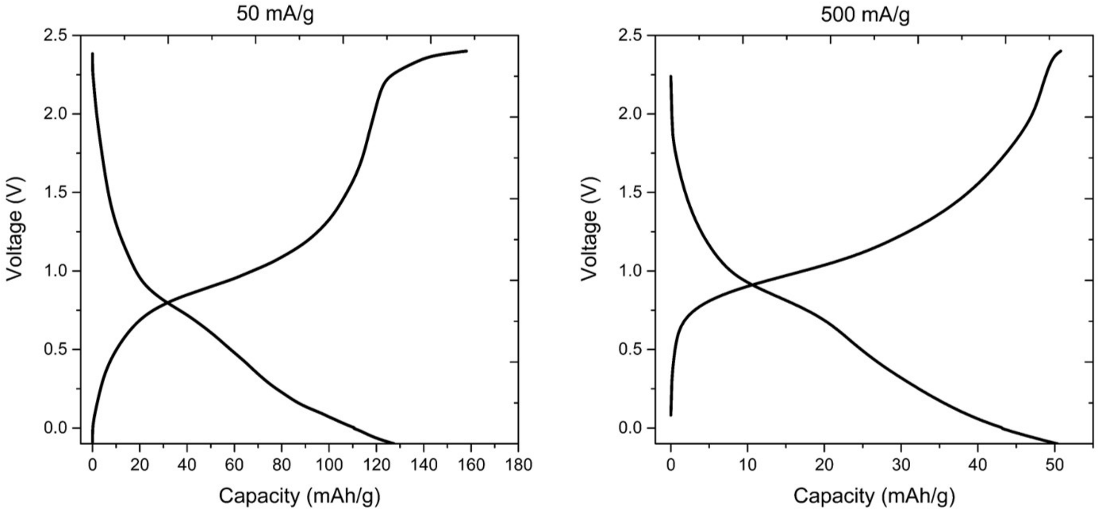

FIGURE 5.8: Side by side comparison of GCDC curves of a lithium ion battery charged and discharged at 50 mA g^{-1} and 500 mA g^{-1}. It was clear that the same redox reactions are occurring, there were just less of them occurring.

One final observation from these curves was that the apparent potential of the redox reactions is changing. In cycle 50, there was an inflection point at approximately 1.8 V where as in cycle 100 this same inflection is seen at 2.2 V. The plateau at 0.25 V in cycle 50 appeared to shift upward in potential into cycle 100, it became less defined but appears to begin around 0.8 V.

It is likely that at least one phase change is accompanying the intercalation reactions at each electrode. It is possible that one or more of these phases has a higher lithium ion conductivity than the initial phases. This might reduce the over-potential associated with the redox reaction leading to a different observed voltage in the GCDC curves.

Using pre-lithiated electrode materials would allow for a good comparison and an evaluation of the validity of this hypothesis. As previously mentioned, obtaining these materials proved difficult and synthesising them in-house was beyond the scope of this work.

Another technique that could be used to validate this hypothesis would be *in situ* or *in operando* X-ray diffraction (XRD). This technique probes the evolution of the electrode materials as the cell is charged and discharged. It reveals things like phase changes or lattice parameters. However, this is still a relatively specialised technique and is not widely available yet.

5.6 Cyclic voltammetry

In order to investigate the development of the reactions inside the cell, cyclic voltammetry studies were conducted, the results of which are summarised in Figure 5.9. These results agree with what is shown in the GCDC curves shown in Figure 5.5. Before cycling, an oxidation peak was observed at 1.1V, however there was no corresponding reduction peak. This is likely the same redox event that is seen in the first cycle in Figure 5.5. However in the CV the lack of a reduction peak was unexpected.

As outlined in Chapter 2.10, the cathode was connected as the working electrode and the anode was connected as the counter and reference electrode. This means that the forward scan in the CV is equivalent to charging the cell and the backward scan is equivalent to discharging the cell. Therefore an oxidation peak in the CV implies an oxidation was occurring at the cathode and a reduction was occurring at the cathode.

This observation is consistent with the reasoning in Section 5.5. Since the anode was in the discharged state and the cathode is in the charged state, it is expected that no complete redox pair would be observed. This evidence suggests that the intercalation at the anode is being driven by an irreversible oxidation at the cathode. This oxidation at the cathode cannot be from lithium deintercalation as there is no lithium in the cathode as assembled.

This result also implies that the electrochemical window of this cell is potentially cathode limited. If the window was anode limited then a reduction peak might be seen in the CV corresponding to intercalation at the cathode driven by an irreversible oxidation at the anode. Since lithium intercalation into V_2O_5 is facile, there must be oxidation reactions that can occur at the anode within the potential range scanned. Further investigation is required to confirm this hypothesis.

The CV after cycling however was markedly different. Firstly, the current density had increased substantially, by about a factor of 10. Also 3 redox events were now visible, all with corresponding reductions. There were oxidation peaks at 0.25 V, 1.1 V and 1.75 V, with reduction peaks visible at 0.15 V, and less noticeable peaks at 1 V and 1.6 V.

The difference in voltage of the oxidation and reduction peaks (known as peak separation) of 100 mV for all of these peaks indicated good electrochemical reversibility of each of these processes. However, the ratio of peak currents, which is another measure of the reversibility tells a different story. For the two higher voltage sets of peaks, the ratio of peak oxidative current to peak reductive current is roughly 2:1. For the lower voltage peak the ratio of peak oxidative current to reductive current was approximately 1:3.

What was also noticeable from the CVs was the behaviour at approximately 2 V in the two scans. In the first cycle the current starts to increase at approximately 1.8 V in a manner that suggests solvent decomposition, or at least it indicated that it was near/over the electrochemcial window of the system. However, after cycling that is no longer the case. This could be indication of the formation of an SEI layer. Perhaps on sites where the EEI is less robust some side reactions are allowed to occur which

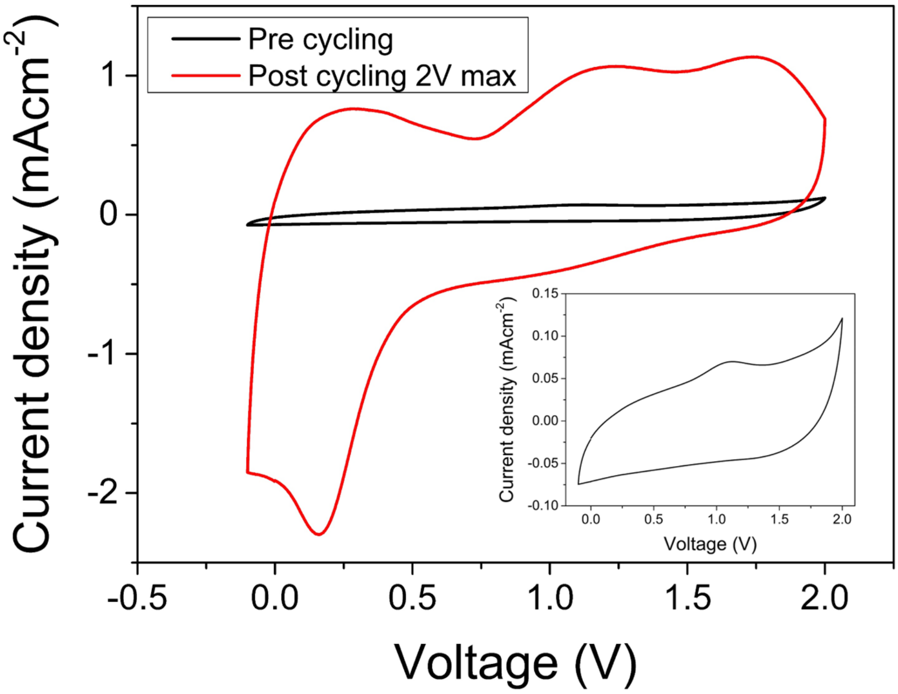

Figure 5.9: Cyclic Voltammograms run on freshly assembled cells (that had sat for 48 hours) and a cell that had been cycled 50 times. Inset is a zoomed in version of the precycled scan. These scans were recorded at 50 mV s^{-1} using a two electrode set up with the cathode (V_2O_5) as the working electrode and the anode (TiO_2) as the counter and reference electrode. Cycles presented are the third cycle in a set of 3

causes an SEI to form. If this SEI was sufficiently hydrophobic, then it could improve the robustness of the EEI and strengthen the effect of the extended window.

By extending the CV to 2.4 V as seen in Figure 5.10 it can be seen that there is an increase in the current at around 2.2V which indicates that this may in fact be the stability limit of the cell. This may be the reason for the lower coulombic efficiencies when the cell was cycled with this higher cut off. The GCDC tests however, show that there is some reversible capacity gained within this voltage range. If it were purely beyond the stability limit of the cell then the extra (non-reversible) faradaic reactions occurring would increase the charge capacity dramatically. However, the discharge capacity would only be expected to increase minimally as the undesired faradaic reactions are assumed to be non-reversible and the extra capacity that arises from coulombic reactions over this extra 0.4 V would be small.

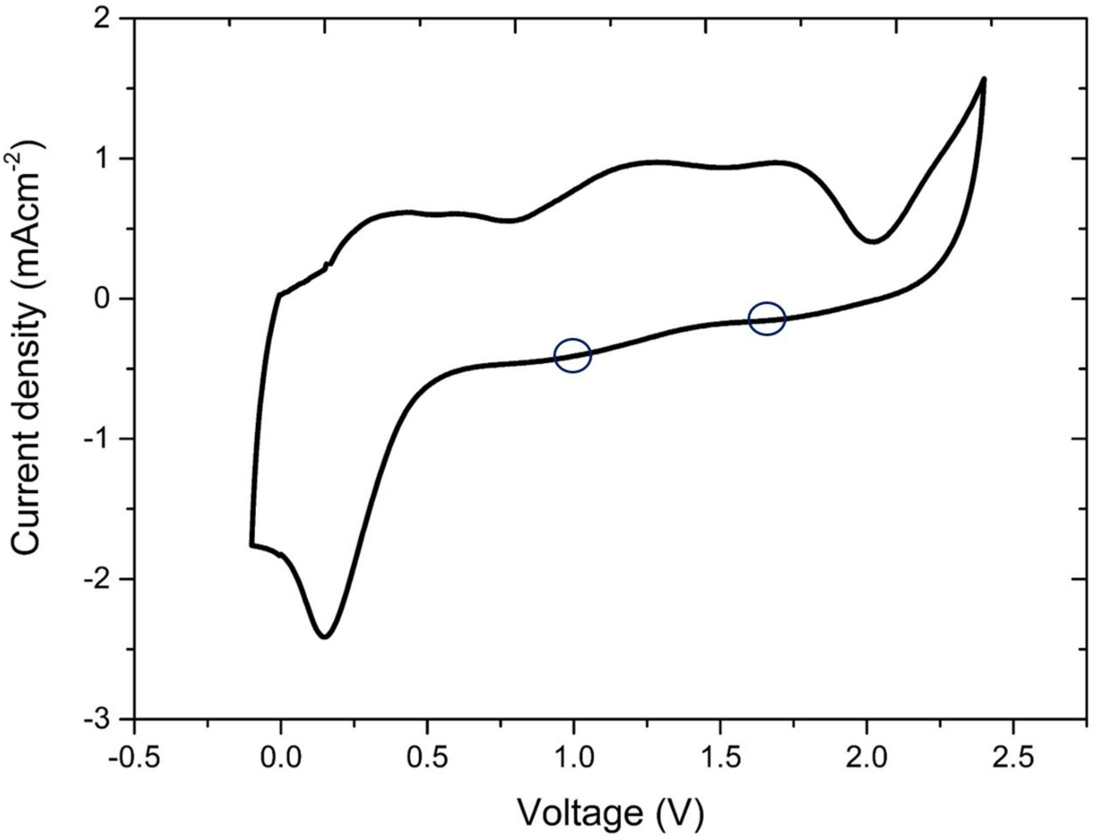

FIGURE 5.10: Cyclic Voltammograms of a lithium ion battery run with a higher voltage limit of 2.4 V run at 50 mV s^{-1}. The increase in current around 2.3 V is indicative of solvent splitting but more tests would be required to confirm this.

5.7 X-ray diffraction

With the electrochemical tests showing evidence of both electrodes being active, attention turned to other techniques that can give insight into the underlying mechanism of the cell. Two cells were constructed with the same components as the other cells discussed so far in this chapter, and cycled to a maximum voltage of 2.4 V at 50 mA g^{-1} for 100 cycles. After 100 cycles, one cell was recharged to its maximum voltage (2.4 V) then disconnected from the battery analyser and disassembled immediately. Another cell was left in the discharged state (at 0 V) and disassembled after being disconnected. Electrodes were washed with distilled water and left to dry overnight. XRD patterns for both the anode and cathode in both the charged and discharged state were then collected and compared to patterns of the pristine electrodes.

5.7.1 Vanadium pentoxide

The pattern of pristine V_2O_5 is shown in Figure 5.11. The two reflections that are marked at 26 and 55 degrees 2θ belong to the graphite foil that the active material was pasted on (See Appendix A). These reflections were observed in all scans of all materials and so are ignored.

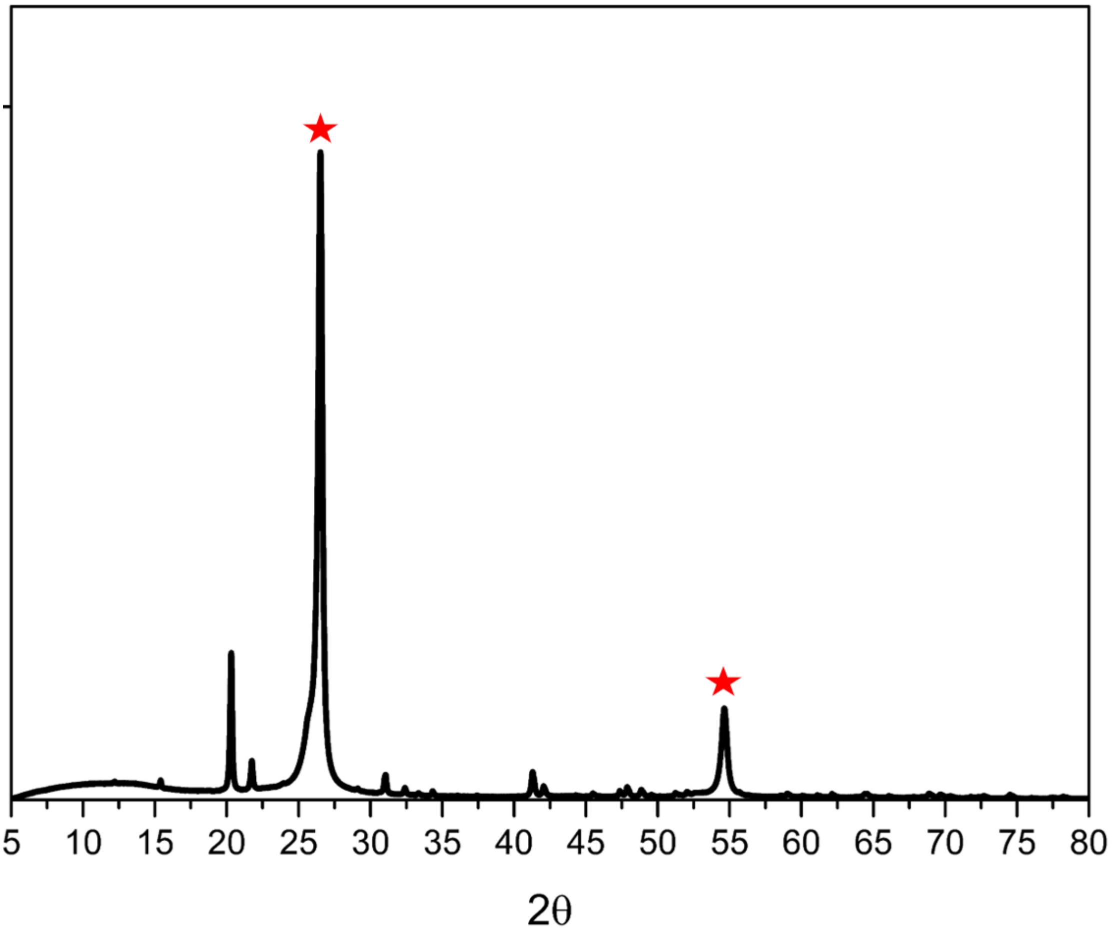

Figure 5.11: The full XRD scan of a pristine vanadium pentoxide cathode from 5 to 80 degrees 2θ at a scan rate of 0.125 degrees per minute. The two marked reflections are of the graphite foil on which the material was pasted

By magnifying a portion of this pattern and comparing it to charged and discharged cathodes changes in the structure can be observed. This is shown in Figure 5.12.

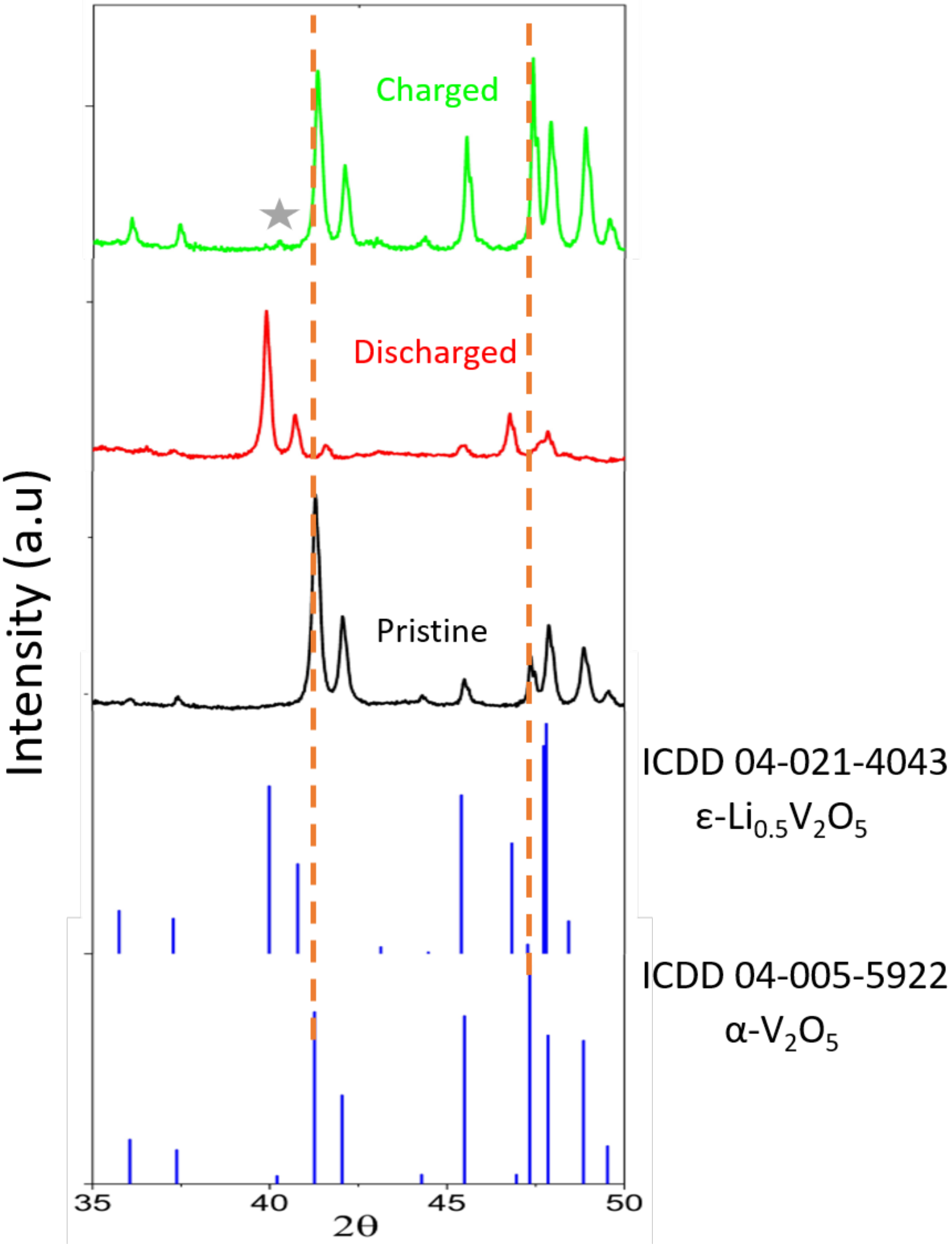

Figure 5.12: A combined XRD pattern of V_2O_5 cathodes in the charged, discharged and pristine states. Two reference patterns are also included for ε-$Li_{0.5}V_2O_5$ and V_2O_5 to allow for comparison. Orange dotted lines are added so that the slight contraction of the lattice of the charged sample compared to the pristine sample is more visible.

First, the pattern of the pristine sample matches well with the reference pattern 04-005-5922 from the ICDD database. This is of the orthorhombic or α phase of vanadium pentoxide. For this phase, ions are generally intercalated into the octahedral sites within the a-b plane [123].

As the V_2O_5 is acting as a cathode, the lithium ions should intercalate into the structure during discharge and then de-intercalate during charge. Therefore, if no irreversible phase change is occurring during cycling, the pristine and charged samples should be similar to each other. This was observed. The relative reflection intensities were slightly different, for example the reflection at 45.5 degrees 2θ, which represents the [141] plane, was more intense in the charged sample than in the pristine sample.

There reflections in the charged sample were also slightly offset to higher 2θ from those in the pristine sample (see the dotted lines in Figure 5.12). In order to correct for any shifts due to a misplaced sample in the detector, the reflections in all patterns were referenced to the carbon foil reflection at 26.3 degrees 2θ. This offset would represent a slight contraction of the lattice relative to the pristine sample which would be unexpected. It could also be the result of a variation in the thickness of the coatings.

The discharged sample matched well with the reference pattern 04-021-4043 from the ICDD database shown in Figure 5.12 which is for ε-$Li_{0.5}V_2O_5$. In particular reflections at 41.2 and 42 degrees 2θ in the pristine pattern (which represent the [002] and [012] planes respectively) shift to 40 and 40.8 degrees 2θ (which again represent the [002] and [012] planes). This move to lower 2θ represents an expansion of the lattice along these planes, which is consistent with lithium ion intercalation. This is strong evidence that intercalation is indeed occurring at the cathode during discharge and de-intercalation is occurring upon charge.

In the charged sample there was still some evidence of some the ε-$Li_{0.5}V_2O_5$. for example, the marked peak in Figure 5.12. This is expected as each charge cycle may not fully extract all the lithium from the cathode and leave behind some of the lithiated phase.

5.7.2 Titanium dioxide

The titanium dioxide used in these studies was the anatase phase as this is what was available. Unlike the V_2O_5, no change is visible in the XRD pattern for this material as seen in Figure 5.13.

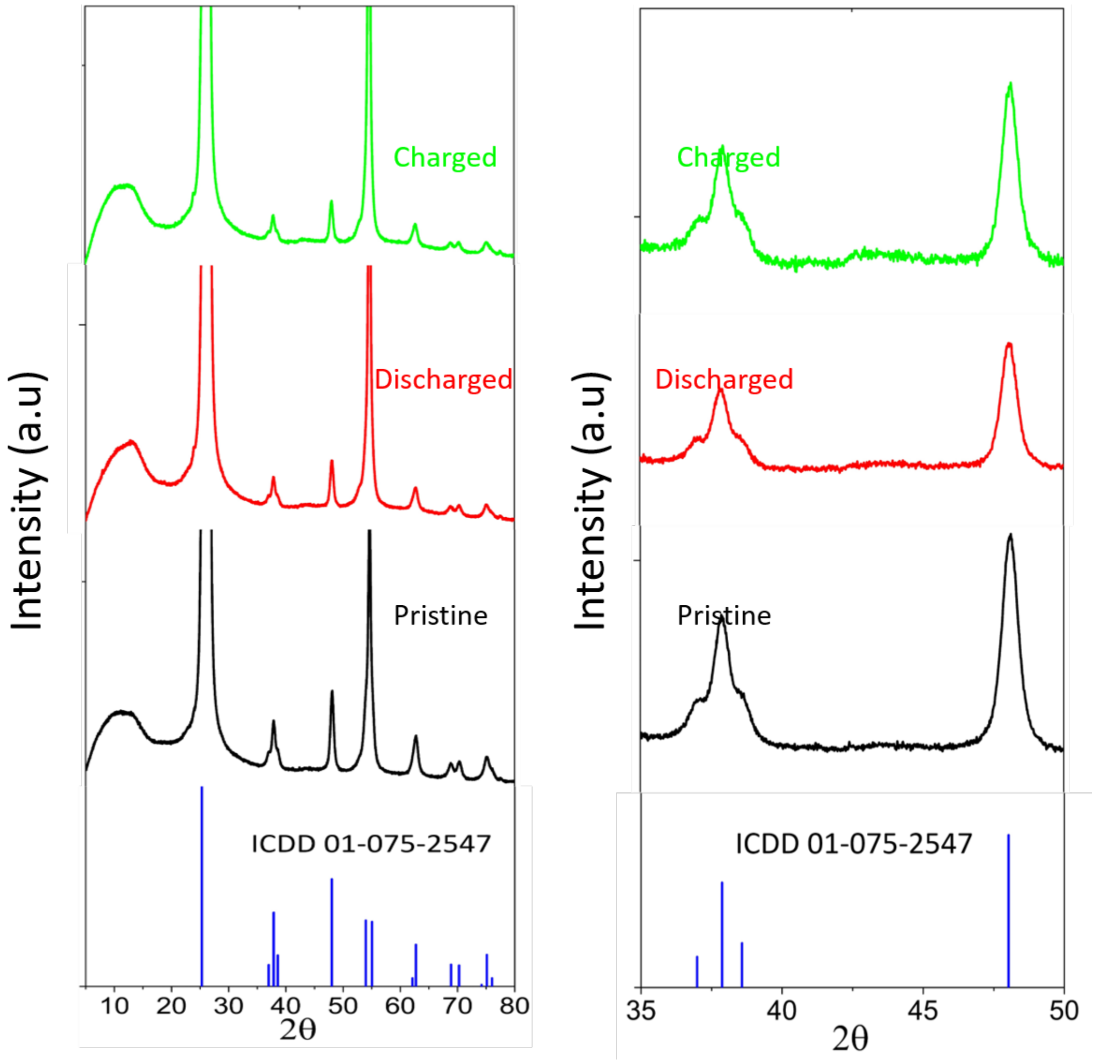

FIGURE 5.13: XRD patterns of TiO_2 in the pristine, charged and discharged state. These patterns all look identical to each other and correlate well to the anatase pattern shown. Both charged and discharged electrodes were taken after 100 cycles.

The patterns did correlate well with the anatase pattern shown in Figure 5.13. Given that change is observed in the cathode and there is good electrochemical evidence that there is activity at both electrodes during cycling, these results are unexpected. This does not necessarily disprove that there is intercalation at the electrode is occurring.

Despite lithium titanate being a better starting anode material for lithium ion batteries, the intercalation of lithium into anataste TiO_2 has been studied previously [124, 125]. Ren *et al.* synthesised mesoporous anatase microparticles and studied the XRD patterns as the amount of lithium intercalation increased [126].

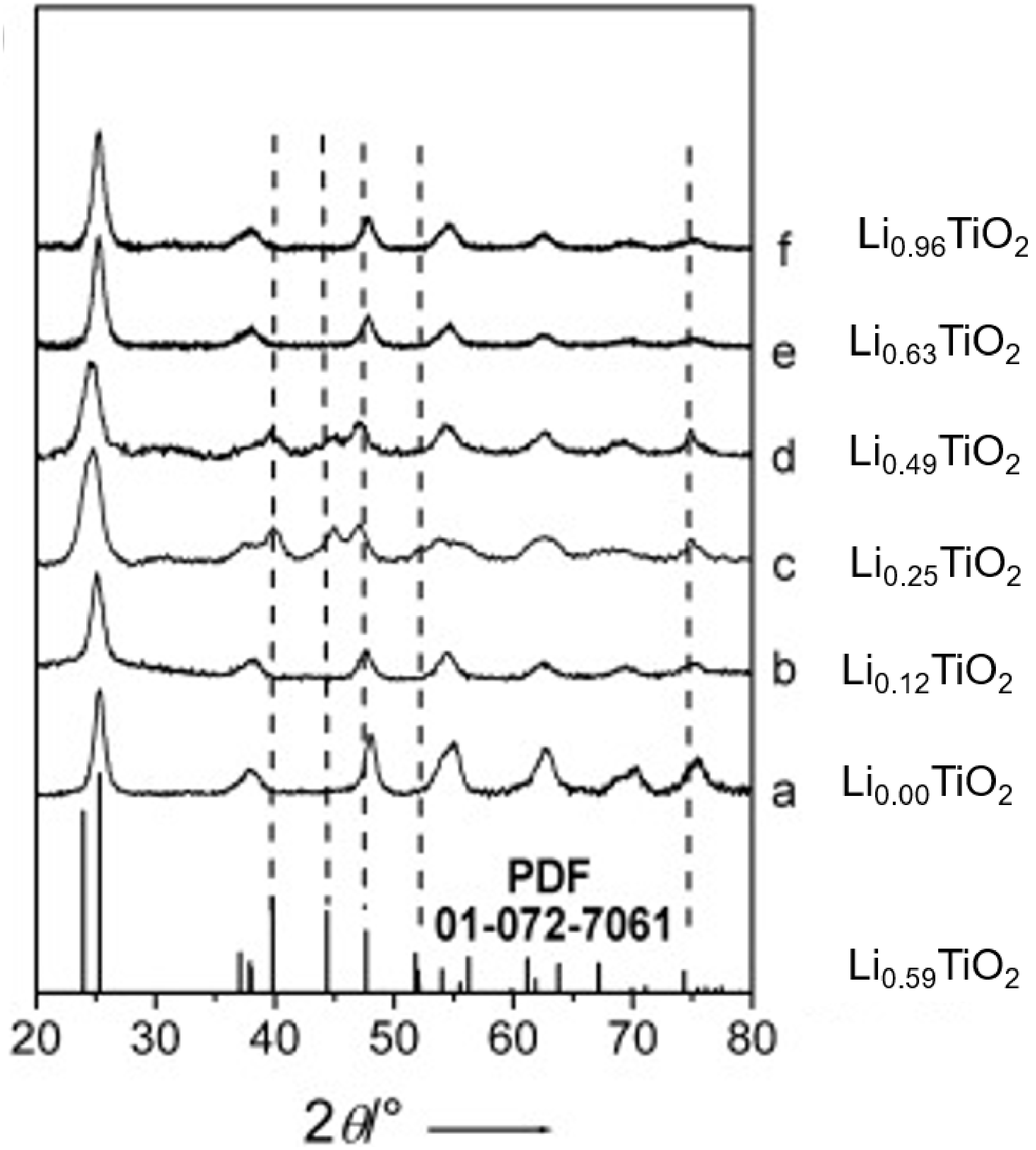

FIGURE 5.14: XRD patterns of mesoporous anatase TiO_2 particles as a function of lithium intercalation. Reproduced from "Lithium Intercalation into Mesoporous Anatase with an Ordered 3D Pore Structure" Angew. Chem. Int. Ed., Volume: 49, Issue: 14, Pages: 2570-2574, with minor alterations with permission from John Wiley and Sons.

While the reference pattern in Figure 5.14 does not match with the reference pattern in Figure 5.13, some conclusions can still be drawn. First, as the proportion of lithium inside the structure increased, the changes in the XRD pattern were minor. In particular the reflection at just below 45 degrees 2θ appeared and disappeared over this process. It is noticeable in Figure 5.14 that pattern a, that has no lithium in the structure, and pattern f which has 0.96 lithium atoms per TiO_2 unit, have remarkably similar reflection positions. The intensities in the reflections were different however. In Figure 5.13, the intensities of the peaks were slightly different to each other which is in agreement to the finding shown in Figure 5.14. It is difficult to claim the different intensities in Figure 5.13 as significant however, as there will be variation exactly how much of the material is exposed to the X-rays in each sample due to slight variations in coating thickness or positioning within the instrument which could also give the same result.

To conclusively show intercalation into the anode is occurring, several techniques are available. First, *ex Situ* XRD patterns could be collected at various states of charge as was done by Ren *et al.*. This is a time consuming pocess but it would allow for the subtle changes that occur to be observed. Second, *in situ, operando* XRD would allow patterns to be collected in real time as the cell is charging and discharging. This is a very advanced technique and currently only available in a few select places globally. Finally, X-ray photoelectron spectroscopy (XPS) could confirm the presence of lithium and observe the oxidation state change of the titanium centres from +4 to +3 in the charged state.

While the difference in patterns was not as noticeable as it was with the V_2O_5 cathode, given the results of Ren et al, this similarity does not rule out intercalation occurring at the anode as well.

5.8 Scanning electron microscopy

XRD will pick up bulk structural changes and not surface changes, since SEIs are a surface phenomenon, another technique was required. Scanning electron microscopy (SEM) can be used to see the surface of samples, and can be used to suggest the formation of an SEI. In reality however, proving the formation of an SEI requires much more detailed analysis. [13]

Samples of both electrodes were taken in both a pristine and discharged state after having been cycled at least 100 times to 2.4 V. No change was immediately obvious between the two samples for either electrode.

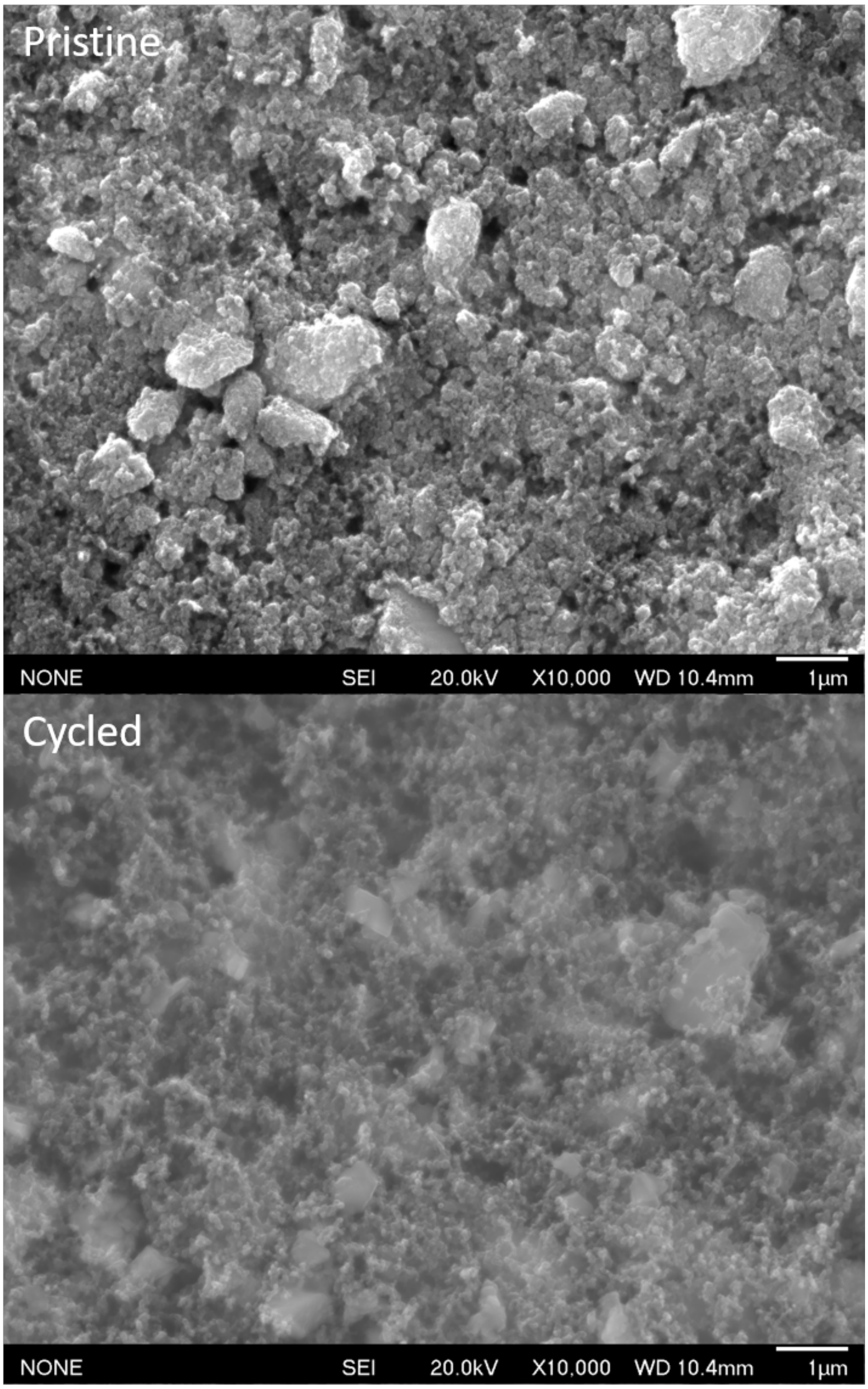

FIGURE 5.15: SEM images of TiO_2 electrodes in a pristine state and in a cycled state. There was no apparent difference in the morphology of the two samples.

Figure 5.15 shows the TiO_2 anodes in a pristine state and a cycled state. There is no visible difference in the surface of the two samples. It is seen that the TiO_2 particles have a wide size distribution. The smaller particles visible are the Super-P conductive carbon present in the slurry. The particle size between the two samples was roughly similar and there was no evidence of any films forming on this electrode.

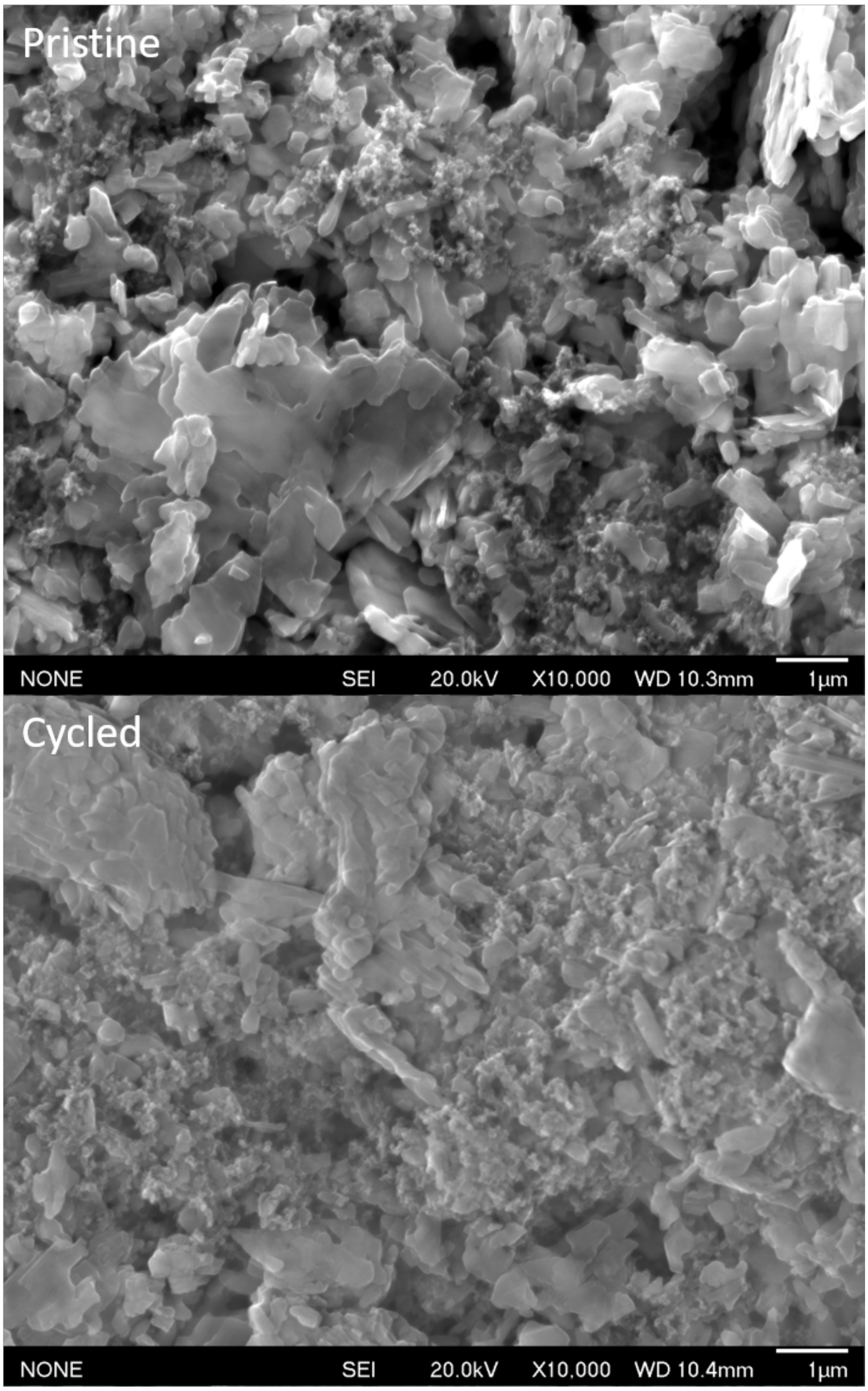

FIGURE 5.16: SEM images of V_2O_5 electrodes in a pristine state and in a cycled state. Again, there was no visible difference in the morphology of the two samples.

Likewise for the V_2O_5 electrodes (Figure 5.16) there is no apparent difference between the two samples in terms of the surface morphology.

These observations do not on their own rule out the formation of an SEI film as it may be very thin or it may have been damaged during sample preparation. Transmission electron microscopy could be a tool to investigate this further however these studies were not performed due to the lack of evidence of an SEI in the SEM images.

Since the surface of the electrode is central to the function of the ME electrolytes, how the SEI and EEI develops over time will have to be investigated in greater detail in future studies.

5.9 Comparison to literature

No cell has ever been made with this combination of anode and cathode. One example does exist of a TiO_2-V_2O_5 composite by Zhou *et al.*, [10] however in this work the TiO_2 was there as a suppourt only and provided no capacity. However both of the electrode materials can be examined individually.

V_2O_5 has been studied extensively as a cathode material for lithium ion batteries [127–130]. Three separate insertions and corresponding phase transformations that can take place.

$$V_2O_5 + 0.5\,Li^+ + 0.5\,e^- \rightleftharpoons \varepsilon\text{-}Li_{0.5}V_2O_5 \tag{5.1}$$

$$\varepsilon\text{-}Li0.5V_2O_5 + 0.5\,Li^+ + 0.5\,e^- \rightleftharpoons \delta\text{-}LiV_2O_5 \tag{5.2}$$

$$\delta\text{-}LiV_2O_5 + Li^+\,e^- \rightleftharpoons \gamma\text{-}Li_2V_2O_5 \tag{5.3}$$

In CV studies in the literature, the first two peaks are almost always seen, whereas the third peak is seen less often due to an apparent lower reversibility of this step [12]. The redox activity of V_2O_5 is best seen in the work by Zhou *et al.*, [10] in Figure 5.17.

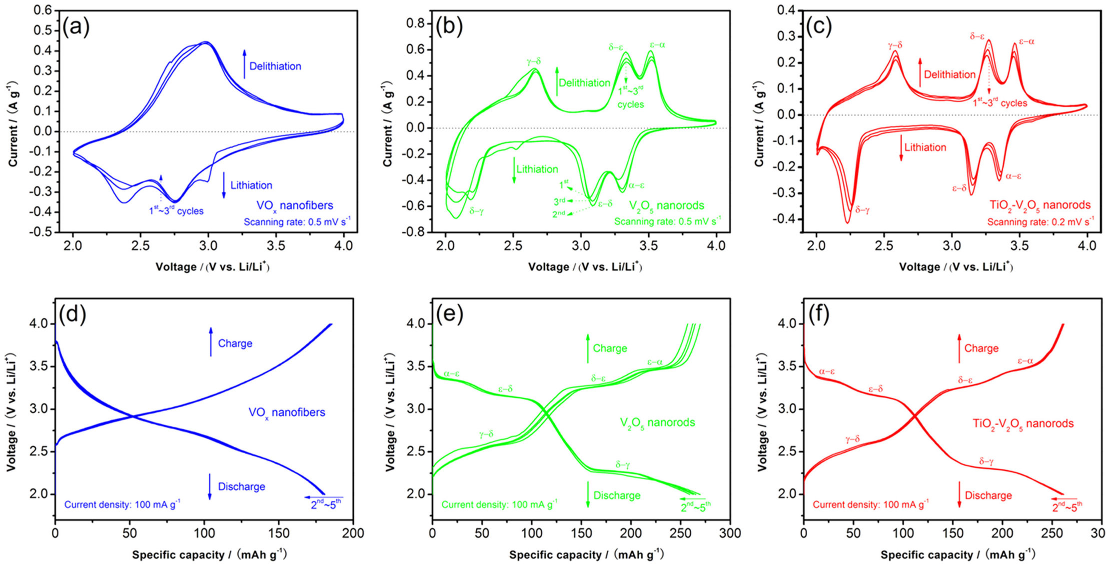

FIGURE 5.17: CV results and corresponding GCDC curves for VO_x Nanofibers (the precursor material in this study) in blue. V_2O_5 Nanoribbons in green and the TiO_2-V_2O_5 nanoribbons which was the focus of the study. Reprinted from A scalable strategy to synthesize TiO2-V2O5 nanorods as high performance cathode for lithium ion batteries from VOx quasi-aerogel and tetrabutyl titanate, Ceramics international Vol. 43 Issue 15, Zhou *et al.*, 12689-12697, Copyright (2017) [10], with permission from Elsevier.

From these results it can be seen that there are 3 redox peaks associated with lithium intercalation into V_2O_5. The two reactions at higher potential appear to be more reversible than the lower potential reaction as indicated by the peak separation. Peaks that are more separated are generally less reversible.

The potential of the three oxidation peaks from Figure 5.17 are 2.6 V, 3.25 V and 3.5 V (all vs. Li/Li^+). The oxidation peaks in Figure 5.10 are 0.6 V, 1.2 V and 1.75 V. The voltage separation between the first and second peak are similar but the third peak in the current work is shifted to higher potential than might be expected. This could be because the two higher potential peaks in Figure 5.10 overlap somewhat due to the scan rate used. A slower scan rate can help separate peaks and make them more well defined, especially in battery research where redox process in solid electrodes can be quite slow compared to solution based electron transfer.

What is also of note is that the reduction peak at 2.25 V in Figure 5.17 is also much larger than the corresponding oxidation peak, similar to Figure 5.10. This gives a rough indication of where the potential of this cell is relative to Li/Li^+. The peak separation of the low potential couple in Figure 5.17 is 335 mV whereas in Figure 5.10 it is only 150 mV which suggests that this 'irreversible' reaction is more reversible in the ME system than in non-aqueous solvents.

When it comes to comparing the GCDC curves for this cell it is seen in Figure 5.17 that three distinct plateaus are observed in both the charge and discharge curves at the correct potentials. This is not the case with the current results shown in Figure 5.5 where in cycle 100 only one charging plateau is observed at approximately 1 V and the discharge profile has no well defined plateaus. The curve in Figure 5.5 is more reminiscent of the $\mathrm{VO_x}$ (blue) curves in Figure 5.17 which show similarly undefined peaks. CV results do not always agree with GCDC curves, one method can often reveal somewhat well defined redox process that are not seen in the other method.

Finally, the capacity of the cells shown in Figure 5.17 is higher than than what recorded for the cell in Figure 5.5. As with all ion battery cells in this work, the anode was in large (5x) excess in terms of loading to make sure its potential remained relatively constant and so the capacity was known to be cathode limited.

The capacity of a battery follows the following relationship:

$$\frac{1}{C_a \times m_a} + \frac{1}{C_c \times m_c} = \frac{1}{C_{total} \times m_{total}} \tag{5.4}$$

Where $\mathrm{C_a}$ and $\mathrm{C_c}$ represent the specific capacitance of the anode and cathode respectively and $\mathrm{m_a}$ and $\mathrm{m_c}$ represent the mass loading of the anode and cathode respectively. As the mass loading of the anode increases, the first term in Equation 5.4 becomes less significant and the capacity is solely influenced by the cathode. In this special case the $\mathrm{m_{total}}$ term on the right hand side of Equation 5.4 is treated only as the mass of the cathode.

The theoretical capacity of an active material is given by the following equation

$$C = \frac{n \times F}{3.6 \times M} \tag{5.5}$$

Where C is the specific capacity of the material in mAh $\mathrm{g^{-1}}$, n is the number of moles of electrons stored in the material, F is Faraday's constant, M is the molar mass of the material. For V_2O_5 the number of moles of electron that can be stored is either 1 or 2 depending on whether or not the third phase transformation is used. This gives specific capacities of 74 mAh g^{-1} for the first lithium insertion, a total of 147 mAh g^{-1} for the one electron process (the first two insertions combined) and a total of 294 for the full two electron process (all three insertions).

The capacity values in the work of Zhou *et al.* are calculated purely on the mass of active material in the electrode rather than the mass of all components. Only 70% of the electrode was the active material. Converting the numbers seen in Figure 5.17 to a more realistic number based on the whole mass of the electrode, the capacity is 180 mAh g^{-1}. The results obtained with the ME electrolyte work were approximately 130 mAh g^{-1}. This shows the ME system and the formation of the EEI is not too detrimental to the potential capacity of a system. If the capacity of the ME system is calculated only on the basis of the active material, then the cell presented in this work achieved a cathode limited capacity of 153 mAh g^{-1} which shows that at least some of the third phase transformation is taking place in the V_2O_5 as the capacity exceeded the theoretical capacity if just one electron transfer is considered.

However, there is only evidence for the first lithium insertion in the XRD as seen in Figure 5.12. Given that the theoretical capacity of just the first insertion is only 74 mAh g^{-1}, the observed capacity of 130 mAh g^{-1} exceeded this and is evidence of the further reactions occurring. If these cells were tested on a larger scale then maybe these other phases would be visible in the XRD patterns. XPS could also be useful to determine the oxidation states of the vanadium centres and potentially their relative amounts and would provide evidence of the more lithiated phases.

There is a strong possibility that with more careful optimisation of the electrode preparation or exact V_2O_5 used (such as nanostructured samples) that this capacity could be improved to match literature capacities.

Direct literature comparisons for the anode are harder to find given that most research focuses on lithium titanate and not TiO_2. Some research does exist using titanium dioxide nanoparticles such as the work of Ren *et al.* [131].

The results shown in Figure 5.18 show roughly the same voltage profile regardless of morphology. With only one long plateau that is somewhat sloped. Therefore, any well

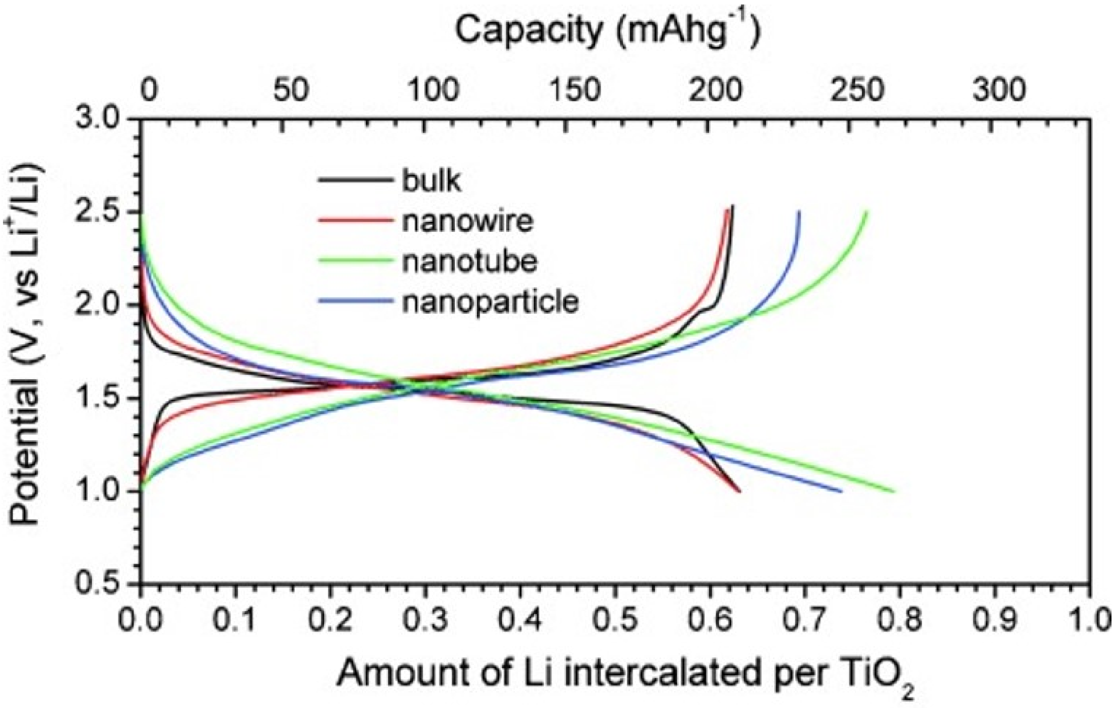

FIGURE 5.18: GCDC curves showing the capacity of various forms of TiO_2. Reproduced with minor alterations from Ren *et al.* Nanoparticulate TiO2(B): An Anode for Lithium-Ion Batteries, Angew. Chem. Int. Copyright © 2012 WILEY-VCH Verlag GmbH Co. KGaA, Weinheim.

defined redox peaks in the CV scan can be attributed to the V_2O_5 as was discussed earlier in this section. Whenever an oxidation happens at the cathode it must be followed by a reduction at the anode, whenever the cathode reaction is finished the potential of the cell increases or decreases until the next oxidation can occur at the cathode. During this time, no reaction happens at the anode as there is no corresponding reaction at the other electrode.

Combining these two results allows an estimation of the expected cell potential for this combination. Lithium insertion into titanium dioxide has an apparent potential of approximately 1.6 V vs Li/Li$^+$ (taken from the midpoint of the plateau). V_2O_5 has reversible reactions at 3.21 V and 3.49 V vs Li/Li$^+$. This means that the potential of the V_2O_5-TiO_2 cell presented in this work should be somewhere from 1.6 V - 1.9 V. However this is not materialised in the GCDC curves in Figure 5.5.

Firstly, from the shape of the curves (i.e. the lack of strong plateaus) it is hard to ascribe a nominal potential to this cell in the first place. There is a prominent plateau in the charge curve centred at approximately 1V but this distinct feature is lacking in the discharge curve. Internal resistance of the cell could lead to lower than expected voltages. This could also come in the form of other overpotetnials, perhaps one step during the discharge (delithiation of the anode or lithiation of the cathode) was slower or requires a slightly higher over-potential than the reverse step. For example the phase transformations that accompany the lithiation/delithiation of the V_2O_5 might be slower in one direction than in the other. The CVs only probed a very small amount of the reactions occurring whereas the CDC experiments theoretically complete each individual reaction before moving to the next one. Given the broad nature of many of the peaks in the CV it is possible that these might just be smearing together and overlapping in the GCDC experiments.

5.10 Conclusion

In conclusion, a lithium ion battery has been constructed using an ME based on Triton X-100 as an electrolyte. The addition of diglyme to the ME was crucial as it acted as a phase transfer catalyst to allow the lithium ions to reach the electrodes.

The lack of pre-lithiated electrode materials meant that the performance of the battery continued to improve as it was cycled, eventually producing one of the highest discharge capacities for an aqueous lithium ion battery ever recorded. XRD investigations coupled with the electrochemical evidence gave strong evidence of reversible intercalation occurring at both electrodes.

By working with pre-lithiated electrode materials the cell could be understood in greater detail. The voltages observed for this cell were also relatively low and the shape of the GCDC curve is not the ideal flat plateaus. This could be improved by finding other viable electrode materials that fit within the window of the electrolyte. While the choice of anodes was somewhat limited there are a range of cathode materials that may be viable alternatives.

Chapter 6

Sodium Ion Batteries

6.1 Introduction

To investigate whether the ME system is applicable beyond lithium, sodium ion batteries were also studied. Being one period lower in the group than lithium, Na^+ ions have a similar chemistry to Li^+ ions. Sodium is also much more earth abundant than lithium, which makes it an attractive alternative to lithium for large scale applications. However, sodium's molar mass, and ionic radius, are larger than that of lithium which means that the specific and volumetric capacities of sodium ion batteries are generally lower than those of lithium ion batteries.

The aims of this chapter are similar to those of Chapter 5. Finding an appropriate ME and electrode, materials to be used in a sodium ion battery and to study the assembled battery electrochemically and using XRD and SEM.

6.2 Electrode materials

The choice of electrode materials for sodium ion batteries is similar to that of lithium ion batteries, with anode materials being somewhat limited and a wider range of cathode materials in the literature.

For anodes, most research is limited to carbonaceous anodes. Unlike lithium, intercalation of sodium ions into graphite is not very favourable [12]. Instead, hard carbons, first demonstrated by Dahn *et al.*, are favoured. These are made by pyrolising cellulose at high temperatures [132]. However, the insertion potential of sodium into these materials is very low [12]. This means that it is probably unusable in the ME system much like graphite was unuseable in the ME based lithium ion battery. Similar to lithium ion batteries, titanates have been used as an anode in various forms [133–137]. The insertion potential of sodium into these titanates is higher than it is for hard carbon and so could find use with MEs much like lithium titanate was viable for the ME based lithium ion batteries. Sodium titanate was available to be used in these studies.

For a cathode, Prussian blue was selected. Prussian blue (Iron (III) hexacyanoferrate (II) or Iron (III) ferrocyanide) is a dark blue pigment with a cubic crystal structure similar to a metal organic framework. This highly porous structure can accommodate metal cations in the middle of the cubes made by the lattice. This very porous structure also allows ions to flow through it easily. Many Prussian blue analogue electrodes exist where some of the iron atoms are replaced with other transition metals such as manganese or cobalt. This changes the redox characteristics of the material and can have an effect on the overall capacity [138–141].

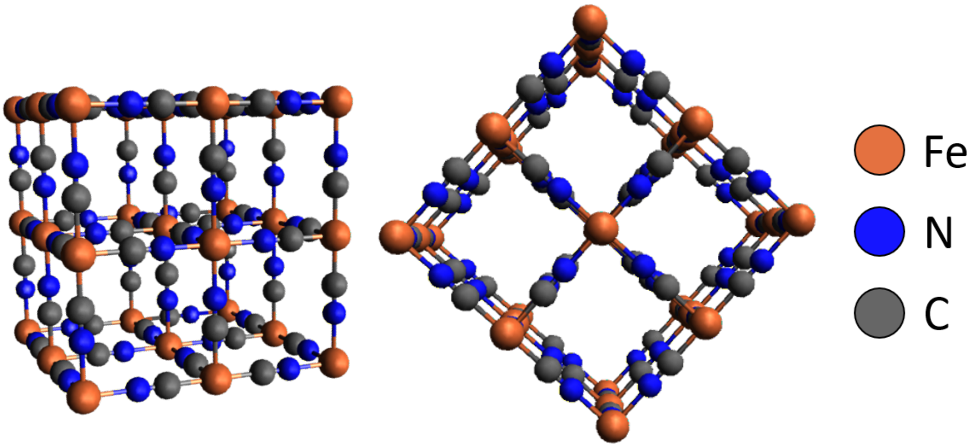

FIGURE 6.1: Prussian blue unit cell showing the channels which ions can flow into and out of.

For this work, standard iron based Prussian blue was chosen due to its ease of synthesis. The material was prepared by mixing a saturated solution of iron (III) chloride (>99.9% Sigma) (3.7 g in 5 mL distilled water) into a vigorously stirred saturated solution of potassium ferrocyanide $K_4[Fe(CN)_6]$ (>99.9% Sigma) (1.39 g in 5 ml distilled water).

The blue precipitate formed instantly and was recovered by vacuum filtration. The precipitate was washed with distilled water and ethanol before leaving to dry in air.

With the anode and cathode materials selected, focus turned to the electrolyte. The Triton X-100 based electrolyte is appropriate to use for these systems except the LiCl was substituted for NaCl at the same 1m concentration. Diglyme was also included in the composition as it was with the lithium ion batteries.

6.3 Sodium ion batteries - GCDC

Cells were assembled in a similar fashion to the lithium ion cells in Chapter 5. GCDC tests showed clear redox activity with two plateaus, one at approximately 1.75 V and the other at approximately 1 V (Figure 6.2. Observing two plateaus is expected for iron based Prussian blue analogues [138]. Prussian blue analogues containing other transition metals may only show one redox plateau [140]. The two redox events visible in Figure 6.2 both arise from the $Fe^{2+/3+}$ couple, one from the iron atoms that are coordinated by 6 carbon atoms in the framework (referred to as the FeC_6 centre) which are in a low spin state, and one from the iron atoms coordinated by 6 nitrogen atoms (FeN_6 centres) which are in a high spin state. These redox events being separated by approximately 0.75 V agrees with literature results [139, 140].

The higher voltage plateau is attributed to the FeC_6 centres [139]. The more positive the reduction potential of a reaction, the more thermodyamically favourable it is (by ΔG=-nFE). The 3d orbitals of the FeC_6 centres are split more because the C is a stronger ligand than the N. This means that reducing the FeC_6 centres is more energetically favourable as there is more energetic gain from placing an electron in a lower energy orbital which leads to a greater voltage output. Said another way, removing an electron from a lower energy orbital (oxidation) requires more energy and so this process will happen at a higher voltage.

Comparable to the lithium ion batteries in Section 5.5, there was some conditioning that took place. Like the Li cells, this conditioning was electrochemical in nature and could not avoided by leaving the cells to rest after assembly. What was most unusual, was that the higher voltage plateau showed no need for such conditioning, being active to a similar extent (shown by the overlapping of the discharge curves) in the first 100

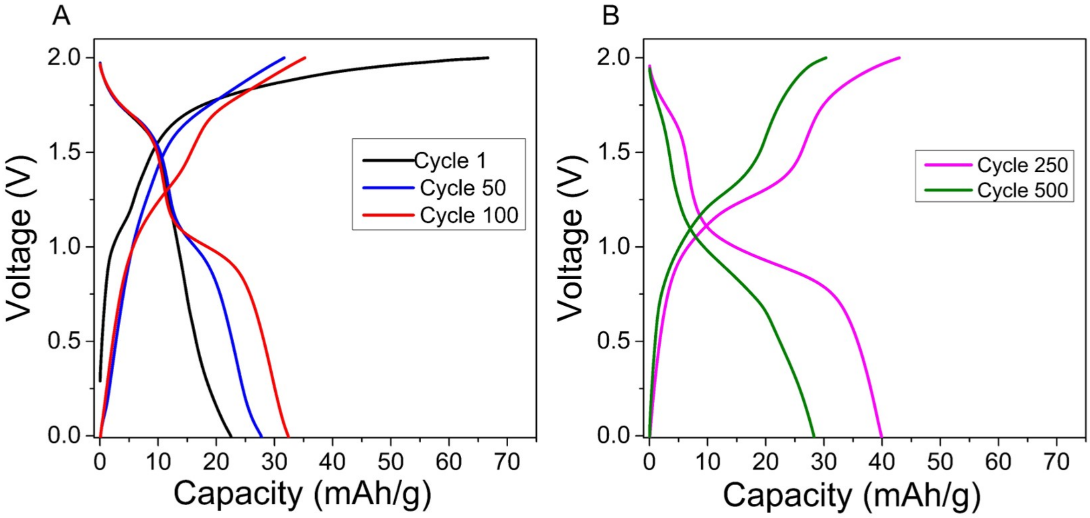

FIGURE 6.2: GCDC curves of a sodium ion battery constructed with a Prussian blue cathode and a sodium titanate anode. Results from the first 500 cycles are shown. The charging and discharging currents used were both 50 mA g^{-1}. A: cycles 1 50 and 100, B:cycles 250 and 500

cycles. The lower voltage plateau, however, grew in over the same time period, being non-existent in the first cycle. The reaction underlying this potential was responsible for most of the capacity of this cell by cycle 250.

As this was the cathode material, it would undergo reduction upon discharge and oxidation upon charging. In the fully charged state, all the iron centres should therefore be in a +3 oxidation state. In the fully discharged state all the iron centres should be in a +2 oxidation state. As synthesised the material was $Fe_7(CN)_{18}$, or $Fe_4[Fe(CN)_6]_3$ which has 4 of the 7 iron atoms in the oxidised (+3) state.

During the first charge in Figure 6.2 there was an apparent plateau at approximately 1.1 V as well as 1.8 V. While there was a corresponding discharge plateau for the second plateau at approximately 1.7 V, there was no discharge plateau for the lower potential reaction. This may represent the iron atoms that were in the +2 oxidation state in the pristine material being oxidised to the +3 state in this initial charge. Interestingly, this charging feature at 1.1 V was absent in cycle 50 shown in Figure 6.2 but reappeared by cycle 100.

Why these lower potential FeN_6 centres were able to be oxidised in the first cycle, then were inactive for the next 100 cycles before becoming the dominant contribution to the capacity by cycle 250 is unclear. In the fully reduced state (with all iron centres +2) the charge on the compound is $Fe_4[Fe(CN)_6]_3{}^{4-}$. This would support the intercalation of 4 sodium ions to maintain charge balance. However, in the fully charged state (with all iron centres in the +3 state) the charge on the compound is $Fe_4[Fe(CN)_6]_3{}^{+3}$. In order to satisfy charge balance in the structure a negative ion must be intercalating. How this could occur in the presence of the EEI is unclear. As established in Chapter 5, transport of cations across the EEI is not possible unless they are complexed with diglyme. The major anion in the electrolyte are the chloride ions from the NaCl. The chloride ions will be complexed by the water, but only weakly. This might mean it is easier to break the solvation shell and transport the chloride across the EEI to a thermodynamic minimum inside the cathode. There is also the potential of CN^- from the ferricyanide being displaced and existing free in the solution. However, given how strongly this ligand binds to the iron centre this was viewed as unlikely.

The electrodes were also placed in a sample of ME and left for 1 week to test if the electrode material would dissolve into the ME. After this period of time no change in colour of the solution was observed. The slurry also appeared to still be adhered to the carbon foil surface.

In order to investigate this further, a cell containing 1 m aqueous NaCl was constructed using the same electrodes. The hypothesis is that the lower potential reaction should still be able to happen but the onset of water splitting reactions will happen before the higher potential reaction is reached. Due to the lack of EEI, it is easier for the chloride ions to reach the electrode, the lower potential reaction should be observed more quickly.

However, this is not what was observed. The assembled cell was cycled at 50 mA g^{-1} and the upper cut off was raised sequentially every 10 cycles from 1.2 V to 2 V. Below 1.8 V no faradaic reactions were observed as seen by the straight diagonal lines in the GCDC experiments (Figure 6.3). Above 1.8 V, a faradaic reaction is observed at a similar potential to that of the ME electrolyte shown in Figure 6.2. This aqueous cell is able to achieve this high voltage due to the glassy carbon current collectors as per Figure 5.2. Above a voltage of 1.9 V significant solvent splitting is observed.

This disproved the above hypothesis of chloride transport to the electrode limiting the appearance of the lower potential redox event. Another possibility was that the lack of reaction could be limited by the anode. A phase change may be required in the anode before sodium ions can be intercalated and deintercalated reversibly. Even though the cathode reactions may be able to proceed, since no anode reactions could, no faradaic

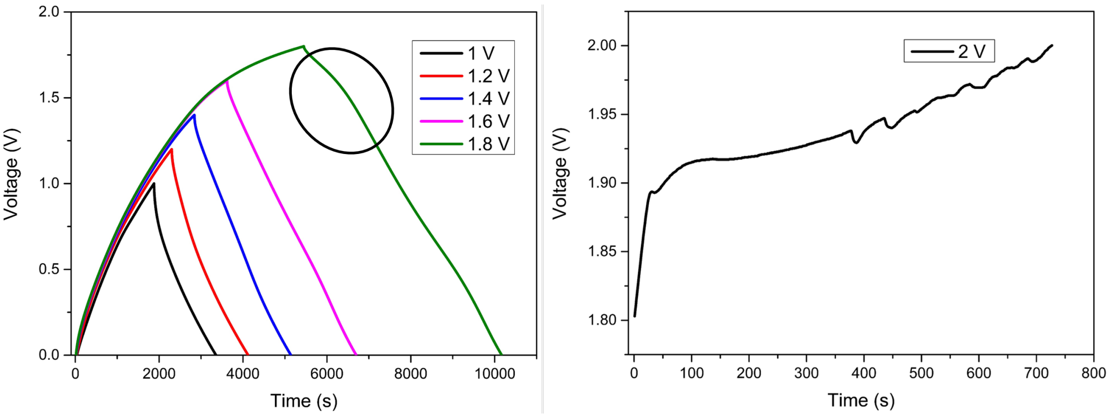

Figure 6.3: Left: The results of the test cell using an aqueous 1 m NaCl electrolyte. The upper voltage cut offs were raised sequenctially by 0.2 V every 10 cycles. Cycles shown are the 5th in every set of 10. The charging current used was 50 mA g^{-1}. No faradaic reactions were observed until the cut off is raised to 1.8 V at which point only the upper voltage reaction was observed (circled). Right: when the cut off was raised above 1.8V significant solvent splitting is observed as this is an aqueous electrolyte so does not benefit from the electrochemical stability of the ME.

processes occur in the cell. It is possible that this phase change happens only at high potentials (1.8 V and above). Only once the cell has been raised to this potential and the phase change has happened the anode is ‘active’ for intercalation. Maybe only once the cell has been cycled a few times at this higher potential will the phase change be complete. Once it is complete then the intercalation-deintercalation process is facile enough to proceed at the lower voltages.

This could be elucidated by XRD studies (See Section 6.5) as well as incorporating a reference electrode into the cell while it is running. This would allow the potential of both the anode and cathode to be monitored individually, rather than monitoring the difference in potential between the two.

The behaviour of the capacity and coulombic efficiency of a cell with a ME electrolyte over the first 500 cycles are presented in Figure 6.4. The discharge capacity increased from around 20 mAhg^{-1} to a maximum of 40 mAhg^{-1} between cycles 200 and 250. This is not an outstanding capacity for a sodium ion battery with numbers getting over 100 mAhg^{-1} for non aqueous and aqueous systems. The coulombic efficiency of these cells was also high at approximately 95% after cycle 75.

What is of note is the cell voltages achieved by this combination of electrodes. One of the voltage plateaus occurred at 1.75 V. This was noteworthy at this was well above the 1.23 V threshold of water splitting. While aqueous supercapacitors can push past the

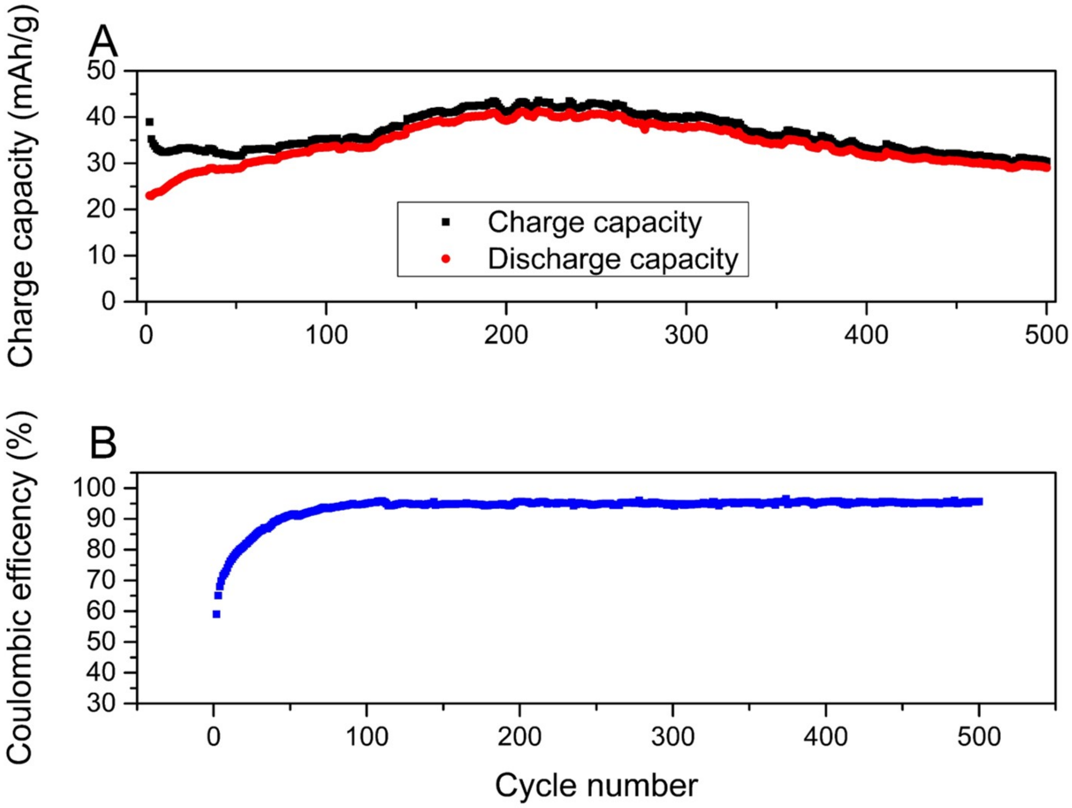

FIGURE 6.4: Results of the first 500 cycles of a sodium ion battery constructed with a Prussian blue cathode and a sodium titanate anode. A) The dicharge and charge capacities which peaked at around 40 mAhg^{-1} between cycle 200 and 250. B) coulombic efficiency was low in early cycles but increased to 95% by cycle 75.

window a little bit if the system is engineered correctly (See Chapter 1.8) an aqueous battery that achieves such voltages without resorting to a ”water-in-salt” methodology has never been seen.

The rate capability of these cells was also tested by increasing the current rate to 500 mA g^{-1}. The results of these are shown in Figure 6.5. The redox reactions were still visible with clear plateaus although the capacity had reduced by over 50% which indicate that the rate capability could be improved.

6.4 Cyclic voltammetry

Cyclic voltammetry studies were carried out in the same manner as for the lithium ion batteries with scans before and after 100 cycles. Figure 6.6 shows the results of this experiment. Similar to what was seen for the lithium ion battery in Figure 5.9, the current density does increase over time. This is not unexpected given the results from

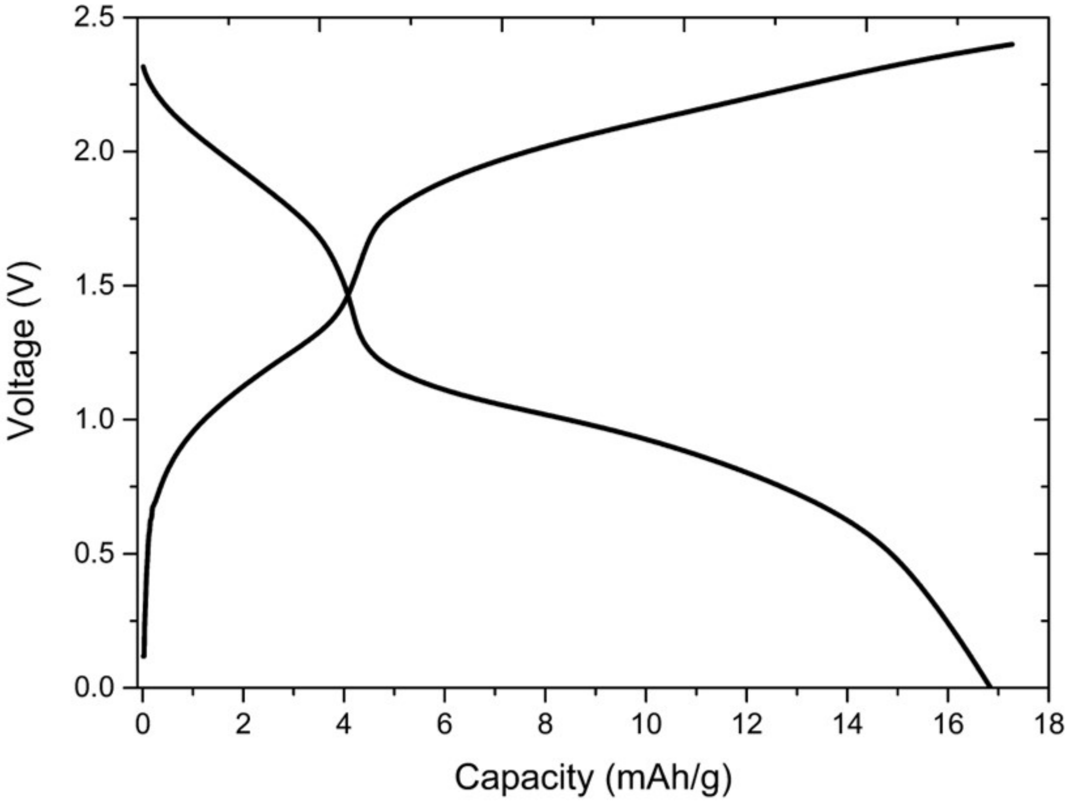

FIGURE 6.5: A sodium ion battery cycled at 500 mA g^{-1}. The redox reactions were still visible but the capacity was dramatically reduced by over 50%

the GCDC tests. Much like the lithium ion batteries, no redox processes were visible in the first cycle but do become visible after cycling. The current density also increased over this time.

When the cell is scanned at a slower scan rate (10 mV s^{-1}), those same redox process visible in the later cycles at higher scan rates become visible (see Figure 6.7). Solid state electrochemistry (such as intercalation) happens much more slowly than solution phase electrochemistry. At fast scan rates, reactions may happen too slowly to be picked up by the measurement. Slower scans allow for these processes to be distinguished as the cell is closer to equilibrium at all times. However the observed current density is lower at slower scan rates. It is not uncommon to see scan rates of 0.1 mVs^{-1} in the battery literature.

There are two reactions observed in these CVs and their potential remains constant before and after cycling. The potentials of the two reactions (taken as the mid-point between the oxidative and reductive peaks) is 1.71 V for the lower potential reaction (a peak separation of 180 mV) and 2.1 V for the reaction at higher potential (200 mV

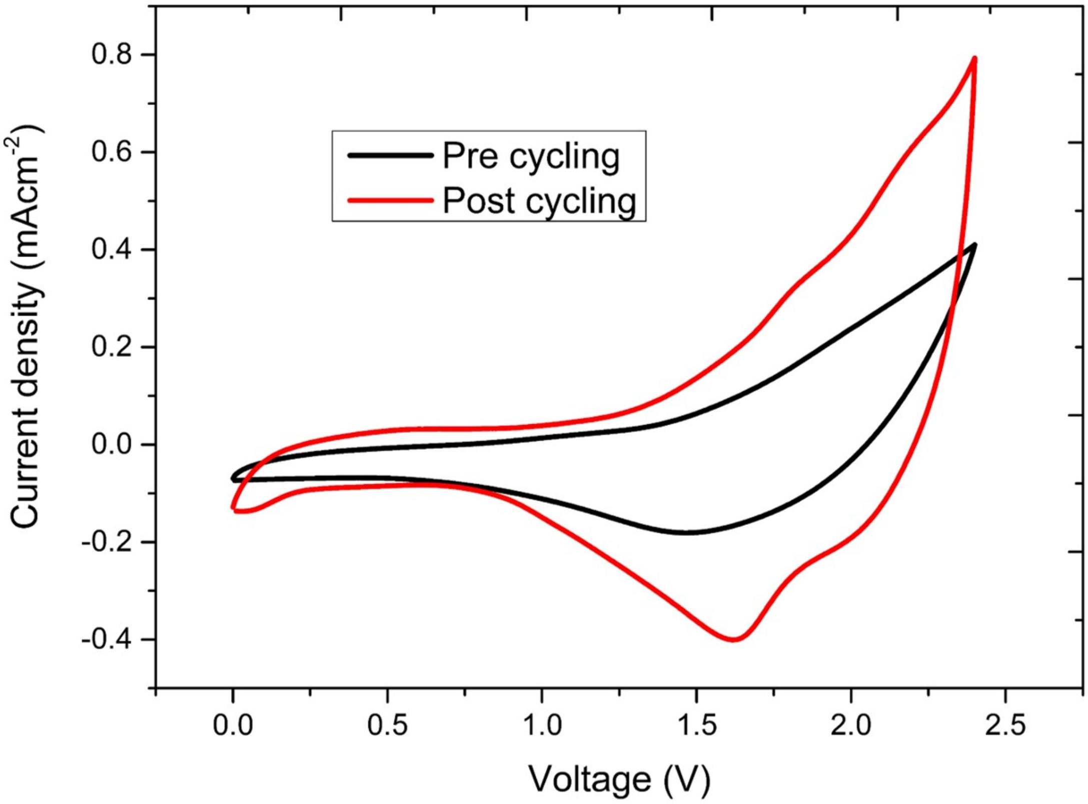

FIGURE 6.6: CVs of a sodium ion battery run at 100 mV s^{-1} before and after running for 100 cycles

peak separation). This is a divergence from the potentials measured in the GCDC tests where the observed discharge plateaus were at 1.75 V and 1 V. The difference in the potential of the reactions as observed in the CV was 0.4 V, whereas in the GCDC tests the difference in the voltage of the plateaus was 0.7 V.

As previously mentioned, the GCDC and CV measurements do not always match exactly. This is for a number of reasons. One can be the internal resistance of the cell being different when run galvanostatically compared to being run as a CV. This would shift the potentials of the reaction slightly. It could also be a result of the CV only probing a very small amount of the material whereas the GCDC curves theoretically hold at a given potential until the reaction is finished.

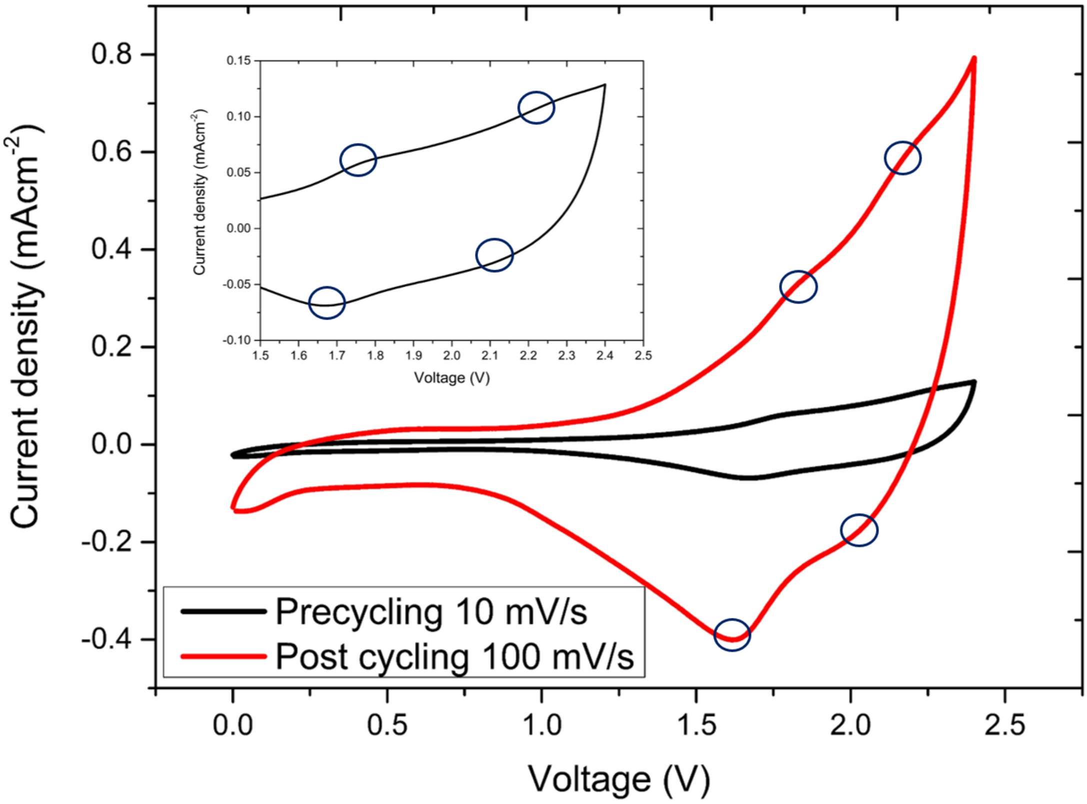

FIGURE 6.7: CVs of a sodium ion battery recorded at 100 mVs^{-1} after running for 100 cycles and one before cycling recorded at 10 mVs^{-1}. Inset, a zoomed in view of the precycling scan

6.5 X-ray diffraction studies

As with the lithium ion batteries in Chapter 5, X-ray diffraction studies were undertaken to investigate the proposed intercalcation mechanisms at both electrodes. Testing conditions were identical to those used in Chapter 5 with pristine electrodes being compared against charged and discharged electrodes.

6.5.1 Prussian blue

Given the cubic network structure of Prussian blue, the lattice parameters are not expected to change too much on intercalation. This is because the sodium ions should occupy the vacancies in the middle of the cubes (See Figure 6.1). This may mean additional reflections may be seen in the XRD pattern representing these interstitial sodium ions.

As with previous results presented in Chapter 5, the main reflections visible at 26 and 55 degrees 2θ, were of the graphite foil on which the electrodes were coated (Figure 6.8). A zoomed in version of this data is visible in Figure 6.9.

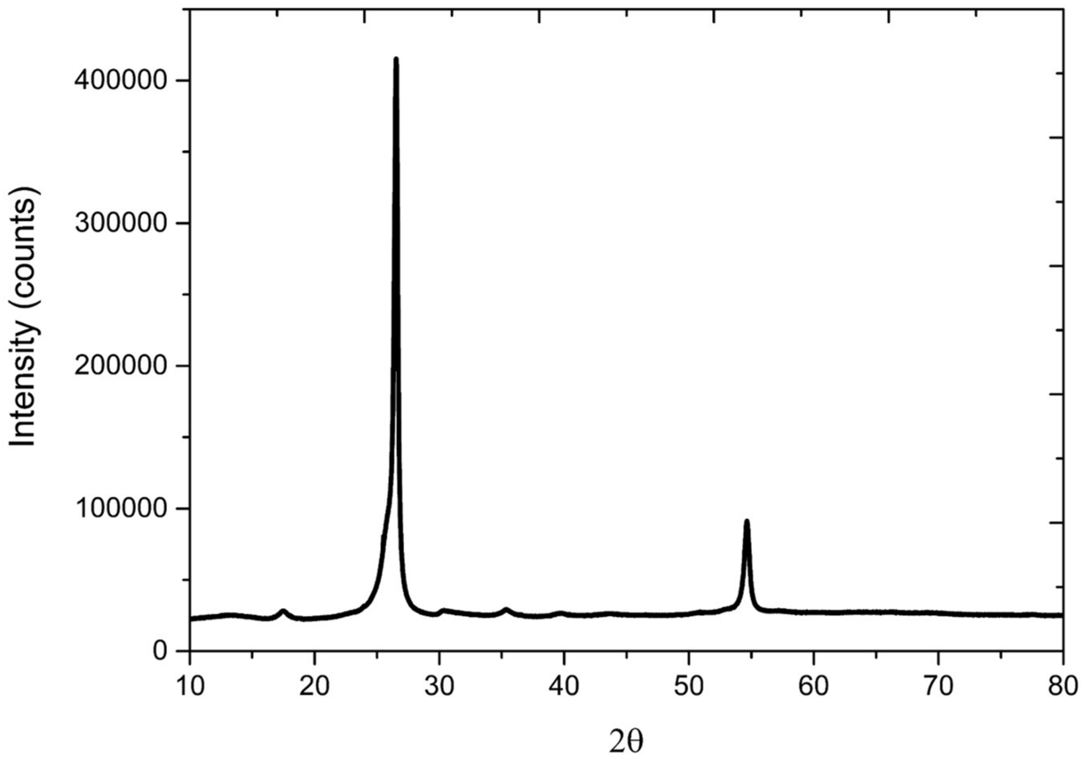

Figure 6.8: The full XRD scan of a pristine Prussian blue sample from 10° 2θ to 80° 2θ at a scan rate of 0.125 degrees per minute. The two most intense reflections are that of the graphite on which the material was pasted.

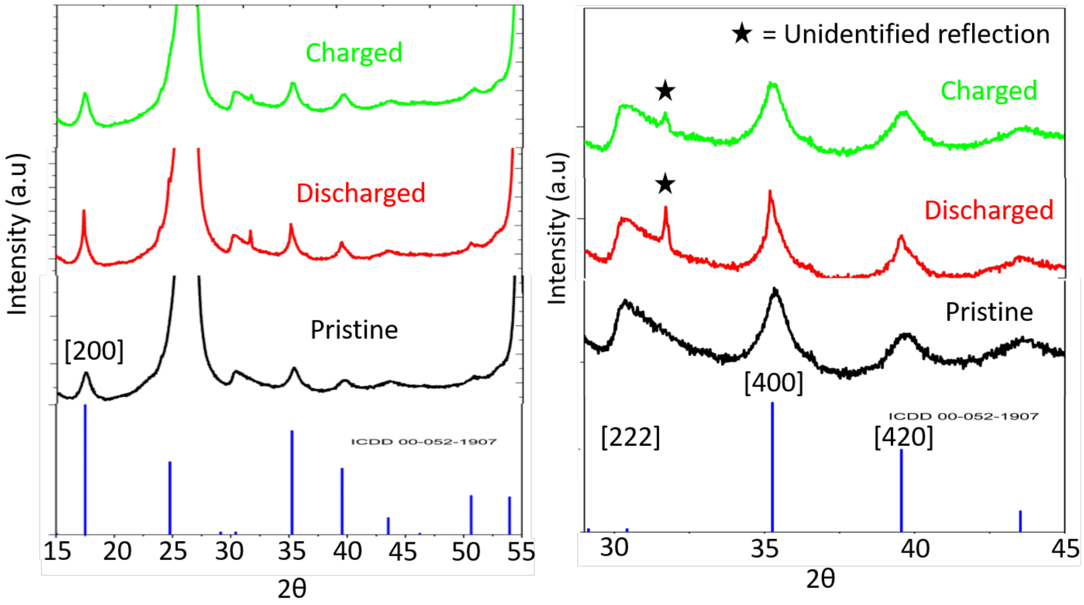

Figure 6.9: A zoomed in section of Figure 6.8 reflections show a good agreement with the reference pattern. reflections in the discharged sample appeared sharper indicating a higher crystallinity of the sample in this state. Another reflection also gradually appears at 32° 2θ which is more prominent in the charged state than the discharged state. The Miller indices [hkl] of certain peaks are indicated.

First, the pristine sample agreed well with the chosen pattern for Prussian blue which confirmed that the synthesis was successful. However, the reflections in the pristine sample were somewhat broad indicating a lower degree of crystallinity compared to the highly crystalline samples seen in the literature [142–144]. Crystallinity is generally important for battery materials that use an intercalation mechanism as it allows for easier diffusion through the interstitial sites in the lattice. Higher crystallinity also makes for a flatter voltage plateau which is commercially desireable. However, in some materials a more amorphous structure may allow for easier diffusion and higher capacities [145–147]. Crystallinity is particularly important for Prussian blue and a lot of the literature focuses on making samples as crystalline as possible [142]

The simple synthesis method used caused rapid precipitation of the Prussian blue, which might result in a lower crystallinity than expected. This lower crystallinity might also be the cause of the lower capacity compared to other literature results (see Section 6.8).

As Prussian blue acts as the cathode material, the sodium ions should intercalate upon discharge and deintercalate upon charging. From Figure 6.9, as expected, the peak positions do not change greatly upon cycling. However, the crystallinity of the sample in the discharged state appears to increase upon discharge (indicated by the peaks getting sharper).

This could be due to the intercalated sodium ions providing a more rigid support structure for the framework. The reflections that are influenced the most by the intercalation are the [200] and [400] planes and to a lesser extent the [420] plane whereas the [222] plane appears to be unaffected by this process. All of these planes except the [200] plane have a sodium ion in them in the intercalated state. The presence of sodium ions in particular planes ([222], [400], [420]) is not a predictor of how the long range order of the planes changes upon intercalation.

In the pattern for the Prussian blue cathode a reflection appeared at approximately 32^{o} 2θ upong charging and discharging. This reflection was not present in the pristine sample. It is more prominent in the discharged state, but is still present in the charged state.

This reflection could not be matched from a variety of candidates including NaCl, sodium containing Prussian blues and $FeCl_3$. Sodium titatante was also checked as a potential match in case some of the anode material had dissolved in the electrolyte and migrated to the cathode. This reflection might hold the answers behind why the second voltage plateau develops over time in the GCDC curves. No other new reflections were visible in the entire pattern.

6.6 Sodium titanate

Unlike Prussian blue which has a well defined crystal structure, ‘sodium titanate’ can refer to a range of materials with different stochiometries [148]. The sodium titanate used was purchased from Sigma Aldrich as sodium metatitanate (catalogue number 401307, CAS number 120-34-36-5) with a chemical formula of $Na_2Ti_3O_7$. One of the listed applications of this material is as a low voltage anode in sodium ion batteries.

The results of XRD studies on pristine, charged and discharged electrodes are presented in Figure 6.10.

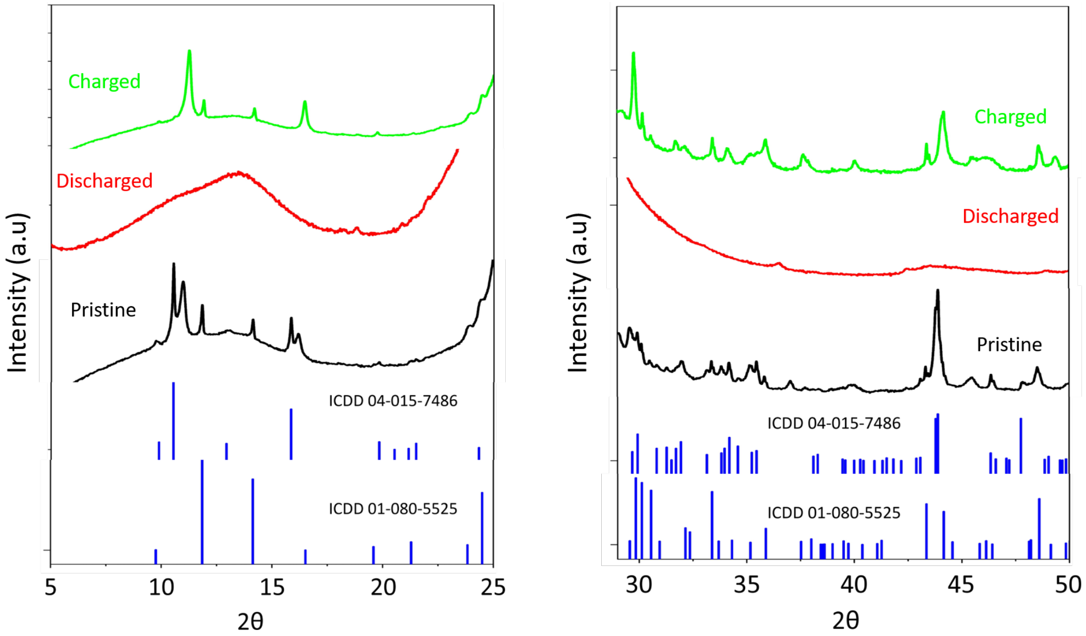

FIGURE 6.10: XRD pattern of sodium titanate electrodes in the pristine charged and discharged state. Both charged and discharged electrodes were measured after 100 cycles. The pristine state shows a mixture of phases that do not correlate perfectly to any database pattern. In the charged state the structure is crystalline but no database match could be found for the structure. The discharged state is amorphous or polycrystalline.

Firstly, in the pristine state, this material could not be matched to a singular pattern in the ICDD database. Two of the more representative patterns, ICDD 04-015-7486 and 01-080-5525, are presented in Figure 6.10. These patterns represent structures with the formula $Na_2Ti_3O_7$ and $Na_2Ti_6O_{13}$ respectively. Even the combination of these two patterns do not account for all the observed reflections, such as the reflection at 36° 2θ in the pristine sample in Figure 6.10. This means that the pristine sample is most likely a mixture of different phases (and stoichiometries) of sodium titanate.

After 100 cycles, the structure of the materials changed dramatically. Since this material acts as the anode, the sodium ions should be intercalated in the charged state and deintercalated in the discharged state. The titanium ions should be in the +4 state when discharged and in a lower oxidation state, +2 or +3, in the charged state.

In the charged state, the material maintains its crystalinity showing several well defined reflections. However it is a totally different phase to the one observed in the pristine state. The pattern obtained could not be matched to any patterns in the ICDD database. This was likely due to there still being a mixture of phases present and also that the charged state is made up of non-stoichiometric compounds (e.g. Na_xTiO_2) which will make it harder to match to a pattern in a database. Regardless, the large difference in the XRD pattern observed between the pristine and charged state is strong evidence that intercalation is occurring.

In the discharged state, it is expected that the sodium ions are deintercalated from the anode. In Figure 6.10 it is seen that the sample becomes amorphous with no well defined reflections. This implies that any crystalinity is lost once the sodium ions are removed from the structure and the titanium ions are reoxidised. Given that the material does not return to its pristine state upon discharge implies that there is an irreversible phase transition that occurs as the material is cycled.

One hypothesis is that the pristine state is a mixture of phases of sodium titanate, but, as synthesised, these are individually large enough moieties to produce an XRD pattern. As the material is cycled, the lattice may indeed be returning to its original state, but the individual phases are spread homogeneously throughout the solid which has the effect of making the material appear amorphous.

Another possibility is that the sodium ions removed upon discharge can come from random sites within the lattice. In the pristine material the sodium ions have fixed positions. When new sodium ions are introduced into the lattice they take different positions to the original sodium ions. However, upon discharge sodium ions could be removed from either the original positions or the new positions. If the energy required to remove the ions were similar to each other then there would be a distribution of ions in both new and old sites once the discharge was finished. The resulting irregular placement of sodium ions through the structure would result in a poly-crystalline structure giving no clear XRD pattern. Upon charge, the sodium ions go back to fully occupying all possible sites which makes the sample crystalline again but in a different phase (or mixture of phases) to the pristine state.

Further study into this electrode is required. *In situ* XRD would be very valuable as the structural changes this electrode undergoes are large, going from a mixture of crystalline phases in the pristine state, to oscillating between amorphous and crystalline states, as the cell is discharged and charged. XPS would also reveal a lot about how many sodium ion environments there are in each state as well as the distribution of oxidation states and environments of the titanium ions.

6.7 Scanning electron microscopy

As with Section 5.8, SEM was used to investigate the surface of the electrodes before and after cycling.

Pristine Prussian blue cathodes showed rather large, irregularly sized crystals which is expected given the method of synthesis used (Figure 6.11). After cycling however, the particles appear to become less well defined with smudged edges rather than the sharper edges seen in the pristine sample. This could the be formation of an SEI layer or it could be caused by the stress induced by the ions inserting and de-inserting over the course of many cycles.

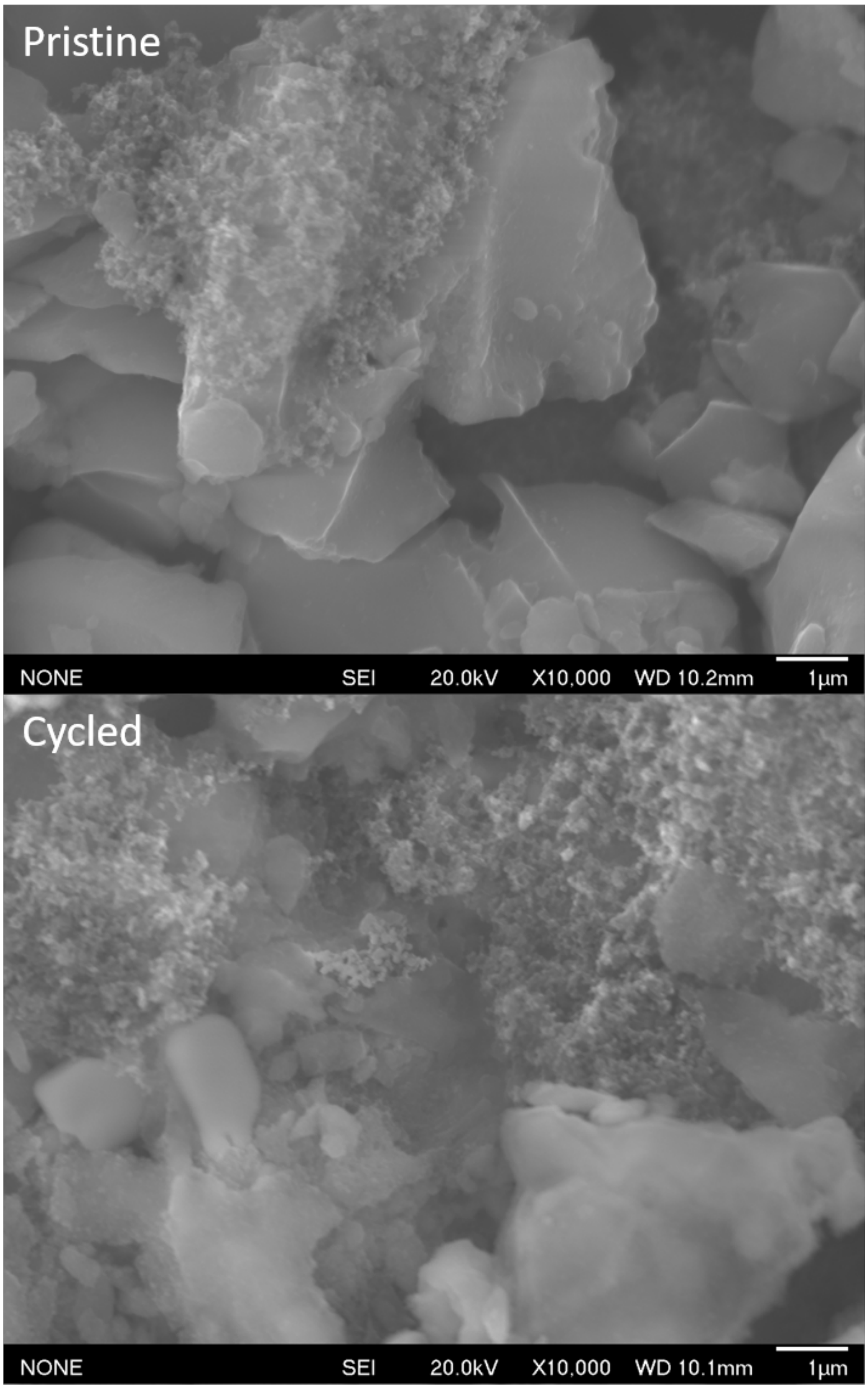

FIGURE 6.11: SEM images of a Prussian blue cathode before and after cycling.

The shape of the crystals also suggests why the capacity of the material may be low. In a perfectly cubic lattice, sodium ions will be able to diffuse through the whole solid and have access to all available positions. In a more disordered lattice, this diffusion will be more difficult so not all the material will be electrochemically accessible leading to lower capacities than expected.

The sodium titanate electrodes show a similar pattern to those in Section 5.8 where no real change is noticeable between the charged and discharged state.

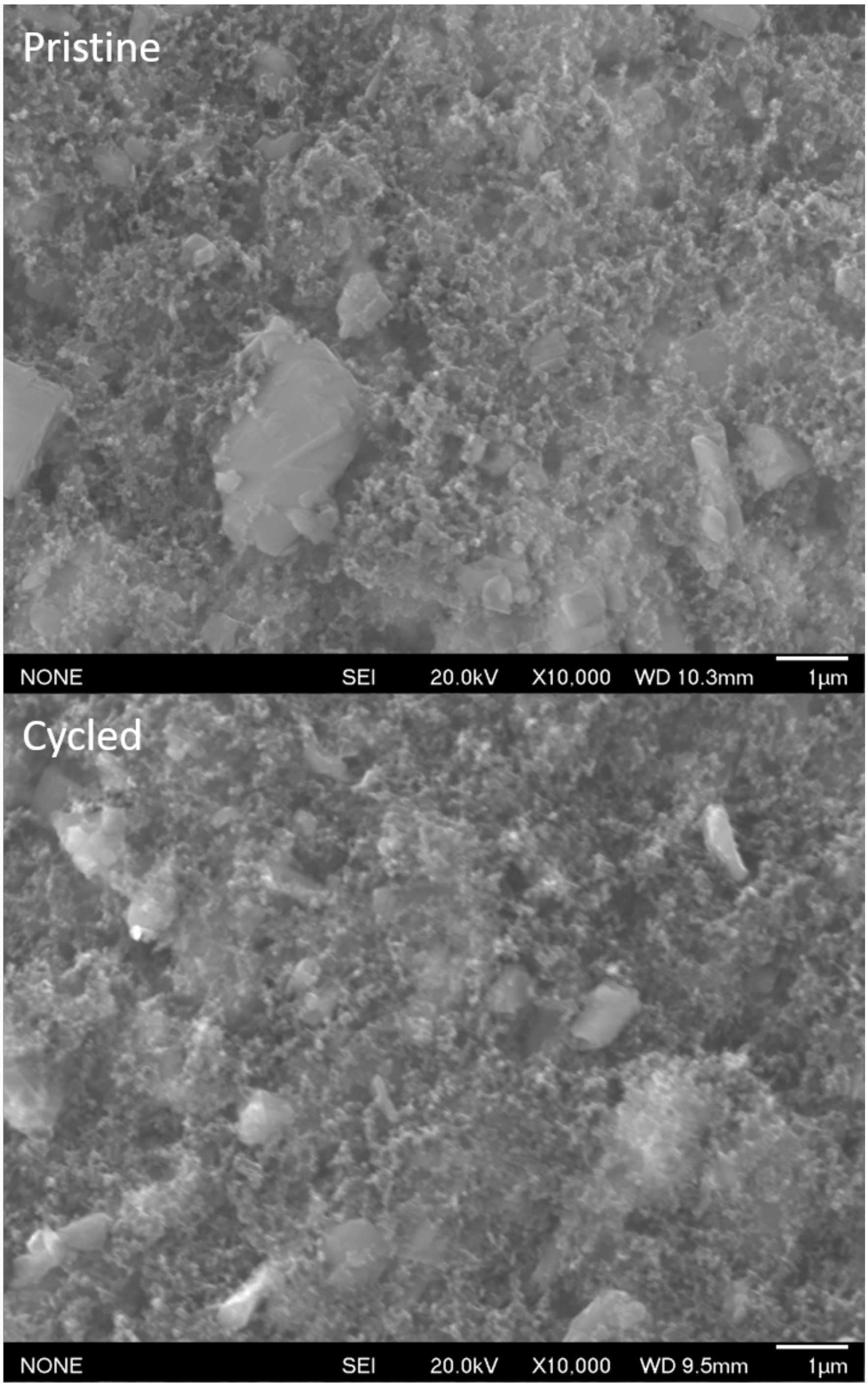

Figure 6.12: SEM images of a Sodium titanate anode before and after cycling.

6.8 Literature comparison

The theoretical capacity of Prussian blue is 218 mAh g^{-1}. This assumes that all seven iron centres are accessible electrochemically and can be changed between the +2 and +3 state i.e. undergo a one electron reaction. Generally the lower voltage reaction displays a higher capacity than the higher voltage reaction [149]. The likely reason for this is due to this reaction being more reversible than the higher voltage process.

In the literature, the observed capacity of Prussian blue is reported to be between 100 and 120 mAh g^{-1}, which is much lower than the theoretical limit [142, 150, 151]. Prussian blue analogues where some of the iron is replaced by another transition metal such as manganese or cobalt generally show better voltage characteristics as well as higher capacities.

The cells made in this work do show lower capacities than those in the literature. This could be for a number of reasons. Firstly, the Prussian blue used in this work was synthesised using a simple technique. Most Prussian blue in literature is synthesised in such a way that it is free of any coordinating water or defects, which are known to have a detrimental effect on the capacity [142, 144]. Nanosynthesis techniques are also often employed to synthesis Prussian blue with enhanced rate capabilities improved capacity [152]. Given the importance of crystal size and the lack of defects it is unsurprising that the rudimentary, aqueous, synthesis method employed to make the Prussian blue would yield a cell with lower than normal capacities.

As mentioned previously, pre-sodiating the cathode material, i.e. synthesising it in its reduced form, could also lead to improved capacities from the first cycle rather than the electrochemical conditioning that was required in the present cells.

Only one cell that uses sodium titanate as an anode and Prussian blue as a cathode has been reported in the literature. The focus of this study by Mukherjee *et al.* [11] was on the anode and therefore the assembled cells were run with the anode as the limiting electrode compared to the cathode being limiting in the cells described in this work. This means that comparing capacities is impossible. It is noted that they achieved capacities of approximately 90 $mAhg^{-1}$ for $Na_2Ti_3O_7$ which was higher than than the 50 $mAhg^{-1}$ recorded for pristine TiO_2.

As part of this research, Mukherjee *et al.* also tested their cells in both aqueous and organic electrolytes (Figure 6.13). They note that charging the cells above 0.7 V in the aqueous electrolyte was impossible due to water splitting on the electrodes. The cells using the ME electrolyte presented above were able to be charged to 2.4 V. This again highlights the advantages of the ME system. When using an organic electrolyte, the voltage characteristics are totally different to what was observed in Figure 6.2. The organic solvent based batteries show sloped curves and while there are plateaus somewhat visible, they are not as clear as those shown in Figure 6.2. This could be due to these cells being constructed with a limiting anode rather than a limiting cathode.

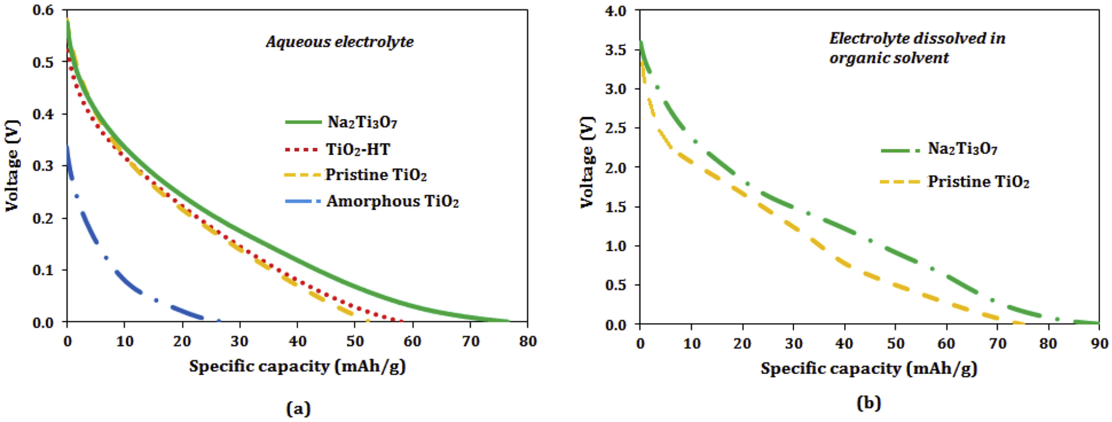

FIGURE 6.13: GCDC curves for aqueous (a) and organic electrolytes (b). The capacities for the organic electrolyte are larger than what was recorded with the ME electrolyte however the voltage characteristics are totally different. Reprinted from "A study of a novel Na ion battery and its anodic degradation using sodium rich Prussian blue cathode coupled with different titanium based oxide anodes", Vol 286, Mukherjee *et al.* [11], Pages 276-289, Copyright (2015), with permission from Elsevier

6.9 Conclusion

In summary, a sodium ion battery using an ME electrolyte was developed. The cathode material selected was Prussian blue, synthesised on site. The anode material was a commercial sample of sodium titanate.

GCDC and CV experiments confirmed that two separate redox events were occurring in the assembled cells, which is consistent with the two electron reduction of Prussian blue reported in literature. The cells achieved a capacity of approximately 40 mAhg^{-1} and two voltage plateaus at 1.7 V and 1 V. The higher potential peak is well beyond the thermodynamic limit for the splitting of water, which is only made possible by the ME.

XRD analysis gave strong evidence for intercalation at both electrodes as well as a phase change at the anode. Further analysis of these samples with XPS would help to identify a mechanism as well as the structure of the materials and how they develop over time.

As with the lithium ion cells, a certain amount of electrochemical conditioning or activation was required to see both faradaic reactions in the GCDC experiments. Capacities increased over time with the lower potential reaction only being observed after 100 cycles.

More study is needed to see how these electrodes develop structurally over time as the cell operates. Also further optimisation of the ME composition and electrode materials is needed to increase the performance of the cells.

Chapter 7

Other Ion Batteries

7.1 Introduction

With ME electrolytes demonstrated in lithium and sodium ion batteries, attention turned to other ion batteries. This was not only to strengthen the intellectual property position of the research, but also to see if MEs could be applied beyond the two most successful ion battery chemsitries. In particular, potassium, magnesium, calcium and zinc ion batteries were investigated.

7.2 Overview

There is comparatively less literature on these batteries for a variety of reasons. Potassium ions are much heavier and larger than both and lithium and sodium ions while still being monovalent. This means that the choice of potassium as the active ion automatically means a lower theoretical specific and volumetric energy density of the cell.

However, potassium ion batteries have been shown to have a greatly improved cycle life over their sodium ion counterparts [153, 154]. This means that over their lifetime the levelised cost of electricity (LCOE) may actually be lower for potassium systems than sodium or lithium. Having similar chemistry to sodium and lithium ions means there is also a raft of available electrode materials. Anodes are primarily based on hard carbons or graphite with Prussian blue analogues making up the majority of cathode materials.

Because potassium chemistry is so similar to lithium and sodium, the same electrolytes, organic carbonates with PF_6^- or ClO_4^- counterions for the salt, can be used for potassium ion batteries as well.

Aqueous potassium ion batteries have been recently demonstrated. Most of the work reports half cell results with the major focus on Prussian blue analogues as cathodes [155]. The lack of available anode materials led Liu *et al.* to investigate sodium titanium phosphate [156]. They discovered that this electrode uses a dual ion mechanism where both potassium and sodium ions intercalate into (and deintercalate from) this electrode during operation. Combined with a Prussian blue analogue cathode this cell was able to achieve a capacity of 160 mAh g^{-1} at a voltage of 1.4 V.

Magnesium and calcium ion batteries present an entirely different set of problems. At a first look, both seem like obvious choices for battery ions. Being divalent means that 2 electrons can be transferred per ion. This means the theoretical capacity of these systems is approximately twice that of its group one neighbour, e.g. Na theoretical capacity is 1165 mAh g^{-1}, Mg theoretical capacity is 2205 mAh g^{-1}.

However, their divalent nature presents a large problem in terms of their solid state diffusion. Magnesium ions are smaller than lithium ions yet bear twice the amount of charge. This means the charge density of a magnesium ion is very high which will hinder its ability to move through a solid reversibly due to the strong electrostatic interactions with the host lattice. As a result very few viable cathode materials have been discovered for magnesium ion batteries. The Cheverel phase Mo_6S_8 was the first material discovered that enabled reversible Mg ion insertion [157] and is still one of the best performing cathodes in literature with a specific capacity of approximately 70 $mAhg^{-1}$ and an insertion potential only 1.1 V above Mg/Mg^{2+}.

Magnesium in particular also has problems in regards to anodes. Magnesium insertion into graphite or other carbons is negligible [12] and so one of the only viable anodes is the parent metal. However, most electrolytes spontaneously decompose on the Mg metal surface to create a passivating SEI layer [158]. This occurs in lithium systems as well, however, the lower charge density lithium ions are able to pass through the SEI whereas magnesium ions are not. Conversion anodes such as tin and bismuth have also been demonstrated, however these have shown limited success [159, 160].

The electrolyte of magnesium ion batteries are also very constrained because of the reactivity of the magnesium metal mentioned previously. Typically they are based on ethers such as THF and glymes. Aqueous magnesium ion batteries have been produced in literature, however many of these only show half cell results given the lack of compatible redox couples [161, 162]. Some full cell examples do exist such as the one presented by Wang *et al.* [163]. This cell used an organic anode and a vanadium phosphate cathode. The full cell was only able to achieve a capacity of 50 mAhg^{-1} and an average voltage of 1 V.

Calcium ions do not suffer from the extreme charge density of magnesium ions but still retain the possibility for multiple electrons transferred per atom. Calcium ion batteries are one of the least studied systems because at first glance, the increased mass and volume of the ion rules it out from being competitive with the other ions. Calcium deposition and stripping in traditional carbonate electrolytes was only observed in 2016 [164]. This is typically paired with Prussian blue analogues for cathodes [165].

Very few examples of aqueous calcium ion batteries exist, even less so in a full cell configuration. Both Adil *et al.* [166] and Cang *et al.*[167] used organic based anodes in their full cell demonstrations. Adil *et al.* paired this with a copper based Prussian blue analogue as the cathode whereas Cang *et al.* used a Ca_2MnO_4 cathode. Both cells prodcued capacities close to 140 mAhg^{-1} but showed low voltage, only recording an average of 0.4 V and 0.2 V respectively.

Aqueous zinc ion batteries are one of the more developed aqueous ion batteries due to the relatively high standard reduction potential of zinc (-0.76 V vs. the standard hydrogen electrode). This means that deposition and stripping of zinc is possible in aqueous solutions. In basic conditions, this reduction potential is reduced to approximately -1.2 V vs the standard hydrogen electrode. Manganese oxides, Prussian blue analogues and vanadium phosphates are all viable cathode materials and can achieve voltages from 1.2 V up to 1.7 V [168] in a full cell configuration.

Therefore, zinc ion batteries have the least to gain from an ME based electrolyte. Using the parent metal as an anode is always the best option as they have the highest gravimetric and volumetric capacities possible for a given ion as there are no ‘wasted’ atoms in the structure. If a higher voltage electrode couple could be found to exploit the microemulsion, it would likely compete with Zn deposition which, if deposited, would break the EEI and provide a surface to split water.

Trials were still attempted to see whether any zinc deposition was observed in the cell at all and if the cells behaved significantly differently to the other ions tested in this chapter.

7.3 Cell assembly

For all cells in this chapter, the cathode material was the same Prussian blue electrode used in the sodium ion batteries in Chapter 6. As seen in Section 7.2, Prussian blue analogues make up the most of the cathode materials in literature because they are well characterised and easily synthesised.

For an anode material, the titanium dioxide used in the lithium ion batteries in Chapter 5 was used. The sodium titanate anodes from Chapter 6 were considered, however it would be hard to claim that the resulting cell was a true single ion battery. It is possible the sodium ions already in the anode could drive the anode reactions with the other ion driving the cathode reactions. Dual ion batteries are an important area of research and show great promise, however they are beyond the scope of this research. The aim of this research is to prove that ME electrolytes can be useful beyond the two most well studied battery chemistries.

The electrolyte used was the same for as in Chapters 5 and 6, except the salt in question was replaced with 1 m of the chloride salt of the given ion.

7.4 Results: Potassium and calcium ion batteries

Both potassium and calcium ion batteries showed remarkably similar voltage curves to the sodium ion batteries in Chapter 6. These were both able to run for 1000 cycles and the results are presented in Figure 7.1.

First, the capacities of these cells are much lower than what was observed for the sodium ion batteries. This is likely due to the size (in the case of potassium) or charge density (in the case of calcium) making it harder for them to move through the solid.

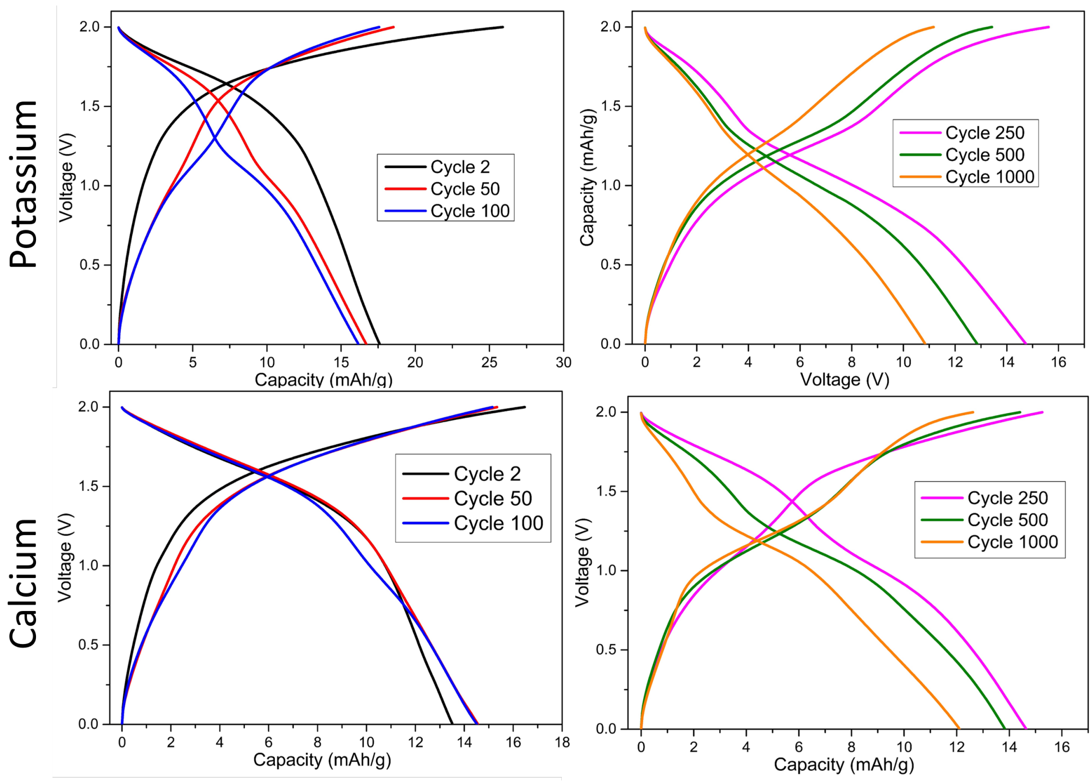

FIGURE 7.1: GCDC curves of a potassium and calcium ion battery constructed as outlined previously. Over these cycles the voltage maximum was 2 V and a current rate of 50 mA g^{-1} was used.

Second, the potential of the reactions observed evolve in a similar way. Over the first few cycles only the high potential reaction is visible at ca. 1.7 V and then the lower potential reaction at ca. 1 V develops in later cycles. This second reaction develops much more quickly for the potassium ion battery compared to the calcium ion battery. However the high potential reaction fades much more quickly for the potassium ion battery, being mostly gone by cycle 250 whereas it is evident in the calcium ion system until cycle 500.

As with the sodium ion batteries, these are the highest voltage aqueous batteries ever observed for these ions.

The similarity of these curves to the sodium ion battery curves is not surprising. The underlying redox reactions that are occurring are the same in all cases, the Fe^{2+}/Fe^{3+} couple of the Prussian blue and the Ti^{3+}/Ti^{4+} couple of the TiO_2.

The lower capacity is most likely attributable to the same problem encountered with the lithium ion batteries. In the assembled configuration, the anode is in the discharged state but the cathode is in the charged state. This could have been avoided by using sodium titanate as the anode but as mentioned previously it would be difficult to to the categorically claim these as potassium or calcium ion batteries. This is definitely an avenue for further research.

The cyclic voltammograms of these two cells are also remarkably similar to each other and to the sodium ion battery CV. These experiments were done after the cells had been cycled 100 times at the maximum voltage and a rate of 50 mA g^{-1}. The scan rate used was 10 mV s^{-1} with an upper voltage cut-off of 2.4 V. It is possible that at slower scan speeds that the individual peaks would be distinguishable as they are in Figure 6.6.

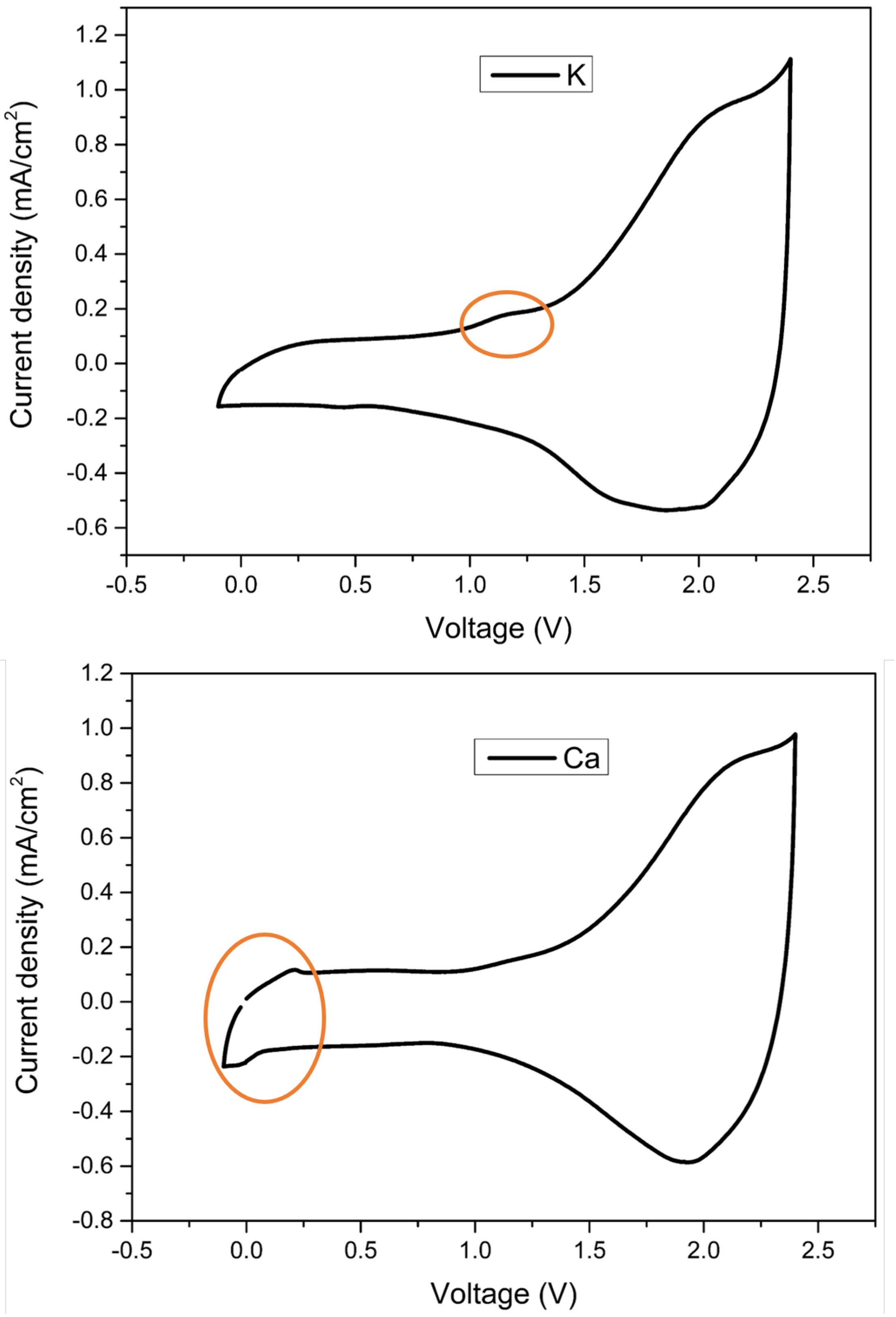

FIGURE 7.2: Cyclic voltammograms of Ca and K ion batteries after 100 cycles had been completed. The scan rate was 10 mV s^{-1}. Both look very similar to each other though an extra oxidative peak is visible at 1.2 V for the potassium ion battery and a lower potential peak being visible in the calcium ion battery.

Some differences in the CV are visible (highlighted in orange in Figure 7.2). These are only minor variations which may not show up in the GCDC curves. Further investiagtion is required as to why these two are so similar in terms of performance.

7.5 Results: Zinc and Magnesium ion batteries

While the potassium ion and calcium ion batteries behave in a similar way to each other and to sodium, both zinc and magnesium behave very differently to each other. These ions *should* have very similar properties given their size is almost identical (145 pm for Mg and 142 pm for Zn) identical charge. Not much work has been done on comparing these two in batteries because most zinc ion batteries use aqueous electrolytes and almost all magnesium ion batteries use organic electrolytes. This makes substituting one for the other in a system quite difficult.

In this instance, despite the system being essentially identical, the performance of these two ion was very different, with the zinc ion battery performing much better than the magnesium counterpart.

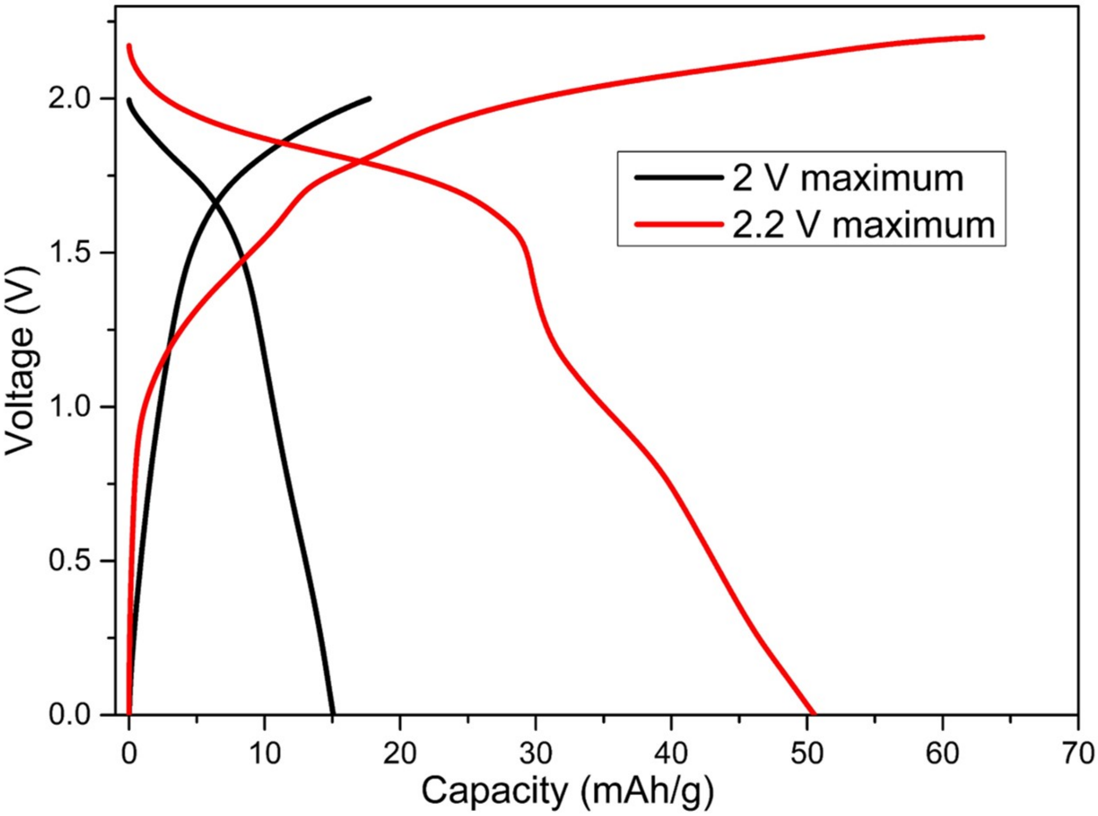

Figure 7.3: GCDC curves of a zinc ion battery constructed as outlined previously. Over these cycles the voltage maximum was 2.2 V and a current rate of 50 mA g^{-1} was used.

The calcium and magnesium batteries were only charged to 2 V, which still allowed for both redox reactions of the Prussian blue to be observed. However only one redox reaction was observed in the zinc ion battery when the cell was charged to 2 V and cycled 100 times. When the cell was charged to 2.2 V a large increase in capacity was observed and a second redox reaction became visible at a lower potential.

In the sodium ion battereis in Chapter 6 and the potassium ion and calcium ion batteries presented in Figure 7.1, the higher potential reaction was observed at 1.7 V where as the higher potential reaction for this zinc ion battery is at 1.85 V (taken as the midpoint of the plateau). The reaction at lower potential appears to be at the same potential as in previous cells, though since this reaction is not very prominent in Figure 7.3, this may not be an accurate conclcusion.

This shift to higher potentials could be a result of the higher charge density of the zinc ion. When intercalated into the Prussian blue structure, the higher charge density could be polarising the electronic environment of the iron centres such that the energy of the orbitals changes, altering the potential of the redox reactions. This could also be to changes at the anode where the intercalation of the higher charge density zinc ion requiring an increased voltage in order to force the ions into the structure and get them to migrate through the solid.

CV experiments were also performed to see the differences between this cell and the previous ones the results of which are presented in Figure 7.4. This CV looks has a large reduction peak at 1.75 V with a corresponding oxidation peak at 2.25 V. Taking the mid-point of these peaks as the formal potential of the reaction, a plateau in the GCDC would be expected at approximately 2 V which is close to what was observed in Figure 7.3. A lower potential reaction is less prominent but still visible (circled).

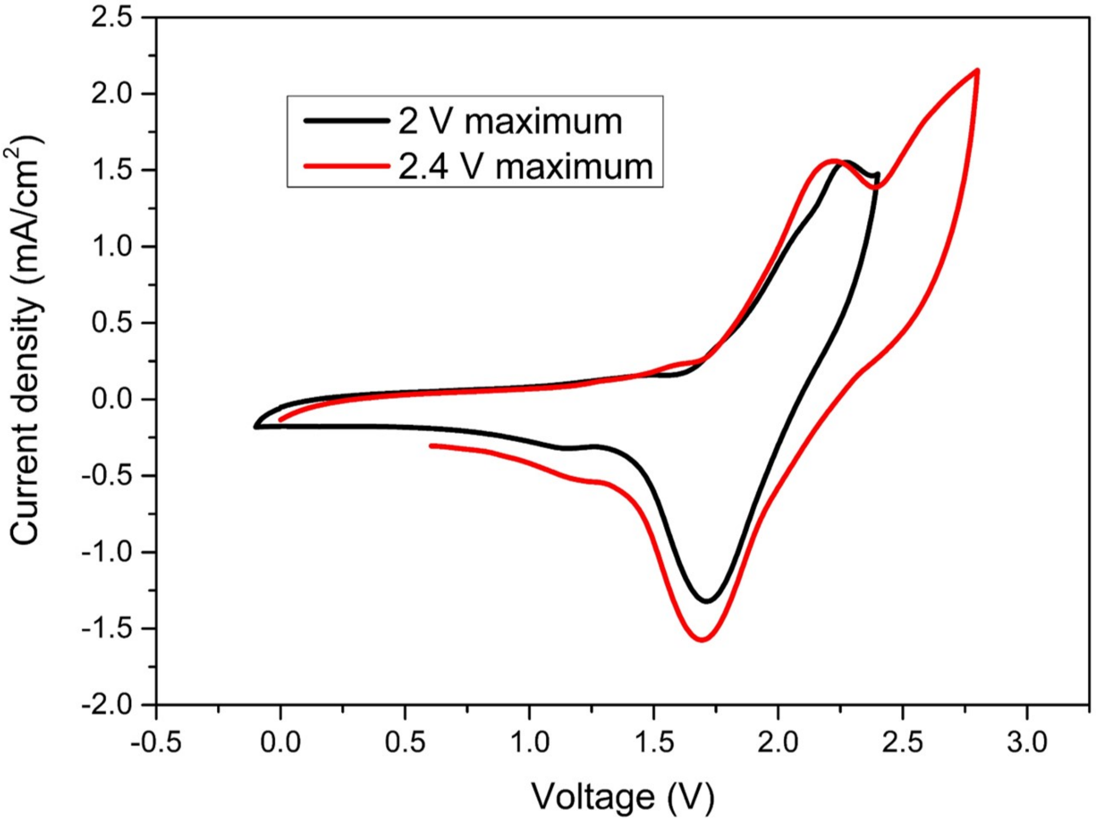

Figure 7.4: Cyclic voltammograms of a zinc ion battery after 100 cycles had been completed. The scan rate was 10 mV s^{-1}.

When the upper cut-off for these cells was raised to 2.4 V, 'infinite charging' behaviour was observed which indicated irreversible side reactions occurring. The curves were relatively flat and so these side reactions are probably not gas evolution from solvent decomposition.

The results of the magnesium ion batteries are presented in Figure 7.5. With the voltage cut-off set to 2 V, a high potential reaction at approximately 1.7 V decayed rapidly over the first 50 cycles. A low potential reaction at 0.5 V grew in over these first 50 cycles which is at a completely different potential to all other cells that used the electrode configuration.

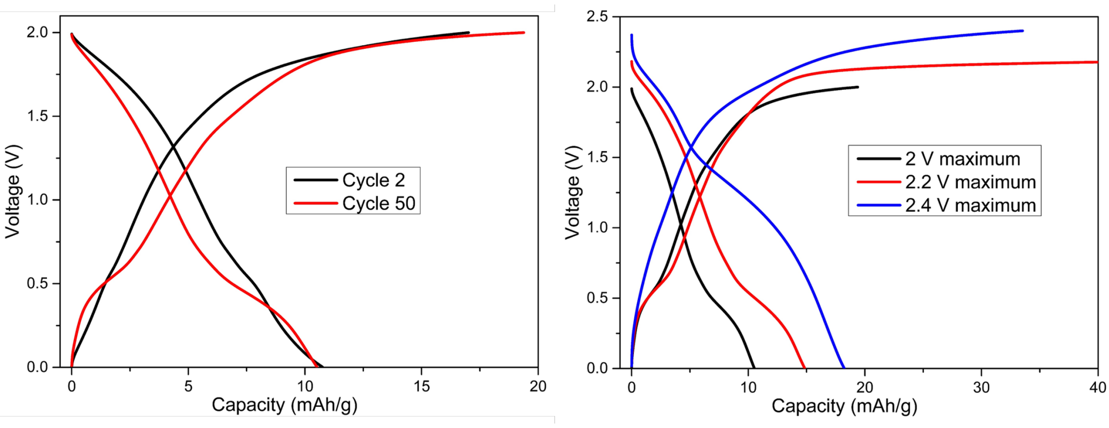

Figure 7.5: GCDC curves of a magneisum ion battery constructed as outlined previously. Over these cycles a current rate of 50 mA g^{-1} was used.

The capacity of these magnesium ion cells is also much lower than the other ion batteries, only reaching 11 mAh g^{-1} at this voltage cut off. What is also noticeable about these cells is that the coulombic efficiency of them is much lower than all the other ion batteries presented thus far in this chapter. The other cells all have coulombic efficiencies of 90% or higher whereas these magnesium ion batteries have a coulombic efficiency of only 65%. There is still no evidence of solvent splitting in these cells, so the degree of side reactions occurring in magnesium ion batteries must be much higher. The only difference between these cells is the salt that is being used. Why magnesium chloride would lead to a much greater amount of side reactions at a lower voltage than zinc chloride is unclear.

When the upper voltage cut off was raised to 2.2 V (after 100 cycles at 2 V) the high potential reaction reappears slightly, and the capacity increases to 15 mAh g^{-1}. Once the upper cutoff is raised again to 2.4 V, the lower potential reaction moves to a much higher potential, approximately 1.25 V. Such a shift in the potential of the reactions was also observed in the lithium ion batteries in Chapter 5 though the cause is still unclear.

The CVs of this cell are also unique compared to all the batteries tested so far as seen in Figure 7.6. There is a large, broad peak from 0 V to approximately 1.5 V. What is also noticeable is that there is a large spike in current density above 2 V in this CV which is not observed in any of the other ion battery CVs. This is most likely the irreversible side reactions that lead to the low coulombic efficiency of these cells.

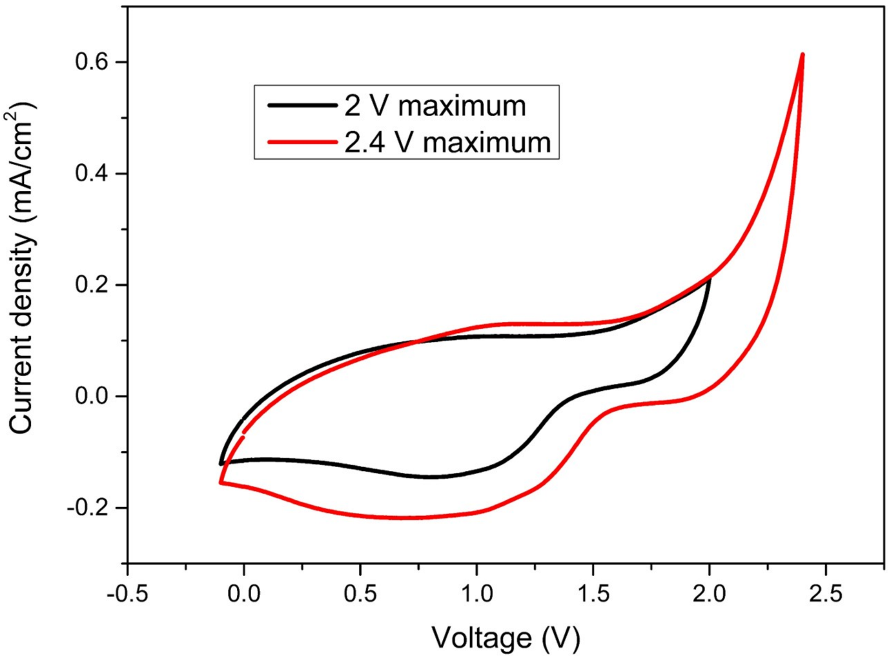

Figure 7.6: Cyclic voltammograms of a magnesium ion battery after 100 cycles had been completed. The scan rate was 10 mV s^{-1}.

For literature comparison, it is still rare to see fully functional magnesium ion batteries in literature, with most reports focusing on half cells using organic electrolytes. Zinc ion batteries are much more common though seeing functioning aqueous battery without a zinc metal anode is rare. This makes comparing these results difficult. Zinc ion batteries in literature regularly reach over 100 mAh g^{-1} though the voltage is often low at around 0.8 to 1.2 V [12, 169–171].

7.6 Conclusion

In this chapter, potassium, calcium, zinc and magnesium ion batteries were all briefly investigated in order to strengthen the IP position of the ME electrolytes and to investigate whether or not MEs could be used in more diverse settings beyond the most well understood battery systems. These experiments were successful, generating batteries based on all the ions tested though much more investigation is required to fully understand the mechanisms underpinning all of these cells.

Chapter 8

Summary and Outlook

8.1 Summary

In this thesis, microemulsion electrolytes were used for the first time in electrical energy storage devices. Custom glassy carbon based current collectors (Chapter 3) were constructed that allowed for Swagelock-type cells to be produced. With these cells, supercapacitors, lithium ion, sodium ion, potassium ion, calcium ion, zinc ion and magnesium ion batteries were all assembled with microemulsion electrolytes.

- Supercapacitors were constructed with an SDS based ME and were able to achieve 2.7 V on activated carbon electrodes. This is a record for aqueous electrolytes. The ME based supercapacitors showed similar capacitance values to cells assembled that used typical quarternary ammonium salts in acetonitrile as an electrolyte. While the rate capability of the ME based cells was lower than comparable acetonitrile supercapacitors, the ageing characteristics were similar suggesting a good stability of the ME electrolyte under these conditions.
- Lithium ion batteries were constructed using a Triton X-100 based ME. The use of a phase transfer catalyst in the form of diglyme was crucial in allowing the metal ions to pass through the EEI and enter the electrodes. One of the highest capacities ever observed for an aqueous lithium ion battery of 130 mAhg^{-1} was recorded using a TiO_2 anode and a V_2O_5 cathode. XRD results showed evidence of intercalation at the cathode but liitle to no change was observed in the anode

material using this method. Based on literature comparisons, this does not rule out lithium intercalation into the anode and further investigation is required to elucidate this.

- Sodium ion batteries were constructed using the same Triton X-100 ME with the additon of diglyme. With a Prussian blue cathode and a sodium titanate anode, the assembled cells achieved a record voltage of 1.7 V for the higher potential plateau seen in GCDC experiments. XRD experiments showed good agreement with intercalation at both electrodes.
- Potassium ion, calcium ion, zinc ion and magnesium ion batteries were assembled using Prussian blue cathodes and TiO_2 anodes. Despite the similarity in the systems the performance of these cells were markedly different to one another. The potassium and calcium ion batteries were similar in both CVs and GCDC experiments where as the zinc and magnesium cells were distinct from each other in both experiments.

8.2 Future outlook

Energy storage technology is advancing rapidly to try and cope with the global transition away from fossil fuels. A key part of this development is improving the sustainability and lowering the cost of the current energy storage and transportation technologies to ensure that there is equitable access to energy globally.

The use of aqueous electrolytes in ion batteries and supercapacitors would be step in the right direction due to a lower cost of materials and processing. However, water-based devices historically suffer from low energy densities due to the small electrochemical window of water. Microemulsions can be mostly water and yet have a much larger electrochemical window, sometimes as much as 5 V, compared to the 1.23 V window of water. Therefore, microemulsions have a huge potential as electrolytes for batteries and supercapacitors.

It is postulated that the ME electrolytes work by creating an oil rich layer on the electrode surface which prevents water from reaching the electrode and being split into hydrogen and oxygen gasses. Further investigation is required into this EEI in terms of not only its structure but how it evolves over time and changes as the devices are operating. For example, supercapacitors usually rely on the formation of a double layer at the electrode surface. How an ME based supercapacitor can still achieve a similar capacitance to an acetonitrile based supercapacitor (that lacks an EEI) requires more study. Solving this problem will likely involve electrochemical modelling combined with more in-depth EIS studies to not only determine the mechanism of double layer formation but figure out how to improve the performance of the supercapacitors that use and ME electrolyte. Further, only one ME and one electrode material has been tested in these supercapacitors, refining the composition and electrode materials is going to be important in the future.

Ion batteries are much more mechanistically complicated than supercapacitors, and so there are even more unanswered questions about the results presented in this thesis. First, while XRD analysis is a good indication of intercalation process occurring at the electrodes, XPS is a standard literature technique as it can identify which species are in the electrode, including the intercalating ion and confirming the oxidation states of the transition metal centres which can help to establish the mechanism of the cell. Beyond this, as with the supercapacitors, only one ME has been tested and only one pair of electrode materials for each ion. Much more work is needed, both at the cell and individual electrode level, to determine how to improve the cell across all metrics. As mentioned previously, the entire library of electrode materials for lithium ion batteries has been developed around the constraints of the electrochemical window of the solvents (and the SEIs that they create over time) on the electrodes. Moving to an electrolyte system with a window that is equally wide (if not wider) but in a different location (relative to the standard hydrogen electrode), means that a lot of this library is invalid e.g. graphite as an anode for lithium ion batteries. Much more research is required to find a set of electrode materials compatible with the ME electrolyte that exploit the window to the fullest.

Microemulsions show great promise as an electrolyte, being cheap and sustainable as well as more environmentally friendly. While there is no doubt a long way to go before they can be fully implemented in a commercial technology, microemulsions have the potential to disrupt and advance the electrical energy storage market.

(12) INTERNATIONAL APPLICATION PUBLISHED UNDER THE PATENT COOPERATION TREATY (PCT)

(19) World Intellectual Property Organization
International Bureau

(43) International Publication Date
25 June 2020 (25.06.2020)

WIPO | PCT

(10) International Publication Number
WO 2020/130857 A1

(51) International Patent Classification:
H01G 11/60 (2013.01) *H01M 10/26* (2006.01)

(21) International Application Number:
PCT/NZ2019/050164

(22) International Filing Date:
20 December 2019 (20.12.2019)

(25) Filing Language: English

(26) Publication Language: English

(30) Priority Data:
2018904852 20 December 2018 (20.12.2018) AU
2019903154 29 August 2019 (29.08.2019) AU

(71) Applicant: **VICTORIA LINK LIMITED** [NZ/NZ]; RB905 Rankine Brown Building, Kelburn Parade, Kelburn, Wellington, 6012 (NZ).

(72) Inventors: **BORAH, Rohan**; Level 7, NIER A, 70 Vale Street, Shortland, New South Wales 2307 (AU). **NANN, Thomas**; 71 Railway Street, Cooks Hill, New South Wales 2300 (AU). **HUGHSON, Fraser Ross**; 100 Hobson Street, Thorndon, 6011 (NZ).

(74) Agent: **CATALYST INTELLECTUAL PROPERTY**; Level 5, 45 Johnston Street, Wellington, 6011 (NZ).

(81) Designated States *(unless otherwise indicated, for every kind of national protection available)*: AE, AG, AL, AM, AO, AT, AU, AZ, BA, BB, BG, BH, BN, BR, BW, BY, BZ, CA, CH, CL, CN, CO, CR, CU, CZ, DE, DJ, DK, DM, DO, DZ, EC, EE, EG, ES, FI, GB, GD, GE, GH, GM, GT, HN, HR, HU, ID, IL, IN, IR, IS, JO, JP, KE, KG, KH, KN, KP, KR, KW, KZ, LA, LC, LK, LR, LS, LU, LY, MA, MD, ME, MG, MK, MN, MW, MX, MY, MZ, NA, NG, NI, NO, NZ, OM, PA, PE, PG, PH, PL, PT, QA, RO, RS, RU, RW, SA, SC, SD, SE, SG, SK, SL, SM, ST, SV, SY, TH, TJ, TM, TN, TR, TT, TZ, UA, UG, US, UZ, VC, VN, ZA, ZM, ZW.

(84) Designated States *(unless otherwise indicated, for every kind of regional protection available)*: ARIPO (BW, GH, GM, KE, LR, LS, MW, MZ, NA, RW, SD, SL, ST, SZ, TZ, UG, ZM, ZW), Eurasian (AM, AZ, BY, KG, KZ, RU, TJ, TM), European (AL, AT, BE, BG, CH, CY, CZ, DE, DK, EE, ES, FI, FR, GB, GR, HR, HU, IE, IS, IT, LT, LU, LV, MC, MK, MT, NL, NO, PL, PT, RO, RS, SE, SI, SK, SM, TR), OAPI (BF, BJ, CF, CG, CI, CM, GA, GN, GQ, GW, KM, ML, MR, NE, SN, TD, TG).

Published:
- *with international search report (Art. 21(3))*
- *in black and white; the international application as filed contained color or greyscale and is available for download from PATENTSCOPE*

(54) Title: ELECTROLYTE COMPOSITIONS

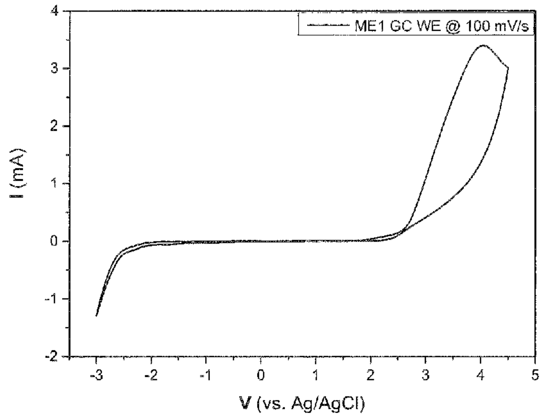

Figure 1

(57) Abstract: Disclosed are electrolyte compositions for electrochemical devices, where the electrolyte compositions comprise a microemulsion and where the microemulsion comprises an aqueous phase and a water-immiscible phase. Also disclosed are microemulsion electrolyte compositions for electrically rechargeable electrochemical energy storage devices, including ion batteries (such as lithium ion, sodium ion, magnesium ion, calcium ion, and aluminium ion batteries), redox flow batteries and supercapacitors.

WO 2020/130857 A1

ELECTROLYTE COMPOSITIONS

TECHNICAL FIELD

The present invention relates to microemulsion electrolyte compositions, and their use in electrochemical energy storage devices.

BACKGROUND

Electrochemical systems, in particular batteries, need an electrolyte which can facilitate dissolution and migration of ions and electrochemically active species. Desirable, or even necessary, properties of an electrolyte are good conductivity, a wide electrochemical window, and an ability to solubilise salts and electrochemically active species used in the battery. Low cost is an economic consideration for commercial applications of electrolytes.

Water is a desirable electrolyte solvent because it is a cheap solvent that is non-toxic and can be safely handled.

A drawback of water for use as an electrolyte solvent is that the electrochemical stability window of water, 1.23 V, is too narrow to support many electrochemical couples used in modern batteries.

Water can be oxidised to form oxygen gas and reduced to form hydrogen gas (commonly referred to as water splitting) at a potential of 1.23V:

$$2H_2O \rightarrow O_2 + 4H^+ + 4e^- \quad E^o = +1.23V$$

$$2H^+ + 2e^- \rightarrow H_2 \quad E^o = 0.00V$$

Therefore: $2H_2O \rightarrow O_2 + 2H_2 \quad E^o = +1.23V$

Batteries using aqueous electrolytes are therefore limited to operate with cell voltages below 1.23 V to avoid degradation. Reactions with potentials which fall outside of the electrochemical stability window would cause water splitting and the evolution of hydrogen and/or oxygen. These reactions deteriorate the electrochemical system, and present a safety hazard to the user. This is a significant limitation because modern batteries, for example, are able to run at potentials significantly greater than 1.23 V, meaning that water cannot be used as an electrolyte.

It is worth noting that the thermodynamic potential of the water splitting reaction is about -0.2 V vs. Ag/AgCl for reduction and about 1 V vs. Ag/AgCl for oxidation, resulting in an overall theoretical window of 1.23 V. However, practical applications of the water splitting reactions experience a non-trivial over-potential. The measured magnitude of the onset potential for oxidation and/or reduction is typically a larger voltage than what is theoretically expected. Whilst it is therefore possible to operate an aqueous battery beyond the thermodynamic limit of 1.23 V, known aqueous electrolytes undergo significant decomposition beyond this limit in normal use, and so exceeding the thermodynamic limit of the aqueous electrolyte is avoided.

Attempts to extend the electrochemical stability window of water have been made in the past. Aqueous electrolytes have been reported to widen electrochemical stability windows compared to bulk water, but these advances have not been sufficient to replace non-aqueous electrolytes in many applications. Further, materials used in electrodes and as electrolyte additives required in these attempts are costly and/or hazardous.

Non-aqueous solvents having electrochemical windows wider than bulk water are used in many electrochemical cells including some batteries. However, there are drawbacks to non-aqueous solvents, such as their expense compared to water, toxicity, flammability and/or their reduced ability to solubilise salts.

Since water as a solvent can solubilise salts, including inorganic and many organic salts, it is an ideal solvent (in this respect) for use as a battery electrolyte. Increasing the concentration of dissolved salts in an aqueous solution increases the charge conductivity of the solution. Further, water also has the ability to solubilise some non-ionic compounds, such as some redox active organic molecules, and allows the aqueous electrolyte to be applied to a range of batteries with different electrochemically active species.

The current of an operating electrochemical cell is dependent on the concentration of the electrochemically active species involved in an electrochemical reaction. The more an electrochemically active species is dissolved in the electrolyte, the higher the concentration of active species and hence the higher the current that can be extracted from the electrochemical cell. For water-soluble electrochemically active species such as metal salts, using water as a solvent allows for a relatively high salt concentration. However, the current that can be produced by an electrochemical cell with an aqueous electrolyte is reduced where electrochemically active species are less soluble in water. As water-insoluble electrochemically active species are often incompatible with aqueous solvents, and water soluble active species are often incompatible with organic solvents, there are significant difficulties in finding compatible solvents and active species in which the conductivity of the electrolyte and the concentration of the active species in the electrolyte can be simultaneously maximised.

An example of the limitations in known electrolyte compositions can be found in ion batteries including magnesium ion batteries, sodium ion batteries, aluminium ion batteries and lithium ion batteries. For example, magnesium ion batteries have been plagued by the cost and complexity of the magnesium salts and organic solvents necessary to achieve the requisite conductivity, solubility and electrochemical window to make a useful magnesium battery.

Limitations of known electrolyte compositions are also apparent in flow batteries. Flow batteries, such as redox flow batteries, are characterised by the use of an electrolyte (specifically, an anolyte and catholyte) that flows over the surface of non-reactive electrodes separated by an exchange membrane. Anolytes and catholytes comprising electrochemically active species are contained in separate compartments. In use, anolytes and catholytes are pumped over their respective electrodes, and electrical current is generated by the transfer of charge between the compartments. As energy is stored in the electrolyte, the storage capacity of the battery scales with improvements to the electrolyte composition and electrolyte volume. Increasing the volume of electrolyte increases the energy that can be stored. Consequently, the economic cost of energy from flow batteries is, in part, proportionate to the cost of the electrolyte. As with other types of electrochemical cells, the efficiency of redox flow batteries may be enhanced by electrolytes that can support higher concentrations of electrochemically active species and electrolytes that have a wider electrochemical stability window.

As a result, the performance of batteries is highly dependent on many factors including the physicochemical properties of the materials from which the electrode(s) of the battery are made and the electrolyte solutions. Such factors affect battery performance by decreasing the battery voltage, affecting coulombic efficiency, lowering the rate capability (maximum charge/discharge rate) of the cell, and cell stability.

There is therefore a need for an electrolyte composition that provides a wide electrochemical window in which electrochemistry can be performed; exhibits good conductivity; is low cost; and has the ability to dissolve compounds across a range of polarities.

It is an object of the present invention to provide an electrolyte composition, and/or its use in an electrochemical cell such as an ion battery, redox flow battery and supercapacitor that overcomes at least one of the abovementioned disadvantages, or addresses or partially addresses at least one of the abovementioned needs, or at least provides the public with a useful choice.

SUMMARY OF THE INVENTION

In an aspect, there is provided an electrolyte composition suitable for, adapted for, or configured for an electrochemical cell, wherein the electrolyte composition comprises a microemulsion. The microemulsion comprises an aqueous phase and a water-immiscible phase.

In an example, the aqueous phase is a continuous phase. The water-immiscible phase may be dispersed in a continuous aqueous phase or alternatively, the microemulsion may be a bicontinuous microemulsion such that the water-immiscible phase and the aqueous phase are both continuous phases.

In a preferred embodiment, the microemulsion is an oil-in-water microemulsion or a bicontinuous microemulsion.

The microemulsion may comprise between 1% and 99% water by weight of the microemulsion, including, for example, between 10% and 99% water by weight of the microemulsion, and between 20% and 99% water by weight of the microemulsion.

Where the microemulsion comprises a continuous aqueous phase and a dispersed water-immiscible phase (i.e. an oil-in-water microemulsion), the microemulsion may comprise between 80% and 99% water by weight of the microemulsion. Where the microemulsion is a bicontinuous microemulsion, the microemulsion may comprise between 20% and 80% water by weight of the microemulsion.

The microemulsion may comprise a dissolved salt, for example to increase the electrical conductivity of the microemulsion. The dissolved salt may be an organic salt, an inorganic salt, or a combination thereof. In an example, the dissolved salt is selected from the group consisting of: a lithium salt, a sodium salt, a potassium salt, a magnesium salt, a calcium salt, an aluminium salt, and a combination thereof. In an example, the concentration of salts in the microemulsion electrolyte composition is between 0 and 10 M, between about 0.001 M and 10 M, more preferably between about 0.01 M and 5 M, more preferably between 0.05 M and 1 M, most preferably between about 0.05 M and 0.5 M. In another example, the concentration of salts in the microemulsion electrolyte composition is between 0 and 10 mol/kg, more preferably between about 0.001 mol/kg and 10 mol/kg, more preferably about 0.01 mol/kg and 5 mol/kg, more preferably between 0.05 mol/kg and 1 mol/kg.

The microemulsion may comprise one or more electrochemically active species. The electrochemically active species are dissolved in the water-immiscible phase or aqueous phase of the microemulsion. The electrochemically active species may be redox active organic species. Redox active organic species, and electrochemically active species, would be readily known and understood to those of skill in the art. Examples of redox active organic species that may be dissolved in the microemulsion include: ferrocene, (2,2,6,6-tetramethylpiperidin-1-yl)oxyl (TEMPO), phenothiazines, dimethoxybenzene, menadione and 2,1,3-benzothiadiazole.

The water-immiscible phase of the microemulsion may comprise an organic solvent. In an example, the water-immiscible phase may be selected from: aliphatic solvents such as hexane, cyclohexane, petroleum ether; aromatic solvents such as benzene, toluene, p-xylene, 1,2-dichlorobenzene; halogenated solvents such as dichloromethane, chloroform, dichloroethane; substantially water immiscible ketone solvents such as acetophenone; substantially water immiscible ester solvents such as ethyl benzoate, ethyl acetate; ether solvents such as diethyl ether; and a combination thereof.

The microemulsion may comprise one or more amphiphiles, such as a surfactant, a co-surfactant and/or co-solvent. Suitable surfactants and co-surfactants for the preparation of microemulsion electrolyte compositions will be known in the art. Examples of suitable surfactants include anionic surfactants, cationic surfactants, zwitterionic surfactants and non-ionic surfactants. Examples of preferred surfactants include Triton X-100 (*t*-octylphenoxypolyethoxyethanol), cetyltrimethylammonium chloride (CTAC), cetylpyridinium chloride (CPC), benzalkonium chloride, benzethonium chloride, sodium dodecyl sulfate (SDS), and sodium lauryl ether sulfate (SLES). Examples of suitable co-surfactants or co-solvents include aliphatic alcohols, such as C2-C6 alcohols, and amines, such as C2-C6 alkyl amines. Preferred co-surfactants and/or co-solvents for the present invention include ethanol, propanol, butanol and pentanol.

The microemulsion may comprise one or more phase transfer catalysts. An example of a suitable phase transfer catalyst is bis(2-methoxyethyl) ether (diglyme).

In an example of the present invention, the microemulsion has a conductivity of more than 0.1 $mS.cm^{-1}$, more than 1 $mS.cm^{-1}$, more than 3 $mS.cm^{-1}$, more than 5 $mS.cm^{-1}$, between 1 and 12 $mS.cm^{-1}$, between 3 and 10 $mS.cm^{-1}$.

In an example of the present invention, the microemulsion has an electrochemical stability window of greater than 1.23 V, greater than 1.5 V, greater than 2 V, greater than 2.5 V, greater than 3 V, greater than 3.5 V, or greater than 4 V.

In a further aspect of the present invention, there is provided an electrolyte composition suitable for, adapted for, or configured for an ion battery, wherein the electrolyte composition comprises the microemulsion.

In another aspect of the present invention, there is provided an electrolyte composition suitable for, adapted for, or configured for redox flow battery, wherein the electrolyte composition comprises the microemulsion.

In a further aspect of the present invention, there is provided an electrolyte composition suitable for, adapted for, or configured for a supercapacitor, wherein the electrolyte composition comprises the microemulsion.

In a further aspect of the present invention, there is provided a microemulsion which is suitable for use, or adapted for use, or configured for use as an electrolyte in an electrochemical cell.

In an example of the present invention, the electrolyte composition consists essentially of the microemulsion.

In a further aspect of the present invention, there is provided a microemulsion comprising one or more electrochemically active species.

In an example according to this aspect of the present invention, the microemulsion comprises an aqueous phase and a water-immiscible phase. Preferably, the microemulsion is an oil in water microemulsion or a bicontinuous microemulsion.

In an example according to this aspect of the present invention, the one or more electrochemically active species is dissolved in the water-immiscible phase. In an alternative example, the one or more electrochemically active species is dissolved in the aqueous phase.

The electrochemically active species may be a dissolved salt. The electrochemically active species may be a redox active organic species.

In an example according to this aspect of the present invention, at least one of the electrochemically active species or redox active organic species have a reaction potential, or redox potential, of greater than 1.23 V (compared to a standard hydrogen electrode). That is, the electrochemical reaction of the electrochemically active species or redox active organic species would cause water splitting of bulk water.

In a further aspect of the present invention, there is provided a microemulsion comprising an aqueous phase, wherein the electrochemical stability window of the microemulsion is greater than 1.23 V.

The microemulsion may comprise an electrochemically active species. In an example, at least one of the electrochemically active species have a reaction potential, or redox potential, of greater than 1.23 V.

The electrochemically active species may be a redox active organic species, examples of which are described herein.

In a further aspect of the present invention, there is provided an electrochemical cell comprising an electrolyte, wherein the electrolyte comprises a microemulsion. The microemulsion comprises an aqueous phase and a water-immiscible phase.

In an example, the electrochemical cell is an electrochemical energy storage device (EESD). EESDs store energy in the form of chemical energy. Electrical energy, in the form of an electrical current, is released during discharging of the device by converting chemical energy to electric energy. EESDs include two electrodes (e.g. an anodic electrode and a cathodic electrode), an electrolyte in electrical contact with the electrodes and, optionally, an ion permeable separator. EESDs generate an electrical potential difference between the electrodes. Examples of EESDs include supercapacitors, ion batteries and flow batteries.

In an example, the EESD is an electrically rechargeable EESD. Electrically rechargeable EESDs comprise electrochemically active species that reversibly react to either generate (during discharge) or store (during charge) electrical energy. Electrically rechargeable EESDs are charged by the input of electrical energy, which restores the electrochemically active species. During discharge, the electrochemically active species react to generate an electrical current. During charging, an externally applied potential drives the reverse reaction to restore the electrochemically active species. Examples of electrically rechargeable EESDs include supercapacitors, ion batteries and flow batteries.

In an example, the EESD is not a fuel cell. In an example, the electrically rechargeable EESD is not a fuel cell.

In an example of the present invention, the electrolyte consists essentially of a microemulsion.

In an example, the electrochemical cell has a cell voltage of greater than 1.23 V, greater than 1.5 V, greater than 2 V, greater than 2.5 V, greater than 3 V, greater than 3.5 V, or greater than 4 V. In an example of the present invention, the electrochemical cell has a cell voltage of between 0.01 V and 4 V, between 1.0 and 4.0 V, between 1.23 V and 4.0 V, between 1.23 and 3.5 V, between 1.23 and 3.0 V, between 1.23 and 2.5 V, or between 1.23 and 2.0 V.

In an example, the aqueous phase is a continuous phase. The water-immiscible phase may be dispersed in a continuous aqueous phase or alternatively, the microemulsion may be a bicontinuous microemulsion such that the water-immiscible phase and the aqueous phase are both continuous phases.

In a preferred embodiment, the microemulsion is an oil-in-water microemulsion or a bicontinuous microemulsion.

In an example, the electrolyte is in electrical contact with the electrodes of the electrochemical cell.

In an example, the electrochemical cell may be selected from an ion battery. The ion battery may be a lithium ion battery, a magnesium ion battery, a calcium ion battery, an aluminium ion battery, a potassium ion battery or a sodium ion battery. In an example, the battery includes an anode, a cathode, the microemulsion electrolyte composition and, optionally, an ion-permeable separator, such as an ion-permeable membrane (e.g. disposed between the anode and the cathode). In an example, the electrolyte composition is in electrical contact with the anode and cathode.

The battery may include a current collector. Preferred current collectors comprise a substantially hydrophobic or lipophilic surface which is configured to contact the electrolyte.

Examples of substantially hydrophobic or lipophilic surfaces include non-metallic conductive surfaces, conductive carbon (e.g. graphite and carbon black), and conductive polymers such as conjugated polymers (polypyrrole, polythiophene, polyanilines). Preferred examples of substantially hydrophobic or lipophilic surfaces include glassy carbon and graphite surfaces.

In an example, the electrochemical cell is a supercapacitor. The supercapacitor may comprise anodic and cathodic electrodes, optionally, an ion-permeable separator, and the microemulsion electrolyte composition of the present invention. The electrodes may comprise a substantially hydrophobic or lipophilic surface in contact with (or configured to contact) the microemulsion. The electrodes may comprise high surface area materials such as zeolites and molecular sieves. The electrodes should comprise conductive materials.

Suitable conductive materials include graphite or carbon black. The electrolyte of the supercapacitor is the microemulsion electrolyte composition of the present invention.

In an example, the electrochemical cell is a sensor.

In a further aspect of the present invention, there is provided an electrochemical cell comprising an electrolyte, wherein the electrolyte comprises or consists essentially of a microemulsion and wherein the microemulsion has an electrochemical stability window of greater than 1.23 V, greater than 1.5 V, greater than 2 V, greater than 2.5 V, greater than 3 V, greater than 3.5 V, greater than 4 V.

In a further aspect of the present invention, there is provided an electrochemical cell comprising an electrolyte, wherein the electrolyte comprises or consists essentially of a microemulsion, wherein the electrochemical cell has a cell voltage of greater than 1.23 V, 1.5 V, greater than 2 V, greater than 2.5 V, greater than 3 V, greater than 3.5 V, greater than 4 V.

In a further aspect of the present invention, there is provided a sodium ion battery comprising an electrolyte, wherein the electrolyte comprises or consists essentially of a microemulsion.

In a further aspect of the present invention, there is provided a magnesium ion battery comprising an electrolyte, wherein the electrolyte comprises or consists essentially of a microemulsion.

In a further aspect of the present invention, there is provided a lithium ion battery comprising an electrolyte, wherein the electrolyte comprises or consists essentially of a microemulsion, wherein the microemulsion comprises a lithium salt.

In a further aspect of the present invention, there is provided an aluminium ion battery comprising an electrolyte, wherein the electrolyte comprises or consists essentially of a microemulsion, wherein the microemulsion comprises an aluminium salt.

In a further aspect of the present invention, there is provided a potassium ion battery comprising an electrolyte, wherein the electrolyte comprises or consists essentially of a microemulsion, wherein the microemulsion comprises a potassium salt.

In a further aspect of the present invention, there is provided a calcium ion battery comprising an electrolyte, wherein the electrolyte comprises or consists essentially of a microemulsion, wherein the microemulsion comprises a calcium salt.

In a further aspect of the present invention, there is provided a redox flow battery comprising an electrolyte, wherein the electrolyte comprises or consists essentially of a microemulsion. In an example, the electrolyte may be an anolyte, a catholyte, or both.

In a further aspect of the present invention, there is provided a supercapacitor comprising an electrolyte, wherein the electrolyte comprises or consists essentially of a microemulsion.

In an example, the electrochemical cell comprises electrodes which have a substantially hydrophobic or lipophilic surface in contact with (or configured to contact) the microemulsion. Preferred examples of substantially hydrophobic or lipophilic surfaces include glassy carbon and graphite surfaces. In an example, the anode has a substantially hydrophobic or lipophilic surface in contact with (or configured to contact) the microemulsion. In another example, the cathode has a substantially hydrophobic or lipophilic surface in contact with (or configured to contact) the microemulsion.

The electrochemical cell may include a current collector. Preferred current collectors comprise a substantially hydrophobic or lipophilic surface which is in contact with or configured to contact the microemulsion. Preferred examples of substantially hydrophobic or lipophilic surfaces include glassy carbon and graphite surfaces.

The electrochemical cell may be positioned within a housing. For example, the housing may contain components including the microemulsion electrolyte composition, electrodes, and, optionally, the ion permeable separator (e.g. located between the anodic and cathodic electrodes).

In a further aspect of the present invention, there is provided an electrolyte composition when used in an electrochemical cell, wherein the electrolyte composition comprises or consists essentially of a microemulsion. The microemulsion comprises an aqueous phase and a water-immiscible phase.

The electrochemical cell may be selected from an ion battery, a supercapacitor, an electrolytic cell and a flow battery. The ion battery may be selected from a lithium ion battery, a magnesium ion battery, a calcium battery, an aluminium ion battery, and a sodium ion battery. The flow battery may be a redox flow battery.

In a further aspect of the present invention, there is provided a use of a microemulsion in an electrochemical cell wherein the microemulsion comprises an aqueous phase and a water-immiscible phase.

In a further aspect of the present invention, there is provided a microemulsion when used as an electrolyte for an electrochemical cell wherein the microemulsion comprises an aqueous phase and a water-immiscible phase.

In a further aspect of the present invention, there is provided an electrolyte composition when used in a redox flow battery, wherein the electrolyte composition comprises or consists essentially of a microemulsion, wherein the microemulsion comprises an aqueous phase and a water-immiscible phase.

In a further aspect of the present invention, there is provided an electrolyte composition when used in a sodium ion battery, wherein the electrolyte composition comprises or consists essentially of a microemulsion, wherein the microemulsion comprises an aqueous phase and a water-immiscible phase.

In a further aspect of the present invention, there is provided an electrolyte composition when used in a lithium ion battery, wherein the electrolyte composition comprises or consists essentially of a microemulsion, wherein the microemulsion comprises an aqueous phase and a water-immiscible phase.

In a further aspect of the present invention, there is provided an electrolyte composition when used in a magnesium ion battery, wherein the electrolyte composition comprises or consists essentially of a microemulsion, wherein the microemulsion comprises an aqueous phase and a water-immiscible phase.

In a further aspect of the present invention, there is provided an electrolyte composition when used in an aluminium ion, wherein the electrolyte composition comprises or consists essentially of a microemulsion, wherein the microemulsion comprises an aqueous phase and a water-immiscible phase.

In a preferred embodiment, the ion batteries described herein further comprise a phase transfer catalyst.

In a further aspect of the present invention, there is provided an electrolyte composition when used in a supercapacitor, wherein the electrolyte composition comprises or consists essentially of a microemulsion, wherein the microemulsion comprises an aqueous phase and a water-immiscible phase.

In a further aspect of the present invention, there is provided use of a microemulsion in an electrochemical cell, wherein the microemulsion increases the electrochemical cell's electrochemical window above 1.23 V, wherein the microemulsion comprises an aqueous phase and a water-immiscible phase.

In a further aspect of the present invention, there is provided a microemulsion when used in an electrochemical cell to increase the electrochemical cell's electrochemical stability window above 1.23 V, wherein the microemulsion comprises an aqueous phase and a water-immiscible phase.

In an example of the foregoing uses of the present invention, the aqueous phase is a continuous phase. The water-immiscible phase may be dispersed in a continuous aqueous phase or alternatively, the microemulsion may be a bicontinuous microemulsion such that the water-immiscible phase and the aqueous phase are both continuous phases.

In a preferred embodiment, the microemulsion is an oil-in-water microemulsion or a bicontinuous microemulsion.

In a further aspect of the present invention, there is provided a method of improving the conductivity of an organic electrolyte for an electrochemical cell, comprising the step of combining the organic electrolyte with an aqueous phase and converting the organic electrolyte into a microemulsion, wherein the microemulsion comprises an aqueous phase and a water-immiscible phase.

In a further aspect of the present invention, there is provided a method of increasing the electrochemical stability window of an aqueous electrolyte for an electrochemical cell, comprising the step of combining the aqueous electrolyte with an organic solvent and converting the aqueous electrolyte into a microemulsion, wherein the microemulsion comprises an aqueous phase and a water-immiscible phase.

In a further aspect of the invention, there is provided a method for increasing an electrochemical window in an electrochemical cell above 1.23 V, the method comprising combining an aqueous phase and a water-immiscible phase to provide a microemulsion, wherein the microemulsion comprises an aqueous phase and a water-immiscible phase.

In a further aspect of the invention, there is provided a method for using an electrochemical cell of the present invention comprising connecting the electrochemical cell comprising the microemulsion electrolyte composition of the present invention to a load and supplying a charge to the load.

In an example of the foregoing methods of the present invention, the aqueous phase is a continuous phase. The water-immiscible phase may be dispersed in a continuous aqueous phase or alternatively, the microemulsion may be a bicontinuous microemulsion such that the water-immiscible phase and the aqueous phase are both continuous phases.

In a preferred embodiment, the microemulsion is an oil-in-water microemulsion or a bicontinuous microemulsion.

BRIEF DESCRIPTION OF THE FIGURES

Figure 1 is a cyclic voltammogram of ME1, scan speed 100 mV.s^{-1}.

Figure 2 is a cyclic voltammogram of ME2, scan speed 100 mV.s^{-1}.

Figure 3 is a cyclic voltammogram of ME3, scan speed 100 mV.s^{-1}.

Figure 4 is a cyclic voltammogram of ME4, scan speed 100 mV.s^{-1}.

Figure 5 is a cyclic voltammogram of ME5, scan speed 100 mV.s^{-1}.

Figure 6 is a cyclic voltammogram of ME6, scan speed 100 mV.s^{-1}.

Figure 7 is a cyclic voltammogram of ME10, scan speed 100 mV.s^{-1}.

Figure 8 is a cyclic voltammogram of ME11, scan speed 100 mV.s^{-1}.

Figure 9 is a cyclic voltammogram of ME12, scan speed 100 mV.s^{-1}.

Figure 10 is a cyclic voltammogram of ME13, scan speed 100 mV.s^{-1}.

Figure 11 is a cyclic voltammogram of ME2b, scan speed 100 mV.s^{-1}.

Figure 12 is a cyclic voltammogram of 0.1 M aqueous solution of KCl, scan speed 100 mV.s^{-1}.

Figure 13 is a cyclic voltammogram of ferrocene in ME1, scan speed 100 mV.s^{-1}.

Figure 14 is a cyclic voltammogram of ferrocene in ME2, scan speed 100 mV.s^{-1}.

Figure 15 is a cyclic voltammogram of ferrocene in ME3, scan speed 100 mV.s^{-1}.

Figure 16 is a cyclic voltammogram of ferrocene in ME4, scan speed 100 mV.s^{-1}.

Figure 17 is a cyclic voltammogram of ferrocene in ME5, scan speed 100 mV.s^{-1}.

Figure 18 is a cyclic voltammogram of ferrocene in ME6, scan speed 100 mV.s^{-1}.

Figure 19 is a cyclic voltammogram of ferrocene in ME10, scan speed 100 mV.s^{-1}.

Figure 20 is a cyclic voltammogram of ferrocene in ME11, scan speed 100 mV.s^{-1}.

Figure 21 is a cyclic voltammogram of ferrocene in ME12, scan speed 100 mV.s^{-1}.

Figure 22 is a cyclic voltammogram of ferrocene in ME13, scan speed 100 mV.s^{-1}.

Figure 23 is a cyclic voltammogram of ferrocene in ME2b, scan speed 100 mV.s^{-1}.

Figure 24 is a chronopotentiogram of a magnesium ion battery comprising 0.5 mol.dm^{-3} $MgSO_4$ in ME1.

Figure 25 is a chronopotentiogram of a sodium ion battery comprising 0.1 mol.dm^{-3} NaCl in ME2.

Figure 26 is a chronopotentiogram of a lithium ion battery comprising 0.1 mol.dm^{-3} LiCl in ME2.

Figure 27 is a chronopotentiogram of an aluminium ion battery comprising 0.1 mol.dm^{-3} $AlCl_3$ in ME2.

Figure 28 is a chronopotentiogram of a magnesium ion battery with an aqueous electrolyte.

Figure 29 is a chronopotentiogram of a redox flow battery comprising an ME2-based electrolyte described in Example 6.

Figure 30 is a charge-discharge curve of Cell 1 after 30 charge/discharge cycles.

Figure 31 shows the charge capacity (mAh/g), discharge capacity (mAh/g) and coulombic efficiency over repeated charge/discharge cycles of Cell 1.

Figure 32 is a charge-discharge curve of Cell 1 after 30 charge/discharge cycles, tested at 1A/g.

Figure 33 shows the charge capacity (mAh/g), discharge capacity (mAh/g) and coulombic efficiency over repeated charge/discharge cycles of Cell 1, tested at 1A/g.

Figure 34 is a charge-discharge curve of Cell 2 after 90 charge/discharge cycles

Figure 35 shows the charge capacity (mAh/g), discharge capacity (mAh/g) and coulombic efficiency over repeated charge/discharge cycles of Cell 2.

Figure 36 is a charge-discharge curve of Cell 3 after 40 charge/discharge cycles.

Figure 37 shows the charge capacity (mAh/g), discharge capacity (mAh/g) and coulombic efficiency over repeated charge/discharge cycles of Cell 3.

Figure 38 is a charge-discharge curve of Cell 4 after 50 and 100 charge/discharge cycles

Figure 39 shows the charge capacity (mAh/g), discharge capacity (mAh/g) and coulombic efficiency over repeated charge/discharge cycles of Cell 4.

Figure 40 is a charge-discharge curve of Cell 4 after 750 charge/discharge cycles

Figure 41 shows the charge capacity (mAh/g), discharge capacity (mAh/g) and coulombic efficiency over repeated charge/discharge cycles of Cell 4 for charge/discharge 750 cycles.

Figure 42 shows the charge capacity (mAh/g), discharge capacity (mAh/g) and coulombic efficiency over repeated charge/discharge cycles of Cell 5.

Figure 43 is a cyclic voltammogram of Cell 5 (V_2O_5 electrode).

Figure 44 is a cyclic voltammogram of Cell 5 (TiO_2 electrode).

Figure 45 is a cyclic voltammogram of Cell 6 (TiO_2 electrode).

Figure 46 shows charge-discharge curves of the supercapacitor of Example 8 for charge-discharge cycles 495-500.

Figure 47 shows the charge capacity and discharge capacity (mAh/g) of the supercapacitor of Example 8 over repeated cycles.

Figure 48 shows the coulombic efficiency of the supercapacitor of Example 8 over repeated cycles.

DEFINITIONS

Unless specifically defined otherwise, all technical and scientific terms used herein shall be taken to have the same meaning as commonly understood by one of ordinary skill in the art (for example, in materials science and chemistry).

It is intended that reference to a range of numbers disclosed herein (e.g. 1 to 10) also incorporates reference to all related numbers within that range (e.g. 1, 1.1, 2, 3, 3.9, 4, 5, 6, 6.5, 7, 8, 9 and 10) and also any range of rational numbers within that range (for example 2 to 8, 1.5 to 5.5 and 3.1 to 4.7) and, therefore, all sub-ranges of all ranges expressly disclosed herein are expressly disclosed. These are only examples of what is specifically intended and all possible combinations of numerical values between the lowest value and the highest value enumerated are to be considered to be expressly stated in this application in a similar manner.

The term "and/or", e.g., "X and/or Y" shall be understood to mean either "X and Y" or "X or Y" and shall be taken to provide explicit support for both meanings or for either meaning.

Throughout this specification the word "comprise", or variations such as "comprises" or "comprising", will be understood to imply the inclusion of a stated element, integer or step, or group of elements, integers or steps, but not the exclusion of any other element, integer or step, or group of elements, integers or steps i.e. including but limited only to.

Throughout this specification, unless specifically stated otherwise or the context requires otherwise, reference to a single step, composition of matter, group of steps or group of compositions of matter shall be taken to encompass one and a plurality (i.e. one or more) of those steps, compositions of matter, groups of steps or group of compositions of matter.

The term "cyclic voltammetry" refers to a type of potentiodynamic electrochemical measurement. To obtain a cyclic voltammogram, the voltage is varied in a solution and the change in current is measured with respect to the change in voltage. It is a specific type of voltammetry used for studying the redox properties of chemicals and interfacial structures.

The term "electrochemical window" or "electrochemical stability window" of an electrolyte refers to the voltage range between which the electrolyte is not substantially oxidised or reduced. For example, the electrochemical stability window of water is the difference between the potential at which water is reduced to hydrogen (H_2), and at which water is oxidised to oxygen (O_2). Electrochemical stability may be measured or described in terms of a cyclic voltammetry measurement, in which the electrochemical stability window is the potential difference between the onset potential (the potential at which the current begins to rise or fall) of each of the cathodic and anodic reactions

The term "immiscible", with reference to two or more materials, means that a material will not dissolve or combine with another material. With reference to immiscible liquids in biphasic systems such as the microemulsions described herein, "immiscible" means that the liquids are insoluble with each other, or are so sparingly soluble in each other that for all practical purposes the liquids are conventionally considered to be insoluble with each other. When two immiscible liquids are combined in a system, it will form a biphasic system of immiscible liquids.

A microemulsion is a thermodynamically stable mixture of two immiscible liquid phases. Microemulsions can be "oil-in-water", "water-in-oil", or "bicontinuous"; these terms which define a microemulsion structure are well known in the art. In oil-in-water microemulsions, a water-immiscible phase is dispersed in a continuous aqueous phase. In water-in-oil microemulsions, an aqueous phase is dispersed in a continuous water-immiscible phase. In bicontinuous microemulsions, an aqueous phase and a water-immiscible phase are each interconnected and interspersed throughout the mixture.

In this specification, the terms "water" and "oil" (e.g. as used in reference to oil in water microemulsions and water in oil microemulsions) are understood to represent the aqueous phase and the water-immiscible phase. The term "water-immiscible phase" is used to describe any liquid that is immiscible with the aqueous phase. "Water phase" and "aqueous phase", as used herein, may be used interchangeably.

As used herein, the terms "active species" and "electrochemically active species" mean compounds (including charged compounds, neutral compounds, radicals and the like) that are reactants of an electrochemical reaction. The reactions of electrochemically active species are, at least in part, responsible for the generation of a charge which flows within an electrochemical cell and as a result are responsible for the generation of an electric current.

The term "redox active organic species" means an organic electrochemically active species that undergoes reduction or oxidation in an electrochemical reaction. The reaction of redox active organic species are, at least in part, responsible for the generation of a charge which flows within an electrochemical cell and as a result are responsible for the generation of an electric current. See, for example: J. Winsberg, T. Hagemann, T. Janoschka, M. D. Hager, U. S. Schubert, *Angew. Chem. Int. Ed.* 2017, *56*, 686; P. Leung, F.C. Walsh *et al., Journal of Power Sources*, 2017, 360, 243-283; X. Wei, *et al.*, *ACS Energy Lett*. 2017, 2, 9, 2187-2204.

DETAILED DESCRIPTION

The present invention is predicated, at least in part, on 1) the surprising discovery that microemulsions which comprise an aqueous phase have an electrochemical stability window which is greater than that of bulk water, i.e. greater than 1.23 V, and/or 2) the surprising discovery that microemulsions, in which redox reactions of electrochemically active species occur in the water-immiscible (and substantially non-conductive) phase, enhance charge conductivity such that the microemulsions are able to conduct charge to an electrode and generate an electrical current.

The inventors have further shown that the microemulsion electrolyte compositions of the present invention may be used as electrolytes in an electrochemical cell. The microemulsion electrolyte compositions are able to support electrochemical redox reactions which generate a potential difference of greater than 1.23 V.

Accordingly, the present invention relates to the new use and application of microemulsions as electrolytes for electrochemical cells, and, more specifically, electrochemical energy storage devices (EESDs). The present invention further relates to new microemulsion electrolyte compositions which are adapted for use, configured for use, useful, or suitable for use, in electrochemical cells.

Microemulsions have a micro-heterogeneous liquid biphasic structure, which, at the macroscopic level, appears homogenous. The aqueous and water-immiscible phases of the microemulsion are immiscible at the desired operating temperature (which is usually at or around room temperature). Microemulsions are thermodynamically stable, and therefore are able to form spontaneously (without application of energy), and do not separate out into their constituent phases over time once formed. Therefore, the electrochemical characteristics of microemulsions are also constant and persist over time. As described herein, microemulsions yield surprising electrochemical properties compared to the materials of each phase in their bulk state.

It should be emphasised that 'emulsions' or 'emulsified electrolytes' are very different to microemulsions, despite similar nomenclature. Emulsions are thermodynamically unstable (kinetically stable) mixtures of immiscible liquids. This means that, in contrast to microemulsions, the two immiscible phases of an emulsion will separate out over time.

The microemulsion electrolyte composition comprises an aqueous phase and a water-immiscible phase.

Preferably, the water-immiscible phase is dispersed in the aqueous phase, and the aqueous phase is a continuous phase (i.e. the microemulsion is an "oil-in-water" microemulsion). Alternatively, but still preferably, the water-immiscible phase and the aqueous phase are bicontinuous. In a less preferred embodiment, the microemulsion may be a water-in-oil microemulsion (i.e. the water-immiscible phase is a continuous phase and the aqueous phase is a dispersed phase).

Suitable solvents for the water-immiscible phase of the microemulsion electrolyte composition include a water-immiscible solvent or a combination of two or more water-immiscible solvents. Water-immiscible organic solvents, and mixtures thereof, are particularly suitable. By way of example only, a non-limiting list of solvents that are suitable for the water-immiscible phase of the microemulsion electrolyte compositions include aliphatic solvents (e.g. cyclic and non-cyclic, branched and non-branched alkanes, such as hexane, cyclohexane and petroleum ether, alkenes, alkynes); aromatic solvents (e.g. benzene, toluene, p-xylene, 1,2-dichlorobenzene); halogenated solvents (e.g. dichloromethane, chloroform, dichloroethane); ether solvents (e.g. diethyl ether, diphenyl ether); ketone solvents, such as acetophenone; esters, such as ethyl benzoate, ethyl acetate; or a combination thereof.

A preferred solvent for the aqueous phase of the microemulsion electrolyte composition is water. Alternative aqueous phases include combinations of water and water-miscible solvents, such as methanol and ethanol. Clearly, the aqueous phase of the microemulsion electrolyte composition must be immiscible with the water-immiscible phase.

The relative proportions of the aqueous phase and the water-immiscible phase in the microemulsion electrolyte composition are naturally limited by the overall thermodynamic stability of the mixture of components that make up the microemulsion electrolyte composition (e.g. aqueous phase, water-immiscible phase, and the presence of any other compounds such as amphiphiles, salts and electrochemically active species). There are natural limitations on the relative proportions of each phase in which it is thermodynamically favourable for the composition to exist as a microemulsion. There are further natural limitations on the relative proportions of each phase to achieve an oil-in-water microemulsion or a bicontinuous microemulsion. The relative proportions of each phase may be determined theoretically, or by routine experimentation by a person skilled in the art.

For the microemulsion electrolyte compositions of the present invention, the relative proportions of the aqueous phase and water-immiscible phase include any and all proportions and ranges thereof in which a microemulsion is formed. As oil-in-water and bicontinuous microemulsion systems are preferred, the preferred proportions of the aqueous phase and water immiscible phase are those that yield oil-in-water and bicontinuous microemulsions.

A factor for determining preferred relative proportions of the aqueous phase and water-immiscible phase is an aim of maximising the concentration of the dissolved electrochemically active species. Where the electrochemically active species is dissolved in the water-immiscible phase, maximising the proportion of water-immiscible phase in the microemulsion electrolyte composition will maximise the concentration of active species in the composition, and thereby maximise energy density. Similarly, where the active species are dissolved in the aqueous phase, maximising the proportion of the aqueous phase in the microemulsion electrolyte composition will maximise the concentration of active species.

In some embodiments, the microemulsion electrolyte composition comprises between about 1% and 99% water by weight of the microemulsion, more preferably between about 10% and 99% water by weight of the microemulsion, more preferably between about 20% and 99% water by weight of the microemulsion.

Microemulsion electrolyte compositions may be prepared with a high water content or with a low water content.

For microemulsions with higher proportion of aqueous phase (i.e. greater than about 75% by weight), and low proportion of water-immiscible phase (i.e. less than about 10% by weight) the electrochemical stability window is significantly greater than bulk water, and enables electrochemical reactions with potentials beyond the electrochemical stability window of an aqueous environment.

For microemulsions with lower water content (i.e. less than about 50% by weight), these microemulsions are particularly useful in electrochemical cells where the electrochemically active species are dissolved in the water-immiscible phase. Microemulsion electrolyte compositions with low water content are desirably not water-in-oil compositions, and are more preferably either bicontinuous or oil-in-water (where feasible). Water-in-oil microemulsions that have been tested by the inventors have low conductivity, or are non-conductive, and are therefore unsuitable as electrolyte compositions for electrochemical cells.

In embodiments where the microemulsion electrolyte composition comprises an oil-in-water microemulsion, the microemulsion electrolyte composition preferably comprises between about 80% and about 99% water by weight of the composition.

In embodiments where the microemulsion electrolyte composition comprises a bicontinuous microemulsion, the microemulsion electrolyte composition preferably comprises between about 20% and about 80% water by weight of the composition.

Another factor for determining preferred relative proportions of the aqueous phase and water-immiscible phase is the aim of maximising charge conductivity. Conductivity of the microemulsion electrolyte composition is predominantly provided by the aqueous phase, and therefore microemulsion electrolyte compositions in which the aqueous phase is a continuous phase (i.e. oil-in-water and bicontinuous microemulsions) are preferred.

The conductivity of the aqueous phase enables electrochemical redox reactions to take place in substantially non-conductive water-immiscible phases. For example, where the water-immiscible phase is an organic solvents such as an aliphatic or aromatic solvent, the water-immiscible phase of the microemulsion electrolyte compositions is substantially non-conductive. The electrochemical redox reaction that is observed to occur within the water-immiscible phase (see, for example, Example 4 below) is facilitated by the conductivity of the aqueous phase.

The aqueous phase may further comprise added dissolved salts to provide ions for the electrolyte composition. The dissolved salts may be selected from the group including Group 1 salts, Group 2 salts, transition metal salts, aluminium salts, or a combination thereof. Examples of dissolved salts include but are not limited to LiCl, NaCl, KCl, LiOH, NaOH, KOH, $MgSO_4$, $MgCl_2$, $Zn(NO_3)_2$, and $AlCl_3$. The aqueous phase may include dissolved Group 1 ions, Group 2 ions, transition metal ions, aluminium ions, or a combination thereof. Examples of dissolved ions include lithium, sodium, potassium, magnesium, aluminium, calcium, chromium, manganese, iron, cobalt, copper, nickel, zinc, silver, halogen ions (e.g. fluorides, chlorides, chlorates, bromides, bromates, iodides, iodates), sulfate ions, nitrate ions, and a combination thereof. The concentration of dissolved ions in the aqueous phase may be between 0% and a saturated aqueous solution. The dissolved ions may contribute towards the conductivity of the microemulsion electrolyte composition, so the concentration of dissolved ions may be as high as possible. Exemplary ranges of dissolved ions include between 0 and 10 M, more preferably between about 0.01 M and 5 M, more preferably between 0.05 M and 1 M, most preferably between about 0.05 M and 0.5 M.

The conductivities of the oil-in-water and bicontinuous microemulsion electrolyte compositions shown in the Examples of the present invention are between 3 and 8 $mS.cm^{-1}$. It will be appreciated by those skilled in the art that the conductivity of the microemulsion electrolyte compositions may be increased beyond what has been specifically exemplified. The conductivity of the microemulsion electrolyte composition may be increased by adding additional charged species (such as by dissolving salts), which will be solubilised by the aqueous phase of the electrolyte composition. The salts may be added to the microemulsion electrolyte composition once it is already formed, or may be added to the aqueous component prior to preparation of the microemulsion electrolyte composition.

The microemulsion electrolyte composition should be sufficiently conductive to permit the flow of electric current through the electrolyte. The microemulsion electrolyte composition preferably has a conductivity of more than 0.1 $mS.cm^{-1}$, preferably more than 1 $mS.cm^{-1}$, preferably more than 3 $mS.cm^{-1}$, preferably more than 5 $mS.cm^{-1}$, or between 0.1 and 12 $mS.cm^{-1}$, preferably between 1 and 12 $mS.cm^{-1}$, preferably between 3 and 10 $mS.cm^{-1}$.

The microemulsion may include one or more amphiphiles. The amphiphile may be a surfactant, co-surfactant or a co-solvent. Suitable surfactants and co-surfactants for the preparation of microemulsion electrolyte compositions and will be known in the art. Examples of suitable surfactants include anionic surfactants, cationic surfactants, zwitterionic surfactants and non-ionic surfactants. Examples of preferred surfactants include Triton X-100, cetyltrimethylammonium chloride (CTAC), cetylpyridinium chloride (CPC), benzalkonium chloride, benzethonium chloride, sodium dodecyl sulfate (SDS), and sodium lauryl ether sulfate (SLES). Examples of suitable co-surfactants or co-solvents include aliphatic alcohols, such as C2-C6 alcohols, and amines, such as C_2-C_6 alkyl amines. Preferred co-surfactants and/or co-solvents for the present invention include ethanol, propanol, butanol and pentanol.

The microemulsion electrolyte composition may include, or be adapted to include, dissolved electrochemically active species. The reactions of the electrochemically active species in an electrochemical cell generate a flow of charge and as a result generate an electric current. In particular, the microemulsion electrolyte composition may include redox active organic species.

As the microemulsion electrolyte compositions comprise aqueous and water-immiscible phases, the compositions are able to dissolve electrochemically active species and redox active organic species across a wide range of polarities and solubilities. The compositions may comprise electrochemically active species that are soluble in the aqueous phase, the water-immiscible phase, or both. Examples of electrochemically active species that may be dissolved in the microemulsion electrolyte compositions include salts (organic and inorganic), neutral organic molecules, stable organic radicals, oil-soluble metal-based compounds, organometallic compounds. Specific examples of redox active organic species that may be dissolved in the microemulsion include: ferrocene, (2,2,6,6-tetramethylpiperidin-1-yl)oxyl (TEMPO), phenothiazines, dimethoxybenzene, menadione and 2,1,3-benzothiadiazole. Where the microemulsion electrolyte composition is used in electrochemical cells, in particular for redox flow batteries, the concentration of redox-active species in the composition is preferably maximised. For electrochemically active species that are insoluble in water or an aqueous solution, a water-immiscible phase solvent in which the electrochemically active species is soluble is selected.

For example, the inventors have performed electrochemical reactions in redox flow battery using ferrocene in a microemulsion electrolyte composition (see Example 4 and Figures 13 to 23). Ferrocene is insoluble in water, indicating that the electrochemical reactions of ferrocene occur in the water-immiscible phase of the microemulsion electrolyte composition. This shows that the microemulsion electrolyte composition can solubilise organic (including organometallic) components which are not soluble in aqueous solvents, and that such components can co-exist in the same electrolyte composition as polar and ionic components.

The microemulsion electrolyte compositions have an electrochemical stability window that is greater than that of bulk water (1.23 V). Preferably, the electrochemical stability window of the microemulsion electrolyte composition is greater than 1.5 V, preferably greater than 2 V, preferably greater than 2.5 V, preferably greater than 3 V, preferably greater than 3.5 V, preferably greater than 4 V.

Preferably, in an experiment using a glassy carbon working electrode, a platinum counter electrode and a Ag/AgCl reference electrode, at room temperature and sea-level pressure, the microemulsion electrolyte composition is stable (i.e. not degrading) at voltages more negative than -0.25 V, more preferably more negative than -0.5 V, more preferably more negative than -1 V, more preferably more negative than -1.5 V, and most preferably more negative than -2 V. The microemulsion electrolyte composition is also preferably stable (i.e. not degrading) at positive voltages greater than 1.25 V, more preferably greater than 1.5 V, more preferably greater than 2 V, and more preferably greater than 2.25 V.

It is preferable that the water-immiscible phase of the microemulsion electrolyte composition does not degrade in use. In particular, it is preferable that the water-immiscible phase is stable and/or does not electrochemically degrade in use, for example, it is preferable that the water-immiscible phase is stable at potentials between -2 V and +2.5 V (Ag/AgCl reference electrode, ambient temperature at sea level). Preferably, the electrochemical stability window of the water-immiscible phase is greater than 1.5 V, preferably greater than 2 V, preferably greater than 2.5 V, preferably greater than 3 V, preferably greater than 3.5 V, preferably greater than 4 V. Similarly, it is preferable that any amphiphile present in the microemulsion does not degrade in use. In particular, it is preferable that the amphiphile is stable and/or does not electrochemically degrade in use, for example, it is preferable that the amphiphile is stable at potentials between -2 V and +2.5 V (Ag/AgCl reference electrode, ambient temperature at sea level).

From the foregoing description, it will be clear that the amounts of each component in the microemulsion electrolyte compositions (e.g. aqueous phase, water-immiscible phase, salts, amphiphiles, and electrochemically active species) may be configured or adjusted to optimise parameters such as the conductivity of the compositions, the electrochemical stability window of the compositions and the solubility of the electrochemically active species. Such optimisations would be a matter of routine experimentation and are within the scope of this invention.

In a further aspect, there is provided an electrochemical cell, such as a battery cell, comprising the microemulsion electrolyte composition of the present invention.

In preferred embodiments, the electrochemical cell comprises electrodes which have a substantially hydrophobic or lipophilic surface in contact with the microemulsion electrolyte composition. Examples of hydrophobic or lipophilic electrodes include carbon electrodes, such as glassy carbon and graphite electrodes. The surface of non-hydrophobic or non-lipophilic electrodes may be treated such that the surface becomes hydrophobic or lipophilic. Suitable electrodes having these features would be familiar to those of skill in the art.

The electrochemical cell may be suitable for any type of battery. The electrochemical cell may be an ion battery, or a flow battery. Preferably, the electrochemical cell may be a lithium ion battery, a magnesium ion battery, a sodium ion battery, an aluminium ion battery, or a redox flow battery.

Where the electrochemical cell is a flow battery, or redox flow battery, the microemulsion electrolyte composition may be used as an anolyte, catholyte or both. The microemulsion electrolyte compositions for anolyte and catholyte may be configured to optimise parameters such as conductivity of the compositions, electrochemical stability window of the compositions and the solubility of the electrochemically active species. Therefore, the anolyte and catholyte may comprise microemulsion electrolyte compositions having substantially the same formulations (except for the identity of the electrochemically active species), or the anolyte and catholyte may comprise different formulations.

The microemulsion electrolyte compositions of the present invention may be prepared according to known methods of preparing microemulsions that are familiar to those skilled in the art. The microemulsions of the present invention may be prepared by the combination of the individual components. As microemulsions are thermodynamically stable, they are able to form spontaneously. However, agitation of the microemulsion components may be performed so that the microemulsion forms in a suitably short amount of time. For example, the combined components may be agitated by stirring, shaking or sonication.

The microemulsions of the present invention may require amphiphiles, such as surfactants co-solvents and/or co-surfactants. Preferred amphiphiles are described above and a selection of amphiphiles are used in the Examples, but the invention is not limited to these specific compounds. As will be appreciated by those skilled in the art, the choice of amphiphile is dependent on the type of microemulsion desired (oil-in-water, bicontinuous or water-in-oil), and on the specific identities and proportions of the components in the microemulsion electrolyte composition.

The microemulsion electrolyte composition may be prepared in ambient conditions, and batteries comprising the microemulsion electrolyte composition may also be prepared in ambient conditions. That is, at room temperature and in the presence of ambient moisture, oxygen, carbon dioxide and other atmospheric constituents.

The microemulsion electrolyte compositions are useful as electrolytes in electrochemical cells including metal ion batteries, such as lithium ion batteries, magnesium ion batteries, sodium ion batteries, and aluminium ion batteries. The microemulsion electrolyte composition enables an operating potential of greater than 1.23 V, while still allowing for dissolution of the metal ions used in metal ion batteries.

The microemulsion electrolyte compositions are also useful as electrolytes in flow batteries, such as redox flow batteries. The microemulsion electrolyte compositions may be used as catholyte and/or anolyte.

Batteries may be prepared using the microemulsion electrolyte composition of the present invention in accordance with known methods. For example, a battery may be prepared using electrodes comprising graphite and/or vanadium pentoxide, current collectors of any type (such as steel), and a body of any suitable material, such as plastic or metal, and which would be readily apparent to those of skill in the art.

Ion batteries may be constructed in ambient conditions using the microemulsion electrolyte composition of the present invention. For example, a first current collector is placed into a body (e.g. a plastic cell). A first electrode is placed on top of the current collector with the active material of the electrode facing the interior. Glass microfiber filters are cut to size and then placed on top of the first electrode to act as a separator. For small batteries, between about 0.1 ml and about 1 ml of the electrolyte of the present invention is added on top of the glass microfiber before a second electrode is placed in the cell with its active material facing the interior of the cell. A second current collector is then placed on top of the second electrode. The components are secured and the cell is closed, for example by screwing the cell closed.

Flow batteries may similarly be constructed using the microemulsion electrolyte composition of the present invention. For example, the microemulsion electrolyte composition may be used as the catholyte and/or anolyte in a flow battery. Such catholyte and/or anolyte include dissolved electrochemically active species, such as redox active organic species. Activation of the flow battery causes the redox active organic species to react in the flow battery to generate a flow of charge and an electrical current.

Supercapacitors may similarly be constructed using the microemulsion electrolyte composition of the present invention. The supercapacitors comprise two high surface area electrodes (anodic and cathodic) in contact with the microemulsion electrolyte composition, typically separated by an ion permeable separator located between the two electrodes. The microemulsion electrolyte composition, in contact with the surface of the electrodes, forms an electrical double layer to store charge.

EXAMPLES

Example 1: Preparation of electrolyte compositions

Microemulsion samples were prepared according to the following method.

Each microemulsion sample comprised an aqueous component and a water-immiscible component, optionally a surfactant and/or optionally a co-surfactant. The components of each microemulsion sample are shown in Table 1.

The surfactant was weighed into an Erlenmeyer flask to which the water-immiscible component and co-surfactant were added. This mixture was stirred thoroughly to form a uniform slurry, and the aqueous component was then added. The mixture was turbid and white, which upon sonication in an ultrasonic bath or stirring, led to the formation of a clear microemulsion.

ME1 was prepared according to the method described in Menger, F. M. & Elrington, A. R. "Organic reactivity in microemulsion systems" *J. Am. Chem. Soc.* **113**, 9621–9624 (1991), and the methods of preparing ME2, ME3, ME5, ME12 and ME13 were based on this disclosure. ME2b was prepared according to the method described in Lang, Djavanbakht, Zana, "Ultrasonic absorption study of microemulsions in ternary and pseudoternary systems", *J. Phys. Chem.*, 1980, *84* (12), pp 1541–1547. ME6 was prepared according to the method described in Sun, B. *et al.* "A surfactant-free microemulsion consisting of water, ethanol, and dichloromethane and its template effect for silica synthesis" *J. Colloid Interface Sci.* 526, 9–17 (2018). ME10 was prepared according to the method described in Mukherjee, K., Mukherjee, D. C. & Moulik, S. P. "Thermodynamics of Microemulsion Formation" *J. Colloid Interface Sci.* 187, 327–333 (1997). ME11 was prepared according to the method described in Gorel, F. "Assessment of agar gel loaded with microemulsion for the cleaning of porous surfaces" *CeROArt Conserv. Expo. Restaur. D'Objets D'Art* (2010).

For the microemulsions with dissolved salts (e.g. ME6), the required amount of salt was weighed and added to the prepared microemulsion.

Example 2: Electrochemical stability window of microemulsions

Cyclic voltammetry analysis of each sample was performed using a glassy carbon working electrode, a platinum counter electrode and a Ag/AgCl reference electrode, using a Metrohm Autolab PGSTAT302 potentiostat. A scan rate of 100 mV/s was used.

Voltammograms of each sample are shown in Figures 1 to 11.

The electrochemical stability window of each microemulsion sample was determined as the potential difference between the onset potential (the potential at which the current begins to rise or fall) of each of the cathodic and anodic reactions. The electrochemical stability window of each microemulsion electrolyte composition sample is shown in Table 1.

Figure 12 shows a cyclic voltammogram of a 0.1 M aq. KCl solution, having an onset potential (potential at which the current starts to rise or fall) for O_2 evolution at ~1.25V vs. Ag/AgCl and an onset potential for H_2 evolution at ~ -1V vs. Ag/AgCl. Most of the microemulsions (except for ME6 and ME10) show an onset potential for O_2 evolution higher than 1.25V, depending on the microemulsion composition. The onset potentials for H_2 evolution are also lower than -1.0V, ranging from -2.0V to -2.5V, again depending on the microemulsion composition. It should be noted that onset potentials can differ between electrolytes, due to factors such as pH differences as well as differences between reference electrodes. Therefore, merely comparing, for example, the reduction reaction onset potentials of electrolytes cannot give meaningful information about the electrochemical stability windows of those electrolytes. Onset potentials become meaningful for electrochemical stability of electrolyte compositions when both the reduction and oxidation onset potentials are known, as the difference between the two gives the electrochemical stability window. In case of the microemulsions of the Examples, the electrochemical stability windows are significantly wider than that of the window for 0.1 M aq. KCl (e.g. a maximum of ~4.5V for ME1 compared to 2.25 V for aqueous KCl).

Example 3: Conductivity of microemulsions

The conductivity tests for all samples were performed using a ECTestr11 (Eutech Instruments) conductivity meter. The device was calibrated using an Enviroquip conductivity calibration standard (1413 µS/cm @ 25°C) before the measurements were made. Conductivity measurements for each microemulsion samples are shown in Table 1.

	Type	**Non-polar (water-immiscible)**	**(weight %)**	**Polar (aqueous)**	**(weight %)**	**Surfactant**	**(weight %)**	**Co-surfactant/co-solvent**	**(weight %)**	**Window (vs Ag/AgCl)**	**Window, V**	**Conductivity (mS/cm)**
ME1	O/W microemulsion with anionic surfactant	Cyclohexane	3.2	Water	82.1	SDS	4.9	Butanol	9.8	-2 to 2.5	4.5	7.5
ME2	O/W microemulsion with anionic surfactant	Toluene	3.2	Water	82.1	SDS	4.9	Butanol	9.8	-2 to 1.5	3.5	7.5
ME2b	Bicontinuous microemulsion with anionic surfactant	Toluene	31	Water	40	SDS	9.67	Butanol	19.34	-2 to 1.5	3.5	6.7
ME3	O/W microemulsion with anionic surfactant	1,2-dichlorobenzene	3.2	Water	82.1	SDS	4.9	Butanol	9.8	-2 to 2	4	7.9
ME4	O/W microemulsion with cationic surfactant	Hexane	3	Water	82	CTAC	5	Butanol	10	-2.5 to 1.25	3.75	7.2
ME5	O/W microemulsion with anionic surfactant	p-xylene	3.2	Water	82.1	SDS	4.9	Butanol	9.8	-2.25 to 1.5	3.75	7
ME6	Bi-continuous microemulsion	Dichloromethane	26	0.1M KCl	36.5			Ethanol	37.5	-2 to 1.25	3.25	1.49
ME10	O/W microemulsion with cationic surfactant	Chloroform	6.3	Water	89.8	CPC	3.9			-0.25 to 1.25	1.5	3.7
ME11	O/W microemulsion with anionic surfactant	Petroleum ether	5	Water	85	SDS	4	Pentanol	6	-2 to 2	4	6.8
ME12	O/W microemulsion with anionic surfactant	Acetophenone	3.2	Water	82.1	SDS	4.9	Butanol	9.8	-1 to 2	3	7
ME13	O/W microemulsion with anionic surfactant	Ethyl benzoate	3.2	Water	82.1	SDS	4.9	Butanol	9.8	-1.5 to 2	3.5	7.4
ME14	O/W microemulsion with non-ionic surfactant	Cyclohexane	10	Water	65.7	Triton X-100	24.3	-	-	-2 to 2	4	Not measured
Comparison	Aqueous soln of 0.1M KCl			0.1M KCl						-1 to 1.25	2.25	

Table 1: (SDS = sodium dodecyl sulfate, CTAC = cetyltrimethylammonium chloride, CPC = cetylpyridinium chloride); O/W = oil in water.

Example 4: Electrochemical experimentation in microemulsions

For each microemulsion sample, an amount of ferrocene was weighed and dissolved in the water-immiscible phase component to achieve a 100 mM concentration in the oil phase before preparing the microemulsions according to Example 1.

Cyclic voltammetry analysis of each sample was performed using a glassy carbon working electrode, a platinum counter electrode and a Ag/AgCl reference electrode, using a Metrohm Autolab PGSTAT302 potentiostat. Scan rate of 100 mV/s was used.

Voltammograms of ferrocene in each of the samples are shown in Figures 13 to 23.

The redox reactions of ferrocene can be interpreted as follows: During the forward scan (from 0 V to more positive voltages), ferrocene (Fc) is oxidized to ferrocenium (Fc^+) via a 1 electron oxidation, which can be seen in the form a cathodic peak current (i_{pc}) at a potential E_{pc}. During the backward scan, the reduction of Fc^+ to Fc, again via a 1 electron reduction can be seen in the form an anodic peak current i_{pa} at a potential E_{pa}. The redox potential of Fc/Fc^+ is thereby defined as the average of E_{pa} and E_{pc}, whereas the reversibility of the redox process is defined in terms of the ratio i_{pa}/i_{pc} (for a fully reversible process the ratio is 1).

The redox potential for the Fc/Fc^+ couple in each sample is around 0.3V, and the peak current ratios are close to 1, implying reversible electron transfer.

Example 5: Battery construction

Batteries comprising the microemulsion electrolyte compositions of Example 1 were prepared on a benchtop in ambient conditions. Whatman™ glass microfiber filters were used as separators. The cells were made with a polyether ether ketone (PEEK) body, and steel current collectors sandwiching the cell together. Between 0.1 ml and 0.2 ml of the electrolyte composition was added to each cell before the last layer was added.

The electrodes used in the batteries were prepared from a pyrolytic graphite sheet (purchased from MTI Corporation) and a V_2O_5 slurry which was doctor bladed onto pyrolytic graphite sheet. The V_2O_5 slurry was made with 85 wt% V_2O_5, 9 wt% super conductive carbon (Super P) and 6% polyvinylidene fluoride (PVDF) binder. N-methyl pyrrolidone (NMP) was used as the solvent. The slurry was bladed onto the pyrolytic graphite sheet, and then the sheet was heated in a vacuum oven at 120°C overnight to completely evaporate the solvent.

Battery electrolytes were prepared from microemulsion electrolyte compositions comprising:

- ME1 in which the aqueous phase is 0.5 $moldm^{-3}$ $MgSO_4$
- ME2 in which the aqueous phase is 0.1 $moldm^{-3}$ NaCl
- ME2 in which the aqueous phase is 0.1 $moldm^{-3}$ LiCl
- ME2 in which the aqueous phase is 0.1 $moldm^{-3}$ $AlCl_3$

Batteries prepared according to Example 5 were tested on a Neware battery analyser, BTS 3000 at a current density of 10 mAg^{-1} and cycled between the voltages as shown in Figures 24 to 27. All experiments were performed at room temperature. Chronopotentiograms of each battery are shown in Figures 24 to 27. The Figures 24 to 27 show regular charge-discharge behaviour, and indicate that no water-splitting occurs during operation of the cells.

For comparison, Figure 28 shows a chronopotentiogram of a magnesium ion battery comprising an aqueous electrolyte (not a microemulsion). Figure 28 shows that the potential rises to about 0.7 V and then climbs in an irregular manner with many sharp increases and decreases to a maximum of just under 1 V before it slightly falls again. This cell failed to reach the 1 V upper cut-off of the battery analyser, despite charge continually flowing into the cell. The spikes and dips in the curve indicate that the battery is not charging and some other process is going on in the cell, most likely electrolyte decomposition. This is not observed in cells where the electrolyte is a microemulsion electrolyte composition (e.g. Figures 24 to 27), where the curves are smother, indicating regular charge-discharge behaviour as opposed to the behaviour of the aqueous cell.

Example 6: Redox flow battery construction and testing

The efficacy of microemulsion electrolyte compositions described herein was investigated in redox flow battery systems using a laboratory-scale conventional flow battery assembly.

A redox flow battery was prepared comprising carbon cloth electrodes, aluminium metal interdigitated flow plates cum current collectors, and a Celgard 4560 separator. Flow of electrolytes (catholyte and anolyte) was achieved using a peristaltic pump purchased from Schenzen coupled with Masterflex Tygon (E-3603) tubing.

Catholyte and anolyte compositions for the redox flow battery were prepared by adding an electrochemically active species to a microemulsion composition, ME2 (see Table 1). For this test, several different redox active organic species were used, as shown in Table 2 below. For each test, the anolyte and catholyte consisted of 10 mM active species in ME2 microemulsion.

Test no.	**Catholyte active species**	**Anolyte active species**	**Cell voltage, V**
1	Ferrocene	Menadione	~1
2	(2,2,6,6-Tetramethylpiperidin-1-yl)oxyl (TEMPO)	Menadione	~1.2-1.3
3	Phenothiazine	Menadione	~1.5
4	Dimethoxybenzene	Menadione	above 1.5

5	Dimethoxybenzene	2,1,3-benzothiadiazole	~2.5

Table 2

With reference to Table 2, above: Ferrocene is an organometallic redox active organic species. Menadione is neutral organic molecule redox active organic species, specifically a quinone. TEMPO is a stable organic radical. Phenothiazine is a neutral redox active organic species. Dimethoxybenzene is a neutral redox active organic species. 2,1,3-benzothiadiazole is another neutral redox active organic species. It is to be noted that phenothiazine and dimethoxybenzene can be substituted by different substituents, and each compound is part of a class of phenothiazines and dimethoxybenzenes.

In each test, 50 mL each of anolyte and catholyte were used with a constant flow rate of 20 mL/min. The redox flow battery charge/discharge test was carried out in a galvanostatic mode with a 10 mA current. Voltages were set within cut offs of 0 V to 1 V. The chronopotentiogram of the battery cell of Test no. 1 is shown at Figure 29, showing regular charge-discharge behaviour.

Figure 29 shows that the microemulsion electrolyte compositions can act as a conductive medium for the oxidation and reduction reactions of the redox active organic species, and can therefore be used as redox flow battery electrolytes. There are characteristic charging and discharging plateaus around 0.7 V.

Figure 29 further shows that the microemulsion composition has good conductivity as an electrolyte, as the Figure shows the microemulsion composition to have a iR drop (voltage difference at the end of charge and beginning of discharge) expected from a typical redox flow battery of this assembly. The iR drop observed typically comes from the membrane and cell resistance and not from the electrolyte.

As neither ferrocene nor menadione is soluble in water, these redox active organic species are assumed to be dissolved in the water-immiscible phase of the microemulsion electrolyte composition yet regular charge/discharge behaviour is still observed. Thus, Figure 29 is further proof the microemulsion electrolyte composition can dissolve and facilitate electrochemical reactions of the redox active organic species by virtue of having an electrochemically active oil phase.

Example 7: Ion battery construction and testing

The efficacy of microemulsion electrolyte compositions described herein was investigated in ion cell systems. Ion batteries were constructed in Swagelok cells comprising the electrolyte described herein, an anode, a cathode, a polyether ether ketone (PEEK) body, glassy carbon current collectors, and glass microfiber separators.

The anode was prepared according to the following method: 255mg of TiO_2 powder (Degussa, P-25), 27mg super conductive carbon (Super P), and 18mg polyvinylidene difluoride were combined with N-methyl pyrrolidone (NMP) to form a thick slurry. The slurry was then doctor bladed onto a pyrolytic graphite sheet (MTI Corporation) and dried in a vacuum oven at 120° C for 12 hours.

For Cells 1 to 3, a cathode was prepared according to the following method: Prussian blue was prepared by combining equimolar amounts of $FeCl_3$ and potassium ferricyanide ($K_3[Fe(CN)_6]$) in water under vigorous stirring in ambient conditions. The mixture was dried and the resulting solid was crushed. 255mg of Prussian blue powder, 27mg super conductive carbon (Super P), and 18mg polyvinylidene difluoride were combined with N-methyl pyrrolidone (NMP) to form a thick slurry. The slurry was then doctor bladed onto a pyrolytic graphite sheet (MTI Corporation) and dried in a vacuum oven at 120° C for 12 hours.

For Cells 4 and 6, a V_2O_5 cathode was prepared according to the method described in Example 5.

For Cell 5, a MoS_2 cathode and graphite anode were used.

A microemulsion electrolyte (ME14) was prepared according to the following method: 65.7 wt% distilled water, 24.3 wt% Triton X-100 (*t*-octylphenoxypolyethoxyethanol) and 10 wt% cyclohexane were combined, sonicated for about one hour and then left to stir overnight. To ME14, 10 wt% of bis(2-methoxyethyl) ether (Diglyme) was added. The final composition of the microemulsion is therefore: 59.7 wt% distilled water, 22.1 wt% Triton X-100, 9.1 wt% cyclohexane and 10 wt% diglyme.

For Cells 1 to 3, the corresponding metal chloride salt was added to ME14 to give a cation concentration of 1 mol/kg. For Cell 4, LiCl was added to ME14 to give a concentration of 0.1 mol/kg. For Cell 5, $MgCl_2$ was added to ME14 to give a concentration of 0.1 mol/kg.

Accordingly, the constructed cells have the composition described in Table 3:

Cell no.	**Anode**	**Cathode**	**Electrolyte**
1	TiO_2	Prussian blue	ME14 with 1 mol/kg KCl
2	TiO_2	Prussian blue	ME14 with 1 mol/kg $CaCl_2$
3	TiO_2	Prussian blue	ME14 with 1 mol/kg NaCl
4	TiO_2	V_2O_5	ME14 with 0.1 mol/kg LiCl
5	Graphite	MoS_2	ME14 with 0.1 mol/kg $MgCl_2$
6	TiO_2	V_2O_5	ME14 (Control)

Table 3

Between 0.1 ml and 0.2 ml of the electrolyte composition was added to each cell construction before the last layer was added.

Charge/discharge

Figures 30 to 42 show the charge-discharge behaviour of Cells 1 to 5. Cells 1 to 3, 5 and 6 were tested on a Neware battery analyser, BTS 3000 at a current density of 50 mA/g. Cell 4 was tested at a current density of 10 mA/g. Cells were run with a constant charge and discharge current of 100 mA/g between 0 V and about 2.0 V (the exact upper cut-off ranges were from 1.9 V to 2.2 V, depending on cell). All experiments were performed at room temperature.

Figures 30 to 33 show the analysis of Cell 1 (KCl). Figures 34 and 35 show the analysis of Cell 2 ($CaCl_2$). Figures 36 and 37 show the analysis of Cell 3 (NaCl). Testing of Cells 1 to 3, shown in Figures 30 to 37, showed no evidence of water splitting despite operating at greater than 2V. The shape of the charge-discharge curves in Figures 30, 32, 34 and 36 indicate redox reactions are occurring in the cell. The nominal cell voltage (taken as approximately where the charge and discharge curves intersect) is approximately 1.7V which is well above the theoretical 1.23V water splitting potential.

Figures 38 to 41 show the analysis of Cell 4 (LiCl). This cell shows a capacity of greater than 140 mAh/g. The nominal cell voltage is approximately 0.7V. There is no evidence of water splitting even though it is charged to 2.4V.

Figure 42 shows the analysis of Cell 5 ($MgCl_2$).

Regular charge-discharge behaviour was observed over multiple cycles, indicating that water-splitting does not occur during operation of the cells. For example, the Figures show that Cells 1-5 retain their charge and discharge capacity over 30 cycles.

Cyclic voltammetry data

Cyclic voltammetry analysis (Ag/AgCl reference electrode) of Cell 4 (1.0 mol/kg LiCl in ME14) and Cell 6 (ME14 control) was performed using a Metrohm Autolab PGSTAT302 potentiostat. A scan rate of 100 mV/s was used. Voltammograms are shown in Figures 43 to 45.

For the V_2O_5 electrode of Cell 4, the cell was analysed from -1.5 V to 2.0 V (vs Ag/AgCl). For the TiO_2 electrode of Cell 4, the cell was analysed from -1.0 to 1.5 V (vs Ag/AgCl). Analysis of each electrode indicates that water splitting does not occur in this range. These measurements were compared to a cyclic voltammetry measurement of Cell 6 (a control microemulsion of ME14 with no other dissolved salts), which confirmed the electrochemical reactions observed in Cell 4 is due to the action of lithium; Cell 6 shows only capacitance, no electrochemical activity.

Example 8 – Supercapacitor

A supercapacitor comprising the microemulsion electrolyte composition described herein was constructed and analysed.

Electrodes were prepared as follows: A 70 wt% zeolite slurry solution was prepared by adding NMP dropwise until it completely dissolved 0.05 g of PVDF (about 2 mL). To this solution, 0.10 g of carbon black and 0.35 g of 4 Å molecular sieves were added, which formed a viscous black slurry. The slurry was then doctor bladed onto a pyrolytic graphite sheet (MTI Corporation) and dried in a vacuum oven at 120° C for 12 hours to form the zeolite electrodes.

A supercapacitor was assembled comprising zeolite electrodes (as both anode and cathode), glassy carbon current collectors, an electrolyte composition of ME14 comprising 1 mol/kg KCl, a glass microfiber separator, and a polyether ether ketone (PEEK) body.

The supercapacitor was cycled between 0 and 2V at 100mA/g for 500 cycles. As shown in Figures 46-48, the supercapacitor has a reversible capacity of about 4.5 mAh/g (Figures 46 and 47) and a coulombic efficiency of ~98% (Figure 48). The shape of the voltage capacity curve (Figure 46) indicates a purely capacitive process. The capacitance was calculated to be approximately 16.7 F/g.

***

Although the invention has been described by way of example, it should be appreciated that variations and modifications may be made without departing from the scope of the invention as defined in the claims. Furthermore, where known equivalents exist to specific features, such equivalents are incorporated as if specifically referred in this specification. The specific compositions and methods described herein are representative of preferred examples and are exemplary and not intended as limitations on the scope of the invention. Other aspects and examples will occur to those skilled in the art upon consideration of this specification, and are encompassed within the spirit of the invention as defined by the scope of the claims. It will be readily apparent to one skilled in the art that varying substitutions and modifications may be made to the invention disclosed herein without departing from the scope and spirit of the invention. The invention illustratively described herein suitably may be practiced in the absence of any element or elements, or limitation or limitations, which is not specifically disclosed as essential. Thus, for example, in each instance described or used herein, in embodiments or examples of the present invention, any of the terms "comprising", "consisting essentially of", and "consisting of" may be replaced with either of the other two terms in the specification. Also, the terms "comprising", "including", "containing", *etc.* are to be read expansively and without limitation. The assays and methods illustratively described herein suitably may be practiced in differing orders of steps, and that they are not necessarily restricted to the orders of steps indicated herein or in the claims. Further, as used or described herein and in the appended claims, the singular forms "a," "an," and "the" include plural reference unless the context clearly dictates otherwise. Under no circumstances may the patent be interpreted to be limited to the specific examples or embodiments or methods specifically disclosed herein.

The terms and expressions that have been employed are used as terms of description and not of limitation, and there is no intent in the use of such terms and expressions to exclude any equivalent of the features shown and described or portions thereof, but it is recognised that various modifications are possible within the scope of the invention as claimed. Thus, it will be understood that although the present invention has been specifically disclosed by preferred embodiments and optional features, modification and variation of the concepts disclosed herein may be resorted to by those skilled in the art, and that such modifications and variations are considered to be within the scope of this invention as described herein, and as defined by the appended claims.

The invention has been described broadly and generically herein. Each of the narrower species and subgeneric groupings falling within the generic disclosure also form part of the invention. This includes the generic description of the invention with a proviso or negative limitation removing any subject matter from the genus, regardless of whether or not the excised material is specifically recited herein. Other embodiments are within the following claims.

CLAIMS

What we claim is:

1. An electrically rechargeable electrochemical energy storage device comprising an electrolyte composition wherein the electrolyte composition comprises a microemulsion, and wherein the microemulsion comprises an aqueous phase and a water-immiscible phase.

2. The device of claim 1, wherein the aqueous phase is a continuous phase.

3. The device of claim 2, wherein the water-immiscible phase is a dispersed phase.

4. The device of claim 1, wherein the microemulsion is a bicontinuous microemulsion.

5. The device of any one of the preceding claims, wherein the microemulsion further comprises a dissolved salt.

6. The device of claim 5, wherein the dissolved salt is selected from the group consisting of: a lithium salt, a sodium salt, a potassium salt, a magnesium salt, a calcium salt, and an aluminium salt.

7. The device of claim 6, wherein the concentration of the dissolved salt is between 0.001 mol / kg and 10 mol / kg.

8. The device of any one of claims 1 to 4, wherein the microemulsion further comprises one or more redox active organic species.

9. The device of claim 8, wherein the redox active organic species are dissolved in the water-immiscible phase or aqueous phase.

10. The device of claim 8 or 9, wherein the redox active organic species are dissolved in the water-immiscible phase.

11. The device of any one of the preceding claims, wherein the water-immiscible phase comprises an organic solvent.

12. The device of any claim 11, wherein the organic solvent is selected from the group consisting of aliphatic solvents; aromatic solvents; halogenated solvents; substantially water immiscible ketone solvents; substantially water immiscible ester solvents; or a combination thereof.

13. The device of any one of the preceding claims, wherein the microemulsion further comprises a surfactant, a co-surfactant and/or co-solvent.

14. The device of any one of the preceding claims, further comprising an anodic electrode and a cathodic electrode and optionally a current collector, wherein at least a portion

of the surface of one or more of the anodic electrode, cathodic electrode and current collector is substantially hydrophobic.

15. The device of claim 14, wherein the portion of the surface of one or more of the anodic electrode, cathodic electrode and current collector is non-metallic or conductive carbon or a conductive polymer.

16. The device of claim 14 or 15, further including an ion permeable separator located between the cathodic electrode and anodic electrode.

17. The device of any one of the preceding claims, wherein the cell voltage is greater than 1.23 V.

18. A lithium ion battery comprising an electrolyte composition wherein the electrolyte composition comprises a microemulsion, and wherein the microemulsion comprises a lithium salt, an aqueous phase and a water-immiscible phase.

19. A magnesium ion battery comprising an electrolyte composition wherein the electrolyte composition comprises a microemulsion, and wherein the microemulsion comprises a magnesium salt, an aqueous phase and a water-immiscible phase

20. A sodium ion battery comprising an electrolyte composition wherein the electrolyte composition comprises a microemulsion, and wherein the microemulsion comprises a sodium salt, an aqueous phase and a water-immiscible phase.

21. A redox flow battery comprising an electrolyte composition wherein the electrolyte composition comprises a microemulsion, and wherein the microemulsion comprises a redox active organic species, an aqueous phase and a water-immiscible phase.

22. A supercapacitor comprising an electrolyte composition wherein the electrolyte composition comprises a microemulsion, and wherein the microemulsion comprises an aqueous phase and a water-immiscible phase.

23. A method for using an electrically rechargeable electrochemical energy storage device comprising connecting the electrically rechargeable electrochemical energy storage device to a load and supplying a charge to the load, wherein the device comprises an electrolyte composition, wherein the electrolyte composition comprises a microemulsion, and wherein the microemulsion comprises an aqueous phase and a water-immiscible phase.

24. An electrolyte composition when used in an electrically rechargeable electrochemical energy storage device, wherein the electrolyte composition comprises a microemulsion, wherein the microemulsion comprises an aqueous phase and a water-immiscible phase.

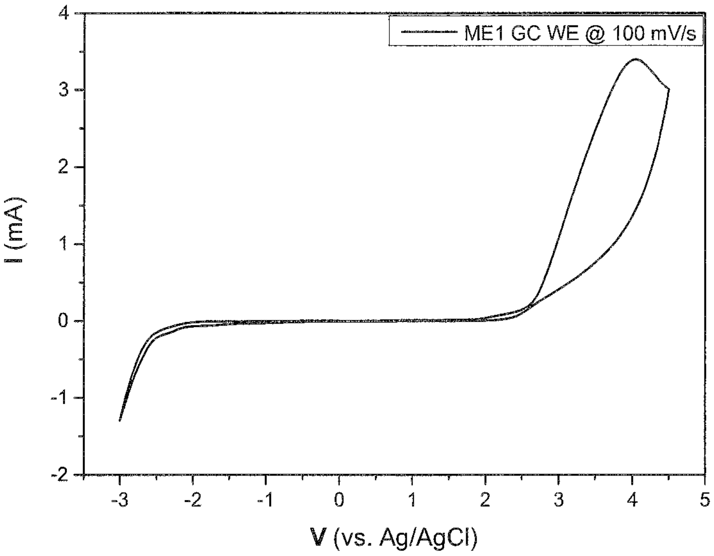

Figure 1

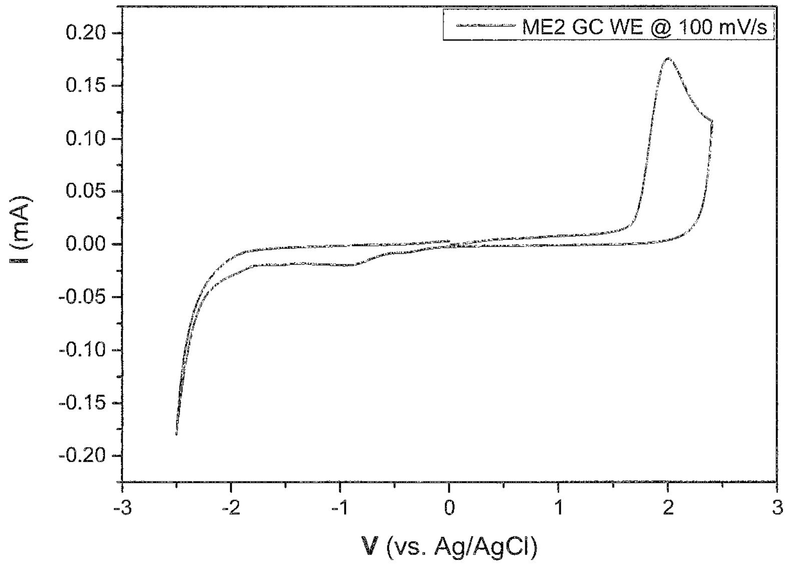

Figure 2

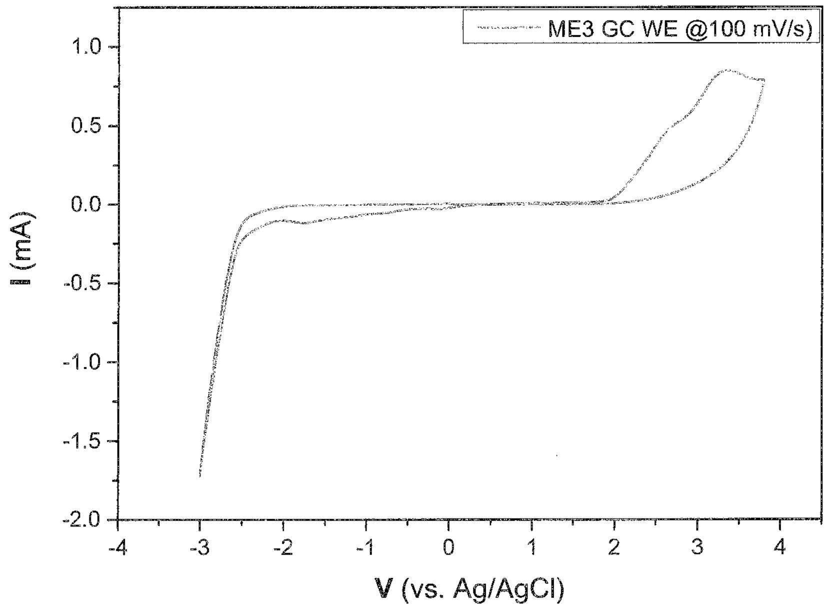

Figure 3

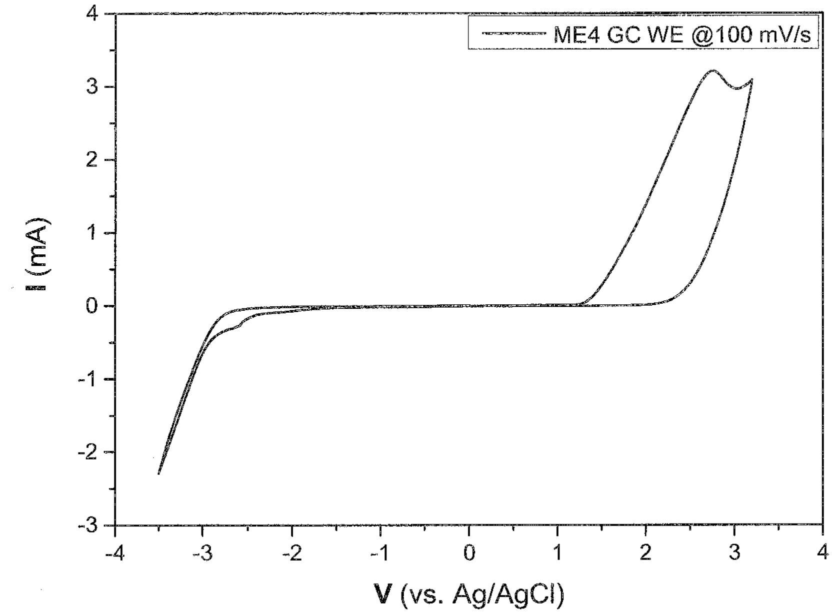

Figure 4

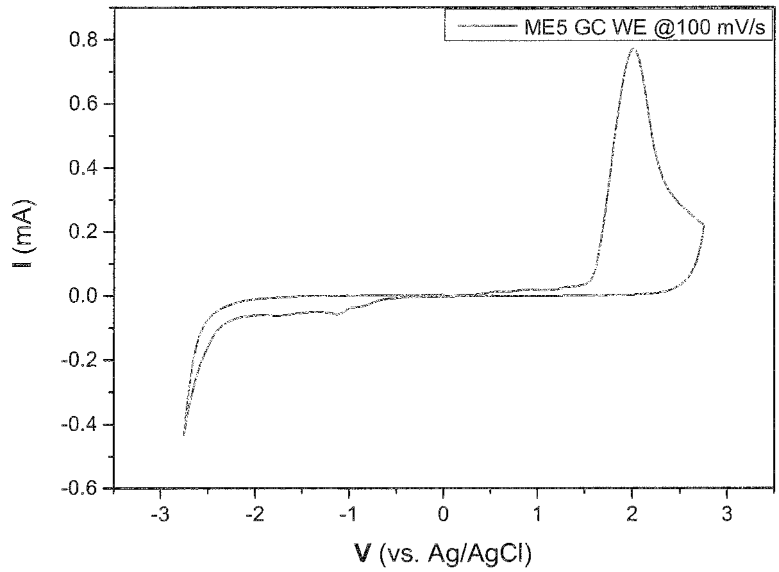

Figure 5

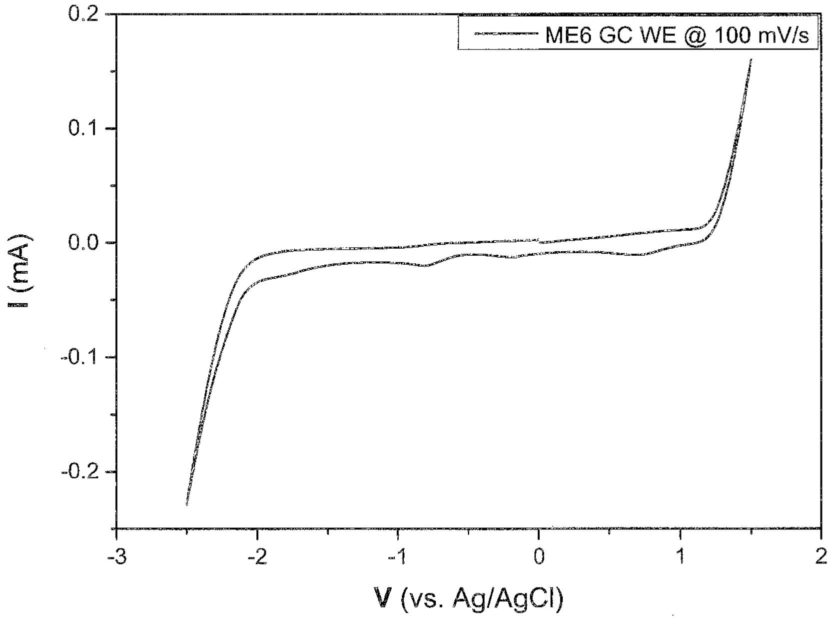

Figure 6

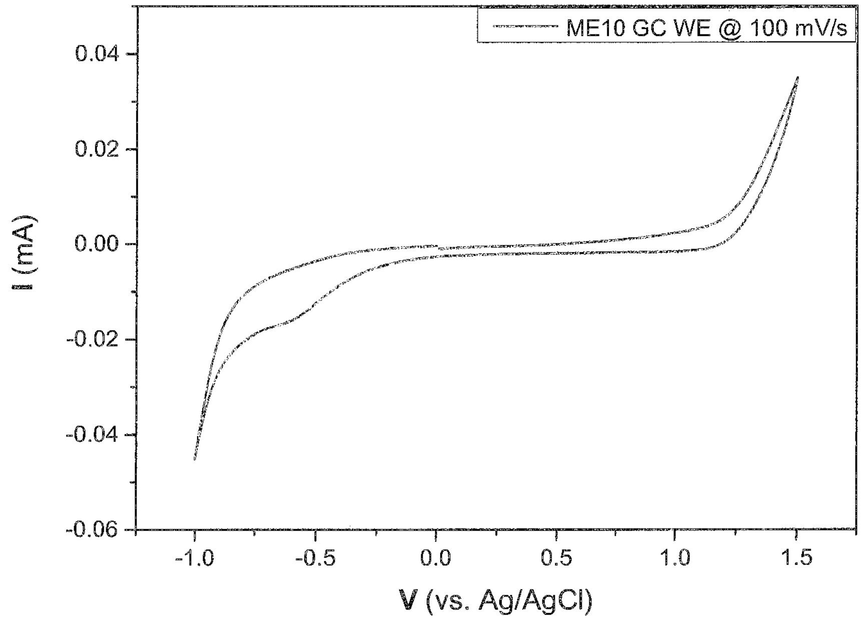

Fiugre 7

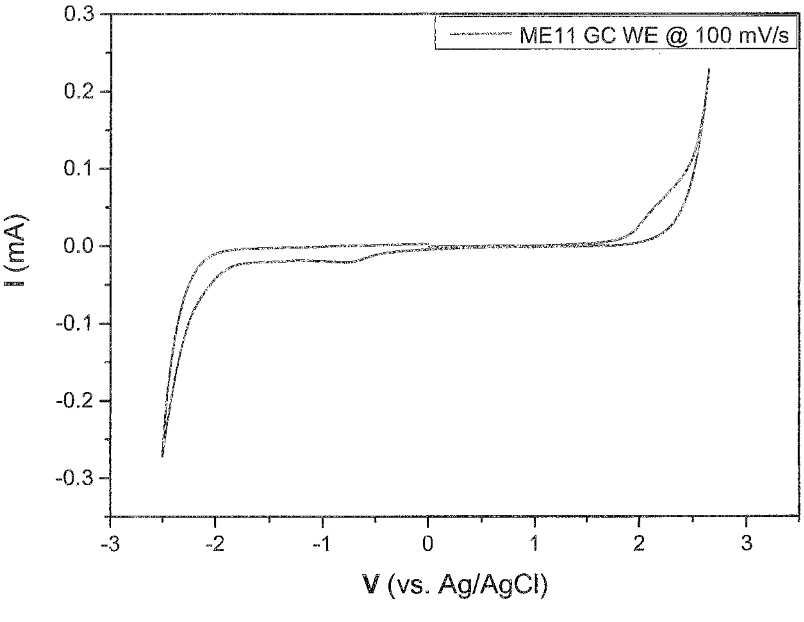

Figure 8

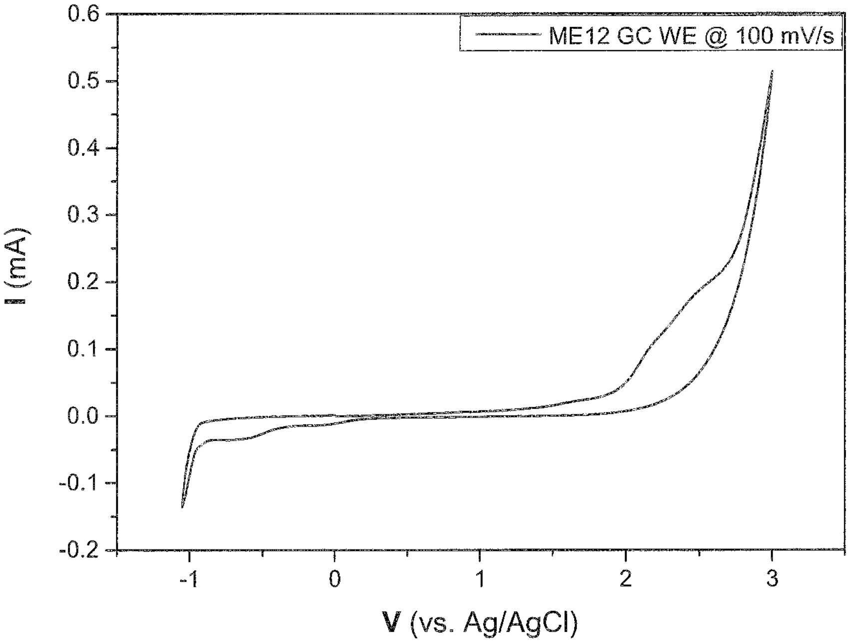

Figure 9

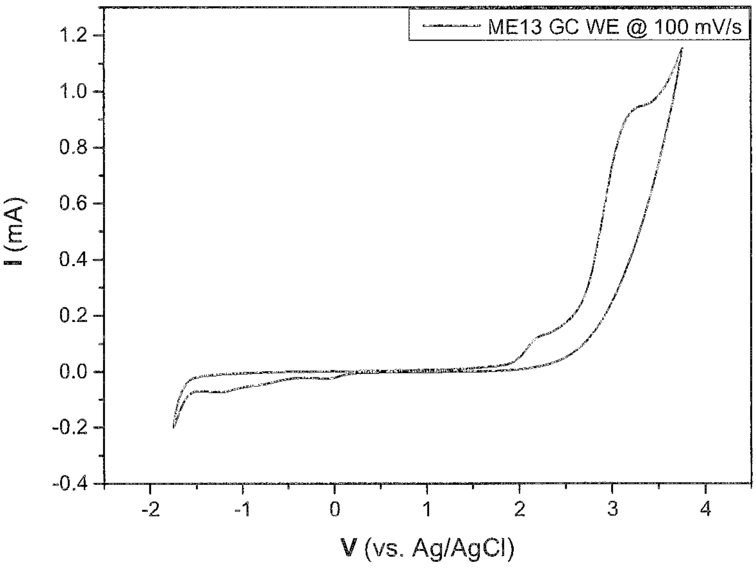

Figure 10

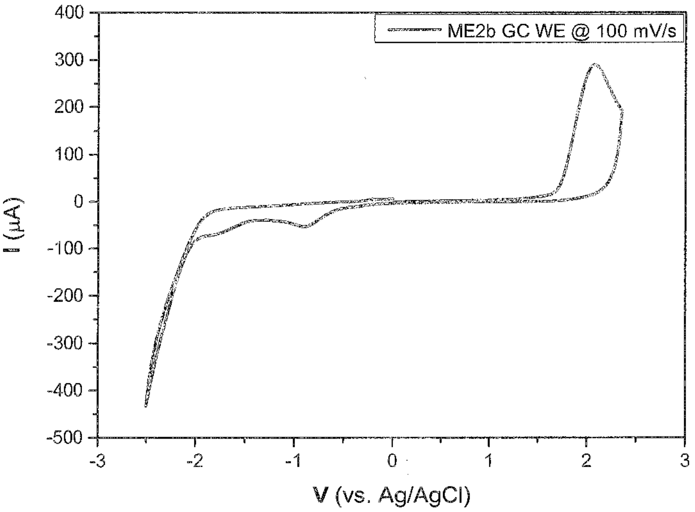

Figure 11

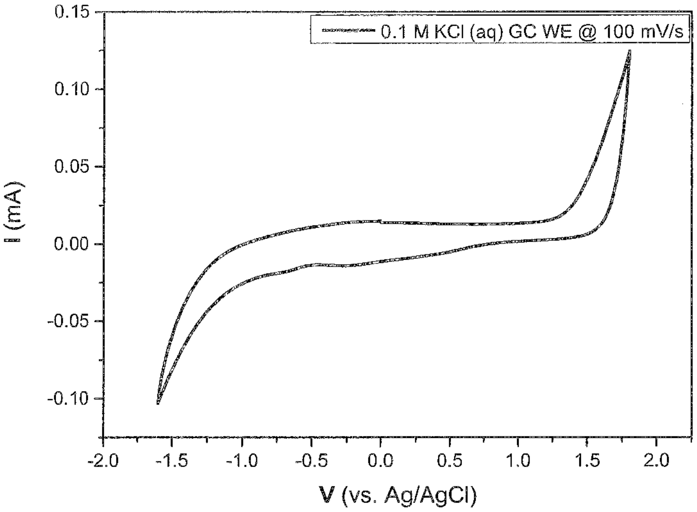

Figure 12

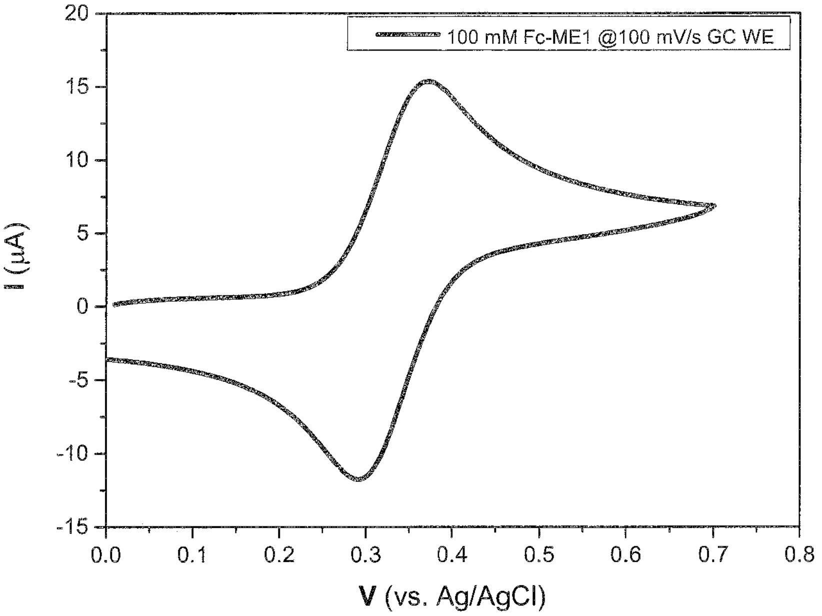

Figure 13

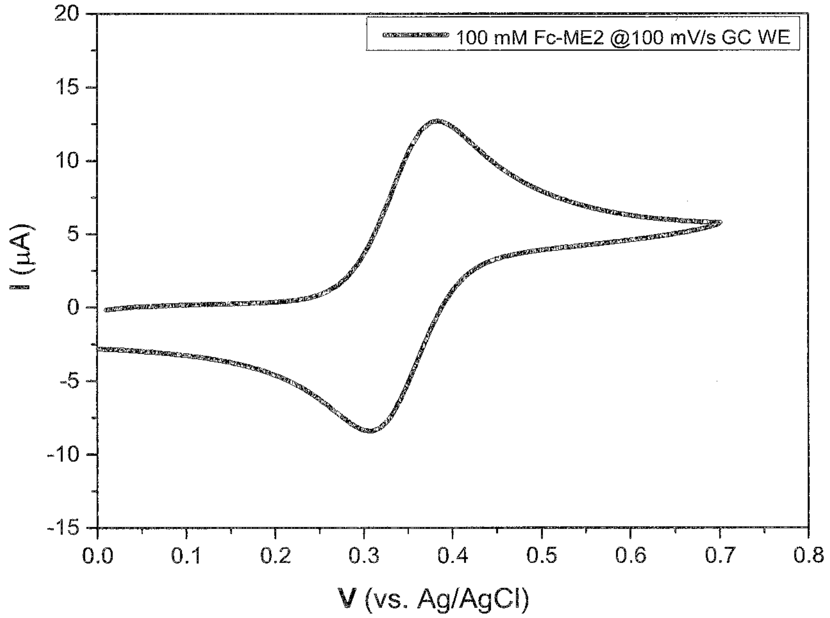

Figure 14

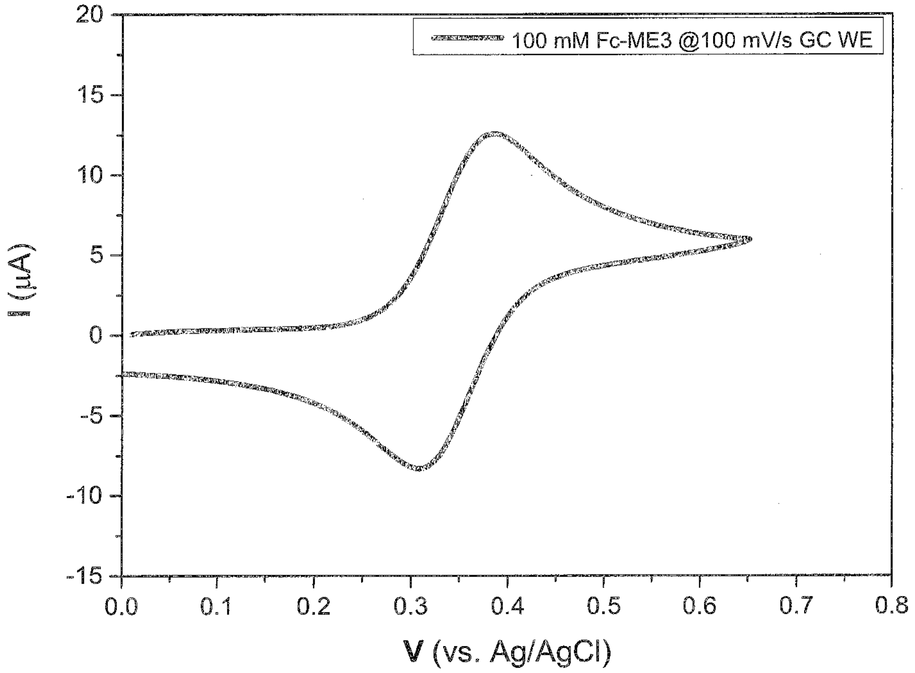

Figure 15

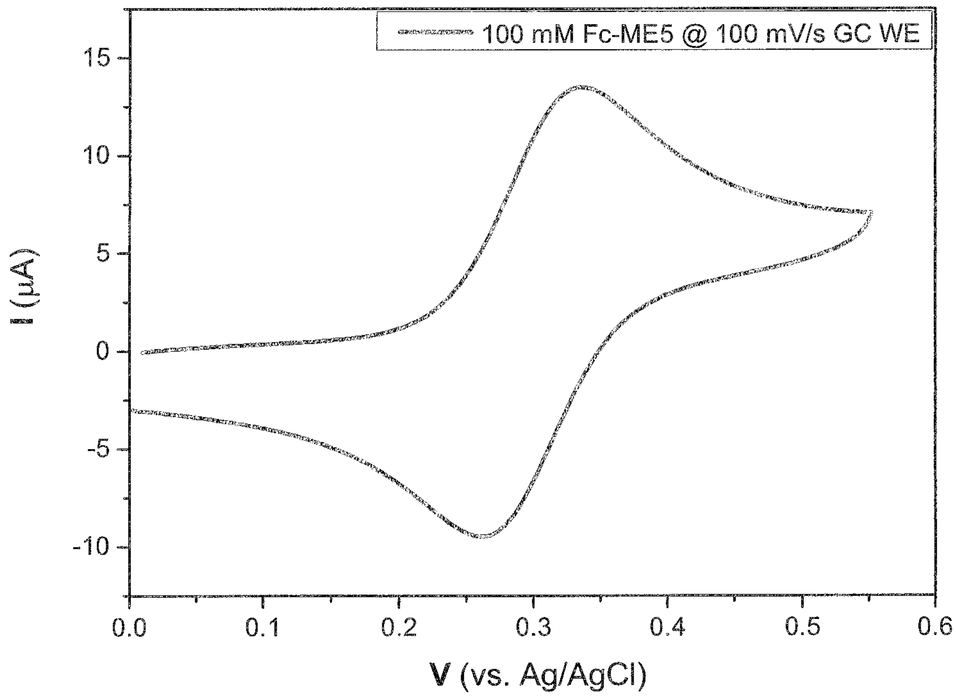

Figure 16

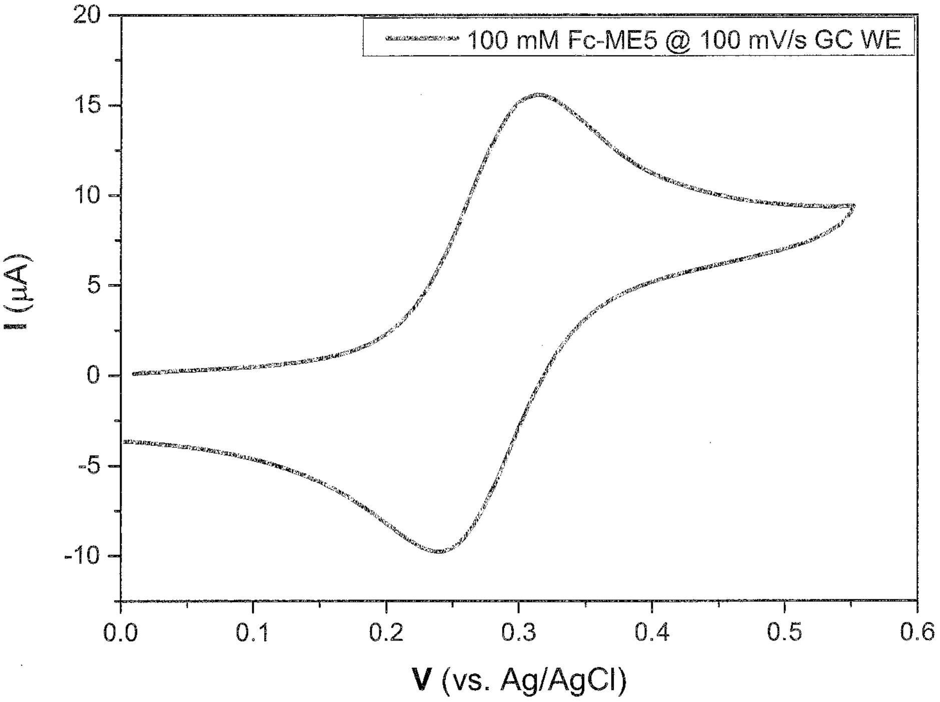

Figure 17

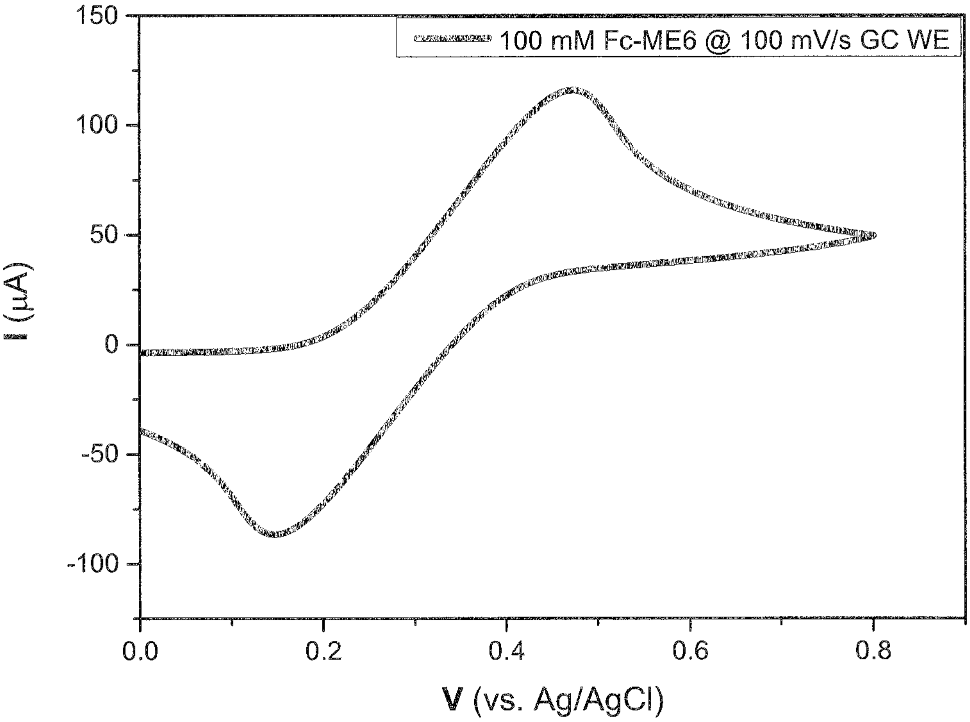

Figure 18

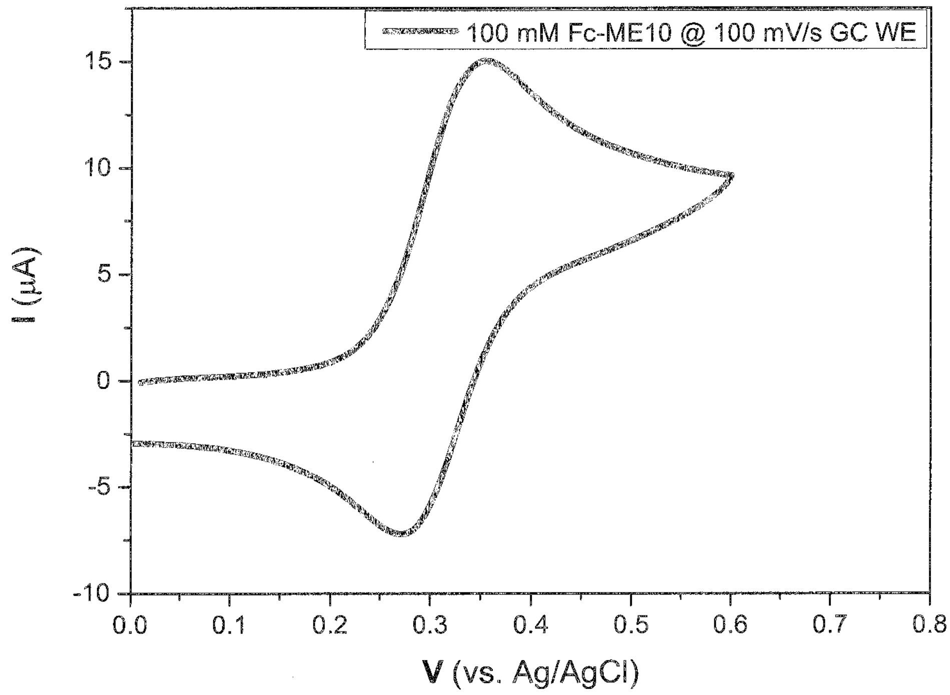

Figure 19

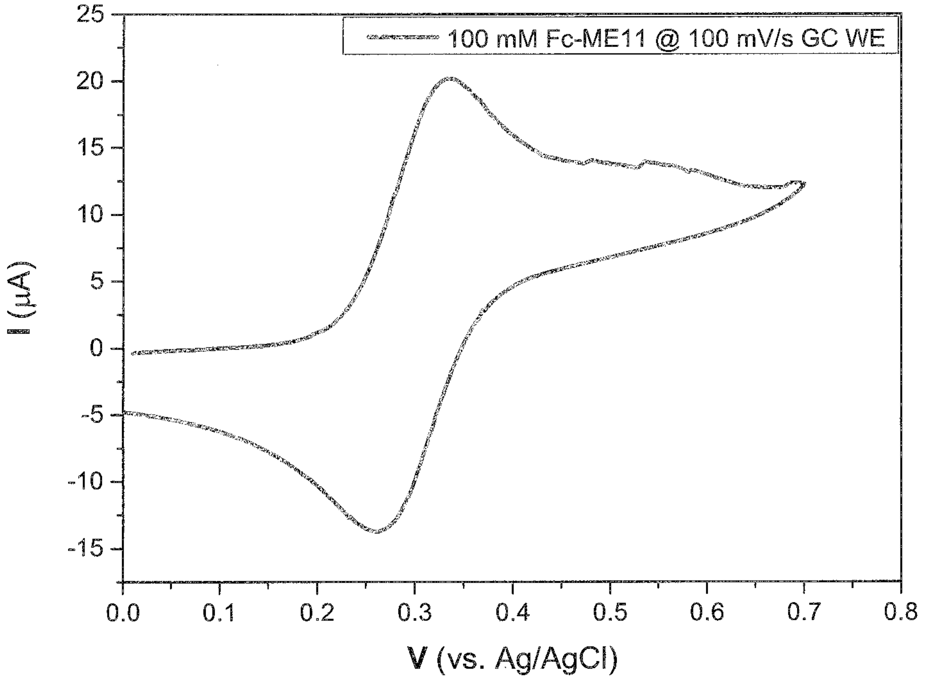

Figure 20

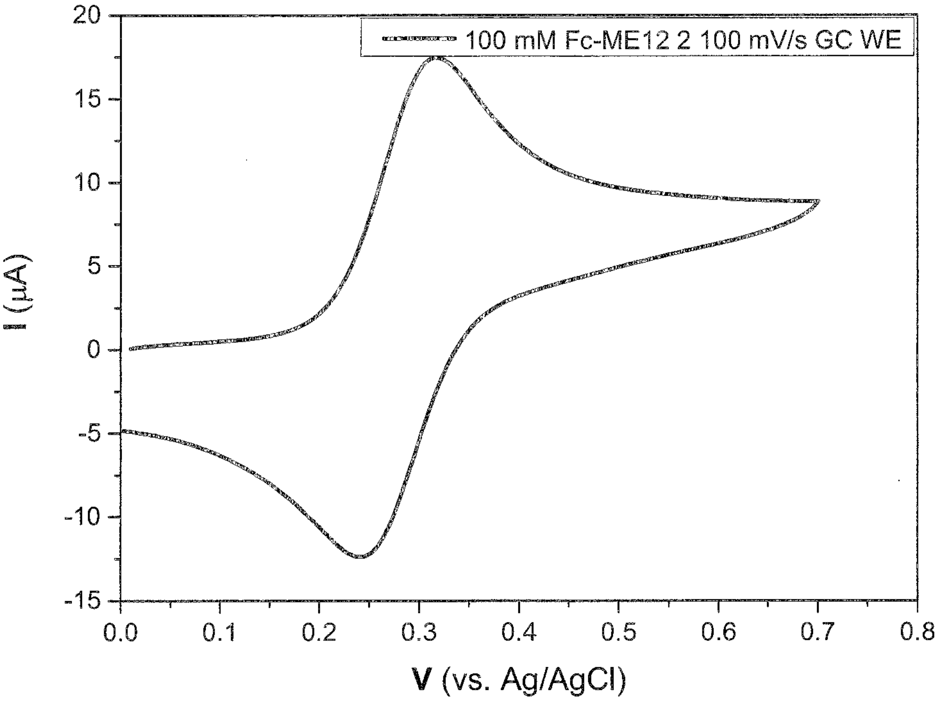

Figure 21

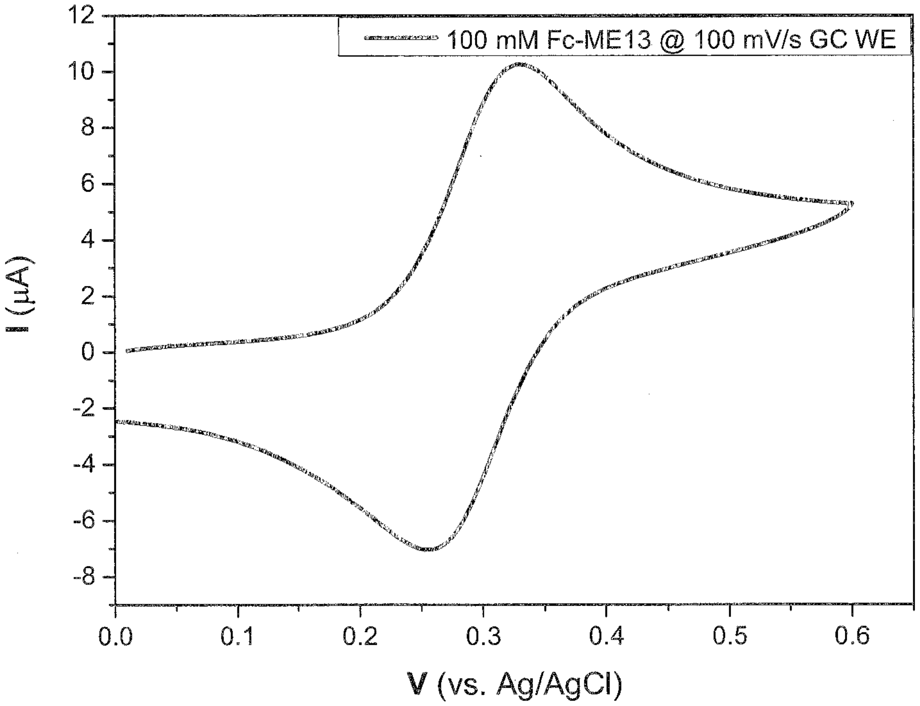

Figure 22

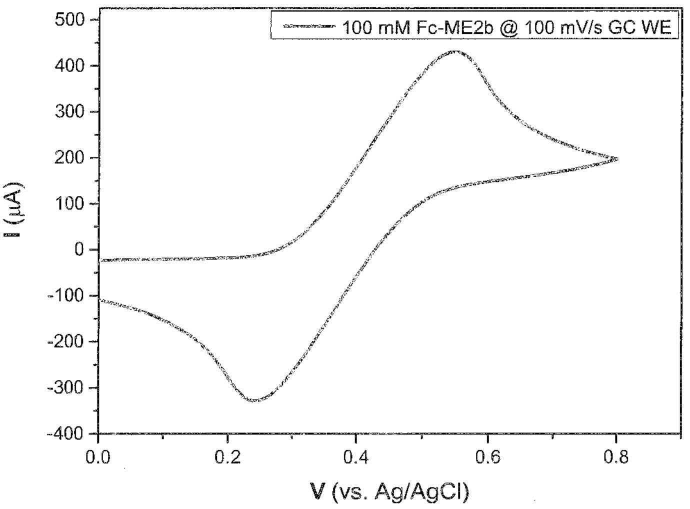

Figure 23

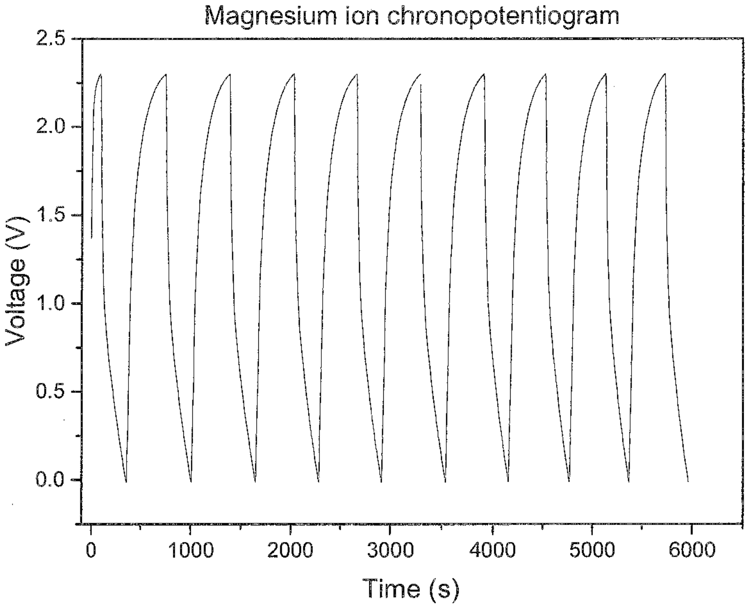

Figure 24

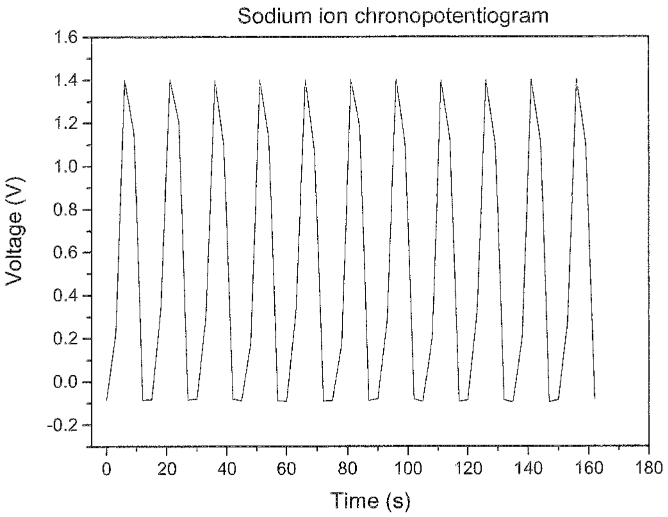

Figure 25

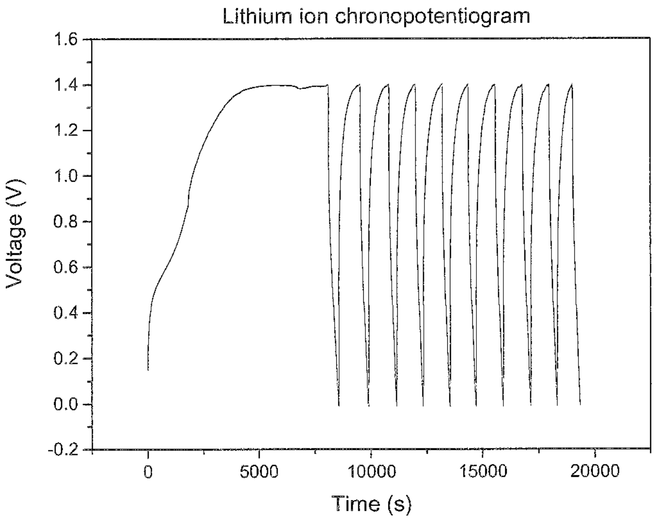

Figure 26

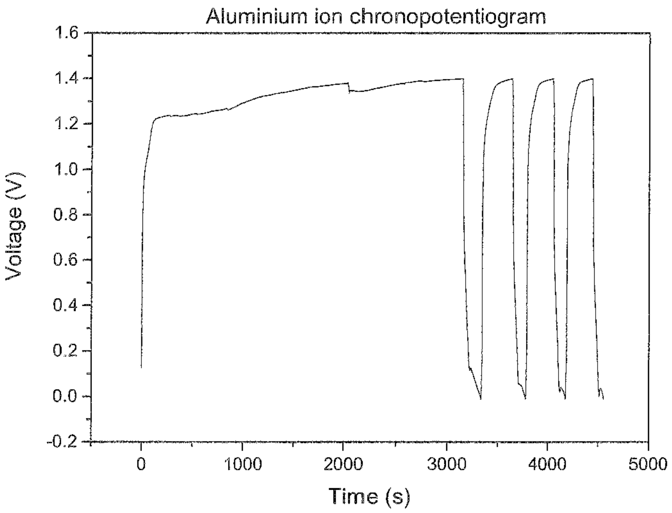

Figure 27

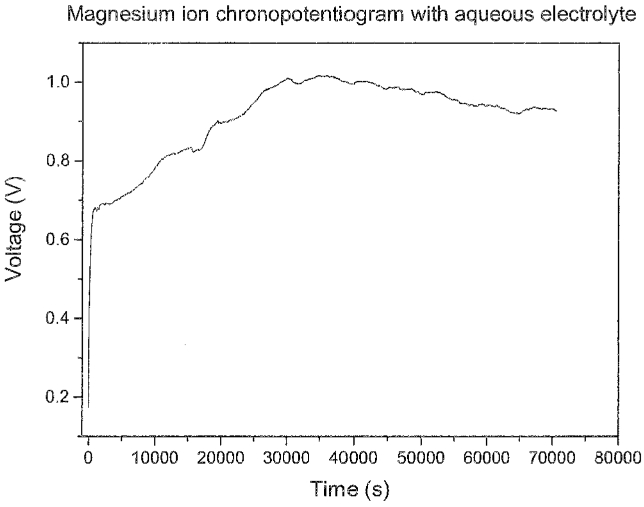

Figure 28

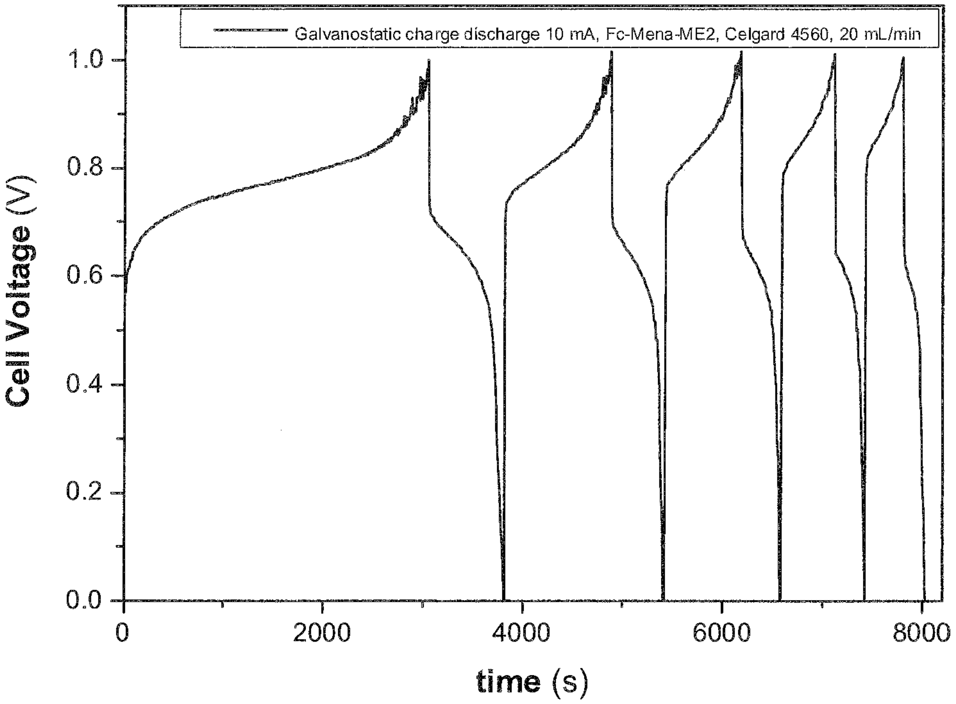

Figure 29

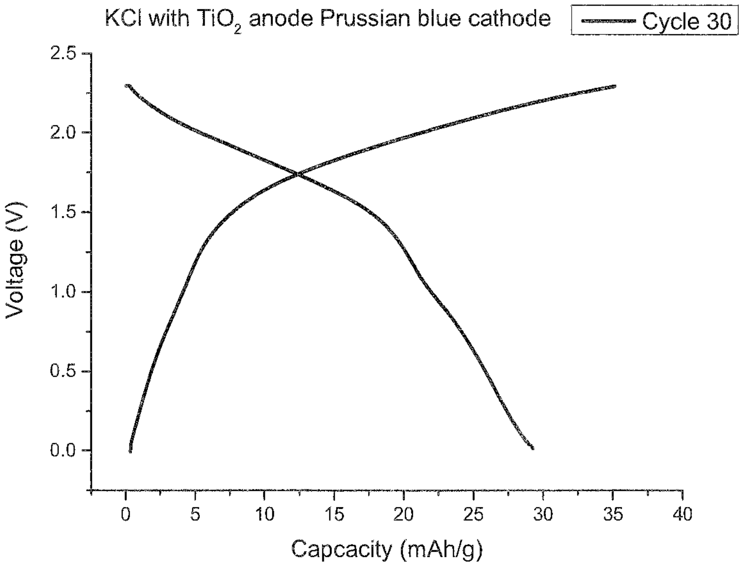

Figure 30

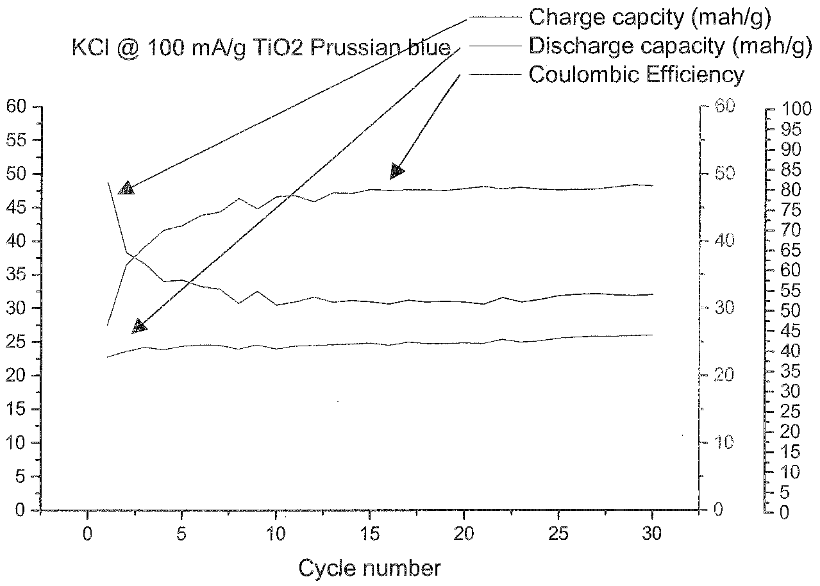

Figure 31

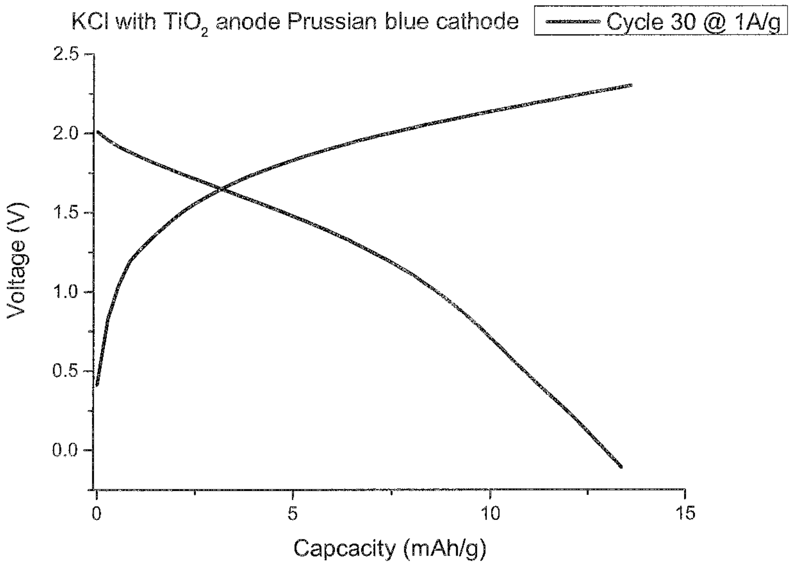

Figure 32

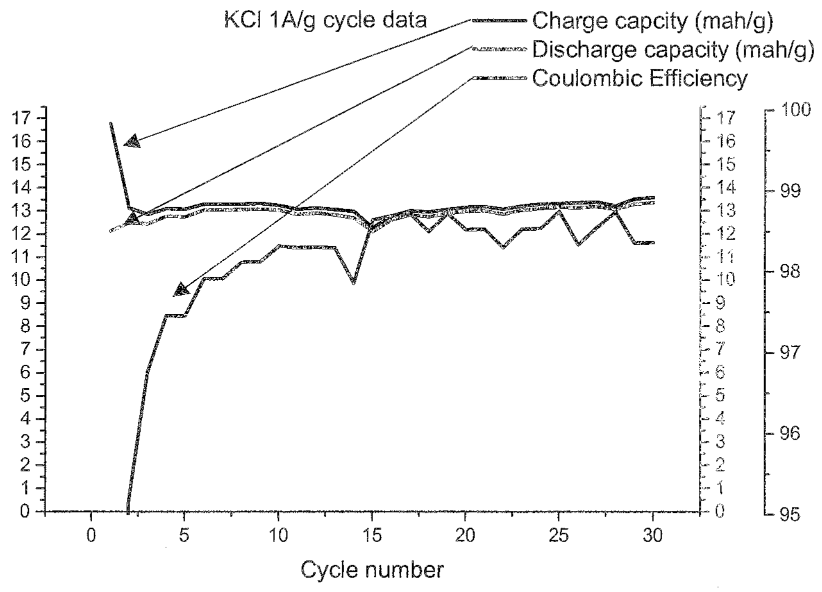

Figure 33

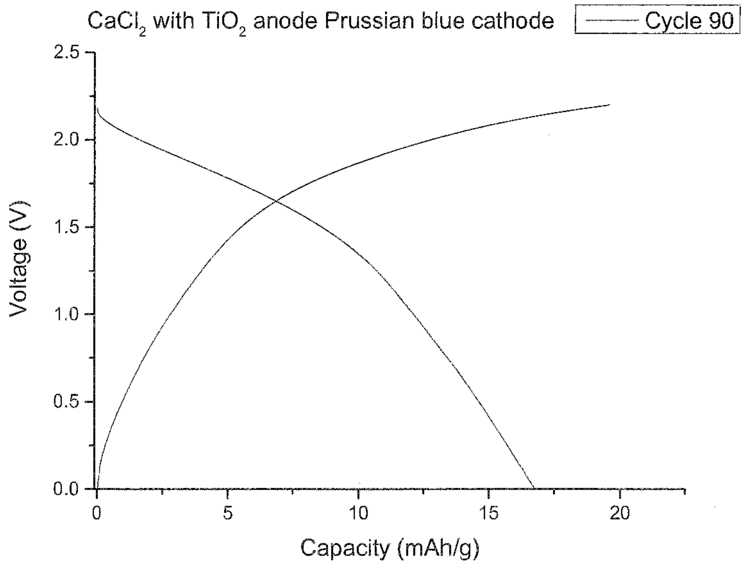

Figure 34

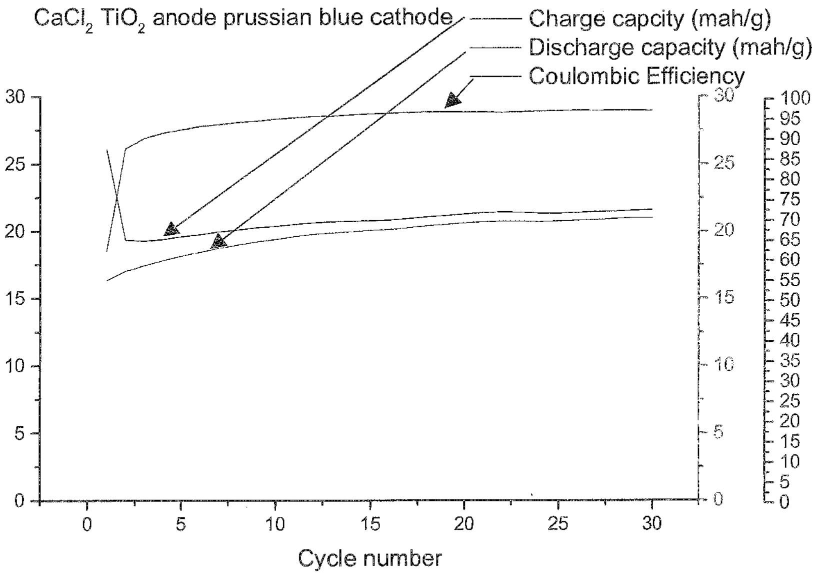

Figure 35

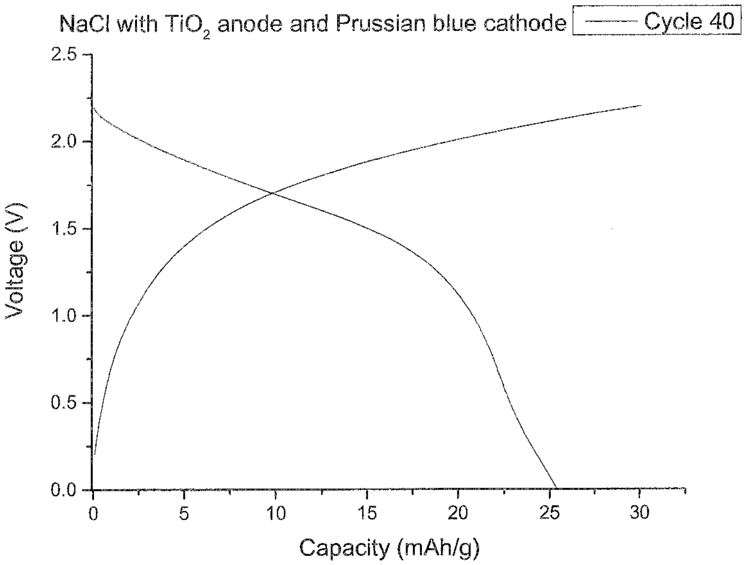

Figure 36

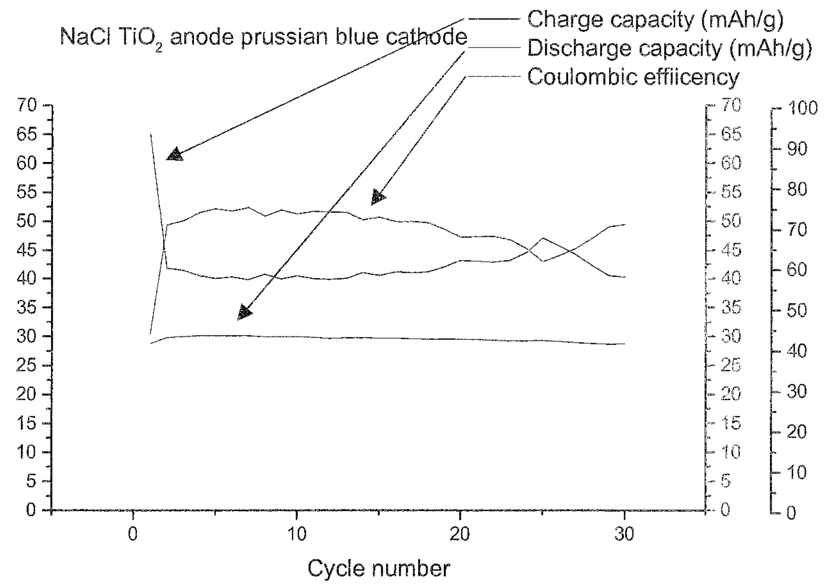

Figure 37

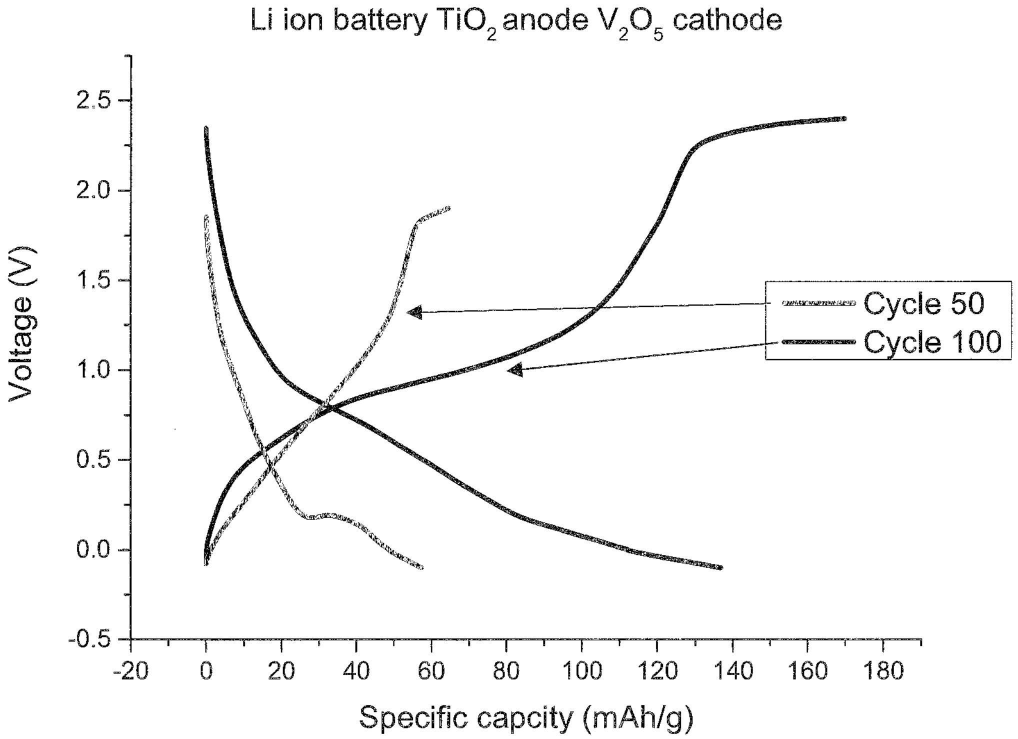

Figure 38

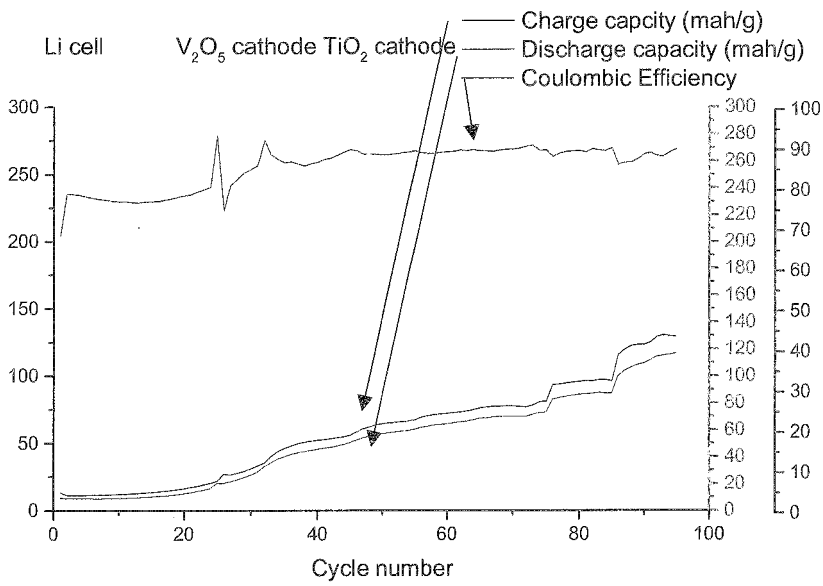

Figure 39

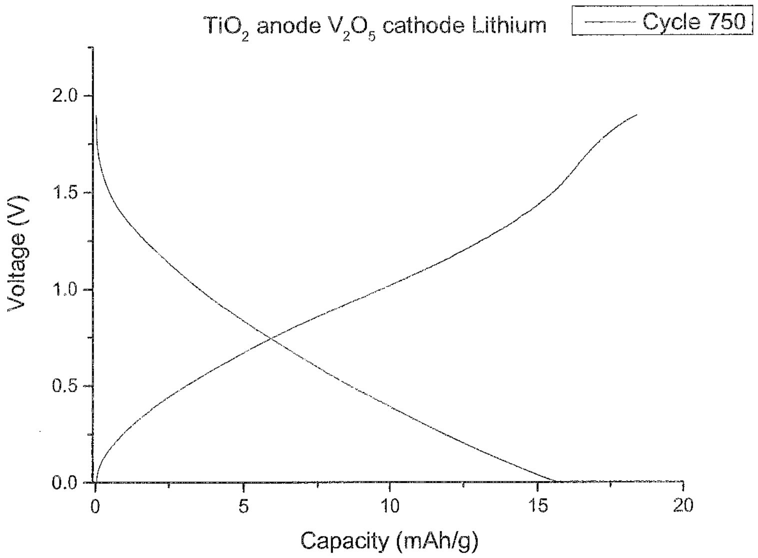

Figure 40

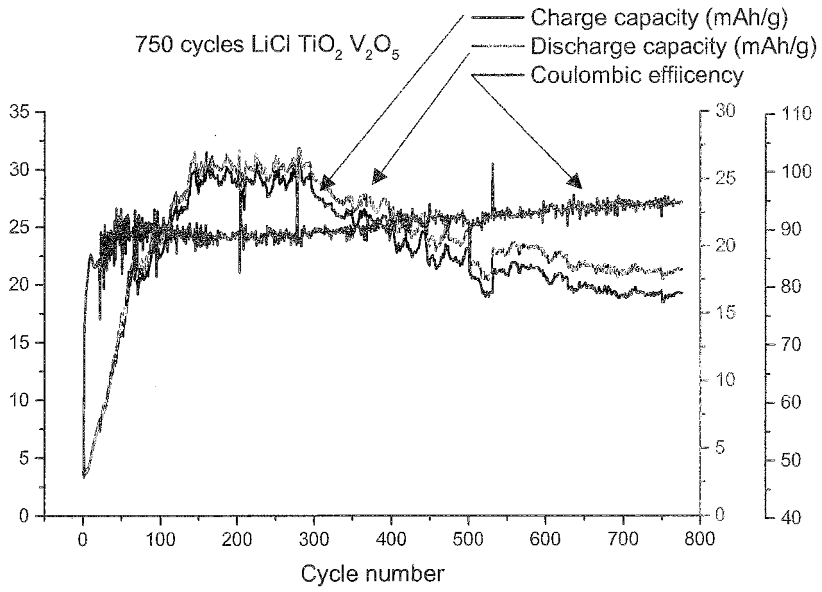

Figure 41

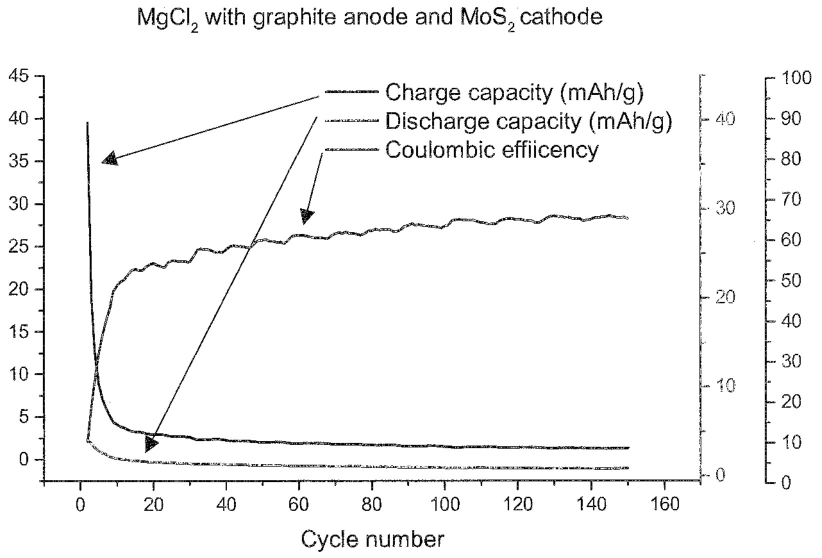

Figure 42

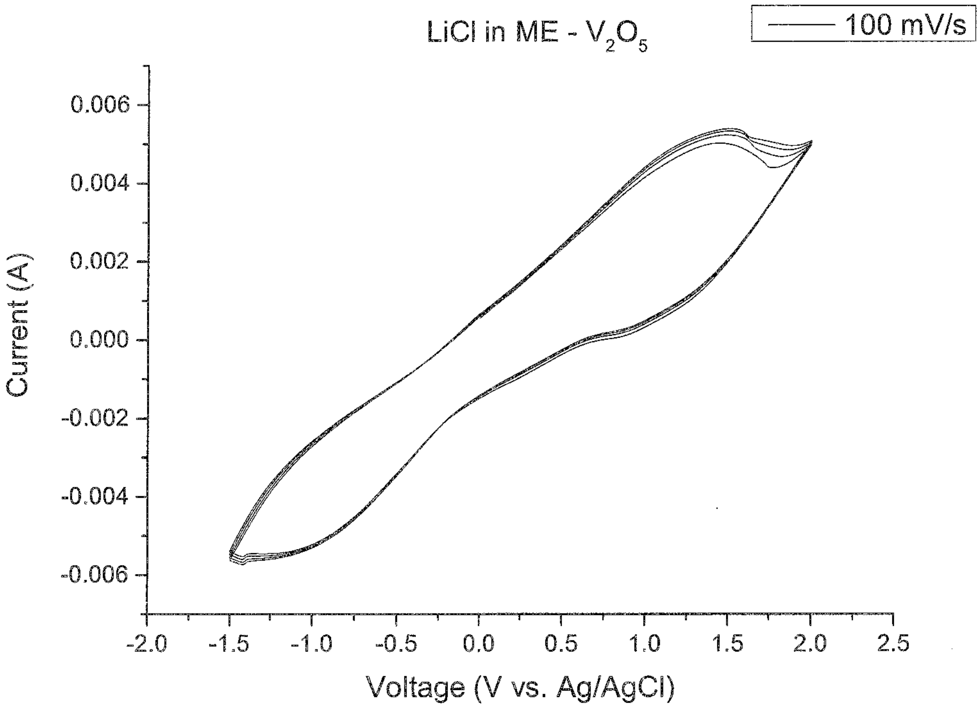

Figure 43

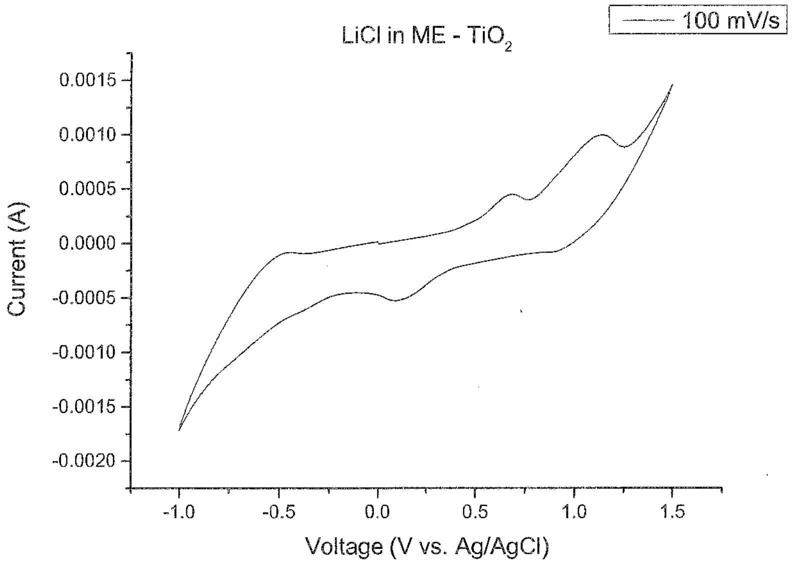

Figure 44

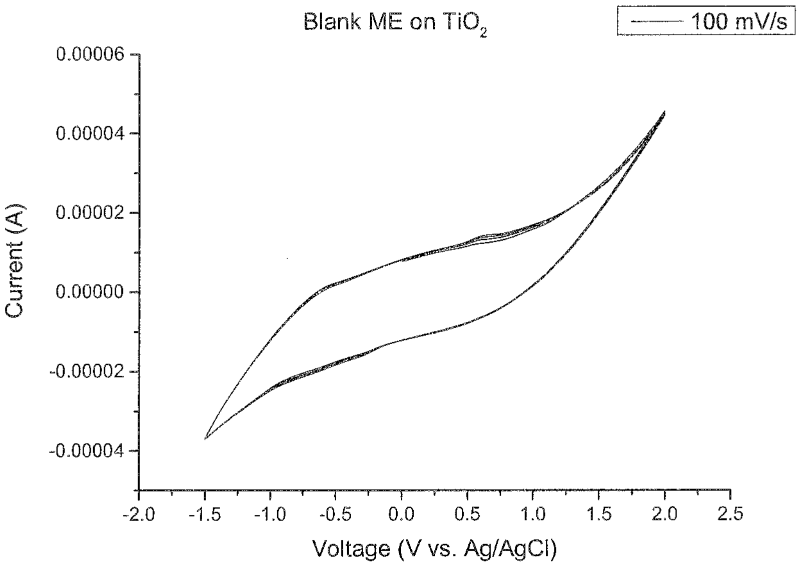

Figure 45

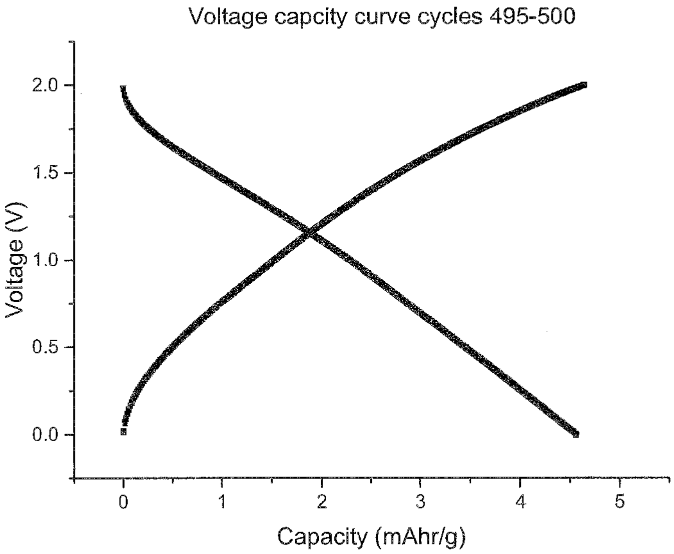

Figure 46

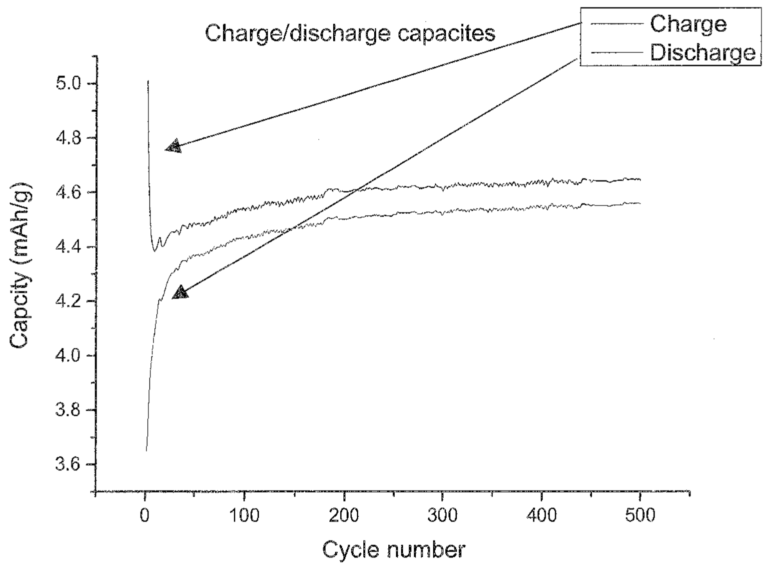

Figure 47

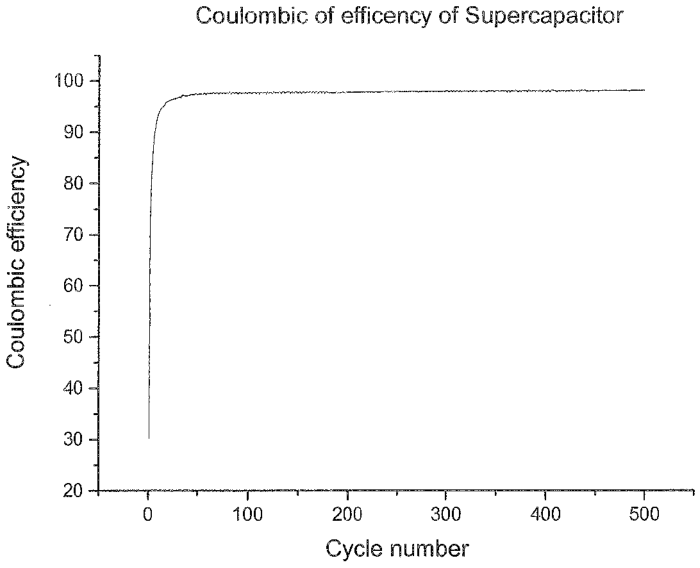

Figure 48

INTERNATIONAL SEARCH REPORT	International application No. **PCT/NZ2019/050164**

A. CLASSIFICATION OF SUBJECT MATTER

H01G 11/60 (2013.01) H01M 10/26 (2006.01)

According to International Patent Classification (IPC) or to both national classification and IPC

B. FIELDS SEARCHED

Minimum documentation searched (classification system followed by classification symbols)

Documentation searched other than minimum documentation to the extent that such documents are included in the fields searched

Electronic data base consulted during the international search (name of data base and, where practicable, search terms used)

PATENW: /C/IC (H01M6/04, H01M10/056, H01M2300/0002, H01G11/60, H01M8/08, H01G9/145, H01G2009/0025, H01M8/18, H01M2300/0088/C, B01F2003/0834, B01F2003/0823, H01M2300/0091, H01G11/60, H01G9/155, H01G9/145) & KEYWORDS: (AQUEOUS, IMMISCIBLE, BICONTINUOUS, EMULSION, MICROEMULSION, ELECTROLYTE, CAPACITOR, BATTERY, CELL and like terms) **COMPENDEX, INSPEC, CAPLUS**: Keywords (MICROEMULSION, ELECTROLYTE, BATTERY, CELL, CAPACITOR, BICONTINUOUS) **GOOGLE PATENTS, GOOGLE, GOOGLE SCHOLAR:** (Marks: H01M10/056, H01M6/04, H01M8/18, H01M2300/0088, H01G9/155, H01G11/60 & Keywords: battery, electrolyte, bicontinuous, electrolyte, microemulsion, aqueous, cell, capacitor, emulsion, assignee:(LOCKHEED MARTIN ADVANCED ENERGY STORAGE) and like terms) Applicant/Inventor searched using both internal (provided by IP Australia) and external databases (Espacenet, Auspat)

C. DOCUMENTS CONSIDERED TO BE RELEVANT

Category*	Citation of document, with indication, where appropriate, of the relevant passages	Relevant to claim No.
	Documents are listed in the continuation of Box C	

☒ Further documents are listed in the continuation of Box C ☒ See patent family annex

* Special categories of cited documents:

"A"	document defining the general state of the art which is not considered to be of particular relevance	"T"	later document published after the international filing date or priority date and not in conflict with the application but cited to understand the principle or theory underlying the invention
"D"	document cited by the applicant in the international application		
"E"	earlier application or patent but published on or after the international filing date	"X"	document of particular relevance; the claimed invention cannot be considered novel or cannot be considered to involve an inventive step when the document is taken alone
"L"	document which may throw doubts on priority claim(s) or which is cited to establish the publication date of another citation or other special reason (as specified)	"Y"	document of particular relevance; the claimed invention cannot be considered to involve an inventive step when the document is combined with one or more other such documents, such combination being obvious to a person skilled in the art
"O"	document referring to an oral disclosure, use, exhibition or other means	"&"	document member of the same patent family
"P"	document published prior to the international filing date but later than the priority date claimed		

Date of the actual completion of the international search 2 March 2020	Date of mailing of the international search report 02 March 2020
Name and mailing address of the ISA/AU AUSTRALIAN PATENT OFFICE PO BOX 200, WODEN ACT 2606, AUSTRALIA Email address: pct@ipaustralia.gov.au	**Authorised officer** Susan Fyfield AUSTRALIAN PATENT OFFICE (ISO 9001 Quality Certified Service) Telephone No. +61262850749

INTERNATIONAL SEARCH REPORT C (Continuation). DOCUMENTS CONSIDERED TO BE RELEVANT		International application No. **PCT/NZ2019/050164**
Category*	Citation of document, with indication, where appropriate, of the relevant passages	Relevant to claim No.
 X Y	US 2011/0250515 A1 (VAN RAALTEN ET AL.) 13 October 2011 paragraphs [0010], [0020], [0049] - [0051], [0066], [0073], [0075], claims 18 & 19 paragraphs [0010], [0020], [0066], [0075], claim 18	 1 – 13, 18 - 24 14 - 16
X	US 2013/0242466 A1 (AVX CORPORATION) 19 September 2013 Abstract, paragraphs [0074], [0075]	1, 5, 23 - 24
X	US 2014/0230679 A1 (ORICA INTERNATIONAL PTE LTD.) 21 August 2014 paragraphs [0054], [0098], [0124]	1, 13, 17, 23 - 24
X	US 2012/0178017 A1 (MURAI et al.) 12 July 2012 Abstract, paragraph [0044], [0105], [0106], [0163], [0247] and claim 1	1 – 3, 13, 18 - 24
Y	US 2003/0180608 A1 (MORI et al.) 25 September 2003 Abstract, paragraph [0013], claim 1	14 - 16
P,X	WO 2019/079047 A1 (LOCKHEAD MARTIN ENERGY, LLC) 25 April 2019 paragraphs [0077],[0088], [0094], [0097] and [0114].	1 - 3, 14 - 16, 19, 23 - 24

INTERNATIONAL SEARCH REPORT Information on patent family members	International application No. **PCT/NZ2019/050164**

This Annex lists known patent family members relating to the patent documents cited in the above-mentioned international search report. The Australian Patent Office is in no way liable for these particulars which are merely given for the purpose of information.

Patent Document/s Cited in Search Report		**Patent Family Member/s**	
Publication Number	**Publication Date**	**Publication Number**	**Publication Date**
US 2011/0250515 A1	13 October 2011	US 2011250515 A1	13 Oct 2011
		US 8669021 B2	11 Mar 2014
		CA 2739714 A1	15 Apr 2010
		CN 102210050 A	05 Oct 2011
		CN 102210050 B	22 Oct 2014
		EP 2335313 A1	22 Jun 2011
		EP 2335313 B1	23 Mar 2016
		JP 2012505497 A	01 Mar 2012
		JP 5480275 B2	23 Apr 2014
		RU 2012110824 A	27 Sep 2013
		SM T201600124 B	01 Jul 2016
		US 2014248553 A1	04 Sep 2014
		US 9543593 B2	10 Jan 2017
		WO 2010041937 A1	15 Apr 2010
US 2013/0242466 A1	19 September 2013	US 2013242466 A1	19 Sep 2013
		US 9076592 B2	07 Jul 2015
		CN 103310984 A	18 Sep 2013
		CN 103310984 B	31 Oct 2017
		DE 102013204358 A1	19 Sep 2013
		FR 2988209 A1	20 Sep 2013
		FR 2988209 B1	05 Aug 2016
		GB 2500988 A	09 Oct 2013
		GB 2500988 B	06 Jan 2016
US 2014/0230679 A1	21 August 2014	US 2014230679 A1	21 Aug 2014
		US 10144678 B2	04 Dec 2018
		AU 2014218506 A1	03 Sep 2015
		AU 2014218506 B2	19 Jul 2018
		CA 2901625 A1	28 Aug 2014
		WO 2014127412 A1	28 Aug 2014
US 2012/0178017 A1	12 July 2012	US 2012178017 A1	12 Jul 2012
		US 9133316 B2	15 Sep 2015
		CN 102498168 A	13 Jun 2012
		CN 102498168 B	10 Sep 2014
		EP 2479212 A1	25 Jul 2012
		JP WO2011034179 A1	14 Feb 2013

Due to data integration issues this family listing may not include 10 digit Australian applications filed since May 2001.

INTERNATIONAL SEARCH REPORT Information on patent family members	International application No. **PCT/NZ2019/050164**

This Annex lists known patent family members relating to the patent documents cited in the above-mentioned international search report. The Australian Patent Office is in no way liable for these particulars which are merely given for the purpose of information.

Patent Document/s Cited in Search Report		**Patent Family Member/s**	
Publication Number	**Publication Date**	**Publication Number**	**Publication Date**
		JP 5461566 B2	02 Apr 2014
		US 2015349366 A1	03 Dec 2015
		US 9406958 B2	02 Aug 2016
		US 2016308232 A1	20 Oct 2016
		US 9627702 B2	18 Apr 2017
		WO 2011034179 A1	24 Mar 2011
US 2003/0180608 A1	25 September 2003	US 2003180608 A1	25 Sep 2003
		US 6818353 B2	16 Nov 2004
		JP 2002015728 A	18 Jan 2002
		WO 0203485 A1	10 Jan 2002
WO 2019/079047 A1	25 April 2019	WO 2019079047 A1	25 Apr 2019

End of Annex

Due to data integration issues this family listing may not include 10 digit Australian applications filed since May 2001.

Appendix A

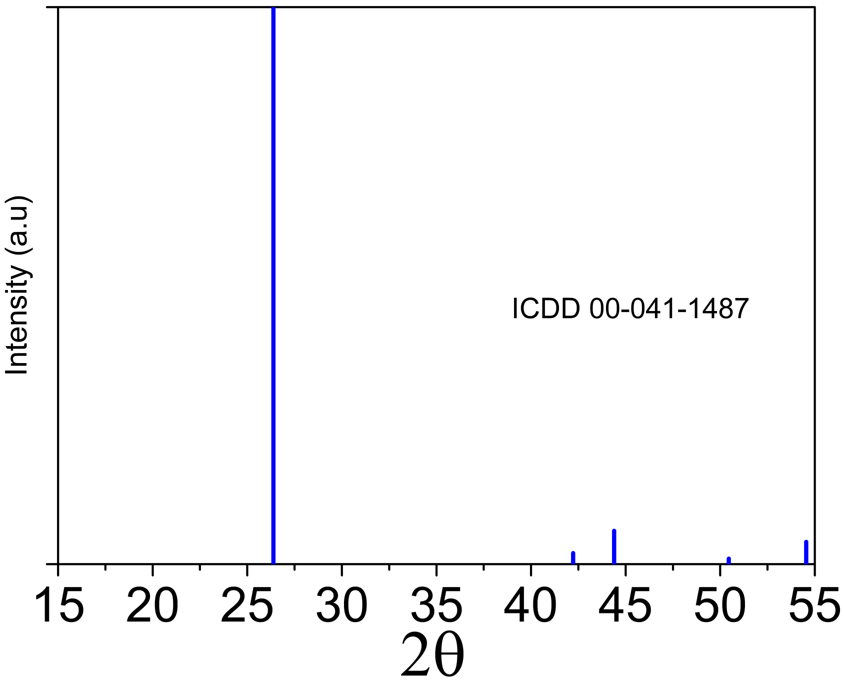

Figure A.1: Reference pattern used for the graphite foil present in all XRD samples. The relative reflectionintensities differ from the pattern due to the foil being made of highly oriented pyrolytic graphite which will emphasise some of the reflections more than others.

Bibliography

[1] Kasper T. Møller, Torben R. Jensen, Etsuo Akiba, and Hai-wen Li. Hydrogen - A sustainable energy carrier. *Progress in Natural Science: Materials International*, 27(1):34–40, February 2017. ISSN 1002-0071. doi: 10.1016/j.pnsc.2016.12.014. URL `http://www.sciencedirect.com/science/article/pii/S1002007116303240`.

[2] Haiwei Du, Xi Lin, Zhemi Xu, and Dewei Chu. Electric double-layer transistors: a review of recent progress. *Journal of Materials Science*, 50(17):5641–5673, September 2015. ISSN 1573-4803. doi: 10.1007/s10853-015-9121-y. URL `https://doi.org/10.1007/s10853-015-9121-y`.

[3] Amin M. Saleem, Vincent Desmaris, and Peter Enoksson. Performance Enhancement of Carbon Nanomaterials for Supercapacitors, August 2016. URL `https://www.hindawi.com/journals/jnm/2016/1537269/`. ISSN: 1687-4110 Pages: e1537269 Publisher: Hindawi Volume: 2016.

[4] Patrick Novinsky, S. Glöser, A. Kühn, and R. Walz. Modeling the Feedback of Battery Raw Material Shortages on the Technological Development of Lithium-Ion-Batteries and the Diffusion of Alternative Automotive Drives, 2014. URL `/paper/Modeling-the-Feedback-of-Battery-Raw-Material-on-of-Novinsky-Gl%C3%B6ser/f417f59ce4f92c2f91a01af1a1a74812609b3566`.

[5] Aoife M. O'Mahony, Debbie S. Silvester, Leigh Aldous, Christopher Hardacre, and Richard G. Compton. Effect of Water on the Electrochemical Window and Potential Limits of Room-Temperature Ionic Liquids. *Journal of Chemical & Engineering Data*, 53(12):2884–2891, December 2008. ISSN 0021-9568. doi: 10.1021/je800678e. URL `https://doi.org/10.1021/je800678e`. Publisher: American Chemical Society.

[6] Maaike C. Kroon, Wim Buijs, Cor J. Peters, and Geert-Jan Witkamp. Decomposition of ionic liquids in electrochemical processing. *Green Chemistry*, 8(3):241–245, 2006. doi: 10.1039/B512724F. URL `https://pubs.rsc.org/en/content/articlelanding/2006/gc/b512724f`. Publisher: Royal Society of Chemistry.

[7] Liumin Suo, Oleg Borodin, Tao Gao, Marco Olguin, Janet Ho, Xiulin Fan, Chao Luo, Chunsheng Wang, and Kang Xu. "Water-in-salt" electrolyte enables high-voltage aqueous lithium-ion chemistries. *Science*, 350(6263):938–943, November 2015. ISSN 0036-8075, 1095-9203. doi: 10.1126/science.aab1595. URL `https://science.sciencemag.org/content/350/6263/938`. Publisher: American Association for the Advancement of Science Section: Research Article.

[8] Masashi Kunitake, Eisuke Kuraya, Dai Kato, Osamu Niwa, and Taisei Nishimi. Electrochemistry in bicontinuous microemulsions based on control of dynamic solution structures on electrode surfaces. *Current Opinion in Colloid & Interface Science*, 25:13–26, October 2016. ISSN 1359-0294. doi: 10.1016/j.cocis.2016.05.004. URL `http://www.sciencedirect.com/science/article/pii/S1359029416300516`.

[9] Bing-Ang Mei, Obaidallah Munteshari, Jonathan Lau, Bruce Dunn, and Laurent Pilon. Physical Interpretations of Nyquist Plots for EDLC Electrodes and Devices. *The Journal of Physical Chemistry C*, 122(1):194–206, January 2018. ISSN 1932-7447. doi: 10.1021/acs.jpcc.7b10582. URL `https://doi.org/10.1021/acs.jpcc.7b10582`. Publisher: American Chemical Society.

[10] Xiaowei Zhou, Xu Chen, Qinsong Bi, Xiaobin Luo, Li Sun, and Zhu Liu. A scalable strategy to synthesize TiO2-V2O5 nanorods as high performance cathode for lithium ion batteries from VOx quasi-aerogel and tetrabutyl titanate. *Ceramics International*, 43(15):12689–12697, October 2017. ISSN 0272-8842. doi: 10.1016/j.ceramint.2017.06.152. URL `http://www.sciencedirect.com/science/article/pii/S0272884217313688`.

[11] Santanu Mukherjee, Alex Bates, Nicholas Schuppert, Byungrak Son, Joo Gon Kim, Jae Sung Choi, Moon Jong Choi, Dong-Ha Lee, Osung Kwon, Jacek Jasinski, and Sam Park. A study of a novel Na ion battery and its anodic degradation using sodium rich prussian blue cathode coupled with different titanium based

oxide anodes. *Journal of Power Sources*, 286:276–289, July 2015. ISSN 0378-7753. doi: 10.1016/j.jpowsour.2015.03.167. URL http://www.sciencedirect.com/science/article/pii/S0378775315006011.

[12] R. Borah, F. R. Hughson, J. Johnston, and T. Nann. On battery materials and methods. *Materials Today Advances*, 6:100046, June 2020. ISSN 2590-0498. doi: 10.1016/j.mtadv.2019.100046. URL http://www.sciencedirect.com/science/article/pii/S2590049819301201.

[13] Nicolò Canever, Fraser R. Hughson, and Thomas Nann. Solid-Electrolyte Interphases (SEI) in Nonaqueous Aluminum-Ion Batteries. *ACS Applied Energy Materials*, 3(4):3673–3683, April 2020. doi: 10.1021/acsaem.0c00132. URL https://doi.org/10.1021/acsaem.0c00132. Publisher: American Chemical Society.

[14] Fraser R. Hughson, Rohan Borah, and Thomas Nann. A 2.7 V Aqueous Supercapacitor Using a Microemulsion Electrolyte. *Batteries & Supercaps*, n/a(n/a). ISSN 2566-6223. doi: https://doi.org/10.1002/batt.202000314. URL https://chemistry-europe.onlinelibrary.wiley.com/doi/abs/10.1002/batt.202000314. _eprint: https://chemistry-europe.onlinelibrary.wiley.com/doi/pdf/10.1002/batt.202000314.

[15] Jillian Ambrose. Renewable electricity overtakes fossil fuels in UK for first time. *The Guardian*, October 2019. ISSN 0261-3077. URL https://www.theguardian.com/business/2019/oct/14/renewable-electricity-overtakes-fossil-fuels-in-uk-for-first-time.

[16] Michael Mazengarb. Tasmania declares itself 100 per cent powered by renewable electricity, November 2020. URL https://reneweconomy.com.au/tasmania-declares-itself-100-per-cent-powered-by-renewable-electricity-25119/.

[17] simionauc. Battery storage: The answer to renewable energy intermittency, April 2018. URL https://auclimate.wordpress.com/2018/04/17/battery-storage-the-answer-to-renewable-energy-intermittency/.

[18] Muhammad Shahzad Javed, Tao Ma, Jakub Jurasz, and Muhammad Yasir Amin. Solar and wind power generation systems with pumped hydro storage: Review

and future perspectives. *Renewable Energy*, 148:176–192, April 2020. ISSN 0960-1481. doi: 10.1016/j.renene.2019.11.157. URL http://www.sciencedirect.com/science/article/pii/S0960148119318592.

[19] Matthew A. Pellow, Hanjiro Ambrose, Dustin Mulvaney, Rick Betita, and Stephanie Shaw. Research gaps in environmental life cycle assessments of lithium ion batteries for grid-scale stationary energy storage systems: End-of-life options and other issues. *Sustainable Materials and Technologies*, 23:e00120, April 2020. ISSN 2214-9937. doi: 10.1016/j.susmat.2019.e00120. URL http://www.sciencedirect.com/science/article/pii/S2214993718302318.

[20] M. T. Lawder, B. Suthar, P. W. C. Northrop, S. De, C. M. Hoff, O. Leitermann, M. L. Crow, S. Santhanagopalan, and V. R. Subramanian. Battery Energy Storage System (BESS) and Battery Management System (BMS) for Grid-Scale Applications. *Proceedings of the IEEE*, 102(6):1014–1030, June 2014. ISSN 1558-2256. doi: 10.1109/JPROC.2014.2317451. Conference Name: Proceedings of the IEEE.

[21] Jorge Omar Gil Posada, Anthony J. R. Rennie, Sofia Perez Villar, Vitor L. Martins, Jordan Marinaccio, Alistair Barnes, Carol F. Glover, David A. Worsley, and Peter J. Hall. Aqueous batteries as grid scale energy storage solutions. *Renewable and Sustainable Energy Reviews*, 68:1174–1182, February 2017. ISSN 1364-0321. doi: 10.1016/j.rser.2016.02.024. URL http://www.sciencedirect.com/science/article/pii/S136403211600232X.

[22] B. B. McKeon, J. Furukawa, and S. Fenstermacher. Advanced Lead–Acid Batteries and the Development of Grid-Scale Energy Storage Systems. *Proceedings of the IEEE*, 102(6):951–963, June 2014. ISSN 1558-2256. doi: 10.1109/JPROC.2014.2316823. Conference Name: Proceedings of the IEEE.

[23] K. Ahmad, N. Mohammad, and M. Quamruzzaman. Review on Frequency Adjustment for Power Systems with Grid Connected Wind Farm. In *2019 International Conference on Robotics,Electrical and Signal Processing Techniques (ICREST)*, pages 617–621, January 2019. doi: 10.1109/ICREST.2019.8644155.

[24] Samuel C. Johnson, Dimitri J. Papageorgiou, Dharik S. Mallapragada, Thomas A. Deetjen, Joshua D. Rhodes, and Michael E. Webber. Evaluating rotational inertia as a component of grid reliability with high penetrations of variable renewable energy. *Energy*, 180:258–271, August 2019. ISSN 0360-5442. doi: 10.1016/j.energy.2019.04.216. URL `http://www.sciencedirect.com/science/article/pii/S0360544219308564`.

[25] Patrice Simon, Yury Gogotsi, and Bruce Dunn. Where Do Batteries End and Supercapacitors Begin? *Science*, 343(6176):1210–1211, March 2014. ISSN 0036-8075, 1095-9203. doi: 10.1126/science.1249625. URL `https://science.sciencemag.org/content/343/6176/1210`. Publisher: American Association for the Advancement of Science Section: Perspective.

[26] Edurne Redondo, Lewis W. Le Fevre, Richard Fields, Rebecca Todd, Andrew J. Forsyth, and Robert A. W. Dryfe. Enhancing supercapacitor energy density by mass-balancing of graphene composite electrodes. *Electrochimica Acta*, 360:136957, November 2020. ISSN 0013-4686. doi: 10.1016/j.electacta.2020.136957. URL `http://www.sciencedirect.com/science/article/pii/S0013468620313505`.

[27] Q. Zhang and G. Li. Experimental Study on a Semi-Active Battery-Supercapacitor Hybrid Energy Storage System for Electric Vehicle Application. *IEEE Transactions on Power Electronics*, 35(1):1014–1021, January 2020. ISSN 1941-0107. doi: 10.1109/TPEL.2019.2912425. Conference Name: IEEE Transactions on Power Electronics.

[28] Eiji Hosono, Tetsuichi Kudo, Itaru Honma, Hirofumi Matsuda, and Haoshen Zhou. Synthesis of Single Crystalline Spinel LiMn2O4 Nanowires for a Lithium Ion Battery with High Power Density. *Nano Letters*, 9(3):1045–1051, March 2009. ISSN 1530-6984. doi: 10.1021/nl803394v. URL `https://doi.org/10.1021/nl803394v`. Publisher: American Chemical Society.

[29] Hiroshi Nagata and Yasuo Chikusa. A lithium sulfur battery with high power density. *Journal of Power Sources*, 264:206–210, October 2014. ISSN 0378-7753. doi: 10.1016/j.jpowsour.2014.04.106. URL `http://www.sciencedirect.com/science/article/pii/S0378775314006077`.

[30] Martin Winter and Ralph J. Brodd. What Are Batteries, Fuel Cells, and Supercapacitors? *Chemical Reviews*, 104(10):4245–4270, October 2004. ISSN 0009-2665. doi: 10.1021/cr020730k. URL `https://doi.org/10.1021/cr020730k`. Publisher: American Chemical Society.

[31] Chenguang Liu, Zhenning Yu, David Neff, Aruna Zhamu, and Bor Z. Jang. Graphene-Based Supercapacitor with an Ultrahigh Energy Density. *Nano Letters*, 10(12):4863–4868, December 2010. ISSN 1530-6984. doi: 10.1021/nl102661q. URL `https://doi.org/10.1021/nl102661q`. Publisher: American Chemical Society.

[32] Li Li Zhang, Rui Zhou, and X. S. Zhao. Graphene -based materials as supercapacitor electrodes. *Journal of Materials Chemistry*, 20(29):5983–5992, 2010. doi: 10.1039/C000417K. URL `https://pubs.rsc.org/en/content/articlelanding/2010/jm/c000417k`. Publisher: Royal Society of Chemistry.

[33] Kai Zhang, Li Li Zhang, X. S. Zhao, and Jishan Wu. Graphene/Polyaniline Nanofiber Composites as Supercapacitor Electrodes. *Chemistry of Materials*, 22(4):1392–1401, February 2010. ISSN 0897-4756. doi: 10.1021/cm902876u. URL `https://doi.org/10.1021/cm902876u`. Publisher: American Chemical Society.

[34] Yu Bin Tan and Jong-Min Lee. Graphene for supercapacitor applications. *Journal of Materials Chemistry A*, 1(47):14814–14843, 2013. doi: 10.1039/C3TA12193C. URL `https://pubs.rsc.org/en/content/articlelanding/2013/ta/c3ta12193c`. Publisher: Royal Society of Chemistry.

[35] Juan Mi, Xiao-Rong Wang, Rui-Jun Fan, Wen-Hui Qu, and Wen-Cui Li. Coconut-Shell-Based Porous Carbons with a Tunable Micro/Mesopore Ratio for High-Performance Supercapacitors. *Energy & Fuels*, 26(8):5321–5329, August 2012. ISSN 0887-0624. doi: 10.1021/ef3009234. URL `https://doi.org/10.1021/ef3009234`. Publisher: American Chemical Society.

[36] C. Muhamed Ashraf, K. M. Anilkumar, B. Jinisha, M. Manoj, V. S. Pradeep, and S. Jayalekshmi. Acid Washed, Steam Activated, Coconut Shell Derived Carbon for High Power Supercapacitor Applications. *Journal of The Electrochemical Society*, 165(5):A900, March 2018. ISSN 1945-7111. doi: 10.1149/2.0491805jes. URL `https://iopscience.iop.org/article/10.1149/2.0491805jes/meta`. Publisher: IOP Publishing.

[37] Marcus Rose, Yair Korenblit, Emanuel Kockrick, Lars Borchardt, Martin Oschatz, Stefan Kaskel, and Gleb Yushin. Hierarchical Micro- and Mesoporous Carbide-Derived Carbon as a High-Performance Electrode Material in Supercapacitors. *Small*, 7(8):1108–1117, 2011. ISSN 1613-6829. doi: 10.1002/smll.201001898. URL https://onlinelibrary.wiley.com/doi/abs/10.1002/smll.201001898. _eprint: https://onlinelibrary.wiley.com/doi/pdf/10.1002/smll.201001898.

[38] M. Arulepp, J. Leis, M. Lätt, F. Miller, K. Rumma, E. Lust, and A. F. Burke. The advanced carbide-derived carbon based supercapacitor. *Journal of Power Sources*, 162(2):1460–1466, November 2006. ISSN 0378-7753. doi: 10.1016/j.jpowsour.2006.08.014. URL http://www.sciencedirect.com/science/article/pii/S0378775306015643.

[39] Cheng Zhong, Yida Deng, Wenbin Hu, Jinli Qiao, Lei Zhang, and Jiujun Zhang. A review of electrolyte materials and compositions for electrochemical supercapacitors. *Chemical Society Reviews*, 44(21):7484–7539, 2015. doi: 10.1039/C5CS00303B. URL https://pubs.rsc.org/en/content/articlelanding/2015/cs/c5cs00303b. Publisher: Royal Society of Chemistry.

[40] A. Jänes, J. Eskusson, T. Thomberg, and E. Lust. Supercapacitors Based on Propylene Carbonate with Small Addition of Different Sulfur Containing Organic Solvents. *Journal of The Electrochemical Society*, 161(9):A1284, June 2014. ISSN 1945-7111. doi: 10.1149/2.0691409jes. URL https://iopscience.iop.org/article/10.1149/2.0691409jes/meta. Publisher: IOP Publishing.

[41] Ping Liu, Mark Verbrugge, and Souren Soukiazian. Influence of temperature and electrolyte on the performance of activated-carbon supercapacitors. *Journal of Power Sources*, 156(2):712–718, June 2006. ISSN 0378-7753. doi: 10.1016/j.jpowsour.2005.05.055. URL http://www.sciencedirect.com/science/article/pii/S0378775305007706.

[42] Mahesh Datt Bhatt and Jin Yong Lee. High capacity conversion anodes in Li-ion batteries: A review. *International Journal of Hydrogen Energy*, 44(21):10852–10905, April 2019. ISSN 0360-3199. doi: 10.1016/j.ijhydene.2019.02.015. URL http://www.sciencedirect.com/science/article/pii/S0360319919305592.

[43] Sheng Shui Zhang. A review on electrolyte additives for lithium-ion batteries. *Journal of Power Sources*, 162(2):1379–1394, November 2006. ISSN 0378-7753. doi: 10.1016/j.jpowsour.2006.07.074. URL http://www.sciencedirect.com/science/article/pii/S0378775306017538.

[44] S. Sato and A. Kawamura. A new estimation method of state of charge using terminal voltage and internal resistance for lead acid battery. In *Proceedings of the Power Conversion Conference-Osaka 2002 (Cat. No.02TH8579)*, volume 2, pages 565–570 vol.2, April 2002. doi: 10.1109/PCC.2002.997578.

[45] Kang Xu, Sheng P. Ding, and T. Richard Jow. Toward Reliable Values of Electrochemical Stability Limits for Electrolytes. *Journal of the Electrochemical Society*, 146(11):4172, November 1999. ISSN 1945-7111. doi: 10.1149/1.1392609. URL https://iopscience.iop.org/article/10.1149/1.1392609/meta. Publisher: IOP Publishing.

[46] R. Kötz, M. Hahn, and R. Gallay. Temperature behavior and impedance fundamentals of supercapacitors. *Journal of Power Sources*, 154(2):550–555, March 2006. ISSN 0378-7753. doi: 10.1016/j.jpowsour.2005.10.048. URL http://www.sciencedirect.com/science/article/pii/S0378775305014266.

[47] Dongping Lv, Terrence Xu, Partha Saha, Moni Kanchan Datta, Mikhail L. Gordin, Ayyakkannu Manivannan, Prashant N. Kumta, and Donghai Wang. A Scientific Study of Current Collectors for Mg Batteries in Mg(AlCl2EtBu)2/THF Electrolyte. *Journal of the Electrochemical Society*, 160(2):A351, December 2012. ISSN 1945-7111. doi: 10.1149/2.085302jes. URL https://iopscience.iop.org/article/10.1149/2.085302jes/meta. Publisher: IOP Publishing.

[48] Fritz Beck and Paul Rüetschi. Rechargeable batteries with aqueous electrolytes. *Electrochimica Acta*, 45(15):2467–2482, May 2000. ISSN 0013-4686. doi: 10.1016/S0013-4686(00)00344-3. URL http://www.sciencedirect.com/science/article/pii/S0013468600003443.

[49] Qingsong Wang, Binbin Mao, Stanislav I. Stoliarov, and Jinhua Sun. A review of lithium ion battery failure mechanisms and fire prevention strategies.

Progress in Energy and Combustion Science, 73:95–131, July 2019. ISSN 0360-1285. doi: 10.1016/j.pecs.2019.03.002. URL `http://www.sciencedirect.com/science/article/pii/S0360128518301801`.

[50] Linda Gaines. The future of automotive lithium-ion battery recycling: Charting a sustainable course. *Sustainable Materials and Technologies*, 1-2:2–7, December 2014. ISSN 2214-9937. doi: 10.1016/j.susmat.2014.10.001. URL `http://www.sciencedirect.com/science/article/pii/S2214993714000037`.

[51] John Muldoon, Claudiu B. Bucur, Allen G. Oliver, Jaroslav Zajicek, Gary D. Allred, and William C. Boggess. Corrosion of magnesium electrolytes: chlorides – the culprit. *Energy & Environmental Science*, 6(2):482–487, 2013. doi: 10.1039/C2EE23686A. URL `https://pubs.rsc.org/en/content/articlelanding/2013/ee/c2ee23686a`. Publisher: Royal Society of Chemistry.

[52] David Muñoz-Torrero, Marc Anderson, Jesús Palma, Rebeca Marcilla, and Edgar Ventosa. Unexpected Contribution of Current Collector to the Cost of Rechargeable Al-Ion Batteries. *ChemElectroChem*, 6(10): 2766–2770, 2019. ISSN 2196-0216. doi: https://doi.org/10.1002/celc.201900679. URL `https://chemistry-europe.onlinelibrary.wiley.com/doi/abs/10.1002/celc.201900679`. _eprint: https://chemistry-europe.onlinelibrary.wiley.com/doi/pdf/10.1002/celc.201900679.

[53] Mengyun Nie, Daniel P. Abraham, Yanjing Chen, Arijit Bose, and Brett L. Lucht. Silicon Solid Electrolyte Interphase (SEI) of Lithium Ion Battery Characterized by Microscopy and Spectroscopy. *The Journal of Physical Chemistry C*, 117(26): 13403–13412, July 2013. ISSN 1932-7447. doi: 10.1021/jp404155y. URL `https://doi.org/10.1021/jp404155y`. Publisher: American Chemical Society.

[54] Hadi Tavassol, Joseph W. Buthker, Glen A. Ferguson, Larry A. Curtiss, and Andrew A. Gewirth. Solvent Oligomerization during SEI Formation on Model Systems for Li-Ion Battery Anodes. *Journal of the Electrochemical Society*, 159 (6):A730, April 2012. ISSN 1945-7111. doi: 10.1149/2.067206jes. URL `https://iopscience.iop.org/article/10.1149/2.067206jes/meta`. Publisher: IOP Publishing.

[55] M. Q. Xu, W. S. Li, X. X. Zuo, J. S. Liu, and X. Xu. Performance improvement of lithium ion battery using PC as a solvent component and BS as an SEI forming additive. *Journal of Power Sources*, 174(2):705–710, December 2007. ISSN 0378-7753. doi: 10.1016/j.jpowsour.2007.06.112. URL `http://www.sciencedirect.com/science/article/pii/S0378775307014164`.

[56] Chongyin Yang, Ji Chen, Tingting Qing, Xiulin Fan, Wei Sun, Arthur von Cresce, Michael S. Ding, Oleg Borodin, Jenel Vatamanu, Marshall A. Schroeder, Nico Eidson, Chunsheng Wang, and Kang Xu. 4.0 V Aqueous Li-Ion Batteries. *Joule*, 1(1): 122–132, September 2017. ISSN 2542-4351. doi: 10.1016/j.joule.2017.08.009. URL `http://www.sciencedirect.com/science/article/pii/S254243511730034X`.

[57] Usha Subramanya, Charleston Chua, Victor Gin He Leong, Ryan Robinson, Gwenlyn Angel Cruz Cabiltes, Prakirti Singh, Bonnie Yip, Anuja Bokare, Folarin Erogbogbo, and Dahyun Oh. Carbon-based artificial SEI layers for aqueous lithium-ion battery anodes. *RSC Advances*, 10(2):674–681, 2020. doi: 10.1039/C9RA08268A. URL `https://pubs.rsc.org/en/content/articlelanding/2020/ra/c9ra08268a`. Publisher: Royal Society of Chemistry.

[58] Jian Zhi, Alireza Zehtab Yazdi, Gayathri Valappil, Jessica Haime, and P. Chen. Artificial solid electrolyte interphase for aqueous lithium energy storage systems. *Science Advances*, 3(9):e1701010, September 2017. ISSN 2375-2548. doi: 10.1126/sciadv.1701010. URL `https://advances.sciencemag.org/content/3/9/e1701010`. Publisher: American Association for the Advancement of Science Section: Research Article.

[59] Mei Han, Jian Zhi, Tuan K. A. Hoang, Yuting Li, Longyan Li, and Pu Chen. Artificial solid electrolyte interphase for thermally stable rechargeable aqueous zinc batteries. *Journal of Power Sources*, 441:227171, November 2019. ISSN 0378-7753. doi: 10.1016/j.jpowsour.2019.227171. URL `http://www.sciencedirect.com/science/article/pii/S0378775319311644`.

[60] R. German, A. Sari, P. Venet, M. Ayadi, O. Briat, and J. M. Vinassa. Prediction of supercapacitors floating ageing with surface electrode interface based ageing law. *Microelectronics Reliability*, 54(9):1813–1817, September 2014. ISSN 0026-2714. doi: 10.1016/j.microrel.2014.07.105. URL `http://www.sciencedirect.com/science/article/pii/S0026271414003011`.

[61] Kijoo Hong, Moonkyu Cho, and Sang Ouk Kim. Atomic Layer Deposition Encapsulated Activated Carbon Electrodes for High Voltage Stable Supercapacitors. *ACS Applied Materials & Interfaces*, 7(3):1899–1906, January 2015. ISSN 1944-8244. doi: 10.1021/am507673j. URL https://doi.org/10.1021/am507673j. Publisher: American Chemical Society.

[62] Zhoufei Yang, Jiarui Tian, Zefang Yin, Chaojie Cui, Weizhong Qian, and Fei Wei. Carbon nanotube- and graphene-based nanomaterials and applications in high-voltage supercapacitor: A review. *Carbon*, 141:467–480, January 2019. ISSN 0008-6223. doi: 10.1016/j.carbon.2018.10.010. URL http://www.sciencedirect.com/science/article/pii/S0008622318309242.

[63] Ali Izadi-Najafabadi, Satoshi Yasuda, Kazufumi Kobashi, Takeo Yamada, Don N. Futaba, Hiroaki Hatori, Motoo Yumura, Sumio Iijima, and Kenji Hata. Extracting the Full Potential of Single-Walled Carbon Nanotubes as Durable Supercapacitor Electrodes Operable at 4 V with High Power and Energy Density. *Advanced Materials*, 22(35):E235–E241, 2010. ISSN 1521-4095. doi: 10.1002/adma.200904349. URL https://www.onlinelibrary.wiley.com/doi/abs/10.1002/adma.200904349. _eprint: https://onlinelibrary.wiley.com/doi/pdf/10.1002/adma.200904349.

[64] Haiyan Liu, Huaihe Song, Xiaohong Chen, Su Zhang, Jisheng Zhou, and Zhaokun Ma. Effects of nitrogen- and oxygen-containing functional groups of activated carbon nanotubes on the electrochemical performance in supercapacitors. *Journal of Power Sources*, 285:303–309, July 2015. ISSN 0378-7753. doi: 10.1016/j.jpowsour.2015.03.115. URL http://www.sciencedirect.com/science/article/pii/S037877531500539X.

[65] Liang Jiang, Jing Wang, Xuyan Mao, Xiangyu Xu, Bo Zhang, Jie Yang, Yunfei Wang, Jun Zhu, and Shifeng Hou. High rate performance carbon nanocages with oxygen-containing functional groups as supercapacitor electrode materials. *Carbon*, 111:207–214, January 2017. ISSN 0008-6223. doi: 10.1016/j.carbon.2016.09.081. URL http://www.sciencedirect.com/science/article/pii/S0008622316308508.

[66] Chi-Chang Hu and Chen-Ching Wang. Effects of electrolytes and electrochemical pretreatments on the capacitive characteristics of activated carbon fabrics for supercapacitors. *Journal of Power Sources*, 125(2):299–308, January 2004. ISSN 0378-7753. doi: 10.1016/j.jpowsour.2003.08.002. URL `http://www.sciencedirect.com/science/article/pii/S0378775303008516`.

[67] Susana Vaquero, Jesus Palma, Marc Anderson, and Rebeca Marcilla. Mass-Balancing of Electrodes as a Strategy to Widen the Operating Voltage Window of Carbon/Carbon Supercapacitors in Neutral Aqueous Electrolytes. *Int. J. Electrochem. Sci.*, 8:15, 2013.

[68] Donghui Zhou, Suqin Liu, Haiyan Wang, and Guiqing Yan. Na2V6O16·0.14H2O nanowires as a novel anode material for aqueous rechargeable lithium battery with good cycling performance. *Journal of Power Sources*, 227:111–117, April 2013. ISSN 0378-7753. doi: 10.1016/j.jpowsour.2012.11.022. URL `http://www.sciencedirect.com/science/article/pii/S0378775312016965`.

[69] Colin Wessells, Riccardo Ruff, Robert A. Huggins, and Yi Cui. Investigations of the Electrochemical Stability of Aqueous Electrolytes for Lithium Battery Applications. *Electrochemical and Solid State Letters*, 13(5):A59, March 2010. ISSN 1944-8775. doi: 10.1149/1.3329652. URL `https://iopscience.iop.org/article/10.1149/1.3329652/meta`. Publisher: IOP Publishing.

[70] Longtao Ma, Shengmei Chen, Hongfei Li, Zhaoheng Ruan, Zijie Tang, Zhuoxin Liu, Zifeng Wang, Yan Huang, Zengxia Pei, Juan Antonio Zapien, and Chunyi Zhi. Initiating a mild aqueous electrolyte Co3O4/Zn battery with 2.2 V-high voltage and 5000-cycle lifespan by a Co(III) rich-electrode. *Energy & Environmental Science*, 11(9):2521–2530, September 2018. ISSN 1754-5706. doi: 10.1039/C8EE01415A. URL `https://pubs.rsc.org/en/content/articlelanding/2018/ee/c8ee01415a`. Publisher: The Royal Society of Chemistry.

[71] Yuko Yokoyama, Tomokazu Fukutsuka, Kohei Miyazaki, and Takeshi Abe. Origin of the Electrochemical Stability of Aqueous Concentrated Electrolyte Solutions. *Journal of The Electrochemical Society*, 165(14):A3299, October 2018. ISSN 1945-7111. doi: 10.1149/2.0491814jes. URL `https://iopscience.iop.org/article/10.1149/2.0491814jes/meta`. Publisher: IOP Publishing.

[72] Yun-Zhao Wu, Yong Ding, Tasawar Hayat, Ahmed Alsaedi, and Song-Yuan Dai. Enlarged working potential window for MnO2 supercapacitors with neutral aqueous electrolytes. *Applied Surface Science*, 459:430–437, November 2018. ISSN 0169-4332. doi: 10.1016/j.apsusc.2018.07.147. URL `http://www.sciencedirect.com/science/article/pii/S0169433218320439`.

[73] David Reber, Ruben-Simon Kühnel, and Corsin Battaglia. High-voltage aqueous supercapacitors based on NaTFSI. *Sustainable Energy & Fuels*, 1(10):2155–2161, 2017. doi: 10.1039/C7SE00423K. URL `https://pubs.rsc.org/en/content/articlelanding/2017/se/c7se00423k`. Publisher: Royal Society of Chemistry.

[74] Hui Xia, Ying Shirley Meng, Guoliang Yuan, Chong Cui, and Li Lu. A Symmetric RuO2/RuO2 Supercapacitor Operating at 1.6 V by Using a Neutral Aqueous Electrolyte. *Electrochemical and Solid State Letters*, 15(4):A60, February 2012. ISSN 1944-8775. doi: 10.1149/2.023204esl. URL `https://iopscience.iop.org/article/10.1149/2.023204esl/meta`. Publisher: IOP Publishing.

[75] Etienne Le Calvez, Sethuraman Sathyamoorthi, Nutthaphon Phattharasupakun, Sangchai Sarawutanukal, and Montree Sawangphruk. High cell-potential and high-rate neutral aqueous supercapacitors using activated biocarbon: In situ electrochemical gas chromatography. *Electrochimica Acta*, 313:31–40, August 2019. ISSN 0013-4686. doi: 10.1016/j.electacta.2019.05.035. URL `http://www.sciencedirect.com/science/article/pii/S0013468619309454`.

[76] Liumin Suo, Oleg Borodin, Yuesheng Wang, Xiaohui Rong, Wei Sun, Xiiulin Fan, Shuyin Xu, Marshall A. Schroeder, Arthur V. Cresce, Fei Wang, Chongyin Yang, Yong-Sheng Hu, Kang Xu, and Chunsheng Wang. “Water-in-Salt” Electrolyte Makes Aqueous Sodium-Ion Battery Safe, Green, and Long-Lasting. *Advanced Energy Materials*, 7(21):1701189, 2017. ISSN 1614-6840. doi: 10.1002/aenm.201701189. URL `https://onlinelibrary.wiley.com/doi/abs/10.1002/aenm.201701189`. _eprint: https://onlinelibrary.wiley.com/doi/pdf/10.1002/aenm.201701189.

[77] Liwei Jiang, Lilu Liu, Jinming Yue, Qiangqiang Zhang, Anxing Zhou, Oleg Borodin, Liumin Suo, Hong Li, Liquan Chen, Kang Xu, and Yong-Sheng Hu. High-Voltage Aqueous Na-Ion Battery Enabled by Inert-Cation-Assisted Water-in-Salt Electrolyte. *Advanced Materials*, 32

(2):1904427, 2020. ISSN 1521-4095. doi: 10.1002/adma.201904427. URL https://onlinelibrary.wiley.com/doi/abs/10.1002/adma.201904427. _eprint: https://onlinelibrary.wiley.com/doi/pdf/10.1002/adma.201904427.

[78] Daniel P. Leonard, Zhixuan Wei, Gang Chen, Fei Du, and Xiulei Ji. Water-in-Salt Electrolyte for Potassium-Ion Batteries. *ACS Energy Letters*, 3(2):373–374, February 2018. doi: 10.1021/acsenergylett.8b00009. URL https://doi.org/10.1021/acsenergylett.8b00009. Publisher: American Chemical Society.

[79] Shengying Cai, Tianwen Bai, Hao Chen, Wenzhang Fang, Zhen Xu, Haiwen Lai, Tieqi Huang, Hanyan Xu, Xingyuan Chu, Jun Ling, and Chao Gao. Heavy Water Enables High-Voltage Aqueous Electrochemistry via the Deuterium Isotope Effect. *The Journal of Physical Chemistry Letters*, 11(1):303–310, January 2020. doi: 10.1021/acs.jpclett.9b03267. URL https://doi.org/10.1021/acs.jpclett.9b03267. Publisher: American Chemical Society.

[80] Jignasa N. Solanki and Zagabathuni Venkata Panchakshari Murthy. Controlled Size Silver Nanoparticles Synthesis with Water-in-Oil Microemulsion Method: A Topical Review. *Industrial & Engineering Chemistry Research*, 50(22):12311–12323, November 2011. ISSN 0888-5885. doi: 10.1021/ie201649x. URL https://doi.org/10.1021/ie201649x. Publisher: American Chemical Society.

[81] James F. Rusling, Thomas F. Connors, and Azita. Owlia. Electrocatalytic reduction of ethylene dibromide by vitamin B12 in a surfactant-stabilized emulsion. *Analytical Chemistry*, 59(17):2123–2127, September 1987. ISSN 0003-2700, 1520-6882. doi: 10.1021/ac00144a025. URL https://pubs.acs.org/doi/abs/10.1021/ac00144a025.

[82] M. O. Iwunze, A. Sucheta, and J. F. Rusling. Bicontinuous microemulsions as media for electrochemical studies. *Analytical Chemistry*, 62(6):644–649, March 1990. ISSN 0003-2700. doi: 10.1021/ac00205a021.

[83] James F. Rusling. Green synthesis via electrolysis in microemulsions. *Pure and Applied Chemistry*, 73(12):1895–1905, January 2001. ISSN 0033-4545, 1365-3075. doi: 10.1351/pac200173121895. URL https://www.degruyter.com/view/journals/pac/73/12/article-p1895.xml. Publisher: De Gruyter Section: Pure and Applied Chemistry.

[84] De-ling Zhou, Jianxin Gao, and James F. Rusling. Kinetic Control of Reactions of Electrogenerated Co(I) Macrocycles with Alkyl Bromides in a Bicontinuous Microemulsion. *Journal of the American Chemical Society*, 117(3): 1127–1134, January 1995. ISSN 0002-7863. doi: 10.1021/ja00108a032. URL `https://pubs.acs.org/doi/abs/10.1021/ja00108a032`.

[85] Shiping Zhang and James F. Rusling. Dechlorination of polychlorinated biphenyls by electrochemical catalysis in a bicontinuous microemulsion. *Environmental Science & Technology*, 27(7):1375–1380, July 1993. ISSN 0013-936X, 1520-5851. doi: 10.1021/es00044a012. URL `https://pubs.acs.org/doi/abs/10.1021/es00044a012`.

[86] Shiping. Zhang and James F. Rusling. Dechlorination of Polychlorinated Biphenyls on Soils and Clay by Electrolysis in a Bicontinuous Microemulsion. *Environmental Science & Technology*, 29(5):1195–1199, May 1995. ISSN 0013-936X, 1520-5851. doi: 10.1021/es00005a009. URL `https://pubs.acs.org/doi/abs/10.1021/es00005a009`.

[87] Jianxin Gao and James F. Rusling. Electrochemical Catalysis of a 5-Endo-Trig Cyclization in Bicontinuous Microemulsions. *The Journal of Organic Chemistry*, 63(2):218–219, January 1998. ISSN 0022-3263. doi: 10.1021/jo971897u. URL `https://doi.org/10.1021/jo971897u`. Publisher: American Chemical Society.

[88] Geoffrey N. Kamau, Naifei Hu, and James F. Rusling. Rate enhancement and control in electrochemical catalysis using a bicontinuous microemulsion. *Langmuir*, 8 (4):1042–1044, April 1992. ISSN 0743-7463, 1520-5827. doi: 10.1021/la00040a004. URL `https://pubs.acs.org/doi/abs/10.1021/la00040a004`.

[89] Shinya Yoshitake, Akihiro Ohira, Masato Tominaga, Taisei Nishimi, Masayo Sakata, Chuichi Hirayama, and Masashi Kunitake. Electrochemistry in Middle Phase Microemulsion Composed of Saline and Toluene with Sodium Dodecylsulfate and n-Butanol. *Chemistry Letters*, 31(3):360–361, March 2002. ISSN 0366-7022. doi: 10.1246/cl.2002.360. URL `https://www.journal.csj.jp/doi/abs/10.1246/cl.2002.360`. Publisher: The Chemical Society of Japan.

[90] Jing Peng, Nelly M. Cantillo, K. McKensie Nelms, Lacey S. Roberts, Gabriel Goenaga, Adam Imel, Brian Andrew Barth, Mark Dadmun, Luke Heroux, Douglas G. Hayes, and Thomas Zawodzinski. Electron Transfer in Microemulsion-Based Electrolytes. *ACS Applied Materials & Interfaces*, 12(36):40213–40219, September 2020. ISSN 1944-8244. doi: 10.1021/acsami.0c07028. URL https://doi.org/10.1021/acsami.0c07028. Publisher: American Chemical Society.

[91] I. M. Kolthoff and Y. Okinaka. Effects of Surface Active Substances on Polarographic Waves of Copper(II) Ions [1]. *Journal of the American Chemical Society*, 81 (10):2296–2302, May 1959. ISSN 0002-7863, 1520-5126. doi: 10.1021/ja01519a004. URL https://pubs.acs.org/doi/abs/10.1021/ja01519a004.

[92] Zhiguo Hou, Xueqian Zhang, Xiaona Li, Yongchun Zhu, Jianwen Liang, and Yitai Qian. Surfactant widens the electrochemical window of an aqueous electrolyte for better rechargeable aqueous sodium/zinc battery. *Journal of Materials Chemistry A*, 5(2):730–738, 2017. doi: 10.1039/C6TA08736A. URL https://pubs.rsc.org/en/content/articlelanding/2017/ta/c6ta08736a. Publisher: Royal Society of Chemistry.

[93] Rohan Borah, Thomas Nann, and Fraser Ross Hughson. Electrolyte Compositions, June 2020. URL https://patentscope.wipo.int/search/en/detail.jsf?docId=WO2020130857&tab=PCTBIBLIO.

[94] Chaofeng Liu, Zachary G. Neale, and Guozhong Cao. Understanding electrochemical potentials of cathode materials in rechargeable batteries. *Materials Today*, 19(2):109–123, March 2016. ISSN 1369-7021. doi: 10.1016/j.mattod.2015.10.009. URL http://www.sciencedirect.com/science/article/pii/S1369702115003181.

[95] F. M. Menger and A. R. Elrington. Organic reactivity in microemulsion systems. *Journal of the American Chemical Society*, 113(25):9621–9624, December 1991. ISSN 0002-7863. doi: 10.1021/ja00025a030. URL https://doi.org/10.1021/ja00025a030. Publisher: American Chemical Society.

[96] Junjie Huang and Zhiyu Jiang. The preparation and characterization of Li4Ti5O12/carbon nano-tubes for lithium ion battery. *Electrochimica Acta*, 53 (26):7756–7759, November 2008. ISSN 0013-4686. doi: 10.1016/j.electacta.

2008.05.031. URL http://www.sciencedirect.com/science/article/pii/S0013468608006865.

[97] E. Senthilkumar, V. Sivasankar, B. Ravindra Kohakade, K. Thileepkumar, M. Ramya, G. Sivagaami Sundari, S. Raghu, and R. A. Kalaivani. Synthesis of nanoporous graphene and their electrochemical performance in a symmetric supercapacitor. *Applied Surface Science*, 460:17–24, December 2018. ISSN 0169-4332. doi: 10.1016/j.apsusc.2017.10.221. URL http://www.sciencedirect.com/science/article/pii/S0169433217331975.

[98] Patrice Simon and Yury Gogotsi. Materials for electrochemical capacitors. *Nature Materials*, 7(11):845–854, November 2008. ISSN 1476-4660. doi: 10.1038/nmat2297. URL https://www.nature.com/articles/nmat2297. Number: 11 Publisher: Nature Publishing Group.

[99] Sun Wen, Joon-Woo Lee, In-Hyeong Yeo, Jongman Park, and Sun-il Mho. The role of cations of the electrolyte for the pseudocapacitive behavior of metal oxide electrodes, MnO2 and RuO2. *Electrochimica Acta*, 50(2):849–855, November 2004. ISSN 0013-4686. doi: 10.1016/j.electacta.2004.02.056. URL http://www.sciencedirect.com/science/article/pii/S0013468604006711.

[100] Megan B. Sassin, Christopher N. Chervin, Debra R. Rolison, and Jeffrey W. Long. Redox Deposition of Nanoscale Metal Oxides on Carbon for Next-Generation Electrochemical Capacitors. *Accounts of Chemical Research*, 46(5):1062–1074, May 2013. ISSN 0001-4842. doi: 10.1021/ar2002717. URL https://doi.org/10.1021/ar2002717. Publisher: American Chemical Society.

[101] Hyeon Jeong Lee, Ji Hoon Lee, Sung-Yoon Chung, and Jang Wook Choi. Enhanced Pseudocapacitance in Multicomponent Transition-Metal Oxides by Local Distortion of Oxygen Octahedra. *Angewandte Chemie International Edition*, 55(12):3958–3962, 2016. ISSN 1521-3773. doi: https://doi.org/10.1002/anie.201511452. URL https://onlinelibrary.wiley.com/doi/abs/10.1002/anie.201511452. _eprint: https://onlinelibrary.wiley.com/doi/pdf/10.1002/anie.201511452.

[102] Hiroyuki Itoi, Hirotomo Nishihara, Takafumi Ishii, Khanin Nueangnoraj, Raúl Berenguer-Betrián, and Takashi Kyotani. Large Pseudocapacitance in Quinone-Functionalized Zeolite-Templated Carbon. *Bulletin of the Chemical Society*

of Japan, 87(2):250–257, November 2013. ISSN 0009-2673. doi: 10.1246/bcsj.20130292. URL https://www.journal.csj.jp/doi/abs/10.1246/bcsj.20130292. Publisher: The Chemical Society of Japan.

[103] Daniela M. Anjos, John K. McDonough, Emilie Perre, Gilbert M. Brown, Steven H. Overbury, Yury Gogotsi, and Volker Presser. Pseudocapacitance and performance stability of quinone-coated carbon onions. *Nano Energy*, 2(5):702–712, September 2013. ISSN 2211-2855. doi: 10.1016/j.nanoen.2013.08.003. URL http://www.sciencedirect.com/science/article/pii/S2211285513001432.

[104] Catherine R. DeBlase, Katharine E. Silberstein, Thanh-Tam Truong, Héctor D. Abruña, and William R. Dichtel. β-Ketoenamine-Linked Covalent Organic Frameworks Capable of Pseudocapacitive Energy Storage. *Journal of the American Chemical Society*, 135(45):16821–16824, November 2013. ISSN 0002-7863. doi: 10.1021/ja409421d. URL https://doi.org/10.1021/ja409421d. Publisher: American Chemical Society.

[105] John Wang, Julien Polleux, James Lim, and Bruce Dunn. Pseudocapacitive Contributions to Electrochemical Energy Storage in TiO2 (Anatase) Nanoparticles. *The Journal of Physical Chemistry C*, 111(40):14925–14931, October 2007. ISSN 1932-7447. doi: 10.1021/jp074464w. URL https://doi.org/10.1021/jp074464w. Publisher: American Chemical Society.

[106] Kyung-Wan Nam, Chang-Wook Lee, Xiao-Qing Yang, Byung Won Cho, Won-Sub Yoon, and Kwang-Bum Kim. Electrodeposited manganese oxides on three-dimensional carbon nanotube substrate: Supercapacitive behaviour in aqueous and organic electrolytes. *Journal of Power Sources*, 188(1):323–331, March 2009. ISSN 0378-7753. doi: 10.1016/j.jpowsour.2008.11.133. URL http://www.sciencedirect.com/science/article/pii/S0378775308022805.

[107] Yu Huang, Yuanyuan Li, Zuoqi Hu, Guangming Wei, Junling Guo, and Jinping Liu. A carbon modified MnO 2 nanosheet array as a stable high-capacitance supercapacitor electrode. *Journal of Materials Chemistry A*, 1(34):9809–9813, 2013. doi: 10.1039/C3TA12148H. URL https://pubs.rsc.org/en/content/articlelanding/2013/ta/c3ta12148h. Publisher: Royal Society of Chemistry.

[108] Chaoji Chen, Ying Zhang, Yiju Li, Jiaqi Dai, Jianwei Song, Yonggang Yao, Yunhui Gong, Iain Kierzewski, Jia Xie, and Liangbing Hu. All-wood, low tortuosity, aqueous, biodegradable supercapacitors with ultra-high capacitance. *Energy & Environmental Science*, 10(2):538–545, 2017. doi: 10.1039/C6EE03716J. URL https://pubs.rsc.org/en/content/articlelanding/2017/ee/c6ee03716j. Publisher: Royal Society of Chemistry.

[109] Dennis Sheberla, John C. Bachman, Joseph S. Elias, Cheng-Jun Sun, Yang Shao-Horn, and Mircea Dincă. Conductive MOF electrodes for stable supercapacitors with high areal capacitance. *Nature Materials*, 16(2):220–224, February 2017. ISSN 1476-4660. doi: 10.1038/nmat4766. URL https://www.nature.com/articles/nmat4766. Number: 2 Publisher: Nature Publishing Group.

[110] Kay Hyeok An, Kwan Ku Jeon, Jeong Ku Heo, Seong Chu Lim, Dong Jae Bae, and Young Hee Lee. High-Capacitance Supercapacitor Using a Nanocomposite Electrode of Single-Walled Carbon Nanotube and Polypyrrole. *Journal of the Electrochemical Society*, 149(8):A1058, June 2002. ISSN 1945-7111. doi: 10.1149/1.1491235. URL https://iopscience.iop.org/article/10.1149/1.1491235/meta. Publisher: IOP Publishing.

[111] D. Weingarth, A. Foelske-Schmitz, and R. Kötz. Cycle versus voltage hold – Which is the better stability test for electrochemical double layer capacitors? *Journal of Power Sources*, 225:84–88, March 2013. ISSN 0378-7753. doi: 10.1016/j.jpowsour.2012.10.019. URL http://www.sciencedirect.com/science/article/pii/S0378775312015741.

[112] Jinwei Xu, Caihong Jia, Bin Cao, and W. F. Zhang. Electrochemical properties of anatase TiO2 nanotubes as an anode material for lithium-ion batteries. *Electrochimica Acta*, 52(28):8044–8047, November 2007. ISSN 0013-4686. doi: 10.1016/j.electacta.2007.06.077. URL http://www.sciencedirect.com/science/article/pii/S0013468607008614.

[113] Na Li, Gang Liu, Chao Zhen, Feng Li, Lili Zhang, and Hui-Ming Cheng. Battery Performance and Photocatalytic Activity of Mesoporous Anatase TiO2 Nanospheres/Graphene Composites by Template-Free Self-Assembly. *Advanced Functional Materials*, 21(9):1717–1722, 2011. ISSN 1616-3028. doi: https://doi.org/10.1002/adfm.201002295. URL

https://onlinelibrary.wiley.com/doi/abs/10.1002/adfm.201002295. _eprint: https://onlinelibrary.wiley.com/doi/pdf/10.1002/adfm.201002295.

[114] Shu-Juan Bao, Qiao-Liang Bao, Chang-Ming Li, and Zhi-Li Dong. Novel porous anatase TiO2 nanorods and their high lithium electroactivity. *Electrochemistry Communications*, 9(5):1233–1238, May 2007. ISSN 1388-2481. doi: 10.1016/j.elecom.2007.01.028. URL http://www.sciencedirect.com/science/article/pii/S1388248107000318.

[115] An-Min Cao, Jin-Song Hu, Han-Pu Liang, and Li-Jun Wan. Self-Assembled Vanadium Pentoxide (V2O5) Hollow Microspheres from Nanorods and Their Application in Lithium-Ion Batteries. *Angewandte Chemie International Edition*, 44(28): 4391–4395, 2005. ISSN 1521-3773. doi: https://doi.org/10.1002/anie.200500946. URL https://onlinelibrary.wiley.com/doi/abs/10.1002/anie.200500946. _eprint: https://onlinelibrary.wiley.com/doi/pdf/10.1002/anie.200500946.

[116] Xiao-Fei Zhang, Kai-Xue Wang, Xiao Wei, and Jie-Sheng Chen. Carbon-Coated V2O5 Nanocrystals as High Performance Cathode Material for Lithium Ion Batteries. *Chemistry of Materials*, 23(24):5290–5292, December 2011. ISSN 0897-4756. doi: 10.1021/cm202812z. URL https://doi.org/10.1021/cm202812z. Publisher: American Chemical Society.

[117] Jun Liu, Hui Xia, Dongfeng Xue, and Li Lu. Double-Shelled Nanocapsules of V2O5-Based Composites as High-Performance Anode and Cathode Materials for Li Ion Batteries. *Journal of the American Chemical Society*, 131(34):12086–12087, September 2009. ISSN 0002-7863. doi: 10.1021/ja9053256. URL https://doi.org/10.1021/ja9053256. Publisher: American Chemical Society.

[118] S. H. Ng, S. Y. Chew, J. Wang, D. Wexler, Y. Tournayre, K. Konstantinov, and H. K. Liu. Synthesis and electrochemical properties of V2O5 nanostructures prepared via a precipitation process for lithium-ion battery cathodes. *Journal of Power Sources*, 174(2):1032–1035, December 2007. ISSN 0378-7753. doi: 10.1016/j.jpowsour.2007.06.166. URL http://www.sciencedirect.com/science/article/pii/S0378775307013080.

[119] Amin Sutjianto and Larry A. Curtiss. Li+Diglyme Complexes: Barriers to Lithium Cation Migration. *The Journal of Physical Chemistry A*, 102(6):968–974, February

1998. ISSN 1089-5639. doi: 10.1021/jp972164g. URL https://doi.org/10.1021/jp972164g. Publisher: American Chemical Society.

[120] Martin Winter, Petr Novák, and Alain Monnier. Graphites for Lithium-Ion Cells: The Correlation of the First-Cycle Charge Loss with the Brunauer-Emmett-Teller Surface Area. *Journal of the Electrochemical Society*, 145(2):428, February 1998. ISSN 1945-7111. doi: 10.1149/1.1838281. URL https://iopscience.iop.org/article/10.1149/1.1838281/meta. Publisher: IOP Publishing.

[121] Laurence J. Hardwick, Patrick W. Ruch, Matthias Hahn, Werner Scheifele, Rüdiger Kötz, and Petr Novák. In situ Raman spectroscopy of insertion electrodes for lithium-ion batteries and supercapacitors: First cycle effects. *Journal of Physics and Chemistry of Solids*, 69(5):1232–1237, May 2008. ISSN 0022-3697. doi: 10.1016/j.jpcs.2007.10.017. URL http://www.sciencedirect.com/science/article/pii/S002236970700594X.

[122] Stefan Seidlmayer, Irmgard Buchberger, Markus Reiner, Thomas Gigl, Ralph Gilles, Hubert A. Gasteiger, and Christoph Hugenschmidt. First-cycle defect evolution of Li1xNi1/3Mn1/3Co1/3O2 lithium ion battery electrodes investigated by positron annihilation spectroscopy. *Journal of Power Sources*, 336:224–230, December 2016. ISSN 0378-7753. doi: 10.1016/j.jpowsour.2016.10.050. URL http://www.sciencedirect.com/science/article/pii/S0378775316314422.

[123] Yun-Hai Zhu, Qi Zhang, Xu Yang, En-Yue Zhao, Tao Sun, Xin-Bo Zhang, Sai Wang, Xi-Qian Yu, Jun-Min Yan, and Qing Jiang. Reconstructed Orthorhombic V2O5 Polyhedra for Fast Ion Diffusion in K-Ion Batteries. *Chem*, 5(1):168–179, January 2019. ISSN 2451-9294. doi: 10.1016/j.chempr.2018.10.004. URL http://www.sciencedirect.com/science/article/pii/S2451929418304844.

[124] Jiwei Ma, Wei Li, Benjamin J. Morgan, Jolanta Światowska, Rita Baddour-Hadjean, Monique Body, Christophe Legein, Olaf J. Borkiewicz, Sandrine Leclerc, Henri Groult, Frédéric Lantelme, Christel Laberty-Robert, and Damien Dambournet. Lithium Intercalation in Anatase Titanium Vacancies and the Role of Local Anionic Environment. *Chemistry of Materials*, 30(9):3078–3089, May 2018. ISSN 0897-4756. doi: 10.1021/acs.chemmater.8b00925. URL https://doi.org/10.1021/acs.chemmater.8b00925. Publisher: American Chemical Society.

[125] Sven Södergren, Hans Siegbahn, Håkan Rensmo, Henrik Lindström, Anders Hagfeldt, and Sten-Eric Lindquist. Lithium Intercalation in Nanoporous Anatase TiO2 Studied with XPS. *The Journal of Physical Chemistry B*, 101(16):3087–3090, April 1997. ISSN 1520-6106. doi: 10.1021/jp9639399. URL `https://doi.org/10.1021/jp9639399`. Publisher: American Chemical Society.

[126] Yu Ren, Laurence J. Hardwick, and Peter G. Bruce. Lithium Intercalation into Mesoporous Anatase with an Ordered 3D Pore Structure. *Angewandte Chemie International Edition*, 49(14):2570–2574, 2010. ISSN 1521-3773. doi: https://doi.org/10.1002/anie.200907099. URL `https://onlinelibrary.wiley.com/doi/abs/10.1002/anie.200907099`. _eprint: https://onlinelibrary.wiley.com/doi/pdf/10.1002/anie.200907099.

[127] Ekaterina Pomerantseva, Konstantinos Gerasopoulos, Xinyi Chen, Gary Rubloff, and Reza Ghodssi. Electrochemical performance of the nanostructured biotemplated V2O5 cathode for lithium-ion batteries. *Journal of Power Sources*, 206: 282–287, May 2012. ISSN 0378-7753. doi: 10.1016/j.jpowsour.2012.01.127. URL `http://www.sciencedirect.com/science/article/pii/S0378775312002303`.

[128] Yang Yang, Lei Li, Huilong Fei, Zhiwei Peng, Gedeng Ruan, and James M. Tour. Graphene Nanoribbon/V2O5 Cathodes in Lithium-Ion Batteries. *ACS Applied Materials & Interfaces*, 6(12):9590–9594, June 2014. ISSN 1944-8244. doi: 10.1021/am501969m. URL `https://doi.org/10.1021/am501969m`. Publisher: American Chemical Society.

[129] Jie Shao, Xinyong Li, Zhongming Wan, Longfei Zhang, Yuanlei Ding, Li Zhang, Qunting Qu, and Honghe Zheng. Low-Cost Synthesis of Hierarchical V2O5 Microspheres as High-Performance Cathode for Lithium-Ion Batteries. *ACS Applied Materials & Interfaces*, 5(16):7671–7675, August 2013. ISSN 1944-8244. doi: 10.1021/am401854v. URL `https://doi.org/10.1021/am401854v`. Publisher: American Chemical Society.

[130] Huali Wang, Ying Bai, Shi Chen, Xiangyi Luo, Chuan Wu, Feng Wu, Jun Lu, and Khalil Amine. Binder-Free V2O5 Cathode for Greener Rechargeable Aluminum Battery. *ACS Applied Materials & Interfaces*, 7(1):80–84, January 2015. ISSN 1944-8244. doi: 10.1021/am508001h. URL `https://doi.org/10.1021/am508001h`. Publisher: American Chemical Society.

[131] Yu Ren, Zheng Liu, Frédérique Pourpoint, A. Robert Armstrong, Clare P. Grey, and Peter G. Bruce. Nanoparticulate TiO2(B): An Anode for Lithium-Ion Batteries. *Angewandte Chemie*, 124(9):2206–2209, 2012. ISSN 1521-3757. doi: https://doi.org/10.1002/ange.201108300. URL https://onlinelibrary.wiley.com/doi/abs/10.1002/ange.201108300. _eprint: https://onlinelibrary.wiley.com/doi/pdf/10.1002/ange.201108300.

[132] D. A. Stevens and J. R. Dahn. High Capacity Anode Materials for Rechargeable Sodium-Ion Batteries. *Journal of The Electrochemical Society*, 147(4):1271, April 2000. ISSN 1945-7111. doi: 10.1149/1.1393348. URL https://iopscience.iop.org/article/10.1149/1.1393348/meta. Publisher: IOP Publishing.

[133] Marca M. Doeff, Jordi Cabana, and Mona Shirpour. Titanate Anodes for Sodium Ion Batteries. *Journal of Inorganic and Organometallic Polymers and Materials*, 24(1):5–14, January 2014. ISSN 1574-1451. doi: 10.1007/s10904-013-9977-8. URL https://doi.org/10.1007/s10904-013-9977-8.

[134] Yan Zhang, Hongshuai Hou, Xuming Yang, Jun Chen, Mingjun Jing, Zhibin Wu, Xinnan Jia, and Xiaobo Ji. Sodium titanate cuboid as advanced anode material for sodium ion batteries. *Journal of Power Sources*, 305:200–208, February 2016. ISSN 0378-7753. doi: 10.1016/j.jpowsour.2015.11.101. URL http://www.sciencedirect.com/science/article/pii/S0378775315305991.

[135] Ananta Sarkar, C. V. Manohar, and Sagar Mitra. A simple approach to minimize the first cycle irreversible loss of sodium titanate anode towards the development of sodium-ion battery. *Nano Energy*, 70:104520, April 2020. ISSN 2211-2855. doi: 10.1016/j.nanoen.2020.104520. URL http://www.sciencedirect.com/science/article/pii/S221128552030077X.

[136] Xuefeng Wang, Yejing Li, Yurui Gao, Zhaoxiang Wang, and Liquan Chen. Additive-free sodium titanate nanotube array as advanced electrode for sodium ion batteries. *Nano Energy*, 13:687–692, April 2015. ISSN 2211-2855. doi: 10.1016/j.nanoen.2015.03.029. URL http://www.sciencedirect.com/science/article/pii/S2211285515001251.

[137] Zichao Yan, Li Liu, Hongbo Shu, Xiukang Yang, Hao Wang, Jinli Tan, Qian Zhou, Zhifeng Huang, and Xianyou Wang. A tightly integrated sodium titanate-carbon composite as an anode material for rechargeable sodium ion batteries. *Journal of Power Sources*, 274:8–14, January 2015. ISSN 0378-7753. doi: 10.1016/j.jpowsour.2014.10.045. URL `http://www.sciencedirect.com/science/article/pii/S0378775314016541`.

[138] Xiaofei Bie, Kei Kubota, Tomooki Hosaka, Kuniko Chihara, and Shinichi Komaba. Synthesis and electrochemical properties of Na-rich Prussian blue analogues containing Mn, Fe, Co, and Fe for Na-ion batteries. *Journal of Power Sources*, 378:322–330, February 2018. ISSN 0378-7753. doi: 10.1016/j.jpowsour.2017.12.052. URL `http://www.sciencedirect.com/science/article/pii/S0378775317316609`.

[139] Yuhao Lu, Long Wang, Jinguang Cheng, and John B. Goodenough. Prussian blue: a new framework of electrode materials for sodium batteries. *Chemical Communications*, 48(52):6544–6546, 2012. doi: 10.1039/C2CC31777J. URL `https://pubs.rsc.org/en/content/articlelanding/2012/cc/c2cc31777j`. Publisher: Royal Society of Chemistry.

[140] Yanfeng Yue, Andrew J. Binder, Bingkun Guo, Zhiyong Zhang, Zhen-An Qiao, Chengcheng Tian, and Sheng Dai. Mesoporous Prussian Blue Analogues: Template-Free Synthesis and Sodium-Ion Battery Applications. *Angewandte Chemie International Edition*, 53(12):3134–3137, 2014. ISSN 1521-3773. doi: https://doi.org/10.1002/anie.201310679. URL `https://onlinelibrary.wiley.com/doi/abs/10.1002/anie.201310679`. _eprint: https://onlinelibrary.wiley.com/doi/pdf/10.1002/anie.201310679.

[141] Feng Ma, Qing Li, Tanyuan Wang, Hanguang Zhang, and Gang Wu. Energy storage materials derived from Prussian blue analogues. *Science Bulletin*, 62(5):358–368, March 2017. ISSN 2095-9273. doi: 10.1016/j.scib.2017.01.030. URL `http://www.sciencedirect.com/science/article/pii/S2095927317300488`.

[142] Ya You, Xing-Long Wu, Ya-Xia Yin, and Yu-Guo Guo. High-quality Prussian blue crystals as superior cathode materials for room-temperature sodium-ion batteries. *Energy & Environmental Science*, 7(5):1643–1647, 2014. doi: 10.1039/

C3EE44004D. URL https://pubs.rsc.org/en/content/articlelanding/2014/ee/c3ee44004d. Publisher: Royal Society of Chemistry.

[143] Xiao Tang, Hao Liu, Dawei Su, Peter H. L. Notten, and Guoxiu Wang. Hierarchical sodium-rich Prussian blue hollow nanospheres as high-performance cathode for sodium-ion batteries. *Nano Research*, 11(8):3979–3990, August 2018. ISSN 1998-0000. doi: 10.1007/s12274-018-1979-y. URL https://doi.org/10.1007/s12274-018-1979-y.

[144] Changxiu Yan, Along Zhao, Faping Zhong, Xiangming Feng, Weihua Chen, Jiangfeng Qian, Xinping Ai, Hanxi Yang, and Yuliang Cao. A low-defect and Na-enriched Prussian blue lattice with ultralong cycle life for sodium-ion battery cathode. *Electrochimica Acta*, 332:135533, February 2020. ISSN 0013-4686. doi: 10.1016/j.electacta.2019.135533. URL http://www.sciencedirect.com/science/article/pii/S0013468619324053.

[145] Jun John Xu, Andrew J. Kinser, Boone B. Owens, and William H. Smyrl. Amorphous Manganese Dioxide: A High Capacity Lithium Intercalation Host. *Electrochemical and Solid-State Letters*, 1(1):1, July 1998. ISSN 1944-8775. doi: 10.1149/1.1390615. URL https://iopscience.iop.org/article/10.1149/1.1390615/meta. Publisher: IOP Publishing.

[146] Pier Paolo Prosini, Marida Lisi, Silvera Scaccia, Maria Carewska, Francesco Cardellini, and Mauro Pasquali. Synthesis and Characterization of Amorphous Hydrated FePO4 and Its Electrode Performance in Lithium Batteries. *Journal of the Electrochemical Society*, 149(3):A297, January 2002. ISSN 1945-7111. doi: 10.1149/1.1435359. URL https://iopscience.iop.org/article/10.1149/1.1435359/meta. Publisher: IOP Publishing.

[147] Hui Xiong, Handan Yildirim, Elena V. Shevchenko, Vitali B. Prakapenka, Bonil Koo, Michael D. Slater, Mahalingam Balasubramanian, Subramanian K. R. S. Sankaranarayanan, Jeffrey P. Greeley, Sanja Tepavcevic, Nada M. Dimitrijevic, Paul Podsiadlo, Christopher S. Johnson, and Tijana Rajh. Self-Improving Anode for Lithium-Ion Batteries Based on Amorphous to Cubic Phase Transition in TiO2 Nanotubes. *The Journal of Physical Chemistry C*, 116(4):3181–3187, February 2012. ISSN 1932-7447. doi: 10.1021/jp210793u. URL https://doi.org/10.1021/jp210793u. Publisher: American Chemical Society.

[148] R. A. Zárate, S. Fuentes, J. P. Wiff, V. M. Fuenzalida, and A. L. Cabrera. Chemical composition and phase identification of sodium titanate nanostructures grown from titania by hydrothermal processing. *Journal of Physics and Chemistry of Solids*, 68(4):628–637, April 2007. ISSN 0022-3697. doi: 10.1016/j.jpcs.2007.02.011. URL `http://www.sciencedirect.com/science/article/pii/S0022369707000777`.

[149] Yinzhu Jiang, Shenglan Yu, Baoqi Wang, Yong Li, Wenping Sun, Yunhao Lu, Mi Yan, Bin Song, and Shixue Dou. Prussian Blue@C Composite as an Ultrahigh-Rate and Long-Life Sodium-Ion Battery Cathode. *Advanced Functional Materials*, 26(29):5315–5321, 2016. ISSN 1616-3028. doi: https://doi.org/10.1002/adfm.201600747. URL `https://onlinelibrary.wiley.com/doi/abs/10.1002/adfm.201600747`. _eprint: https://onlinelibrary.wiley.com/doi/pdf/10.1002/adfm.201600747.

[150] Dezhi Yang, Jing Xu, Xiao-Zhen Liao, Hong Wang, Yu-Shi He, and Zi-Feng Ma. Prussian blue without coordinated water as a superior cathode for sodium-ion batteries. *Chemical Communications*, 51(38):8181–8184, 2015. doi: 10.1039/C5CC01180A. URL `https://pubs.rsc.org/en/content/articlelanding/2015/cc/c5cc01180a`. Publisher: Royal Society of Chemistry.

[151] Dezhi Yang, Jing Xu, Xiao-Zhen Liao, Yu-Shi He, Haimei Liu, and Zi-Feng Ma. Structure optimization of Prussian blue analogue cathode materials for advanced sodium ion batteries. *Chemical Communications*, 50(87):13377–13380, 2014. doi: 10.1039/C4CC05830E. URL `https://pubs.rsc.org/en/content/articlelanding/2014/cc/c4cc05830e`. Publisher: Royal Society of Chemistry.

[152] Hang Hu, Weifang Liu, Maolan Zhu, Yisheng Lin, Ying Liu, Jianwen Zhang, Tao Chen, and Kaiyu Liu. Yolk-shell Prussian blue nanoparticles with fast ion diffusion for sodium-ion battery. *Materials Letters*, 249:206–209, August 2019. ISSN 0167-577X. doi: 10.1016/j.matlet.2019.04.102. URL `http://www.sciencedirect.com/science/article/pii/S0167577X19306652`.

[153] Xianyong Wu, Daniel P. Leonard, and Xiulei Ji. Emerging Non-Aqueous Potassium-Ion Batteries: Challenges and Opportunities. *Chemistry of Materials*, 29(12):5031–5042, June 2017. ISSN 0897-4756. doi: 10.1021/acs.chemmater.7b01764. URL `https://doi.org/10.1021/acs.chemmater.7b01764`. Publisher: American Chemical Society.

[154] Dawei Su, Andrew McDonagh, Shi-Zhang Qiao, and Guoxiu Wang. High-Capacity Aqueous Potassium-Ion Batteries for Large-Scale Energy Storage. *Advanced Materials*, 29(1):1604007, 2017. ISSN 1521-4095. doi: https://doi.org/10.1002/adma.201604007. URL https://onlinelibrary.wiley.com/doi/abs/10.1002/adma.201604007. _eprint: https://onlinelibrary.wiley.com/doi/pdf/10.1002/adma.201604007.

[155] Wenhao Ren, Xianjue Chen, and Chuan Zhao. Ultrafast Aqueous Potassium-Ion Batteries Cathode for Stable Intermittent Grid-Scale Energy Storage. *Advanced Energy Materials*, 8(24):1801413, 2018. ISSN 1614-6840. doi: https://doi.org/10.1002/aenm.201801413. URL https://onlinelibrary.wiley.com/doi/abs/10.1002/aenm.201801413. _eprint: https://onlinelibrary.wiley.com/doi/pdf/10.1002/aenm.201801413.

[156] Chunyi Liu, Xusheng Wang, Wenjun Deng, Chang Li, Jitao Chen, Mianqi Xue, Rui Li, and Feng Pan. Engineering Fast Ion Conduction and Selective Cation Channels for a High-Rate and High-Voltage Hybrid Aqueous Battery. *Angewandte Chemie*, 130(24):7164–7168, 2018. ISSN 1521-3757. doi: https://doi.org/10.1002/ange.201800479. URL https://onlinelibrary.wiley.com/doi/abs/10.1002/ange.201800479. _eprint: https://onlinelibrary.wiley.com/doi/pdf/10.1002/ange.201800479.

[157] D. Aurbach, Z. Lu, A. Schechter, Y. Gofer, H. Gizbar, R. Turgeman, Y. Cohen, M. Moshkovich, and E. Levi. Prototype systems for rechargeable magnesium batteries. *Nature*, 407(6805):724–727, October 2000. ISSN 1476-4687. doi: 10.1038/35037553. URL https://www.nature.com/articles/35037553. Number: 6805 Publisher: Nature Publishing Group.

[158] Hui Dong, Oscar Tutusaus, Yanliang Liang, Ye Zhang, Zachary Lebens-Higgins, Wanli Yang, Rana Mohtadi, and Yan Yao. High-power Mg batteries enabled by heterogeneous enolization redox chemistry and weakly coordinating electrolytes. *Nature Energy*, 5(12):1043–1050, December 2020. ISSN 2058-7546. doi: 10.1038/s41560-020-00734-0. URL https://www.nature.com/articles/s41560-020-00734-0. Number: 12 Publisher: Nature Publishing Group.

[159] Wei Wang, Lin Liu, Peng-Fei Wang, Tong-Tong Zuo, Ya-Xia Yin, Na Wu, Jin-Ming Zhou, Yu Wei, and Yu-Guo Guo. A novel bismuth-based anode material

with a stable alloying process by the space confinement of an in situ conversion reaction for a rechargeable magnesium ion battery. *Chemical Communications*, 54 (14):1714–1717, 2018. doi: 10.1039/C7CC08206A. URL `https://pubs.rsc.org/en/content/articlelanding/2018/cc/c7cc08206a`. Publisher: Royal Society of Chemistry.

[160] Francisco Nacimiento, Marta Cabello, Carlos Pérez-Vicente, Ricardo Alcántara, Pedro Lavela, Gregorio F. Ortiz, and José L. Tirado. On the Mechanism of Magnesium Storage in Micro- and Nano-Particulate Tin Battery Electrodes. *Nanomaterials*, 8(7):501, July 2018. doi: 10.3390/nano8070501. URL `https://www.mdpi.com/2079-4991/8/7/501`. Number: 7 Publisher: Multidisciplinary Digital Publishing Institute.

[161] Richard Y. Wang, Colin D. Wessells, Robert A. Huggins, and Yi Cui. Highly Reversible Open Framework Nanoscale Electrodes for Divalent Ion Batteries. *Nano Letters*, 13(11):5748–5752, November 2013. ISSN 1530-6984. doi: 10.1021/nl403669a. URL `https://doi.org/10.1021/nl403669a`. Publisher: American Chemical Society.

[162] Xiaoqi Sun, Victor Duffort, B. Layla Mehdi, Nigel D. Browning, and Linda F. Nazar. Investigation of the Mechanism of Mg Insertion in Birnessite in Nonaqueous and Aqueous Rechargeable Mg-Ion Batteries. *Chemistry of Materials*, 28(2): 534–542, January 2016. ISSN 0897-4756. doi: 10.1021/acs.chemmater.5b03983. URL `https://doi.org/10.1021/acs.chemmater.5b03983`. Publisher: American Chemical Society.

[163] Fei Wang, Xiulin Fan, Tao Gao, Wei Sun, Zhaohui Ma, Chongyin Yang, Fudong Han, Kang Xu, and Chunsheng Wang. High-Voltage Aqueous Magnesium Ion Batteries. *ACS Central Science*, 3(10):1121–1128, October 2017. ISSN 2374-7943. doi: 10.1021/acscentsci.7b00361. URL `https://doi.org/10.1021/acscentsci.7b00361`. Publisher: American Chemical Society.

[164] A. Ponrouch, C. Frontera, F. Bardé, and M. R. Palacín. Towards a calcium-based rechargeable battery. *Nature Materials*, 15(2):169–172, February 2016. ISSN 1476-4660. doi: 10.1038/nmat4462. URL `https://www.nature.com/articles/nmat4462`. Number: 2 Publisher: Nature Publishing Group.

[165] Rosalind J. Gummow, George Vamvounis, M. Bobby Kannan, and Yinghe He. Calcium-Ion Batteries: Current State-of-the-Art and Future Perspectives. *Advanced Materials*, 30(39):1801702, 2018. ISSN 1521-4095. doi: https://doi.org/10.1002/adma.201801702. URL https://www.onlinelibrary.wiley.com/doi/abs/10.1002/adma.201801702. _eprint: https://onlinelibrary.wiley.com/doi/pdf/10.1002/adma.201801702.

[166] Md. Adil, Ananta Sarkar, Amlan Roy, Manas Ranjan Panda, Abharana Nagendra, and Sagar Mitra. Practical Aqueous Calcium-Ion Battery Full-Cells for Future Stationary Storage. *ACS Applied Materials & Interfaces*, 12(10):11489–11503, March 2020. ISSN 1944-8244. doi: 10.1021/acsami.9b20129. URL https://doi.org/10.1021/acsami.9b20129. Publisher: American Chemical Society.

[167] Ruibai Cang, Chunlin Zhao, Ke Ye, Jinling Yin, Kai Zhu, Jun Yan, Guiling Wang, and Dianxue Cao. Aqueous Calcium-Ion Battery Based on a Mesoporous Organic Anode and a Manganite Cathode with Long Cycling Performance. *ChemSusChem*, 13(15):3911–3918, 2020. ISSN 1864-564X. doi: https://doi.org/10.1002/cssc.202000812. URL https://chemistry-europe.onlinelibrary.wiley.com/doi/abs/10.1002/cssc.202000812. _eprint: https://chemistry-europe.onlinelibrary.wiley.com/doi/pdf/10.1002/cssc.202000812.

[168] Longtao Ma, Na Li, Changbai Long, Binbin Dong, Daliang Fang, Zhuoxin Liu, Yuwei Zhao, Xinliang Li, Jun Fan, Shimou Chen, Suojiang Zhang, and Chunyi Zhi. Achieving Both High Voltage and High Capacity in Aqueous Zinc-Ion Battery for Record High Energy Density. *Advanced Functional Materials*, 29(46):1906142, 2019. ISSN 1616-3028. doi: https://doi.org/10.1002/adfm.201906142. URL https://onlinelibrary.wiley.com/doi/abs/10.1002/adfm.201906142. _eprint: https://onlinelibrary.wiley.com/doi/pdf/10.1002/adfm.201906142.

[169] Chuan Xia, Jing Guo, Yongjiu Lei, Hanfeng Liang, Chao Zhao, and Husam N. Alshareef. Rechargeable Aqueous Zinc-Ion Battery Based on Porous Framework Zinc Pyrovanadate Intercalation Cathode. *Advanced Materials*, 30(5):1705580, 2018. ISSN 1521-4095. doi: https://doi.org/10.1002/adma.201705580. URL https://onlinelibrary.wiley.com/doi/abs/10.1002/adma.201705580. _eprint: https://onlinelibrary.wiley.com/doi/pdf/10.1002/adma.201705580.

[170] Pan He, Yueli Quan, Xu Xu, Mengyu Yan, Wei Yang, Qinyou An, Liang He, and Liqiang Mai. High-Performance Aqueous Zinc–Ion Battery Based on Layered H2V3O8 Nanowire Cathode. *Small*, 13(47): 1702551, 2017. ISSN 1613-6829. doi: https://doi.org/10.1002/smll.201702551. URL `https://onlinelibrary.wiley.com/doi/abs/10.1002/smll.201702551`. _eprint: https://onlinelibrary.wiley.com/doi/pdf/10.1002/smll.201702551.

[171] Jianhang Huang, Zhuo Wang, Mengyan Hou, Xiaoli Dong, Yao Liu, Yonggang Wang, and Yongyao Xia. Polyaniline-intercalated manganese dioxide nanolayers as a high-performance cathode material for an aqueous zinc-ion battery. *Nature Communications*, 9(1):2906, July 2018. ISSN 2041-1723. doi: 10.1038/s41467-018-04949-4. URL `https://www.nature.com/articles/s41467-018-04949-4`. Number: 1 Publisher: Nature Publishing Group.